COPPER GALLIUM DISELENIDE THIN FILM ABSORBER GROWTH FOR SOLAR CELL DEVICE FABRICATION

By

RYAN KACZYNSKI

A DISSERTATION PRESENTED TO THE GRADUATE SCHOOL
OF THE UNIVERSITY OF FLORIDA IN PARTIAL FULFILLMENT
OF THE REQUIREMENTS FOR THE DEGREE OF
DOCTOR OF PHILOSOPHY

UNIVERSITY OF FLORIDA

2007

To my family – I love you

ACKNOWLEDGMENTS

First, I would like to thank Prof. A. Brad Anton at Cornell University for encouraging me to pursue my doctorate degree when I had no idea what I wanted to do in the future. I express my sincerest gratitude to Dr. Oscar Crisalle for taking me under his guidance. It has been a pleasure working for him. His relaxed attitude has been very beneficial to our working relationship.

I would like to acknowledge the many members of the CIS solar cell team at the University of Florida: Dr. Timothy Anderson and Dr. Sheng Li for your expertise in the solar cell field and bringing these many excellent graduate students together, Billy Stanbery for starting this project, Serkan Kincal for training me on the PMEE reactor, Suku Kim for training me on film deposition, Ryan Acher for helping with reactor maintenance (by far the toughest job) and film characterization, Woo Kyoung Kim and Seokhyun Yoon for growth support, Jiyon Song and Xuege Wang for device characterization, and Andre Baran and Wei Liu for device fabrication. Each one of you was very integral to my success on this project. I would also like to recognize the staff at MICROFABRITECH, especially Scott Gapinski and Diane Badylak.

TABLE OF CONTENTS

LIST OF TABLES

LIST OF FIGURES

Abstract of Dissertation Presented to the Graduate School
of the University of Florida in Partial Fulfillment of the
Requirements for the Degree of Doctor of Philosophy

COPPER GALLIUM DISELENIDE THIN FILM ABSORBER GROWTH FOR SOLAR CELL DEVICE FABRICATION

By

Ryan Kaczynski

May 2007

Chair: Oscar Crisalle
Major: Chemical Engineering

A custom-built migration-enhanced epitaxy reactor originally optimized for $CuInSe_2$ (CIS) deposition was modified to grow gallium-containing compound semiconductor thin films, such as $CuGaSe_2$ (CGS) and $CuIn_{1-x}Ga_xSe_2$ (CIGS). The addition of gallium allows for the manufacturing of solar cell absorber layers with wider band gaps.

Three distinct growth recipes under several growth temperatures and a wide range of metal-composition ratios are used to deposit polycrystalline CGS thin films. The surface morphology of gallium-rich films is typically very uniform, with long needle-like grains when grown by the first recipe, a constant copper-rate process. In contrast, copper-rich films grown by this same recipe or by a modified three-stage process have island structures with very large grains embedded in a matrix region that possesses small grains. The surface morphology becomes more uniform and the grains in the matrix region become larger when a higher growth temperature is used. The third recipe, an emulated three-stage process, does not produce films with an island-matrix structure, and the grains are uniformly large.

The highest conversion efficiency achieved for solar cells based on CGS is 5.3%, delivered by a copper-rich absorber deposited at the highest sustainable growth temperature of 491°C. This device has a large fill factor of 66 %, but the open-circuit voltage of 0.48 V is lower than

what is expected from a wide band-gap absorber. A set of CIGS solar cells was completely fabricated and characterized in-house. This led to the most efficient device produced from an absorber grown in our reactor, in the form of a 9 % CIS solar cell featuring a one-micron film deposited at 491°C.

Finally, a dynamic reactor model was created to describe the deposition environment in our epitaxial reactor. All relevant physical features are incorporated, including the cyclic motion of a rotating platen and the spatial distribution of the flux produced by three metal effusion sources. Reaction occurs under an excess of selenium, and operational variables such as rotational speed and melt height can be simulated. The outputs are predicted film thickness and composition. Further work is proposed to identify the values of adjustable sticking coefficients using experimental data.

CHAPTER 1
INTRODUCTION

This first chapter is intended to give the reader an overall description of the system under study. This information will be followed by the statement of the objectives of the project and finally by the proposed solution strategy to the problems. Not many details will be covered in this chapter; the purpose is to give the reader an overall idea of the rationale behind the remaining sections of the report.

The second chapter is an introduction to photovoltaics and thin film solar cells, especially those based on copper chalcopyrites. Its purpose is to familiarize the reader with energy production, solar cells and the important parameters that affect their efficiency. This chapter may be skipped by readers who are already familiar with the field without a loss of continuity.

The third chapter is an in-depth description of the absorber growth and device fabrication procedures. It is complimented by an explanation of the various techniques used to characterize the respective films and devices. Our techniques are compared to those in the literature.

Chapter 4 is an account of Copper Gallium Diselenide absorber growth in our modified molecular beam epitaxy reactor. The main motivation is the characterization of the films grown under various processing conditions. This chapter is accompanied by Appendix A, which includes the growth conditions for each absorber film described within the course of this work.

The fifth chapter is very similar in structure to the previous one, with the focal point shifting to the device fabrication of $CuGaSe_2$ solar cells. The thin films grown in the PMEE reactor that are discussed in Chapter 4 are used as the absorber layers in solar cell devices. Most cells were finished at the National Renewable Energy Laboratory (NREL), except for the final set which was completely fabricated in-house at the University of Florida.

In Chapter 6, low gallium content $Cu(In,Ga)Se_2$ absorbers are grown and completely fabricated within our facilities. The as-grown absorbers and subsequent devices were characterized to determine the effect of Ga composition on films grown by a simple single-stage process at a substrate temperature below 500°C. Appendix A also contains the reactor conditions pertaining to each of the growth runs.

In the seventh chapter, the focus is shifted to modeling of the reactor. A flux model had already been developed and needed to be incorporated into overall dynamic reactor model. This chapter is complemented by appendix B, which includes the details of model development.

The final two sections of the manuscript are conclusions and the list of references. The conclusions chapter also contains a list of possible future directions this research can take.

System Description

This project was initiated after the Boeing Company decided to terminate its photovoltaics research program and donated some research equipment to the University of Florida. Billy Stanbery, who was part of the Boeing Team, decided to enroll at the University of Florida to pursue a PhD degree. This jump-started a comprehensive, multi-faceted and multidisciplinary CIS solar cell research effort at the University of Florida.

PMEE Reactor

Physical Vapor Deposition (PVD) describes semiconductor thin film growth in a reactor whose high vacuum conditions cause material to flow in the molecular regime. Molecular Beam Epitaxy (MBE) describes this deposition process when epitaxial growth results. The main attributes of MBE compared to other techniques are a low growth temperature that limits diffusion, a slow growth rate that ensures two-dimensional growth, a simple growth mechanism, and compatibility with in situ analysis. Because of its unprecedented control down to the atomic

scale, MBE has been employed for the growth of many novel devices that require "band gap engineering."

Migration Enhanced Epitaxy (MEE) is a variant of MBE based on sequential rather than simultaneous exposure of the substrate to source fluxes. Rather than using shutters to control the material deposition on the substrates, the substrates rotate on a donut-shaped platen that takes them through the different deposition zones as well as fluxless relaxation steps in between. Each substrate is sequentially exposed during a complete cycle to Cu+In+Ga, background vacuum ambient, Se, and the background vacuum ambient again [1]. Chalcopyrite films have been grown by MBE for nearly 30 years [2], but the rotating platen, which is the main concept of MEE, makes our work unique compared to other research groups.

Our own reactor has been named with the acronym PMEE (plasma-assisted migration enhanced epitaxy) because of the incorporation of a plasma cracker for selenium or sulfur deposition. This reactor was originally designed to deposit $CuInSe_2$ (CIS) absorber layers and then was modified to support the growth of $CuGaSe_2$ (CGS) and $CuIn_{1-x}Ga_xSe_2$ (CIGS) films as well. The PMEE reactor can deposit Cu, In, Ga, Se, S, and Na, allowing for the deposition of a wide-variety of Cu-chalcopyrite thin films. It can support device manufacturing based on polycrystalline co-deposited CIS-based films, as well as an assortment of studies such as single crystal growth and bilayer precursor design for RTP studies. This process is low throughput and thus not economically feasible, but this research is concerned with investigating the film properties, not large-scale production. The ultra-high vacuum (UHV) creates an extremely clean condition and makes it possible to generate the molecular beam of each source so that the growth system can be used to grow epitaxial CIS thin films of high crystalline quality. It can overcome,

to a certain extent, a disadvantage of MBE, which is low productivity by processing nine samples in one batch.

There are some disadvantages of the system. Due to the rotational movement of the platen and thus the substrates, direct in-situ measurement of the substrate temperature is virtually impossible. The thermocouple is currently located in the gap between the platen and the heater and reading sort of an average value of those two temperatures. The localized heater position creates non-uniformity of the temperature distribution on the substrates. The growth rate is significantly limited by the selenium flux delivery. Even with a high Se flux rate ([Se]/([Cu]+[In])>5), it is hard to obtain sufficient Se incorporation into a growing film under a high temperature condition since the Se deposition zone is confined, and the high vapor-pressure material is easily re-evaporated from the surface. As a result, maximum flux rates of Cu and In are limited, which makes it difficult to achieve high growth rate. A time-consuming and costly problem is that the PMEE reactor has been custom designed and therefore requires extensive customizations to the regular sources available from manufacturers.

Chamber

The reactor can be divided into four zones as is shown in Figure 1-1: load-lock, chalcogen, heater, and metals. Materials are sequentially deposited as the substrate passes through their respective zones rather than co-deposited. The total flux is highly enriched in the specie evaporating from the nearer of the two sources as the substrate initially enters the metals deposition zone from either side. Hence, substrate rotation direction can result in substantially different compositions within the first metal layer. Counterclockwise rotation results in an initial metal flux during each MEE cycle that is substantially Cu-enriched.

The high-vacuum chamber is divided vertically into two zones by the cryoshroud and is maintained at a base pressure of around 10^{-8} torr by a series of diffusion and mechanical pumps.

Above the cryoshroud is the growth zone, where all the sources and substrates are located. Liquid nitrogen, circulated in the cryoshroud, further reduces the pressure in the growth zone to a base pressure around 10^{-9} torr. Pressure during deposition is in the range of 10^{-7} to 10^{-8} torr depending on the operating conditions. If the chamber is brought to atmospheric pressure, it takes a few days to get the appropriate low pressure back.

Load-lock

A load-lock, attached to a port at the substrate platen level of the chamber, allows the system to remain under vacuum for months during operation. The load-lock is independently pumped with a small turbomolecular pump (TMP) and isolated by a gate valve from the loading chamber. Chamber venting uses argon gas and the load-lock is equipped with a Venturi pump and a liquid nitrogen sorption pump for rough-pumping down to the TMP's crossover pressure of 10^{-3} torr. Up to nine 2" diameter wafers or 2" x 2" square substrates can be loaded onto the donut-shaped molybdenum platen via a two-prong fork, which is then rotated so that each substrate travels through all four zones.

Chalcogen Zone

The chalcogen zone is where a thermal cracker for Selenium (Se) and a low-capacity plasma cracker that can be charged with Selenium or Sulfur (S) are installed. Since Se does not evaporate as a very reactive species, it must be further cracked to be incorporated into the film. The thermal cracker breaks the large molecules into smaller, more reactive molecules by heating them to very high temperatures in a double-oven reactor before deposition. Hence the temperature in the evaporation zone of this double oven controls the flux of the material and the temperature in the cracking zone controls the species distribution [3]. The plasma cracker accelerates particles to make them more effectively reactive, which is an alternative to the high temperature of the thermal cracker. No sensors are used to measure the flux since the Se is

deposited in excess; only the temperatures of the sources are measured. Excess Se deposits everywhere so a chalcogen zone shield was incorporated to isolate this zone from the rest of the reactor.

Heater Zone

After passing through the chalcogen zone, substrates are brought to the desired operation temperature in the heater zone with radiative heating by a boron nitride-coated radiation heater. Most of the substrate platen heating is provided here. In other zones, the substrates are slowly cooled down since there is no direct heating there. Some extent of non-uniformity of the temperature distribution on the platen is expected due to the complex design [4].

Metals Zone

Finally, the substrates enter the metal deposition zone where they are sequentially exposed to Copper (Cu), Indium (In), and Gallium (Ga) fluxes. The Cu, In, and Ga sources are thermal evaporation sources with conical shaped crucibles and free-evaporating surfaces. Deposition uniformity is improved significantly with a conical instead of a cylindrical crucible [5]. The effusion sources are identical in structure: 7.5° tapered angle, 30 cc capacity, and constructed with Pyrolithic Boron Nitride (PBN). Cu and Ga have dual filament heating structures due to their properties, whereas In has only one. The tip filament keeps the tip of the crucible hot so no impurities can condense on the surface. Shielding prevents deposition on each individual substrate except during that portion of each rotation cycle of the substrate platen when it is inside the shield.

The platen then rotates back into the load-lock zone where the entire cycle restarts. The dopant source is located in this area to introduce small quantities of impurities. It is charged with a very small amount of NaF. The metals zone was expanded into the previously allocated load-lock area so that the Gallium source could be added.

Control

Every material source is equipped with thermocouples for monitoring the temperature. The source temperature is actually measured indirectly by putting the thermocouple in thermal contact with the crucible. These are mainly c-type thermocouples, with the exception of the evaporation zone in the two crackers which are fitted by k-type thermocouples due to the lower temperatures involved. The substrate temperature is measured indirectly by means of a c-type thermocouple suspended in between the rotating platen and the substrate heater. The rotating nature of the platen prevents getting direct temperature readings on the substrate [6].

Rate control is provided by a Leybold-Heraeus Inficon Sentinel III with both EIES (Electron Impact Emission Spectroscopy) sensors for monitoring and controlling the metals deposition process and quartz crystal monitors (QCM) for calibration. Closed-loop feedback control is conducted along with the in-situ rate measurement employed by the EIES sensors for Cu and In sources. EIES sensors are calibrated by a QCM that is located right over the source cells whenever source material is reloaded. A single QCM is used to monitor the Ga flux because the reactor modifications were limited by space and the current setup. The dopant flux is monitored by QCM because it doesn't need to be controlled tightly. No instrument is used to measure the Se flux rate in-situ so closed-loop feedback control based on temperature has been adopted.

An instrumentation and control interface for the PMEE reactor was designed to enable the implementation of advanced control strategies envisioned for the local sources as well as the supervisory control structure. A human-machine interface is programmed on a LABVIEW platform so that real time control of the PMEE reactor can be administered through a central computer [6]. Using microprocessor control, one can ensure run-to-run repeatability by constantly monitoring and adjusting the various growth parameters.

Problem Statement

The purpose of this project is to explore the key processing issues associated with growing copper chalcopyrite films containing gallium in a migration enhanced epitaxy reactor. Copper Gallium Diselenide is theoretically a good candidate as the top cell in a tandem solar device, owing to its nearly ideal band gap of 1.7 eV and maximum theoretical efficiency of 26%. Practical use in a tandem cell will require efficiencies greater than the current best cell efficiency of approximately 10%. A low temperature process for the growth of $CuGaSe_2$ absorber layers should be developed to avoid the degradation of the junctions located underneath the top cell in a monolithic tandem structure.

To grow high-quality CGS absorbers, several steps were required. First, a gallium source needed to be retro-fit into a custom-built MEE reactor used for the deposition of $CuInSe_2$ absorber films. Then it needed to be shown that this reactor could grow polycrystalline $CuGaSe_2$ thin films that produced working solar cell devices. Various growth recipes were investigated, along with varying material compositions, growth temperatures, and post-deposition processes. The structural and morphological properties of the films were characterized along with electrical properties of the subsequently fabricated devices.

Another goal was to achieve complete in-house fabrication and characterization of CGS devices. This was intended to decrease the feedback time needed in investigating the effect of processing changes on electrical properties of the solar cell. This required a team effort of several graduate students.

Finally, the flux models of the effusion sources needed to be incorporated into a dynamic reactor model. This model will be the basis for a control feedback scheme that will correlate film properties and hence, device properties with the input conditions of the reactor.

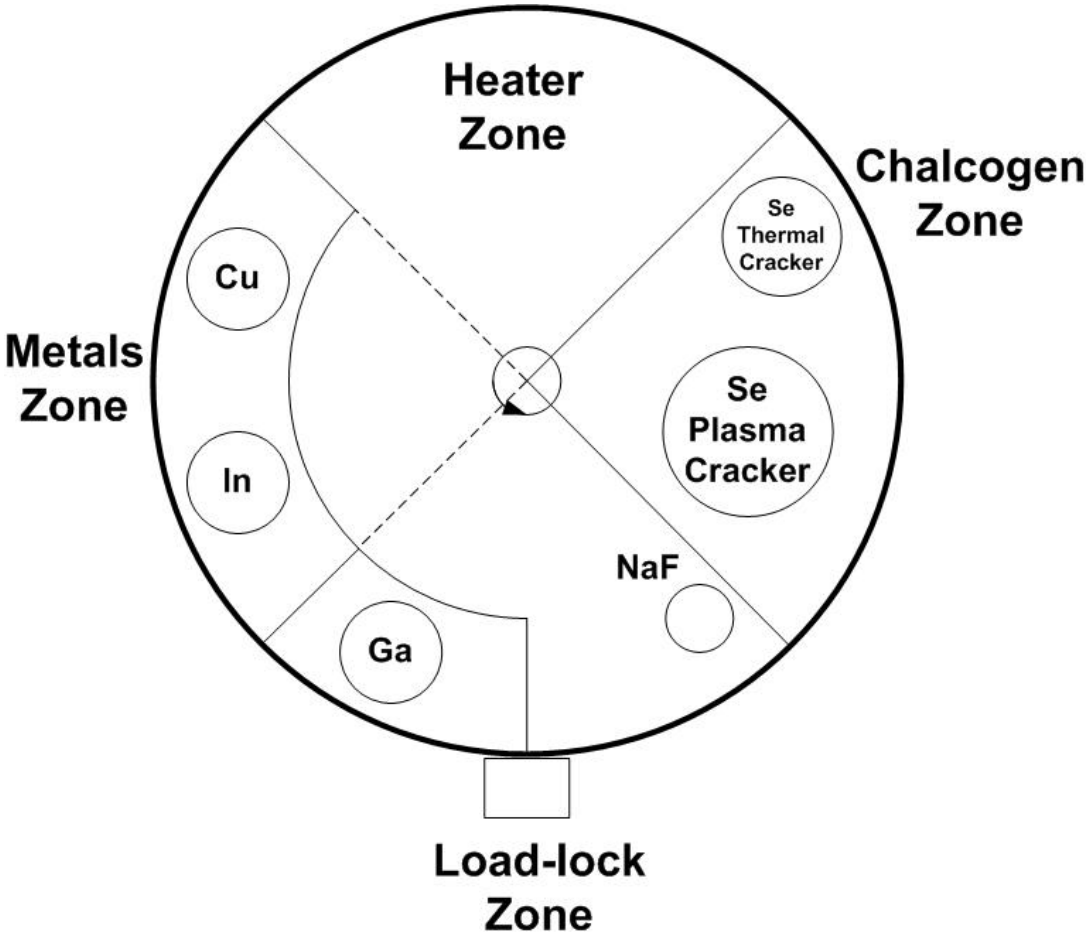

Figure 1-1. Top view of the PMEE reactor.

CHAPTER 2
SOLAR CELLS

Energy

Rapid industrialization combined with an expanding population is driving the world's demand for energy, which is projected to triple by the end of the century (from 13 TW to 46 TW) [7]. The fossil fuel reserves that currently furnish power to the globe will fall short of this demand over the long term, and their continued use produces harmful side effects such as pollution. Finding sufficient supplies of clean energy for the future may be civilization's most difficult challenge. Alternative renewable fuels are currently not competitive with fossil fuels in cost and production capacity, but solar cells have the potential to become a key part of the solution to this problem.

Sunlight

Photovoltaic (PV) systems exploit an inexhaustible resource that is free to use and available anywhere in the world. More energy from sunlight reaches the earth's surface in one hour (4.3×10^{20} J) than is consumed by civilization in an entire year (4.1×10^{20} J) [7]. If 0.16% of the land on Earth was covered with 10% efficient solar cells, 20 TW of power would be provided, which is more than the world's current consumption rate of fossil energy [7]. This illustrates the impressive magnitude of the solar resource and the potential harbored by solar cell technology.

The sun emits energy as a blackbody radiator at a temperature of approximately 6000 K with a spectrum ranging from the ultraviolet (3.5 eV), through the visible, into the infrared (0.5 eV). The energy of the visible region ranges from 3.1 eV (violet) to 1.8 eV (red) with the peak power of the sun occurring at approximately 2.25 eV. This distribution of photons in the spectrum is one of the greatest limiting factors on solar cell performance. Under monochromatic

light, a typical PV cell might be able to convert 60% of the light to electricity, but under the multicolored solar spectrum, the same cell would only be able to convert 10% of the light's energy to electricity [8]. Diffuse light is the portion of sunlight that has been refracted or scattered in the atmosphere before it reaches the Earth's surface. When the sky is completely clear, about 10% of the sunlight is diffuse. Most losses in the spectrum at lower energies are caused by light being absorbed by molecules of water vapor while at energies higher than 3 eV, almost all sunlight is absorbed by ozone [8].

The AM1 solar spectrum represents the sunlight on the Earth's surface when the sun is at its peak. At a solar zenith angle of 48.2°, the equivalent of 1.5 of these noontime air masses (AM1.5) is diminishing the intensity of the sunlight [8]. The AM1.5 condition has an incident power of 84.4 mW/cm^2 and is the most appropriate for calculating the conversion efficiency of a solar cell in the terrestrial environment [9]. The irradiant power of the sun under AM0 conditions is 135.3 mW/cm^2, which is the spectrum measured outside the earth's atmosphere. AM1.5 is compared to AM0 in Figure 2-1 [9]. The "peak watt" (W_P) rating is the power (in watts) produced by a solar cell module illuminated under the following standard conditions: 100 mW/cm^2 intensity, 25°C ambient temperature, and AM1.5. Because of day/night and time-of-day variations and cloud cover, the average electrical power produced by a solar cell over a year is about 20% of its W_P rating [7].

The two most important variables controlling the amount of annual sunlight are latitude and local cloud cover. Latitude is important to the amount of annual sunlight for two reasons: the angle of the sun and the length of the days. The Northeast and Northwest United States are the cloudiest regions, while the Southwest usually has the clearest skies. In Buffalo, NY, there is about 60% and in Sacramento, CA, about 85% of the solar energy available in Albuquerque, NM

[10]. Almost 90% of the country gets between 6 and 8 kWh/m^2 daily, which is enough for the effective use of PV [8]. There is also a seasonal effect on the energy produced by PV modules because in the summer the sun spends more time at high elevation angles (low air mass) than in the winter (high air mass)

Costs

Clearly, solar energy can be exploited on the needed scale to meet the global energy demand. Sunlight is readily available and its use does not harm the environment through pollution or the climate through greenhouse gases. Yet, U.S. electricity production by solar cells currently represents a tiny fraction (<0.02%) of the total electricity supply [7]. The wide-spread use of PV has been hampered by the relatively high price of the solar cell module. The huge gap between our present consumption of solar energy and its enormous undeveloped potential defines a grand challenge in energy research.

Solar cells typically have a lifetime of at least 30 years and incur no fuel expenses, but they do involve a capital cost. The cost for the electricity produced by the cell is estimated by spreading the total capital cost over the entire lifetime of the cell while considering the total electrical energy that will be produced during that time. Higher conversion efficiency thus directly impacts the overall electricity cost because higher efficiency cells will produce more electrical energy per unit cell area over the cell lifetime. The most useful cost calculation for PV cell modules ($/$W_P$) is determined by the ratio of module cost per unit area ($/$m^2$) divided by the maximum amount of electric power delivered per unit of area (module efficiency multiplied by 1000 W/m^2, the peak isolation power) [7]. In addition to module costs, a PV system also has costs related to the non-photoactive parts of the system, called balance of system (BOS) costs. To compete with electricity produced from fossil fuels, solar cell costs must eventually approach $0.40/$W_P$ [7].

Photovoltaic Systems

$$\text{Efficiency} = \frac{\text{power out}}{\text{power in}} \qquad (2\text{-}1)$$

For a solar cell, this is the ratio of the electric power produced by the cell at any time versus the power of the sunlight arriving at the cell. Efficiencies do not fluctuate much over the life of a cell unless it is degrading. By definition, the higher a photovoltaic device's efficiency, the more electricity it produces for a given exposed area. Besides device efficiency, the definition of performance must also include uniformity, reproducibility, throughput, materials utilization, and yield [11].

A single cell is only useful when powering wristwatches and calculators so many cells are connected within a module. The module serves two purposes: it protects the solar cells from the outside environment and it delivers a higher voltage than a single cell. Individual small-area cells must be connected in series so some part of the module area is lost for the interconnection of cells. Another important effect which reduces the performance of modules is the non-uniformity of voltage and current density over a large area, which is mainly related to the compositional variation of the absorber layer [12]. A critical issue that must be resolved is the large gap in efficiency between small-area laboratory devices and large-area modules.

The basic components of a photovoltaic system are the modules, support structures, land, and possibly sun trackers. There are two different kinds of modules: flat plates and concentrators. Flat plates are large panels that can be assembled into even larger arrays. To maximize energy production, a module can be mounted onto a two-axis solar tracker so that it always points directly at the sun [10]. Concentrators use large, concentrating lenses to focus sunlight onto small cells. These lenses replace large areas of expensive semiconductor material, reducing the total module cost. A concentrator does not produce any energy when the weather is

cloudy because it cannot focus diffuse light. Hence, they are geographically limited to sunny locations as opposed to flat plates, which can be useful in cloudy areas.

There are two major market sectors: grid-connected and stand-alone systems. The former delivers power directly to the grid by converting the direct current of solar modules into alternating current by an inverter. The latter supplies power to isolated sites and to small-scale consumer products. Since solar energy is not always available, effective storage and distribution are critical to matching supply with demand. Storage drives up the cost of solar cells. A simplified photovoltaic system is shown Figure 2-2. Besides the terrestrial market, there is also the space market, which has different material and cost requirements.

Future

The primary objective of worldwide solar cell research and development is to reduce the cost of photovoltaics to a level that will be competitive with conventional ways of generating power. The world market grew from less than 10 MW_P/yr in 1980, to 80 MW in 1996 sold at prices close to \$10/W_P [13], to finally exceeding 1000 MW in 2004 at less than \$7/W_P [14]. Costs need to be reduced even more for solar cells to become competitive with the likes of oil, coal, and natural gas. Otherwise, future large-scale use of PV might depend more on environmental concerns rather than economic competitiveness.

Behind the progress of photovoltaics as a technology is a loyalty to PV as an idea. There are technical obstacles that must be overcome and their solutions depend on the funding of fundamental research. As these issues are resolved, the costs will continue to fall. "Solar electricity is part of America's present and its future – as is the R&D that enables it" – Larry Kazmerski, one of the pioneers of thin film solar cells [15].

Solar Cell History

Photovoltaics had its beginnings in the nineteenth century. French Scientist Alexandre-Edmond Becquerel discovered the PV effect in 1839. He observed that a voltage and a current were produced when two electrodes in a beaker full of fluid were exposed to sunlight. And in 1873, Willoughby Smith found that the element selenium conducted far more electricity when it was illuminated than it did when it was dark [8].

Many consider the work accomplished during the 1950s at Bell Laboratories to be the true origin of photovoltaics. Cal Fuller, Darryl Chapin, and Gordon Pearson made a silicon cell that was able to convert 6% of sunlight into electricity [16], which was a large improvement over selenium cells. Fuller and Chapin eventually reached 10% conversion efficiency, but compared to traditional electricity in the 1950s, the cost of PV-produced power was a thousand times as much [8].

From the mid 1950s to the early 1970s, PV research and development was directed primarily toward space applications where it is the conventional power source. In space, payload weight is critical and solar cells weigh very little compared to the power that they produce. Nearly every communications satellite, military satellite, and scientific probe is powered by PV. Satellite manufacturers can endure a high cost because it is a small fraction of their total cost, but they cannot tolerate an unreliable power source that may jeopardize their entire investment. Then in 1973, a greatly increased level of research and development on solar cells was initiated following the oil embargo in that year, which led to the creation of the U.S. Department of Energy, along with its PV program, a few years later.

Researchers at Bell Labs showed three decades ago that the I-III-VI_2 semiconductor $CuInSe_2$ (CIS) allows for efficient solar-to-electrical energy conversion. A single crystal CIS cell of 12% efficiency was made at Bell Laboratories in 1975 [17] and the University of Maine

produced a polycrystalline $CuInSe_2$ cell of nearly 6% efficiency in the following year [18]. Although Bell Labs and Maine initiated the study of CIS, the most important early research was done by a small group at Boeing Aerospace Corporation in Seattle. Boeing's team, led by Reid Mickelsen and Wen Chen, achieved over 10% efficiency with CIS cells in 1982 using elemental co-evaporation of the source materials in vacuum [19].

Solar Cell Device Physics

Photovoltaics (PV) is the direct conversion of sunlight into electricity; solar cells absorb sunlight and change it continuously into electricity. According to quantum theory, light can behave either as waves or as particles. Discrete particle-like packets of light are called photons, and each photon has a well-defined energy and wavelength.

Band Gap

The valence and conduction bands of an inorganic semiconductor are separated by a forbidden energy range that the electrons cannot occupy [20]. This minimum threshold energy is called the energy gap or band gap (E_g), and it varies for different materials because each of them has a different bond strength. Semiconductors with weak bonds have small energy band gaps. Conduction is only possible if we can impart kinetic energy to an electron. When photons with energies $h\nu > E_g$ impinge upon a pn junction solar cell, they are absorbed and the rate of generation of electron-hole pairs as a function of distance x from the surface of the solar cell is given by the following equation [9]:

$$g_E(x) = \alpha\Phi_o(1-R)e^{-\alpha x} \qquad (2\text{-}2)$$

where α is the optical absorption coefficient, Φ_o is the incident photon flux density per unit bandwidth per second, and R is the reflection coefficient. Photons with energies below the band gap pass through the absorber without being absorbed.

Electric Field

Most semiconductor devices incorporate both positive and negative regions, and it is the space-charge region formed between them that leads to their useful electrical characteristics [20]. After a certain number of electrons and holes have flowed from one region to the other, an electric field will be built up, preventing further net flow of the carriers. The greater the density of free carriers initially on each side of the interface, the greater will be the electric field that forms when they mix. This electric field is not tenuous; it does not come and go. The area of the field is also called the depletion region because in that region there are no free carriers. They all are either in bonds or swept away by the field. Under equilibrium conditions, electron-hole pairs are continuously generated everywhere within the semiconductor and in the absence of an applied voltage, the electron-hole pairs recombine and therefore no current flow results. However, when a positive voltage is applied to the n-region of a diode with respect to the p-region, the electron-hole pairs, once generated, will be separated and their probability of recombination is diminished. The most important attribute of these p-n junctions is that they rectify, i.e. they permit the passage of electric current in only one direction [20].

The electric field that drives the current is proportional to the material's band gap. A semiconductor with a small band gap produces an insignificant voltage. As the band gap is increased, more solar photons within the spectrum will lack the energy to produce electrons and holes so a very large band gap would produce a high voltage with a tiny current. For a semiconductor to be a sufficient absorber layer in a solar cell, it must have a band gap that allows for both reasonable current and voltage.

Recombination

Radiative recombination, in which a hole reacts with an electron and produces a photon, is exactly the reverse of absorption; it is the spontaneous transition of an electron from the

conduction band to an unoccupied state in the valence band [21]. In real solar cells, recombination via impurities is the predominant recombination process. Recombination centers located within the electric field can severely reduce the field's strength and thus the voltage. These are called shunts [8]. Defects located at the interface can also be efficient recombination centers because they introduce deep trap levels into the band gap [22].

Defects

In compound semiconductors, intrinsic point defects are introduced to compensate for deviations from the stoichiometry [23]. The simplest point defect is the vacancy in which a single atom is missing from the lattice. An interstitial is an extra atom occupying space between the normal lattice sites. A component atom may also occur on a site intended for another. This is called an antisite defect. Point defects influence the bulk properties of a semiconductor as opposed to grain boundaries or interfaces that only affect the film locally [22].

A grain boundary is the complete fracturing of bonds along an entire surface. They occur when a lattice takes shape in such a way that a defect spreads and makes it impossible for nearby atoms to bond together. According to the grain boundary carrier-trapping theory, grain boundaries work as trapping centers and therefore hinder the transport of charge carriers towards the pn interface [24]. Cell performance would suffer considerably because these lost electrons would not contribute to the cell current. It is very common for crystal defects to cause a polycrystalline structure where the grain boundaries separate regions of different crystallographic orientation. Many of the electrical and optical properties of these materials are determined by the corresponding properties of the grain boundaries and these may differ considerably from a single crystal [22].

When grain boundaries cannot be avoided, they need to be passivated to minimize their effect. This consists of adding some extra material, usually oxygen, that can make the grain

boundary defects less harmful. Most added materials diffuse preferentially down grain boundaries so it goes directly to the region where it can have the most effect. The added oxygen might passivate defects in the grain boundary by grabbing loosely bound electrons, removing many of them as undesirable recombination centers. Some materials have relatively harmless grain boundaries like $CuInSe_2$; they may be self-passivating or some growth step may passivate them. They can be made inexpensively and yet behave almost as if they were single crystals. Others have very harmful grain boundaries, like gallium arsenide (GaAs) and silicon (Si) [8].

Thin Films

Crystalline silicon currently dominates the photovoltaic market despite a complicated manufacturing process and a high production cost. Its advantages are a readily available raw material, mature processing technology, and non-toxicity. Si-based products are also very reliable and are capable of achieving high efficiencies [14]. The preeminence of the element Si, in its amorphous or crystalline form, within the market is an overwhelming 99% [25].

A strategy for reducing costs is to use thin film materials that have a very high absorptivity for solar photons. The leading thin film technologies, a-Si, CdTe, and CIS, offer the potential for significant manufacturing advantages over crystalline Si. They have a lower consumption of materials, independence from Si shortages, fewer processing steps, and a monolithic circuit design so no assembly of individual solar cells into a final product is needed [26]. Less material usage leads to lower material costs, thinner layers leads to faster processes and lower capital costs, and the processing of large-area devices leads to reduced handling costs. They can also be made into flexible and light-weight modules on alternative substrates, which provide multiple advantages in processing [27]. The most serious threat to large-scale deployment of existing thin films is materials availability of key elements such an In, Te, and Ge. Thus, Si-based technology may always be relevant.

Direct vs Indirect Band Gap

Si has an indirect band gap so light absorption is much weaker than for thin films, which are direct band gap semiconductors. The difference in absorption strength between direct and indirect band gap semiconductors comes from the different processes by which they absorb individual photons. Direct transitions are transitions in which the momentum of the electron-hole pair does not change. Light of sufficient energy to free an electron from its fixed state is absorbed by the electron, which is then freed. Light-absorption is more complicated in an indirect band gap material. Promotion of an electron to the conduction band requires the simultaneous interaction of a photon and a thermal vibration of the crystal lattice, called a phonon. When a photon and a phonon of the proper energies are both absorbed, at the same time, by a bound electron, a free electron-hole pair results. Almost all of the energy needed to generate the electron-hole pair is carried by the photon; the phonon just acts to catalyze the process.

Absorption Length

The absorption length of light in a semiconductor is determined by the likelihood that a photon will be absorbed. The absorption length for crystalline Si is approximately 30 microns, while it is about 0.3 microns for CIS. Higher energy photons have a greater probability of interacting with a bound electron and being absorbed than lower energy photons, even though both have more than the band gap energy. For instance, in CIS (Eg = 1.0 eV), the absorption length of high-energy photons (>2.5 eV) is less than 0.1 microns, but a beam of low-energy photons (1.1 eV) might require 1 micron to be equally satisfied [8].

Diffusion Length

Free electrons on the p-side move around randomly before recombining. During this short period of time, called the lifetime, they have a finite chance of encountering the electric field and

being sent to the n-type side of the device. This separation is a result of diffusion and the average distance that minority carriers can move toward the built-in field before they return to their fixed states is called the diffusion length. Materials with longer diffusion lengths are able to produce more current. In solar cells, they can vary from less than a micron to over 100 microns in some single-crystal semiconductors. Large diffusion lengths are a necessity for indirect band gap materials like crystalline silicon, but direct band gap materials absorb enough light within their depletion region that their performance is not critical to diffusion length. If the ratio of diffusion length to absorption length is greater than one, most carriers will be separated. Crystal quality is the most important factor in determining a material's diffusion length because diffusion is constrained by the propensity of free carriers to recombine.

$CuInSe_2$-Based Solar Cells

$CuInSe_2$-based solar cells are the most promising of the thin film solar cells and are the basis for the investigations within this work. Cu-chalcopyrites, of the general composition $Cu(In_{1-x}Ga_x)(S_ySe_{1-y})_2$, offer a wide range of band gaps from 1.0 eV for $CuInSe_2$ to 2.4 eV for $CuGaS_2$. Recently, new world record total-area efficiencies of 15.0, 19.5, and 10.2% for CdS/CIGS solar cells have been achieved for x=0 (CIS), x~0.28 (CIGS) and x=1 (CGS), respectively [28]. Table 2-1 shows these record efficiencies alongside their theoretical output.

Material Properties

The direct optical band gap of single crystal $CuInSe_2$ has a value near 1 eV at room temperature [29]. The absorption coefficient of 10^5 cm^{-1} for light greater than the band gap means the thickness of the absorber can be reduced theoretically to less than 1 micron [30]. CIS-based materials belong to the group of I-III-VI_2 semiconducting compounds. Their lattice elements are tetrahedrally coordinated similar to diamond-like semiconductors [31]. The chalcopyrite cell consists of two zinc blende cells with Cu and In occupying the same lattice sites

in the upper and lower cell, alternately as seen in Figure 2-3 [32]. In the chalcopyrite structure, each I (Cu) or III (In, Ga) atom has four bonds to the VI atom (Se). In turn, each Se atom has two bonds to the Cu and two to the In (or Ga). Because the strengths of the I-VI and III-VI bonds are different, the ratio of the lattice constants c/a is not exactly 2; it varies from 2.01 for CIS [33] to 1.96 in CGS [34].

Doping in chalcopyrites is mainly controlled by compositional variation and thereby induced defects, which lead to strong compensation [35]. This makes the systematic study of their electronic properties more difficult than in extrinsically dopable materials. The band gap can be engineered, which offers a greater possibility of finding the optimum photovoltaic material with respect to cost, efficiency, and stability.

Four different phases have been found to be relevant: α-phase ($CuInSe_2$), β-phase ($CuIn_3Se_5$), δ-phase (high temperature sphalerite phase), and $Cu_{2-y}Se$ [36]. The existence range of single-phase $CuInSe_2$ is very small and does not include the stoichiometric composition of 25% Cu. The Cu content of absorbers for efficient thin-film solar cells typically varies between 22 and 24% (at.) Cu. At the growth temperature of 500-550°C, this region lies within the single-phase region of the α-phase.

Some interesting features of CIS-based solar cells include low open-circuit voltage to band gap ratio compared to Si and III-V devices, insensitivity of the conversion efficiency to the [Cu]/[III] ratio over a wide range, exceptional tolerance to grain boundaries, and loss of performance for CIGS alloys with x greater than 0.3 [37]. Single crystal CIGS efficiencies also lag behind those of polycrystalline CIGS. Optimal sodium incorporation is beneficial to device performance, and excess sodium is detrimental. Na depth profiles typically exhibit some

qualitative features: enrichment at the CIS surface and a relatively lower concentration in the bulk of the CIS with concentration increasing toward a maximum at the CIS/Mo interface [38].

Defects

For Chalcopyrite compounds, intrinsic defects are introduced to maintain the crystal structure for non-stoichiometric composition. There are twelve intrinsic point defects that can be formed in the ABX_2 chalcopyrite lattice: three vacancies (V_A, V_B, V_X), three interstitials (A_i, B_i, X_i), and six antisite defects. In addition to the antisite defects that can be formed by an exchange of anions (X) and cations (A,B) as in binary compounds (A_X, B_X, X_A, X_B), one can also form antisite defects on the same sublattice by an exchange of the cations (A_B, B_A) [22]. The Cu vacancy, V_{Cu}, is considered to be the dominant acceptor in Cu-poor p-type material, while the Se vacancy, V_{Se}, is considered to be the dominant donor in n-type material [36]. Most of the off-stoichiometry defects must be electronically inactive to allow for large deviations from stoichiometry without the deterioration of the electronic quality of the film [39]. A critical issue in regard to CIS-based solar cells is the control of these point defects, which are responsible for recombination in the space charge region of the devices [40].

Gallium Addition

When indium is replaced by gallium, the band gap increases. This is an effect of the smaller size of the Ga atom, when compared to In, and the subsequent formation energies involved. With the addition of gallium, some of the material properties also change. These include structural properties like lattice constants, film morphology, and adhesion, and chemical changes such as defect levels, affinities, and carrier concentrations. The band gap of $CuIn_{1-x}Se_2Ga_xSe_2$ can be tuned from 1.0 to 1.7 eV by adjusting the Ga content (x) from 0 to 1.

Although the Ga/(Ga+In) ratio of roughly 0.65 would provide the optimal band gap by theory, the actual Ga content in the current record device is 28%, which corresponds to a band

gap of approximately 1.2 eV [41]. This disparity implies that there are factors effecting conversion efficiency other than band gap. The increase in efficiency in the range of 0 to 28% Ga is due mainly to the increase of the band gap, and the potential on the grain boundary in this gallium content range stays strong. However, at higher Ga content, the absence of the potential on the grain boundary seems to be significant in comparison to the effect of the band-gap widening [42].

$CuGaSe_2$

Copper Gallium Diselenide, as a member of the I-III-VI_2 compound semiconductors, has a direct energy band gap of 1.7 eV [43], a very high absorption coefficient $\alpha = 3 \times 10^4$ cm^{-1} at 1.7 eV [44], and an easily controllable electrical resistivity in a wide range of 10^{-1} to 10^5 ohm-cm [45]. The band gap of CGS decreases with increasing Cu/Ga ratio [46]. The temperature coefficient is lower for wide gap materials, which means that the efficiency loss at operating temperature is less than for smaller band gap semiconductors [47]. To date, device efficiency of greater than 9.5% is reported using less than 2 microns of CGS absorber film by NREL [48].

$CuGaSe_2$ has been investigated for more than 25 years, but in comparison to the rapid progress made for $CuInSe_2$ and $Cu(In,Ga)Se_2$, the efficiency of CGS-based solar cells is still relatively low. CGS did not overcome a limitation of 6.2% until fairly recently when efficiencies of up to 9.3% for thin films and 9.7% for single crystal devices were achieved [49]. These reported values lie well below the theoretical limit for CGS of $\eta = 26\%$ [50]. The most critical drawback of CGS solar cells is the low open-circuit voltage (V_{OC}) compared to band gap. In the case of CIS or CIGS, the V_{OC} follows a relationship with the band gap according to $V_{OC} \sim E_g/q$-500 mV, where q is the elementary charge. A V_{OC} of 1.2 V should therefore be possible for CGS-based devices, but Cu-rich absorbers have been limited to a V_{OC} of 750 mV [51], while high efficiency Ga-rich absorbers have peaked at 900 mV [48]. The improved device

performance of Ga-rich films results from decreased defect densities in the bulk and a decrease of tunneling-enhanced recombination [52]. Cell performance may be fundamentally constrained since it seems that the Fermi level might be limited to values less than 800 meV above the valence band edge, which would always make CGS p-type [53].

Defects

Wide gap chalcopyrites, such as CGS seem to have extensive material and growth-related problems that limit the device performance. The tetragonal structure is capable of sustaining a large concentration of vacancy and antisite defects in CGS [54]. Devices based on slightly Cu-poor $CuGaSe_2$ absorbers have shown better performances than stoichiometric ones. In Cu-poor material, the deviation from stoichiometry is not facilitated by the formation of a second phase, as in the Cu-rich case, but the material develops a high density of defects. This leads to a high degree of compensation, which in turn causes lateral potential fluctuations in the concentrations of the charged defects [55]. This density of defects is higher at the increased Ga contents because the lattice mismatch in that composition range is anticipated to be larger. Better lattice matching between the surface and the bulk leads to better performance [56]. Optimal growth conditions of CGS thin films are realized by a trade-off between growing Ga-rich films, reducing the density of states in the band gap, and growing stoichiometric CGS to achieve optimal grain size and crystallinity [55].

Recombination

The actual path of recombination, which limits open circuit voltage, is important; it can take place at the interface or within the space charge region, or it can be tunneling supported [57]. Increasing the Ga content in CIGS intensifies the contribution of tunneling, which is observed as a larger characteristic tunneling energy, E_{oo}. This facilitates recombination and in turn increases the recombination loss. For CGS, Rau et al. obtained significant values of E_{oo} and

found that the devices with the highest V_{OC} are those with the lowest charge density and the lowest tunneling currents [58]. At room temperature, the tunneling contribution to recombination is insignificant for low gallium content CIGS [59]. Hence, there is no fundamental difference between CIS and CGS with regard to recombination path, but recombination losses in CGS are enhanced due to a higher contribution of tunneling [57].

Cu-rich CGS devices are controlled by high E_{oo} values due to tunneling enhanced interface recombination. The efficiency gain achieved by the use of Ga-rich absorbers is mainly explained by a reduced doping level and the decreased tunneling rate. All the beneficial device modifications like air-annealing or the increase of CdS deposition temperature lead to a further decrease of E_{oo}. The increased Cd diffusion into the absorber material during CBD explains the reduction of tunneling [51].

Type inversion

The efficiency of a $CuInSe_2$ device is aided by the fact that its surfaces can be inverted to become n-type even though the bulk of the sample is p-type. This is done via deposition of CdS, which leads to band bending. The amount of band bending equals the shift in Fermi level with respect to the valence band maximum from the p-type to the n-type region. A large amount of band bending results in a Fermi level close to the conduction band minimum, which is needed to get n-type conditions. The beneficial effects of this weakly n-type surface layer include the reduction of the recombination rate and the enhancement of the carrier collection efficiency by shifting the electrical junction away from the interface between CdS and the absorber [60].

The photovoltaic performance of CIGS devices deteriorates for $x>0.3$. Due to the lack of type inversion for CIGS with $x>0.3$, the pn junction moves to the 'real' CdS/CIGS interface causing higher recombination losses [61]. CGS has been reported p-type for all compositions, for thin films as well as single crystals; this is true for all deviations from stoichiometry and

molecularity. The doping-pinning rule predicts both n- and p-type behavior for CIS and only p-type behavior for CGS. The maximum Fermi level positions are basically the same for both these materials [57]. Thus, it depends on the relative position of the band edges with respect to those maximum Fermi level positions whether the material can be p-type or n-type or both. As one applies to CGS the same process that converts CIS to n-type, the Fermi level does not rise towards the conduction band minimum [62]. The larger band gap of CGS leads to a higher difference between the Fermi level and the upper edge of the valence band at the interface [63].

In CGS, type inversion cannot be achieved under normal conditions, but it can be reached due to doping via non-equilibrium effects [64]. Schon et al. have demonstrated that n-CGS can be obtained using ion-implantation and Zn, Ge co-doping [65]. As-grown p-type CGS single crystals are first doped by Ge-implantation and then heated in vacuum. Finally, annealing of the implanted samples in Zn atmosphere results in n-type conduction of CGS [66].

Sulfide-based Chalcopyrites

$CuInS_2$ has an optical band gap (E_g) of approximately 1.5 eV [67], which is an excellent match for the solar spectrum. Its high absorption coefficient, $\alpha = 10^4$ cm^{-1} (at $\lambda = 500$ nm) is also very good for solar cell devices [68]. Masse et al. calculated a maximum solar energy conversion efficiency of 28% for a $CuInS_2$ homojunction [69], but to date, the highest reported efficiency for a solar cell is about 12% [70]. Although $CuInS_2$ solar cells are theoretically expected to possess higher efficiencies than CIGS, sulfides have reached only about 60% of the performance of selenides so far. Selenide-based chalcopyrite solar cells that are slightly copper poor have shown the best efficiencies, but sulfide absorbers must be prepared Cu-rich to produce a working device [57]. $CuGaS_2$ has a band gap $E_g = 2.5$ eV [69], but it has not been used in the PV industry to date [71].

Deposition Processes

The progress of the solar industry depends not only on conversion efficiency, but also on the development of techniques, which must be conducive to producing large-area devices at a low cost. The absorber deposition method generally has a significant impact on the resulting film properties as well as on production cost. Common thin film deposition methods for CIS-based solar cells are co-evaporation from elemental sources, selenization of metallic precursor layers, evaporation from compound sources, chemical vapor deposition, closed-space vapor transport, and low-temperature liquid phase methods like electrodeposition, spray pyrolysis, and particle deposition techniques.

Siemens Solar Industries (SSI) was the first company in the world to produce CIS modules using the selenization process. Low temperature (200°C) CIS precursor deposition is followed by high temperature selenization [72]. At 500°C, a complete recrystallization of the precursor film occurs [73]. The material quality of the absorber is determined by the structural features of the precursor and the experimental conditions during selenization. Some disadvantages of this process are that it involves complicated intermediate phases, interdiffusion, and reaction, which can affect the controllability of the film quality.

Usually high-quality I-III-VI_2 absorber thin films are prepared on a laboratory scale by physical vapor deposition (PVD) or molecular beam epitaxy (MBE). These techniques require high temperatures for the source metal evaporation [74]. Molecular beam epitaxy is used to grow CGS epilayers [45] while two and three-stage co-evaporation are the benchmark methods for depositing polycrystalline CIGS. Although these growth methods are relatively easy to implement on a small R&D scale, scale-up to a commercial level proves to be challenging. High-quality CIGS deposition requires a high substrate temperature (>500°C) which limits the selection of substrate materials and decreases throughput due to heat-up and cool down periods.

Co-deposition of the elements requires precise control of the flux of each element and an overpressure of chalcogens (Se or S) during deposition, which results in low material utilization and high equipment maintenance costs. An alternative low temperature route to the formation of CIS is the rapid thermal processing of stacked metal/Se layers [75].

Most PVD deposition techniques are quite wasteful of materials, but printing or electrodeposition techniques are quite efficient in depositing materials. The co-electrodeposition technique [76], where Cu-In-Ga-Se species are present in the same chemical bath, is a simple process to prepare low-cost thin films. It is crucial to control the deposition parameters like pH, chemical bath composition, deposition time, deposition temperature, and the applied potential, owing to their influence on the film properties and quality.

Printing, spraying, or coating of inks involves the deposition of particulate precursor materials onto substrates at low temperatures and the subsequent sintering under chalcogen overpressure. The reaction kinetics of nanoparticle-derived CIGS precursor films, typically 0.5-2.0 microns, is much different than those prepared by evaporation [77]. ISET's non-vacuum process utilizes nanoparticles of mixed oxides of Cu, In, and Ga with a fixed Cu/(In+Ga) ratio that are synthesized into precursor inks [78].

Multijunctions

The major reason for losses in simple photovoltaic devices is the inefficient use of the solar spectrum by cells that have only one built-in electric field. Some proportion of the sunlight is not used because certain photons do not have enough energy to be absorbed and to free electrons. For those photons that do have enough energy, there is no distinction between them; they are all treated as if they have just enough energy to free an electron. The band gap at which these spectrum-driven losses are smallest in single-junction cells is about 1.4 eV [8]. A range of band gap values at which losses are still manageable extends from about 1.0 eV to 1.8 eV.

Theoretical Multijunctions

The single junction thermodynamic limit for solar cell conversion efficiency was determined to be 32% by Shockley and Queisser [79], but the practical lab limit of polycrystalline thin film solar cells is about 20% under 1-sun illumination. The major assumption in the calculation of the theoretical limit is that electrons and holes created by the absorption of photons with energies above the band gap lose their excess energy by phonon emission.

One way to achieve efficiencies above the Shockley-Queisser limit is to use a series of semiconductor pn junctions arranged in tandem configuration. The efficiency of solar cells can be significantly increased by stacking several cells with different band gaps such that the gap energy decreases from top to bottom. This multijunction cell uses more than one electric field to separate electrons and holes. Light is incident on the top cell which has a high band gap. Photons with energies greater than the band gap of the top cell are absorbed while those with lower energies pass through to the next semiconductor where they are absorbed if their energy is greater than the band gap of that cell. Thus, the solar spectrum is split so that photons are used more efficiently; losses due to the mismatch between the energies of the photons and the cell's band gap are reduced. Two cells in series connection have a maximum theoretical efficiency of 41.9% and with a larger number of cells, 50% efficiency can be exceeded [8]. The thermodynamic limit for solar energy conversion is significantly higher still, 66% at 1-sun and 86% at full solar concentration (46,200 suns), for an infinite tandem [21]. The grand challenge is to push solar cell efficiency towards its theoretical limit while maintaining low cost.

The efficiency benefit of a tandem solar cell to that of a single junction has been known for quite some time, but it has only been practically observed in expensive crystalline III-V materials. Multijunction cells under concentrated light have just recently exceeded 40%

efficiency (Spectrolab). Traditionally, they have been used to power satellites and other spacecraft. The use of multijunction cells to generate clean energy for terrestrial applications has been sought because, when combined with high concentration, multijunction cell modules have the potential of producing the lowest $/watt amongst solar cell technologies [80].

Coutts et al. identified optimum band gaps for two-junction tandem thin film solar cells. A current-matched, 28% efficient tandem is possible with a top cell absorber of 1.72 eV and a bottom cell absorber of 1.14 eV [81]. These band gaps are ideally matched to the CIS-CGS material system. Low Ga content CIGS has the band gap and performance to be the low gap cell. The wide band gap top cell material of the tandem is critical; it is estimated that approximately two-thirds of the tandem cell efficiency originates there [82]. A high band gap, transparent top cell with efficiency greater than 17% is needed to form a tandem with an efficiency of at least 25% [83].

Tandem Structure

In typical CIGS thin film solar cells, metallic Mo back contacts are used, which makes it impossible for light to pass through this layer. However, a semitransparent solar cell is required for the top cell of tandem devices. Nakada et al. report that the cell performances of CIGS devices incorporating tin oxide (SnO_2) and indium tin oxide (ITO) back contacts are similar to those using molybdenum [84]. The superstrate configuration, where the glass substrate is not only used as a supporting structure, but also as a window for illumination, has an advantage of easy and reliable encapsulation. Since the diffusion of sodium from the soda-lime glass is strongly inhibited by the front contact in this design, Na-doping is necessary. The addition of Na from co-evaporated Na_2Se has been reported to more than double the efficiency in superstrate cells [85].

Monolithic vs Mechanical

There are pros and cons to monolithic or mechanical tandems. In a two terminal device, the stacked cells are connected at a common boundary where the bottom contact of one is the top contact of another. Current flows continuously between the cells under illumination. Using this monolithic approach, only one thick transparent conducting oxide (TCO), one grid, and one anti-reflective coating (ARC) would be needed. However, current-matching and thermal stability issues arise. The lowest current will limit the entire device so band gaps must be chosen that split the spectrum equally: half of the sunlight absorbed on the top and half transmitted to the bottom cell and absorbed there.

Several difficult technical issues need to be addressed in order for high efficiency monolithic tandem cells to be developed. The bottom, first deposited, cell must not be destroyed by the processing conditions of the top cell. High-efficiency CIGS devices are vulnerable to temperatures greater than 200°C where diffusion destroys the pn junction. Therefore, a successful tandem device fabrication procedure will require a bottom cell that is not affected by the processing conditions of the top cell or a top cell that can be grown at a much lower processing temperature [86]. Some clever tandem structures are being investigated because of the need to grow thin films at temperatures greater than 500°C to obtain high-quality absorbers [87]. Another critical issue for a monolithically interconnected tandem cell is providing a transparent interconnect between the top and bottom cells [86].

The mechanical stack may appear much simpler, but there are other issues involved. In a four-terminal device, each cell has a top and bottom contact connected to an external circuit so their output is taken off separately. Performance of each cell is independent so the spectrum doesn't need to be split between them. More materials (ARCs, TCOs, and glass) are needed for the overall structure, which increases the cost [82].

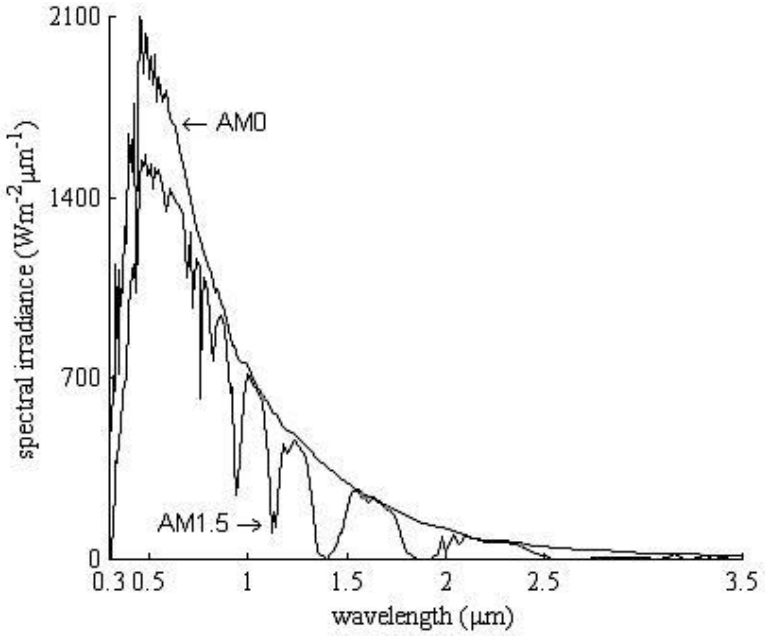

Figure 2-1. Spectral irradiance versus wavelength under AM0 and AM1.5 conditions.

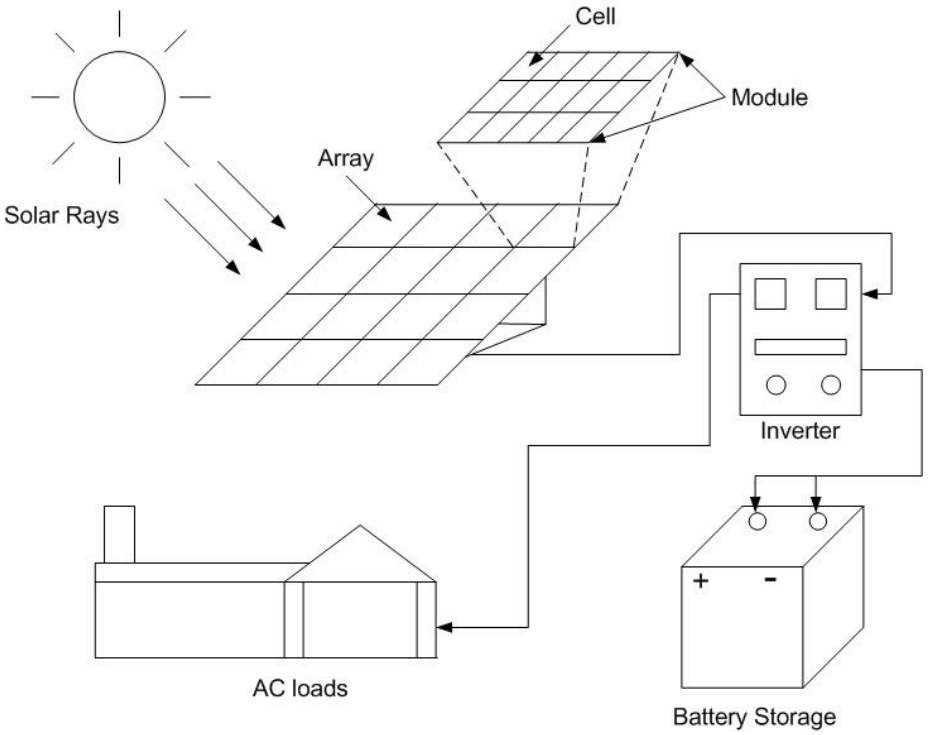

Figure 2-2. Photovoltaic system.

Table 2-1. Efficiencies of copper chalcopyrites.

Material	Band gap (eV)	Theor. η (%)	Achieved η (%)
$CuInSe_2$	1.0 [29]	25 [57]	15.0 [28]
$CuIn_{0.72}Ga_{0.28}Se_2$	1.1 [28]	27.5 [57]	19.5 [28]
$CuInS_2$	1.5 [67]	28.5 [71]	12.2 [70]
$CuGaSe_2$	1.7 [43]	26 [49]	10.2 [28]

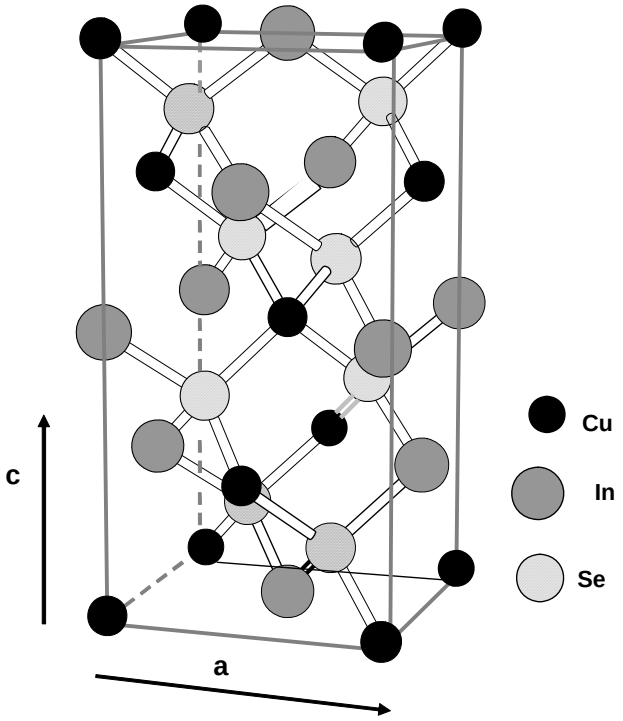

Figure 2-3. Chalcopyrite structure of $CuInSe_2$.

0.5-1.5 μm	ITO	3.7 eV
0.03-0.05 μm	CdS	2.4 eV
1.0-2.0 μm	CGS	1.7 eV
0.01 μm	tunneling junction	3.3 eV
0.01 μm	ITO	3.7 eV
0.03-0.05 μm	CdS	2.4 eV
1.5-2.0 μm	CIGS	1.1 eV
0.5-1.0 μm	Mo	
Glass/SS/Polymer		

Figure 2-4. CIGS/CGS monolithic tandem device structure.

CHAPTER 3
ABSORBER GROWTH AND DEVICE FABRICATION

Growth Calibration

Fabricating and testing a working solar cell requires multiple steps including equipment calibration, the deposition of multiple layers, and film and device characterization. When the source materials are depleted, the reactor must be shut down and brought to atmospheric conditions. Copper (Cu) is annealed in a hydrogen furnace to remove the oxide film present on the Cu pellets received from the supplier. The oxides have a higher melting point than copper so their presence in the source may cause sputtering and thus non-uniformity in the flux distribution. The indium (In) and gallium (Ga) source materials are introduced into the vacuum system in the same condition that they are received from the manufacturer. To add Cu or In to the reactor, the respective source shutter must be disconnected while an optical port must be removed to add Ga.

After the source material is replenished, the Sentinel III rate controller, using Electron Impact Emission Spectroscopy (EIES) sensors, is calibrated by Quartz Crystal Monitors (QCM). Both the Cu and In sources are equipped with an EIES optical sensor located adjacent to the rotating platen at substrate level and a QCM sensor located directly above the source center at a fixed distance above the substrates. EIES is a system of evaporant excitation by electrons that uses the optical intensity of the subsequent de-excitation as a means of process control. These sensors are used for online measurement while the QCMs provide an absolute value of the flux for the calibration of the optical sensors and cannot be used online because they are located directly above the substrates. The Ga source is equipped with a single sensor, which is a QCM that is in an identical position to the EIES sensors used for the Cu and In sources. QCM rate control of gallium was inadequate so a temperature control scheme was implemented. Once the

Sentinel's parameters are adjusted, films can be deposited based upon the deposition rate sensed by the EIES sensors.

Before a growth run series is initiated, the Cu and/or In deposition rates must be calibrated with a specific Ga source temperature. Assumed Cu-rich, Ga-rich, and near-stoichiometric thin films, typically 0.25-0.5 microns, are grown and the composition is measured through ICP analysis. It is assumed that the Ga deposition rate is fixed throughout a run since the temperature is manually controlled to a specific value. Cu and/or In rates can be adjusted based on the ICP results of the previous run. For example, an average Cu rate is determined from the previous run and is divided by the Cu/Ga ratio verified from ICP to give the Cu rate needed to produce stoichiometric CGS. The Cu rate for the current run can be adjusted appropriately to give the desired overall composition. ICP feedback results must be maintained throughout a growth series because reactor conditions may change. This procedure is only as good as the repeatability of reactor conditions between successive runs.

Standard Growth Procedure

System startup is a lengthy process during which stringent guidelines must be followed to ensure proper operation of the reactor. A cryotrap is filled with liquid nitrogen so that the reactor chamber reaches a certain crossover pressure to safely switch the pumping to the diffusion pump, which is necessary to get to high vacuum. As the trap fills, samples can be loaded into and unloaded out of the reactor through the load-lock. After switching the system into high vacuum, the ionization gauges are degassed for a minute to remove any deposits from them. The platen is then started to its desired rotating speed, which is typically 12 rotations per minute. Platen rotation must be started before the substrate heater is engaged so as to not warp it. The PMEE reactor Supervisory Control Panel is then opened on the attached system PC. Film pre-deposition parameters are set for the metals such as soak power, rise time, and soak time.

Heating layers are also set to determine the order in which the heaters are turned on and how much power should be supplied.

When the appropriate parameters are entered into the LABVIEW program, heating can begin. The pyrolytic boron nitride (PBN) substrate heater is started first and brought up to the growth temperature. The inputted temperature is actually the temperature in the gap between the heater and the platen as a thermocouple cannot be directly placed on the rotating platen. As the PBN heater's power is increased, the Cu tip is turned on and the power is gradually increased manually. Before turning on the selenium source heaters, the cryoshroud that surrounds the metal sources is filled with liquid nitrogen. The cryoshroud helps keep the excess Se in its designated reactor zone. First the cracker is heated and then the crucible. As the Se crucible approaches its final temperature set point, the metals primary heaters are switched on. The practice for source preparation in this MBE system before initiating deposition is to hold the sources at a particular soak power for a set period of time. The metal sources first go through a period of rising temperature and then a soaking period so that the solid metal sources become melts. Since the Ga source is manually temperature controlled, control is taken over manually after an initial rise time and the power is adjusted to reach the Ga temperature set point before deposition. The Ga shutter needs to be manually opened when the other metals shutters open automatically after their soak period. If a certain metal source is not being deposited in the film, its heaters are not turned on and its shutter remains closed throughout the run. Selenium is depositing on the substrates as they pass through the chalcogen zone as the Se crucible temperature approaches its final value prior to the start of metals deposition. Startup time leading up to deposition is approximately two hours.

The deposition time begins once the metal shutters are opened and metal beam fluxes are impinging upon the rotating substrates. Cu and In rates are controlled by adjusting the local set point and corresponding offset. Desired element deposition rates are set in advance and layer thickness is controlled by adjusting open shutter time. The average deposition rate over a certain period is calculated and these parameters can be adjusted appropriately to achieve the desired composition. The Se source is kept at a constant temperature during evaporation. The power of the Ga source is manually adjusted to maintain temperature control since QCM rate control was ineffective. The reactor conditions are closely monitored with the cryoshroud periodically being filled throughout the run. Different growth strategies can be administered by closing certain metal shutters during the growth run; selenium is supplied in excess while the Cu and In rates can be adjusted. Dopant NaF can be added at a constant rate for a set period of time. When the appropriate thickness is reached, the metals' shutters are closed and the heaters are shut down. Se can be deposited in an annealing procedure under the designated growth temperature for a set period of time as the metal heaters cool down. Otherwise, power to the Se crucible and the substrate heater are decreased at the end of metals deposition.

When all heaters are cooled to below 200°C, which typically takes at least an hour and a half, the system is taken out of Hi-Vac. Once the system cools completely, the grown films can be removed from the reactor by way of the load-lock. Films to be used for device fabrication are immediately vacuum sealed to isolate them from the atmospheric conditions prior to buffer deposition. The films are also re-sealed after the buffer layer is added and prior to ZnO sputtering. One sample can be cut up and used for absorber characterization. Sometimes, the samples were exposed to a normal room temperature air ambient for over a month between

deposition and analysis. This was also the case for absorbers used for device fabrication prior to the purchase of a vacuum sealing system.

Growth Schemes

High quality absorber layers that are well-controlled are essential to the fabrication of high efficiency solar cells. Thermal evaporation processes have been mainly designed on a basis of experience and intuition to grow polycrystalline thin film layers [88]. Therefore a fundamental understanding of CIGS film deposition is necessary to design the best absorbers.

Single Stage

In the simplest single-step process, all rates as well as the substrate temperature are kept constant during the whole process. A one-stage process typically produces low-quality material when compared to the bilayer or three-stage processes. In CIGS growth, three-stage co-evaporation leads to an absorber with a graded band gap, while single step co-deposition results in a uniform band gap [89].

Bilayer

The first growth strategy used to synthesize highly-efficient $CuInSe_2$ films was developed at Boeing by Mickelesen and Chen. In the Boeing bilayer process, a two-phase film containing CIS and $Cu_{2-x}Se$ is first deposited at low temperature and then reacted with a Cu-deficient flux of co-evaporated Cu, In, and Se vapors at a higher temperature. The precursor deposition and re-growth chemistry are shown in the following equations [90]:

$$Cu(v) + In(v) + Se(v) \rightarrow CuInSe_2(s) + Cu_{2-x}Se(s) \quad (3\text{-}1)$$

$$CuInSe_2(s) + Cu_{2-x}Se(s) + Cu(v) + In(v) + Se(v) \rightarrow CuInSe_2(s) \quad (3\text{-}2)$$

Copper-rich material tends to form larger grains. This is typically true above approximately 525°C because of a liquid phase assisted re-growth process due to the melting of $Cu_{2-x}Se$ in the presence of excess Se. Thus, by first depositing a layer containing excess copper,

larger CIS grains are formed. In-rich layers generally have smaller grains, but when grown on top of Cu-rich layers they are inclined to conform to the same growth pattern [8].

Three-Stage

In the mid 1990s, NREL developed the three-stage process to grow high-quality CIGS films [91]. Indium, gallium, and selenium are evaporated at 260°C to form a $(In,Ga)_2Se_3$ precursor. The temperature is then ramped up to 550°C within a Se flux. At this point, sufficient Cu is co-deposited with Se to make the film Cu-rich. Additional In, Ga, and Se are added to bring the overall composition back to Cu-poor. The amount of In and Ga deposited in the third stage is usually 10% of the total in the first and third stages combined. The film is finally cooled down within a flux of Se at about 350°C. The three-stage process is based on the following reaction chemistry (precursor deposition, re-growth, and titration) [90]:

$$In(v) + Se(v) \rightarrow In_2Se_3(s) \quad (3\text{-}3)$$

$$In_2Se_3(s) + Cu(v) + Se(v) \rightarrow CuInSe_2(s) + Cu_{1-x}Se(l) \quad (3\text{-}4)$$

$$CuInSe_2(s) + Cu_{1-x}Se(l) + In(v) + Se(v) \rightarrow CuInSe_2(s) \quad (3\text{-}5)$$

The intermediate Cu-rich growth stage has been shown to be beneficial to the morphology and electronic quality of CIGS layers. The $Cu_{2-x}Se$ secondary phase has a higher emissivity in the IR range than Cu-deficient CIGS, and the increased emission of heat radiation leads to a lowering of the substrate temperature. $Cu_{2-x}Se$ segregations begin to appear once the film reaches stoichiometric composition, i.e. [Cu]/[III] =1.00. This is reflected in a drop of the substrate temperature, which is recorded by the thermocouple on the sample rear side. When the substrate temperature is ramped up to 550°C after the completion of the first stage, the PID temperature controller is cut off and a constant heating power is supplied [92]. The third stage is

terminated when the temperature reading reaches the value recorded before the film became stoichiometric during the second stage.

Growth Strategies in the PMEE reactor

Three different growth recipes were investigated for the deposition of $CuGaSe_2$ absorber layers. Another growth strategy was employed in the reactor during the earliest investigations of CGS growth, an initial Cu-rich layer followed by a Ga-rich layer similar to the Boeing bilayer process, but it never resulted in quality devices. We refer to each strategy as follows:

- Constant Copper Flux Process (Figure 3-1A)
- Modified Three-Stage Process (Figure 3-1B)
- Emulated Three-Stage Process (Figure 3-1C)

The Constant Cu Flux Process is illustrated in Figure 3-1a. The selenium crucible is maintained at a constant temperature, typically 265°C, so that selenium is provided in excess for all film growth in our PMEE reactor. Since temperature control is used for gallium deposition, we maintained a specific gallium temperature for each growth run. Thus, we can change the overall composition of the absorber by manipulating the copper flux. Calibration runs were performed to determine the relationship between the average copper deposition rate and the Cu/Ga ratio. This strategy simply keeps the same Cu flux over the entire growth run so that the absorber maintains either Cu-richness or Ga-richness throughout the deposition of the film.

Figure 3-1b shows the Modified Three-Stage Process. This growth recipe starts by depositing GaSe for a set period of time, followed by a Cu-rich layer, and ending with a Ga-rich layer. Since the Ga temperature is maintained for the complete growth run, the Cu flux must be adjusted to achieve either a Cu-rich layer or a Ga-rich layer. The overall composition and peak

Cu-richness can be adjusted by varying the duration of growth and the Cu flux employed for each step.

The Emulated Three-Stage Process is illustrated in Figure 3-1c. In contrast to NREL's approach, our Emulated Three-Stage Process does not use end-point detection, but is based on the composition results of previous runs. The thermocouple for substrate temperature measurement is placed in the gap between the heater and the platen for temperature measurement since it could not be placed in contact with the substrate because of the rotating nature of the platen. An additional possibility to control the composition is to monitor the emissivity of the films, but problems with pyrometry were presented by selenium condensation on the optical ports. In this recipe, we deposit GaSe for a certain amount of time and then deposit CuSe until we reach the desired thickness. The greatest copper-richness is reached at this point, and then GaSe is deposited until the overall composition becomes Ga rich. The gallium temperature remains constant throughout the first and third stages, while the same Cu rate is maintained during the second stage.

Absorber Characterization

Characterization of the absorber film is integral to the production of high quality devices. Many research groups have implemented in-situ techniques to observe the growing film, but this is not possible inside our reactor. Typically, one absorber is set aside strictly for characterization purposes. The techniques described below are used extensively within this research.

ICP

Inductively Coupled Plasma-Optical Emission Spectroscopy (ICP-OES) is most commonly used for bulk analysis of liquid samples or solids dissolved in liquids [93]. The ICP operates on the principle of atomic emission by atoms ionized in an argon plasma. Photons are emitted as electrons return to the ground state of the ionized elements, which allows for the quantitative

identification of the species that are present. The strengths of ICP-OES include its speed, low detection limits, and relatively small interference effects, but it is a destructive technique that provides only elemental composition. Calibration curves must be made using a series of standards to relate emission intensities to the concentration of each element of interest. The Perkin-Elmer Plasma 3200 ICP system used in this study is located in the Particle Engineering Research Center, University of Florida. This system is capable of analyzing materials with a detection limit range of less than 1 part per million.

Known concentrations of Cu-In-Ga-Se dissolved in solution (0, 1, 5, and 10 ppm) are used to create a calibration curve for ICP characterization. A small piece of the characterization absorber, typically 2 cm x 1 cm, is dissolved in a 10 mL nitric acid solution. After the film reacts for a few hours, the solution is diluted with 50 mL of deionized water. The overall composition determined from this small sample may not be representative of the entire film if it does not have uniform morphology.

SEM

Scanning Electron Microscopy (SEM) can be used to determine the grain size and shape of absorber films [94]. The SEM is commonly used for image analysis by focusing a source electron beam into a fine probe and rastering over the surface of the sample. Secondary electron and backscattered images are obtained to provide the surface topographical information. SEM, using the SEM JEOL JSM 6400, characterization measurements were done at the Major Analytical Instrumentation Center, Department of Materials Science and Engineering, University of Florida.

XRD

X-ray diffraction (XRD) is a powerful technique used to uniquely identify the crystalline phases present in materials and to measure the structural properties of these phases [95].

Polycrystalline thin films can have a distribution of orientations, which influences the thin-film properties. When sizes of crystal grains are less than about 100 nm, x-ray diffraction lines will become broadened. Hence, grain size can be estimated by measuring the broadening of a particular peak. XRD is noncontact and nondestructive, which makes it ideal for in-situ studies. Characterization measurements, using the XRD Philips APD 3720, were done at the Major Analytical Instrumentation Center, Department of Materials Science and Engineering, University of Florida.

The most important use of thin-film XRD is phase identification. XRD provides positive phase identification by comparing the measured d-spacings in the diffraction pattern with known standards in the JCPDS Powder Diffraction File. Some thin films have a preferred orientation, but the JCPDS file contains measurements for films with random orientations so there can be some disagreement between the measured values and the standard. For films possessing several phases, the proportion of each phase can be determined from the integrated intensities in the diffraction pattern.

Device Fabrication

The most commonly used structure for CIS-based solar cells is the substrate configuration; the absorber layer is evaporated on Mo-coated glass, and on top of this is a thin CdS buffer layer and a transparent ZnO front contact. The universally accepted device design for fabricating high efficiency, thin-film CIGS solar cells: MgF_2/ZnO/CdS/CIGS/Mo/SLG is shown in Figure 3-2 [96].

Substrate and Back Contact

Soda-lime glass (SLG) is commonly used as the substrate for high-efficiency solar cells, but it deforms at the temperatures used for highest device efficiencies, 550-600°C. Soda-lime glass contains significant amounts (15.6 wt %) of sodium in the form of Na_2O [97], and it is

typically coated with molybdenum, which serves as the back contact. When the substrate temperature approaches the softening point of the glass, Na ions diffuse from the glass through the Mo back contact into the growing CIGS film. The extent of Na diffusion is related to the Mo sputtering pressure. At low pressure, the amount of Na out-diffused from the SLG is low, while at the highest pressure, the amount of Na out-diffused exceeds the optimal value required for high-quality devices due the formation of microvoids and microcracks [97].

For good electronic device properties, the formation of an ohmic contact for the majority carriers (holes) from the p-type CIGS and a low recombination rate for the minority carriers (electrons) at the CIGS/back contact interface is essential. The back contact should be inert to the highly corrosive environment during deposition and it must impede the diffusion of impurities from the substrate into the absorber. Finally, a high optical reflectance is necessary to minimize optical losses. Molybdenum, the historical back contact material for CIGS solar cells, complies well with most requirements; it is inert during deposition, allows for the growth of large grains, and forms an ohmic contact via an intermediate $MoSe_2$ layer [98].

CIGS can also be deposited onto various substrates other than glass, even flexible ones. Stainless Steel (SS) can be heated up over 500°C which is necessary to achieve high-quality absorbers, but Na-doping is needed since SS doesn't contain sodium like soda-lime glass. Unlike metal foils, polymer substrates are electrically insulating, which simplifies monolithically-integrated module fabrication. However, polymer substrates have a limited maximum operating temperature and can cause adhesion problems between the CIGS film and the Mo back contact [99]. Stainless steel substrates have generated CIGS films with 17% efficiency [100] while applying a low temperature, 450°C, CIGS deposition process and a

reliable method for controlled Na incorporation on polyimide substrates has yielded cells with 14% efficiency [101].

Post Absorber Deposition

Exposure of CIGS absorbers to the atmosphere for significant amounts of time prior to the buffer layer deposition step leads to surface oxidation. Yamada et al. observed large oxidation rates for polycrystalline films; the surface of the film is likely to be oxidized to a depth of a couple nm in a brief time after removal from the growth chamber [102]. Oxidation of the surface can also lead to large changes in resistivity of up to three orders of magnitude in just a few days [103]. This shows clearly that it would indeed make a difference if the application of the buffer layer and the completion of the solar cells is done immediately after absorber deposition, a few days, or even a few hours later. Nadenau reported a dramatic decrease in cell performance if the CGS layers were exposed to air for one day prior to the CdS deposition [104].

CIGS grown under a large Cu-excess condition contains copper selenide phases at the surface and along the grain boundaries. A cyanide-based chemical treatment is used to remove any secondary phases while being inert to the CIGS phase [105]. The remaining material after potassium cyanide (KCN) etching is expected to be the stoichiometric phase, but a rough surface may remain [102]. This type of morphology may affect the device performance adversely because it can lead to poor metallurgical contact at the interface [106].

Buffer Layer

The main purpose of the buffer layer in a solar cell device is to act as barrier to diffusion of impurities from the transparent conducting oxide layer into the absorber. Other benefits may include interface passivation and the establishment of an inverted region in the absorber [107]. The properties of a buffer layer often depend on the deposition technique used in its fabrication and the ability to control the growth parameters for each technique.

Most high-efficiency CIGS device structures employ a high-resistivity CdS buffer layer deposited by chemical bath deposition (CBD). Because the band gap of CdS is too low (2.4 eV) to permit transmission of all useful light, a balancing act is employed to optimize the structure. If the CdS layer is too thick, unacceptable absorption occurs, leading to the reduction in short circuit current (J_{SC}). If the CdS layer is too thin, shunt paths are generated, which leads to a decrease in the open-circuit voltage (V_{OC}) [108]. The high efficiencies that have been achieved by the CBD process are the result of a set of critical interactions that can produce n-type doping or inversion, compositional grading, and interface passivation [109]. The direct diffusion of cadmium into the CIGS layer has been observed and this may lead to the formation of a buried pn-junction [110].

A CBD bath temperature at 80°C instead of 60°C, which is the common standard for CIGS, is employed for CGS devices. The growth speed increase due to the elevated temperature so the concentrations in the solution are modified. The quality of the buffer layer and the interface with the absorber are improved by the 80°C procedure [111]. Chemical bath deposition also affects the defects in the bulk of the absorber material so tunneling recombination is reduced in samples grown with the higher CdS deposition temperature.

There are a few problems associated with cadmium sulfide technology. The band gap of the CdS layer is still low enough to limit the short wavelength part of the solar spectrum that can reach the absorber, and this leads to a reduction in the current that can be collected. This current reduction becomes proportionally more severe for higher band gap cells [112]. The substitution of the heavy metal compound, CdS, is also desirable from an environmental and economical point of view. A large-scale CBD-CdS buffer deposition process creates extra costs for the

necessary safety precautions needed for the handling and disposal of toxic material, especially for such an inefficient and exceedingly wasteful process [113].

Alternative Buffers

An alternative buffer layer such as ZnS is attractive due to its wide optical band gap and reduced ecological issues. By widening the E_g beyond that of CdS, a higher short-wavelength quantum efficiency is expected in CIGS solar cells, thereby increasing the short-circuit current [114]. Using a ZnS CBD buffer, a champion cell of 18.6% was achieved by Hariskos et al. [115].

Based on Anderson's model of heterojunctions, the electron affinities of both layers should match in order to obtain the maximum built-in potential and hence a high open-circuit voltage. The electron affinity of CdS (4.5 eV) is larger than that of CGS (3.9 eV) so current loss can be minimized by mixing ZnS with CdS to form a ternary compound $Zn_xCd_{1-x}S$ in which the electron affinity can be varied from 3.7 eV to 4.5 eV. Electron affinities are equal at about $x = 0.78$ and any variation in the buffer layer composition from this optimum value results in a deterioration of the cell performance [105]. V_{OC} increases with increasing Zn concentration whereas the J_{SC} decreases. Ramakrishnu et al. produced a CGS cell with moderate efficiency ($\eta \sim 5$ %) with a Zn composition fixed at $x = 0.5$ [105].

Due to good lattice matching and to ideal electronic band offsets, ZnSe is expected to provide a perfect buffer layer for CGS [116]. For the CdS/CGS interface, the CdS conduction band minimum is below that of CGS resulting in a "cliff" structure. Devices with this type of band alignment show interface recombination dominated behavior, and hence suffer from a loss in V_{OC}. In order to avoid this effect, a material with a smaller valence band offset and a larger gap is required. ZnSe has a band gap of 2.7 eV and the lattice constants of ZnSe and CGS are closely matched, which should result in an almost strain-free interface [117]. Rusu et al.

produced ZnSe/CGS heterojunctions with very high voltages, but poor conversion efficiency due to very low current (V_{OC} ~0.96 V and J_{SC} ~2 mA/cm^2) [118].

Window Layers

From the aspect of band alignment, the II-VI buffer layer could be omitted, but solar cells prepared with a direct CIGS/ZnO heterocontact show only poor efficiencies [119]. Ramanathan et al. observed that the direct sputtering of ZnO on CIGS typically yields only 2-5% devices [120]. These cells are characterized by enhanced current losses probably due to tunneling or recombination processes via trap levels associated with impurities that diffuse into the absorber during transparent conducting oxide (TCO) deposition [107].

The basic properties for making high quality transparent conductors are high conductivity, high optical transmission, minimal surface roughness, thermal stability to withstand the processing temperature, chemical stability, and crystallinity. Typical TCOs used in solar cell fabrication have band gaps in the range of 3.3-3.8 eV, carrier concentrations in the range of 10^{20}-10^{21} cm^{-2}, a conductivity of 10^4 (ohm-cm)$^{-1}$, a sheet resistance of about 5-10 ohms/square, and an optical transmission greater than 85% over the visible part of the spectrum [121]. Almost all of the well-known TCOs that are used in solar cell devices, such as ZnO, In_2O_3, and SnO_2 have n-type conductivity [122].

In the fabrication of CIGS solar cells, it is customary to use a high/low resistivity grading of the ZnO layer. An undoped layer of ZnO (high resistivity) is first deposited on CdS, followed by the deposition of a doped layer. Ramanathan reports that solar cells made without the undoped ZnO layer are identical to those made with the bilayer so the undoped ZnO layer may be unnecessary even when CdS is very thin [89].

Metallization

To collect the current, contacts are placed across the entire surface of a PV cell. This is normally done with a "grid" of metal strips. However, placing a large, opaque grid on top of the cell shades the active parts of the cell from the sun so they are designed with many thin, conductive "fingers" spreading to every part of the cell's surface. The fingers of the grid must be thick enough to conduct well with low resistance, but thin enough not to block much of the incoming light. Ni/Al grids are deposited by e-beam evaporation using a mask. Cell areas are then delineated by mechanical scribing to give individual cell areas of 0.429 cm^2 and a final In contact is soldered on after the film is scratched away to reveal the Mo back contact far away from the grid.

Anti-Reflective Coating

Bare solar cells can reflect about 30% of the sunlight. Since the power output is proportional to the amount of sunlight that is absorbed, these losses are detrimental to the device performance. Surface reflection loss can be reduced by adding anti-reflection coatings (ARC) to the solar cell. An ARC is typically deposited onto CIGS devices by the E-beam evaporation of MgF_2 to a thickness of 800-1200 Angstroms. The gain in short-circuit current is typically 4-8% with a corresponding enhancement in conversion efficiency [106].

Device Characterization

Current-Voltage

Current-voltage (I-V) analysis is a critical tool used to study solar cell performance. The electrical parameters, including the conversion efficiency (η), open-circuit voltage (V_{OC}), short circuit current density (J_{SC}), fill factor (FF), series resistance (R_S), shunt resistance (R_{SH}), diode ideality factor (n), and saturation current density (J_o), of a device can be determined from the measured illuminated and dark I-V curves. The conversion efficiency is defined by

$$\eta = \frac{FF\ V_{OC}\ I_{SC}}{P_{IN}} \qquad (3\text{-}6)$$

P_{IN} is the total power of incident light. Considering the general expressions for V_{OC} and I_{SC}, the key material parameters that determine the efficiency of the solar cell are the lifetime and mobility of the minority charge carriers and the surface recombination velocities [22].

The power that a cell provides is a product of its operating current and voltage. Under short-circuit conditions, current is maximum, but voltage is nearly zero so almost no power is provided to the circuit. Under open-circuit conditions, voltage is highest, but no current flows so power is again zero. Fill factor is the percentage of maximum power as compared to the product of open-circuit voltage and short-circuit current. Some cells can have good V_{OC} and good J_{SC}, but a poor FF, which results in not much power and a low efficiency. The series resistance can affect the shape of the photo I-V curve, mainly the FF [9].

To make a good measurement, two other parameters are controlled: total power in the light and the temperature of the cell. Standard power is 100 mW/cm^2, which is approximately the power density of sunlight at the Earth's surface at noon on a cloudless day. The cell is held at a fixed temperature of 25°C because cell voltage and thus power output varies with temperature. To get an accurate efficiency, the precise cell area must be known because the amount of input sunlight depends on the cell area. Total area is the total area of the top surface of the cell, while active area is the surface area of the cell without counting metal contacts even if those are on top of the active portion of the cell. The solar cell to be measured is exposed to simulated sunlight, and as a resistive load is varied from open-circuit voltage through short-circuit conditions, the cell's I-V characteristics are measured [8].

I-V Measurement Technique

The reference cell method, which basically uses a reference cell to adjust the illumination level of the solar simulator, is employed in the performance measurement of CIGS (and CGS) solar cells in this study. The solar simulator intensity is adjusted by changing the distance between the tungsten-halogen lamp and the test plane so that the measured J_{SC} of the reference cell is equal to its calibrated value at the standard measurement intensity of 100 mW/cm^2. We use a CIGS solar cell calibrated against a primary reference cell and the global reference spectrum by NREL to set the illumination level of the solar simulator.

The open-circuit voltage of CIGS solar cells decreases with increasing temperature at 100 mW/cm^2. The temperature of the test cell is maintained at 25°C ± 1°C by a temperature controller that circulates cooling water through the assembly during the illuminated I-V measurement. The temperature controller of the cooling system is set at 20°C to keep the reading of the thermocouple and hence the temperature of the test cell at 25 ± 1°C. The semi-automated I-V measurement system is controlled by a personal computer with the data acquisition and data analysis software LabVIEW [123].

Quantum Efficiency

Quantum efficiency (QE) is defined as the number of electron-hole pairs generated per absorbed photon and is a measure of the effectiveness of a cell in converting light of various energies into electricity [9]. The cell is illuminated with monochromatic light while its electrical output is being recorded. We know the number of photons in the monochromatic light and we can measure the resulting electric current, which tells us how many electrons are being produced by the cell. By slowly changing the monochromatic light to various energies, we can measure the cell's response to the spectrum of solar photons. If the photons making up the monochromatic light have less energy than the cell's band gap, they will pass through it without

producing any current (QE = 0). Just above the band gap of the cell, light will be very weakly absorbed and unless the material's diffusion length is very large, the quantum efficiency will be small. QE will begin to rise sharply as the energy of the incident photons is increased. In very good cells, quantum efficiency of over 90% can be reached across most of the solar spectrum [8].

QE Measurement Technique

A spectral response measurement system employing a grating monochromator is used to analyze the quantum efficiency of our solar cells. The monochromator, which is controlled via a computer program written in LabVIEW, scans the spectral range from 400 to 1400 nm using 10 nm incremental steps. Two order sorting filters are use to block the undesired harmonic terms from the monochromator; one is applied for the range from 630 to 1000 nm and the other for 1000 to 1400 nm. The incident power density on the test plane is first measured by calibrated silicon and germanium photodetectors, and it is saved on the hard disk of the computer. The measured spectral response is calculated from the data stored in the computer previously and the measured photocurrent of the test cell ($I_{test\ cell}(\lambda)$). Finally, the external quantum efficiency as a function of the wavelength can be converted from the spectral response using the following equation [123]

$$QE(\lambda) = \frac{h \cdot c \cdot I_{test\ cell}(\lambda)}{q \cdot \lambda \cdot \text{power density}_{detector} \cdot \text{Area}_{test\ cell}} \times 100\% \qquad (3\text{-}7)$$

where h, c, q, and λ are Planck's constant, the speed of light, the electronic charge, and the photon wavelength, respectively.

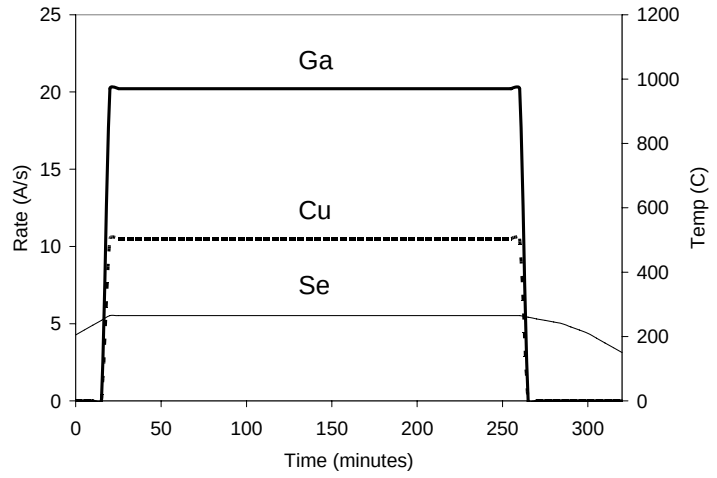

A

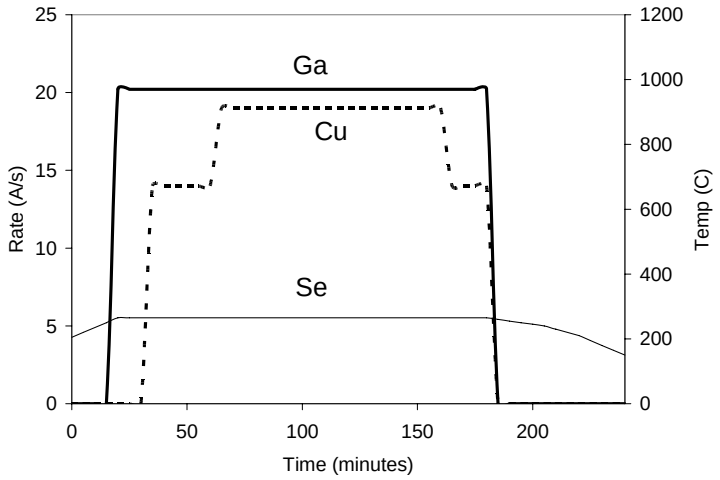

B

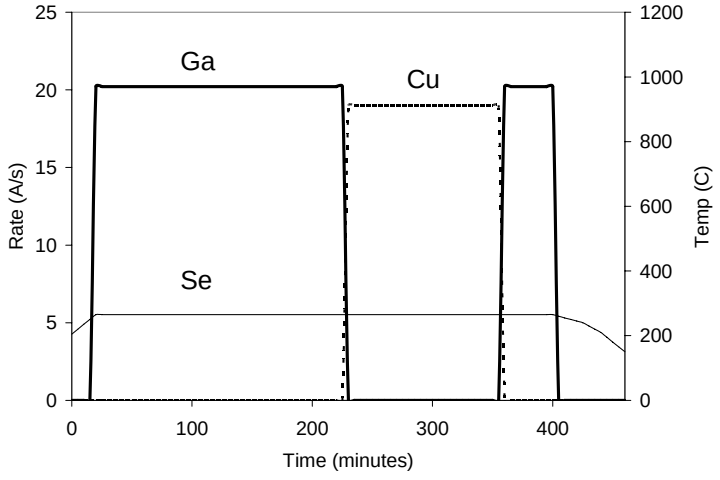

C

Figure 3-1. UF growth recipes. A) Constant Cu-Flux. B) Modified 3-Stage. C) Emulated 3-Stage.

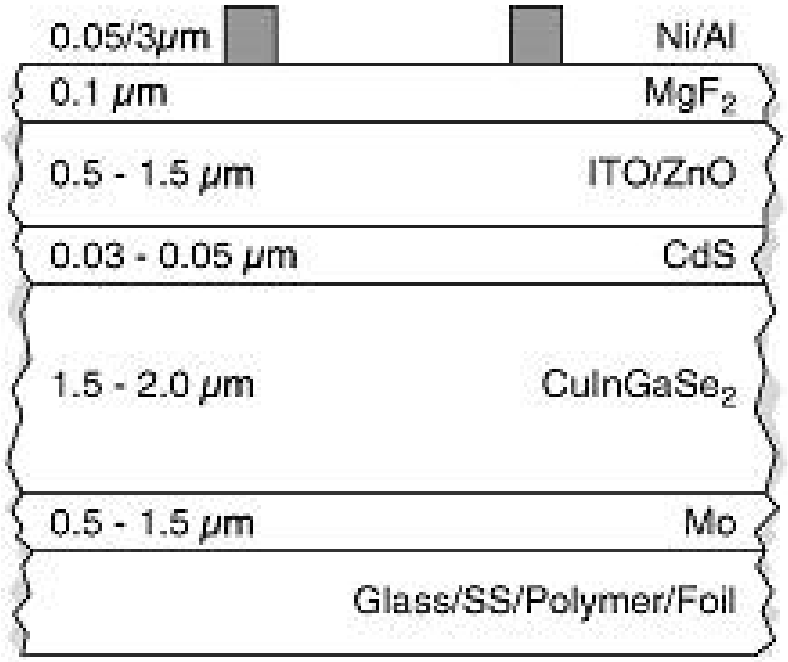

Figure 3-2. Typical CIGS device structure.

CHAPTER 4
COPPER GALLIUM DISELENIDE ABSORBER GROWTH

Like other I-III-VI_2 compounds, $CuGaSe_2$ has a wide phase stability region. The existence range of CGS extends down to a Cu/Ga ratio of approximately 0.7 [53]. Optical and electrical properties are greatly affected by film composition because intrinsic point defects exist in the material as its composition deviates from stoichiometry. It is not surprising that different research groups have presented slightly different results depending on their specific preparation method since the defects present are strongly dependent on the growth method and thermal treatment [124].

Growth Matrix

During the last few years, CGS films were grown in order to optimize the performance of devices. Eight sets of CGS films were grown on Mo coated soda-lime glass substrates in the PMEE system under different growth conditions. The specific PMEE reactor conditions for each growth run described within this document are available in Appendix A. Growth temperature and recipe were adjusted for the films and the growth rate fluctuated from about 0.4 to 0.9 Å/s. The thickness estimated for each run was varied from 1.0 to 1.5 μm based upon the total Cu thickness sensed by the Sentinel III. This estimation method has been a better predictor of thickness for films containing indium rather than gallium. ICP analysis of film composition gives the parts per million of each species in the solution. Knowing the area of the characterization sample and the density of each species allows you to determine a thickness estimate of the film. There is of course error involved in the exact measurement of the characterization sample's area, but this procedure estimates the actual thickness range to be approximately 0.6 to 1.3 μm. Each table related to the specific growth run series summarizes the growth process, as-grown composition and if available, the composition of the film after a KCN

etch for each of the films. The column labeled "growth process" shows the intended composition of each layer of the film.

The first set of films, samples 443 through 447 shown in Table 4-1, was deposited at 386°C. They were grown mostly gallium rich by following a procedure similar to Boeing's bilayer process: Cu-rich deposition followed by a Ga-rich layer. Three different compositional stages were incorporated: an initial Cu-rich stage, an intermediate stage that varied from less Cu-rich, to near stoichiometric, to Ga-rich depending on the desired overall Cu/Ga ratio, and a final Ga-rich layer. The layers were approximately the same thickness with each constituting one-third of the total thickness. The growth rate for these films was approximately 0.5 Å/s and the film thickness was estimated to be about 1.2 μm.

Films with Cu-rich initial stages seem to give poor quality absorber films when grown in the PMEE reactor. We believed this may have to do with poor adhesion of these films to the molybdenum, like in Stacked Elemental Layer processing where only gallium as the first layer led to good adhesion of the absorber layer to the Mo back contact [103]. Klenk et al. suggest that Cu is not useful as the first material deposited onto the Mo as it caused severe adhesion problems [125]. Films that start and finish with Ga sequences should adhere better to the substrate and result in a more uniform morphology [126]. We intended to test this by changing our growth procedure to either include a Ga-rich CGS initial layer or a thin GaSe layer.

The second set of films, samples 452-459 shown in Table 4-2, were also grown at 386°C. The first part of this growth series consisted of films grown overall copper rich followed by gallium rich samples. The intended growth procedure was a Modified Three-Stage Process. A rather thin initial Ga-rich layer was deposited followed by a Cu-rich layer. Most of the films had a thicker final Ga-rich layer deposited on them except for 452, which had only 2 stages, and 453,

whose final layer was composed of GaSe. This Ga-rich layer was typically half the total film thickness. These films were grown at a similar rate to the previous set, but they were much thinner, approximately 0.8 μm. Selenium annealing was performed for 30 minutes after metal deposition was complete at the growth temperature for all the samples. The Se flux remained the same as it was during metals deposition.

Copper selenide is a degenerate p-type solar cell found in CGS cells with overall Cu/Ga ratios greater than one. If present, the $Cu_{2-x}Se$ phase will tend to short-circuit the device, not allowing for a measure of device performance that is representative of the underlying absorber material quality. It must be removed before deposition of the buffer layer [127]. A cyanide etch should remove any $Cu_{2-x}Se$ phase at the surface and between the network of grains in the film so we dipped the $CuGaSe_2$ film in a 10% KCN solution for five minutes. After the removal of the Cu-Se surface phase, the composition of Cu-rich CGS films has been found to be near stoichiometry [35]. It has also been shown to increase the photoluminescence intensity of Cu-rich grown CIGS film up to five times by Keyes [128]. However, the removal of the secondary phase did not result in the Cu-rich sample becoming more like the (In, Ga)-rich samples since the dominant defects and recombination processes are inherent to the CIGS phase. This result should be analogous to $CuGaSe_2$ samples.

The third set of films, samples 472 to 480 shown in Table 4-3, consisted of films that were mostly gallium rich or near-stoichiometric. For many of the films, an initial layer of gallium selenide was grown. This was done to promote adhesion of the film to the substrate. The initial GaSe layer was followed by a Cu-rich CGS layer, and a thin GaSe or Ga-rich layer was deposited on top. For two of these films, the Emulated Three-Stage growth recipe was used. The final GaSe layer was very thin so it is assumed that since the final composition is slightly

Ga-rich for these two samples that the film may have never been Cu-rich during the growth procedure. The gallium primary temperature was increased to 1007°C, compared to 975°C that was used for the previous growth series, to increase the growth rate. The growth rate for these samples ranged from 0.8 to 0.9 Å/s, except for the emulated three-stage process, which had a growth rate of about half that value. The film thickness was approximately 0.9 μm. The same final Se vapor treatment was performed after deposition.

In the PMEE system, the substrates are radiatively heated by a resistive heater located above the rotating substrate platen. This platen carries the substrates through each of the four zones in the system, the metals zone, the fluxless load-lock zone, the chalcogen zone, and the heater zone. A thermocouple is placed in the gap between the heater and the rotating platen for temperature measurement. This temperature is then controlled during growth. Previous work had been done to determine the relationship between the gap thermocouple temperature, T_g, and the actual temperature, T_s, of the substrates, yielding the relationship [6]:

$$T_s = 0.5247\ T_g + 18.856 \qquad (4\text{-}1)$$

It had been previously believed that for the PMEE system, using a T_g greater than 700°C may result in damage to the heater. However, the efficiencies of devices grown at this temperature were relatively low. It was decided that a higher growth temperature was needed to improve device efficiencies. After much investigation, it was concluded that the system could likely be used safely at a higher temperature.

CGS solar cells with the highest performance were for a long time based on Cu-rich composition, but the current record cells incorporate absorber films with an overall as-grown composition that is gallium rich. The disadvantages of an overall as-grown Cu-rich composition are a high doping density and a high concentration of electrically active traps [111]. Air

annealing mainly diminishes the density of deep traps in Cu-rich CGS [52]. It is well known that the grain size of Cu-rich chalcopyrite films is larger as compared to Cu-poor films [129]. The Cu-content of the film determines the activation energy for grain boundary motion. Higher Cu-contents lead to lower activation energies for grain boundary motion and therefore to the formation of larger grains [88].

A Cu-rich growth period has been deemed to have beneficial effects on device performance by some, but others have defined these benefits as limited to depositions at reduced temperatures or times. Comparing different flux profiles, it was shown that at 400°C, Cu-rich growth is necessary to achieve good performance in CIGS by Shafarman et al. At higher substrate temperatures, device performance is insensitive to growth sequence allowing greater process flexibility [130]. Two-stage, rather than three-stage growth was utilized there. The simultaneous deposition of group I and III atoms during the two-stage process may provide more time for the necessary reactions and lessen the benefit of the Cu-rich growth period since the benefit of the Cu-rich growth period has been surmised to come from a fluxing of the CIGS grains by excess liquid Cu_2Se [131].

The lack of quality absorbers obtained by deposition in the PMEE from overall Ga-rich composition is a perplexing phenomenon. It is possible that the films were not grown Ga-rich enough, but many were in the compositional existence range of high quality absorbers. It is possible that the processing conditions arrived at after years of optimizing the performance of the low-Ga absorber material are not optimal for use with higher Ga-containing films, especially when the Cu/III ratio falls much below 1 [128].

Since previous CGS absorber layers grown by PMEE with overall Cu-rich compositions had shown higher efficiencies, subsequent film growth series were grown copper rich. Table 4-4

displays the fourth set, which consisted of seven CGS films. Samples 510-516 were grown at T_g = 750°C, which corresponds to a substrate temperature of 412°C. These samples used growth recipes that were similar to the ones that resulted in our previous best cells at a slightly elevated growth temperature. The growth rate was similar to the previous runs, about 0.4 to 0.5 Å/s, and the films were slightly thinner at 0.6-0.8 μm. Cu-rich samples became nearly stoichiometric after etching them in a 10% KCN solution for 5 minutes to remove the unwanted copper selenide secondary phase. Se annealing was also performed for these films.

High substrate temperatures may be even more important for CGS deposition than for CIS or low gallium content CIGS growth. Purwins et al. found that the formation of CIS is finished before CGS starts to form at an elevated temperature of approximately 390°C [132]. Most of our film growth occurred at a substrate temperature near this lower limit of $CuGaSe_2$ constitution.

Growth temperature seemed to be a limiting factor in producing high-quality films so a much higher gap temperature of Tg = 900°C, corresponding to a growth temperature of 491°C, was used for the fifth set of films, 521-525, shown in Table 4-5. These films had a similar growth rate and thickness to the previous set. Film #523 was grown at a very low growth rate of 0.4 Å/s to a thickness of only about 0.6 μm. The final selenium vapor treatment for 30 minutes occurred at the new elevated growth temperature of 491°C.

The growth temperature used while depositing CGS films in our PMEE reactor is lower than ideal resulting in lower quality films. This may be a result of inadequate sodium incorporation into the film. Na presence is due to diffusion from the soda-lime glass. During absorber growth and potential annealing steps, Na diffuses through the Mo film into the absorber, improving the doping concentration of the absorber. Ideally, a higher Na amount is found closer to the Mo contact and the concentration gradually decreases in the bulk. Rusu et al

found a sodium concentration of 1 atomic percent at the surface [74]. A moderate level of Na improves the efficiency of the cells by enhancing the p-type conductivity. It incorporates into the lattice of the CIGS by reacting with Se and forming Na-Se compounds [97]. These compounds slow the growth of CIGS and facilitate the Se incorporation into the film. Excessive Na diffusion may limit the efficiency of the cells because of the introduction of additional deep states.

Table 4-6 shows a sixth set of films, samples 535-542, which were mostly grown copper rich at 491^{o}C. Growth runs 535-540 used an elevated gallium primary crucible temperature of 1005°C to increase the Ga flux. Previous attempts at growing quality absorbers by the Emulated Three-Stage Process were unsuccessful so the procedure was attempted again for some of these films while maintaining an overall Cu-rich composition. The initial GaSe layer was grown at 450^{o}C and the final two stages were deposited at 491^{o}C. Films #541 and #542 used the same processing sequence as our best absorber to date, #523. Se annealing, as described above, was only performed on absorbers #541 and #542. The thickness of the films ranged from 0.6 to 0.8 μm while employing a growth rate of approximately 0.4 Å/s.

Three-stage co-evaporation imposes stringent limits on the parameter space if highly efficient devices are to result. The growth kinetics, substrate temperature profile, and reaction time will make the outcome of local equilibria unique to the growth process. The Ga and Se delivered in the third stage reacts with the Cu_xSe to form additional $CuGaSe_2$ until the Cu_xSe is consumed. Cu must diffuse out of the CGS grains to react with new Ga and Se while some Ga will diffuse into the bulk grains to bring them to more Cu-poor compositions. By varying the temperature during this stage, the counterdiffusion process can be enhanced or inhibited such that the thickness and/or composition of surface Cu-poor phases can be controlled [91]. The

evolution of the intrinsic defects depends on the dynamics of the reaction pathway, i.e. the composition changes that occur when the film transitions from Cu-rich to Ga-rich [133]. The degree of overall Cu-richness or lack of Cu-richness that the film has after the second stage may have a large effect on the absorber quality.

The three growth strategies described in the preceding chapter were incorporated into a seventh set of runs, 628-641, that produced CGS absorber layers. The second column of Table 4-7 identifies the growth process utilized. For example, Sample #628 was grown using the Constant Cu Flux Process described previously. When the Modified Three-Stage Process was utilized, the second column of the table indicates the target composition of each sublayer of the resulting CGS film. For example, Sample #634 has a growth process denoted as "0/1.2/1.62/1.2". This indicates that the absorber film in this sample is composed of four layers. In the first layer, the ratio of the copper flux to the gallium flux is zero, indicating that the effective metal flux reaching the substrate was composed only of gallium. In the second layer the ratio of the copper flux to the gallium flux is 1.2, indicating that there was a 20% excess of copper relative to gallium reaching the substrate and thus this sublayer was grown under copper-rich conditions. In an analogous fashion, the ratio values of 1.62 and 1.2 describe the relationship between the fluxes imposed when growing the third and fourth sublayers. Finally, Sample #640 incorporates an Emulated Three-Stage Process designated as "GaSe/CuSe/GaSe". This indicates that the growth was done with the intent of defining three sublayers, where the bottom most and the top sublayers are grown under gallium and selenium fluxes, while the middle sublayer is grown under copper and selenium fluxes.

The third column of Table 4-7 indicates the overall ratio of copper to gallium content in the final CGS film, as measured via ICP, and whenever applicable, the fourth column gives the

copper to gallium ratio in the film after a 5 min etch procedure in a 10% KCN solution carried out to eliminate surface CuSe material. For example, Sample #629 had a copper-to-gallium ratio of 1.17 as determined by ICP, and hence was a copper-rich film. The last column shows that after the KCN etch procedure the ratio of copper to gallium in Sample #629 was reduced to 1.00, putting the film in a stoichiometric Cu:Ga composition.

In every growth run the gallium source primary temperature was maintained at 970°C for each run, and the substrate temperature was estimated to be approximately 440°C. Although an elevated substrate temperature of approximately 490°C gave higher quality CGS absorbers, the heat being generated was also warping the rotating platen, which led to scraping and erratic rotational movement of the substrates. A gap temperature of 800°C, corresponding to a substrate temperature of 440°C, was deemed safe so this is the maximum growth temperature that is used in the PMEE reactor. Each absorber layer was estimated to be grown to a thickness of 1.5 microns except for Sample #641, which was grown to a thickness of 2 microns. The actual thickness is more likely to be in the range of 1.1 to 1.3 μm for those grown to an estimated thickness of 1.5 μm by analysis of the component masses over a defined film surface area. A thickness of 1 micron is sufficient for the absorption of photons up to 750 nm, however thicker layers result in a better performance of the solar cell [134]. The film growth rate is estimated to be about 0.8 Å/s, except for those using the emulated three-stage process where the growth rate is about half of this value.

Three samples were grown under the constant copper flux strategy: one was grown under near a 1:1 (i.e., stoichiometric) Ga:Cu fluxes (Sample #628), one under Cu-rich conditions (Sample #629), and one under Ga-rich conditions (Sample #630). Thicker versions of the process that resulted in our best absorber, namely #523, were grown. Overall Ga-rich and near-

stoichiometric films were grown incorporating the modified three-stage process with varying levels of peak copper richness. For this process, a thin initial GaSe layer was deposited followed by Cu-rich layer and then a Ga-rich layer. The final two layers had similar thicknesses incorporating half of the total film thickness.

Gallium rich samples in this growth series were slightly more selenium rich than KCN-etched copper rich samples. Etched samples ranged from 0.490 to 0.494 selenium composition while the overall gallium rich samples varied from 0.494 to 0.500. Epitaxial CGS films grown at a substrate temperature of 500°C by Gu et al. showed a similar trend. The Se content value was slightly higher than 50 at.% in the Ga-rich region and slightly lower than 50 at.% for the Cu-rich region [45].

A final set of films, 647-662, were grown at 440°C by the Constant Copper Flux Process over a range of Cu/Ga ratios from approximately 0.9 to 1.25. Films #648, grown by the procedure that produced our best absorber to date, and #649, grown by the three-stage process, were included for comparison. All of the films were grown at a rate of 0.7 to 0.9 Å/s, except for #649, which was grown at a rate around 0.45 Å/s. Approximate film thickness varied from about 1.0 to 1.3 μm.

A growth series of bilayer precursors was started, represented by growth run #666 in Appendix A, but the Ga source was damaged during or following GaSe deposition. It is likely that the gallium crucible cracked and the metal leaked out and shorted the source. The intent was to grow a low temperature CuSe/GaSe stack that was to be rapidly thermally processed (RTP).

Absorber Characterization

The effect of different growth conditions on the film morphology such as growth temperature, overall Cu to Ga ratio and growth recipe were studied by using Scanning Electron Microscopy (SEM). All CGS films having overall Cu to Ga ratio greater than one at some point

during the growth showed the morphology that had matrix and domain structure. In this structure, the domain region showed highly Cu-rich composition and large grains while the matrix region had small grains and stoichiometric or Ga rich composition. It means at the point we had the overall Cu-rich composition for the film, there was a formation of liquid-like CuSe secondary phase in the film and it made the grain size in the domain region larger than that in the matrix region. As this kind of inhomogeniety was observed in Cu-rich films with large grains that lead to better efficiencies, the growth temperature was increased to get more uniform films.

Figure 4-2 shows that film #523 has better uniformity than the films grown by a similar process at a lower growth temperature as seen in Figure 4-1. More uniform films are more likely to produce high-quality CGS absorbers. Figure 4-3 and 4-4 shows the morphologies of films grown with the similar Cu to Ga ratio profile but at different growth temperatures during the growth. As seen in those figures, the grain size in the domain region appears to be largest at the lowest growth temperature, while the grain size in the matrix region is the smallest. The grain size in domain region was smaller at an intermediate growth temperature and got bigger at the highest growth temperature. It appears that the grains in the matrix region got bigger as the growth temperature increased. This means there might have been possible phase separation between the Cu-rich domain region and Ga-rich matrix region at the lowest growth temperature, and the film got more homogeneous as growth temperature increased. This improved bulk crystal quality may be due to a more ideal incorporation of sodium into the film from the soda-lime glass substrate at an elevated temperature [135].

Shafarman et al. showed that with Cu-rich growth of CIGS, the mean lateral grain area decreases from 1.8 to 0.3 squared microns as substrate temperature is reduced from 550 to 400°C, but only at the highest substrate temperature does the grain size depend on growth recipe

[130]. Films deposited at 400°C have a greater average sodium concentration than those deposited at higher substrate temperatures. Thus, improved device performance with increased substrate temperature cannot be explained by greater availability of Na. Films with smaller grain size or a greater density of grain boundaries may have greater average sodium concentration since nearly all Na probably resides along those boundaries.

In figure 4-5 and 4-6, the morphologies of films grown at the highest growth temperature were compared for three different growth processes. Film #521 was grown by using a reverse Boeing process, which used Ga-rich and then Cu-rich conditions. Film #523 was grown by the Modified Three-Stage Process to utilize the liquid-like CuSe secondary phase to get larger grains. Finally, film #525 was made by a process similar to Boeing's. As shown in those figures, absorbers #521 and #523 have similar morphologies, both for the matrix and the domain regions. And the grain size in domain region is only slightly larger than that in the matrix region for those two films. For film #525, we could see that the grain sizes in two regions appear to be much different from each other and there might have been possible phase separation again.

In figure 4-7, the morphologies of Cu-rich and Ga-rich films grown by the Emulated 3-Stage Process were compared. Even though both films showed good homogeneity, the grains of Cu-rich film are much larger than that of Ga-rich film. The Ga-rich film (#536) has very small grains (~100 nm) while the Cu-rich film has larger grain size (300 ~ 900 nm). Films #541 and #542 have a more uniform morphology, as seen in Figure 4-8, than those grown at lower substrate temperature. They also didn't show the domain (large grain size region) and matrix structure so it is assumed that devices made from both absorbers #541 and #542 will show good performance.

Preference for a certain orientation seems to be dependent upon the growth recipe that was followed in the PMEE reactor. Films grown by similar growth recipes, but at different substrate temperatures, exhibit nearly identical XRD patterns. Shafarman et al. claim that XRD measurements did not show any significant difference in the film orientation for different processes or substrate temperatures. All their films had nearly random orientation [130]. Figure 4-9 shows that films #511 and #522 both have a preference for the (112) orientation of CGS while Figure 4-10 shows that #515 and #523 have comparatively less of a preference for this orientation. Absorbers #515 and #523 were grown with an initial GaSe layer while #511 and #522 had a Ga-rich initial layer and a final layer of GaSe. The films that had no initial Cu flux during deposition had much more intense (220) peaks compared to the (204) peaks, whereas films without this good adhesion layer seem to have slightly more intense (204) peaks than (220) peaks. The full width half maximum of the (112) diffraction peak of film #523 is sufficiently small indicating that the crystalline quality is fairly good. Some groups claim that there is a clear correlation between higher (112) orientation and smoothness of the films [136], but that does not seem to be the case for CGS films grown by PMEE at lower than ideal substrate temperatures.

Figure 4-11 shows two films with the same growth conditions, but grown at different rotational speeds. The XRD patterns are very similar, but the film grown at the higher rotational speed, #479, has slightly sharper peaks. A higher rotational speed may lead to larger grains. The film grown at the lower speed, #476, also seems to have a stronger preference for (112) orientation.

XRD patterns also show which secondary phases are present. Films #452 and #455 were grown at the same low growth temperature, but film #455 has an as-grown Cu/Ga ratio of about 1.4 while #452 has a ratio of 1.1. Figure 4-12 shows that the $Cu_{2-x}Se$ peaks are much more

intense for the very Cu-rich film. After the 10 % KCN etch for five minutes, these $Cu_{2-x}Se$ peaks disappear as shown in Figure 4-13.

As shown earlier, the growth recipe can have an effect on the preferred film orientation. Films grown by the Constant Cu Rate Process have similar XRD patterns no matter the composition. Figure 4-14 shows that the peaks for the KCN-etched Cu-rich film, #629, are nearly identical to the Ga-rich film, #630. The extent to which a film goes copper rich in the Modified Three-Stage Process can also have an affect on the pattern. Films #635 and #636 have nearly identical compositions and similar growth processes, but #636 becomes more Cu-rich during deposition. Figure 4-15 shows a greater (220) peak intensity for the film that has a lower copper peak composition.

The Emulated Three-Stage Process produced absorbers that favored the (204) orientation of CGS rather than (112), which is the more prevalent configuration for the other two growth recipes. Figure 4-16 shows that Cu-rich and Ga-rich films employing GaSe deposition followed by CuSe deposition have (220) CGS peaks that are more intense than even the (112) peaks. The preference for these orientations may be due to the fact that the Emulated Three-Stage Process deposits copper and gallium in separate layers, while they are deposited concurrently in the other growth strategies. Yet, the XRD pattern for film #478 shown in Figure 4-17, which was also grown by a three stage process, but at a lower growth temperature does not show these same characteristic peaks. Due to the very thin GaSe final layer and overall Ga-rich composition, film #478 may not have ever been Cu-rich and hence may have had different growth kinetics.

The surface morphology of films #628 through #641, grown at 440°C by various growth processes, was investigated by SEM. Figure 4-18 shows the Constant Cu Rate Process of a Cu-rich (#629) and a Ga-rich film (#630) at 100X magnification. Both Samples were grown under a

constant Cu flux throughout the entire deposition run with no Cu:Ga profile grading in any sublayers. The Ga-rich film is very uniform while the Cu-rich film has many island structures. Figures 4-19 and 4-20 show the Cu-rich film's grain structure in the field region and the island region at 5000X and 10,000X, respectively. The field region shows very small grains and the island structures have large grains up to a micron in size. The Ga-rich film morphology that is shown in Figure 4-21 exhibits long needle-like grains. The Cu-rich films have $Cu_{2-x}Se$ secondary phase on their surface. Figure 4-22 shows the island region and Figure 4-23 shows the field region of film #634 before and after the 10 % KCN etch. The gaps left by the etching of the copper nodules are very apparent in the island region while the field region appears to be unchanged.

Co-evaporation of Ga-rich samples in an in-line deposition process revealed that a bilayer process yields large, columnar grains, whereas a single layer process leads to absorbers with very small grains. The bilayer-like process had a Cu-rich growth regime at the beginning and the single-layer like process had constant rates throughout [137]. Shafarman et al. showed that at lower temperatures, the uniform flux process appears to give more columnar grains and a smoother surface than CIGS films with a Cu-rich growth period. There is no apparent difference between films grown with Cu-rich flux at either the beginning or middle of deposition [130].

The morphology of CGS films is strongly dependent on composition. Haug et al. observe long and needle-like grains that are of small size for Cu/Ga~0.3. Grains of somewhat Ga-rich CGS layers with Cu/Ga ratios between 0.9 and 0.7 are triangular, and layers deposited at higher temperatures have an increased grain size. The Cu-rich layer consists of grains of irregular shapes with a typical grain size of 1-3 microns (Cu/Ga ~1.1) [134].

Orsal et al. observed slightly different morphology [138]. For slightly Ga-rich, there are grains in the background with thin and long shaped grains starting to grow on the surface. With an even higher Ga-content, the morphology is again homogenous and constituted of platelet-shaped grains that are tilted on the surface. Cu-rich films exhibit small and homogenous grains on the bottom with large polyhedral and packed grains on the surface. While it is not the case for Cu-rich or Ga-rich films, the morphology is very sensitive near stoichiometric composition and seems to depend on growth temperature and kind of substrate. Triangular crystallites are more evident at 450°C with a grain size of approximately 0.6 microns. At 400°C, grains are polyhedral whereas the layer is composed of a melt of triangular and polyhedral grains at 500°C. Columnar growth is observed at each growth temperature.

Films 635-637 and #639 show some very peculiar surface morphology. The growth recipe involved an initial GaSe layer followed by a Cu-rich layer and a Ga-rich layer. The overall composition was either Ga-rich or near stoichiometric. The surface has islands surrounded by rings that show a grain transition of large grains to smaller grains to long thin grains as can be seen in Figure 4-24. Figure 4-25 shows the long needle-like grains present in the field region that are the same as those in films grown Ga-rich by the Constant Cu Rate Process and the large grains in the island region that are of similar size and shape to the ones found in the island region of Cu-rich films grown by the Constant Cu Rate Process. It is likely that these films may have copper selenide phases in the island region although the overall composition may be Ga-rich. The sample taken for ICP compositional characterization may not have been representative of the entire film since it is very non-uniform. This could be the case for film #639 since the Cu/Ga ratio changed to 0.95 after the KCN etch from 1.04. Typically the film becomes nearly stoichiometric, usually very slightly Ga-rich, after the cyanide etch. The pieces of the

characterization absorber used for the as-grown and post-etch composition analysis may have started with drastically different overall compositions because of the non-uniformity of the film.

Smooth surface morphology is characteristic of films deposited by the three-stage process [139]. The Emulated Three-Stage Process produced very uniform films as can be seen in Figure 4-26. Figure 4-27 shows that the Cu-rich process that did not incorporate a final GaSe layer has long tubular grains that have a larger axial diameter than the needle-like grains of the Ga-rich films. A SEM picture on a 45° tilt in Figure 4-26 gives a clear view of these tubular grains. The Ga-rich absorber film, #640 shown in Figure 4-28, seems to have somewhat triangular-shaped grains that have not been produced by any other growth recipe used in the PMEE reactor.

Films 647-662 were mostly grown with a Constant Copper Rate Process to investigate the difference in the absorber film properties based on composition. Figure 4-29 shows a slightly different XRD pattern for the films grown the most Ga-rich like #647. The peak intensity for (220) CGS is slightly greater than that of (204) CGS. Nearer stoichiometric Ga-rich films and Cu-rich films, as can be seen in Figure 4-30, demonstrate the characteristics peaks of a constant copper rate process that were seen in the previous growth series. Figure 4-31 also shows that the Modified and Emulated Three-Stage Processes exhibit the same orientation as those in previous growth series.

In all the diffraction patterns of the CGS films grown in the PMEE reactor, the (220) and (204) peaks are clearly separated, showing that the films have the chalcopyrite type crystallographic structure. This was true for the near-stoichiometric and Cu-rich CGS films grown by MBE by Yamada et al., but they also observed sphalerite crystallite structure for films with Ga-rich composition [140]. But this was for very Ga-rich (Cu/Ga~0.66) films, which we never grew in these growth run series.

Conclusions

Growth temperature, growth recipe, and overall Cu/Ga ratio each had varying yet substantial effects on the film morphology and orientation. Growth temperature seems to be the most critical variable in achieving high-quality absorber films. The fact that Cu-rich absorbers grown by PMEE have been more successful than Ga-rich ones is likely due to the lower deposition temperature. Ga-rich absorbers produce the highest efficiency CGS cells in the literature, but they are also grown at an elevated temperature of at least 550°C. The intrinsic defects produced at different processing conditions results in absorbers with distinct properties.

For the final growth series, we were able to maintain very consistent growth conditions between runs in our reactor, which gave us great confidence in the compositional results for each run, even though we lack in-situ measurement techniques. A packaging system allows us to vacuum seal the absorbers after growth to lessen any degradation that may occur before the cell has been processed. The biggest drawback in using the PMEE reactor to grow polycrystalline films is the limit that we must observe on the maximum substrate growth temperature. A more effective technique may be to grow CGS bilayer precursors at a low substrate temperature and then utilize an RTP system to rapidly raise the temperature for a brief period of time. Klenk et al. performed a post-growth rapid thermal treatment at 550°C for 6 minutes on stacked elemental layers that were deposited by evaporation at a low deposition temperature [103]. Our research group has been successful in the past employing an analogous strategy to grow CIS films via the RTP processing of a bilayer [141]; we anticipate that the RTP processing route is likely to produce similar satisfactory results for the CGS material.

Table 4-1. First CGS growth series.

Film #	Process	Cu/Ga ratio
443	1.1/0.9/0.7	0.89
444	1.15/0.95/0.75	1.00
445	1.15/0.95/0.75	0.96
446	1.3/1.1/0.9	1.13
447	1.15/0.95/0.75	0.98

Note: Process refers to the intended Cu/Ga ratio of each graded layer.

Table 4-2. Second CGS growth series.

Film #	Process	Cu/Ga ratio
452	0.8/1.25	1.11
453	0.8/1.4/0	1.00
454	0.85/1.4/1.1/0.87	1.11
455	0.85/1.4/1.1/0.87	1.40
456	0.85/1.4/1.05/0.81	1.04
457	0/0.85/1.5/1.1/0.75	0.97
458	0.85/1.4/1.2/0.8	0.91
459	0.85/1.2/1.05/0.75	0.85

Table 4-3. Third CGS growth series.

Film #	Process	Cu/Ga ratio	Cu/Ga after KCN-etch
472	0/1.3/0	0.93	--
74	0/1.4/0.96	1.00	0.98
475	0/1.3/0.90	0.97	--
476	0/1.3/0	1.01	--
477	0/1.3/0	0.97	--
478	GaSe/CuSe/GaSe	0.98	--
479	0/1.3/0	1.01	0.99
480	GaSe/CuSe/GaSe	0.95	--

Table 4-4. Fourth CGS growth series.

Film #	Process	Cu/Ga ratio	Cu/Ga after KCN-etch
510	0.8/1.25	1.14	0.99
511	0.8/1.4/0	1.59	1.01
512	0/1.4/0.8	1.07	0.99
513	1.15/0.95/0.75	0.97	0.96
514	0.8/1.25	1.19	0.99
515	0/0.9/1.45/0.9	1.19	0.99
516	Constant	1.06	1.01

Table 4-5. Fifth CGS growth series.

Film #	Process	Cu/Ga ratio	Cu/Ga after KCN-etch
521	0.8/1.25	1.14	--
522	0.8/1.4/0	1.23	1.00
523	0/0.9/1.45/0.9	1.36	--
524	0/1.4/0.8	1.28	0.97
525	1.15/0.95/0.75	1.09	--

Table 4-6. Sixth CGS growth series.

Film #	Process	Cu/Ga ratio
535	GaSe/CuSe/GaSe	1.04
536	GaSe/CuSe/GaSe	0.98
537	GaSe/CuSe/GaSe	1.12
538	0/1.3	1.58
540	GaSe/CuSe/GaSe	1.54
541	0/1/1.6/1	1.80
542	0/1.2/1.6/1	1.67

Note: These samples were etched by KCN, but the composition of the etched samples was not measured.

Table 4-7. Seventh CGS Growth Series.

Film #	Process	Cu/Ga ratio	Cu/Ga after KCN-etch
628	Constant	0.97	--
629	Constant	1.17	1.00
630	Constant	0.89	--
634	0/1.2/1.62/1.2	1.37	0.98
635	0/1.3/0.7	0.89	--
636	0/1.6/0.7	0.90	--
637	0/1.3/0.87	0.98	--
638	GaSe/CuSe	1.26	1.01
639	0/1.6/0.8	1.04	0.95
640	GaSe/CuSe/GaSe	0.91	--
641	0/0.8/1.37/1.35	1.49	0.99

Note: Ga-rich samples were not KCN-etched.

Table 4-8. Eighth CGS growth series.

Film #	Process	Cu/Ga ratio
647	Constant	0.92
648	0/1.2/1.6/1.2	1.41
649	GaSe/CuSe/GaSe	0.95
652	Constant	0.98
653	Constant	0.99
654	Constant	1.23
655	Constant	0.95
656	Constant	1.17
657	Constant	0.98
658	Constant	1.17
659	Constant	1.12
660	Constant	1.04
661	Constant	1.00
662	Constant	1.23

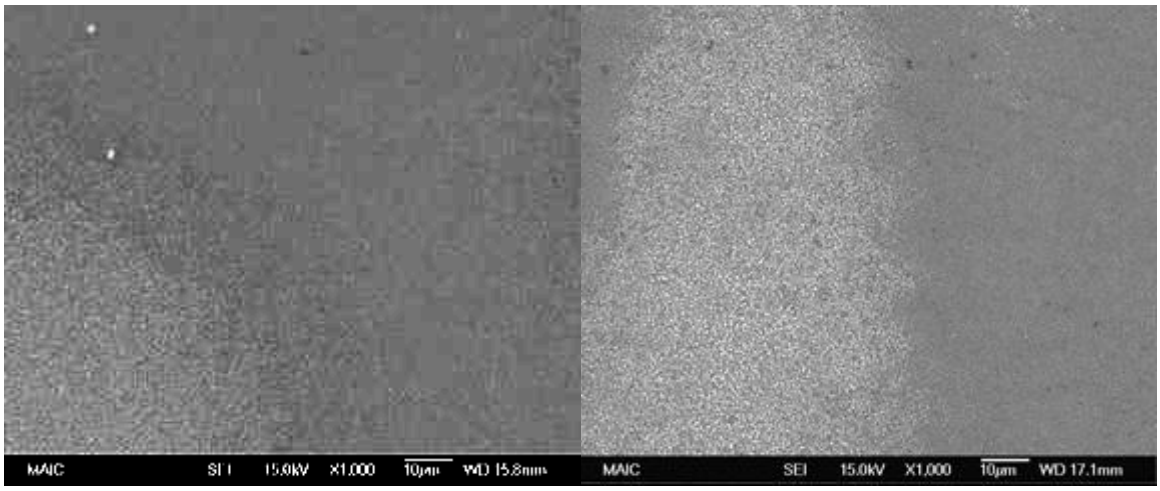

A B

Figure 4-1. Morphologies of films grown at lower growth temperatures by similar growth recipes (X1000). A) T_{sub} = 386°C. B) T_{sub} = 412°C.

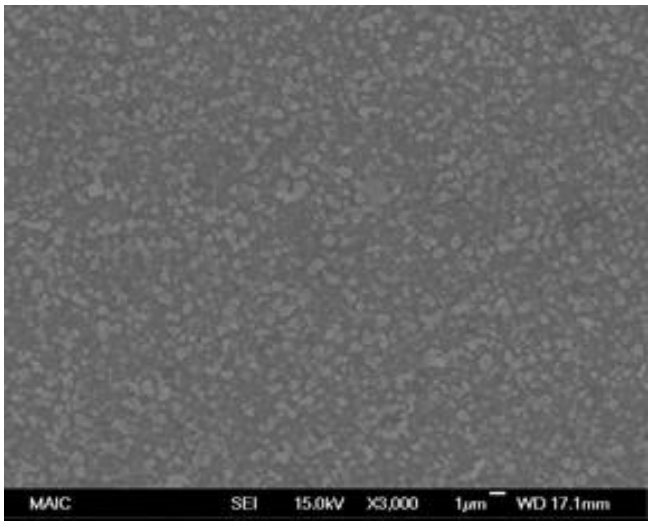

Figure 4-2. Morphology of a film grown at a higher growth temperature (X3000). T_{sub} = 491°C.

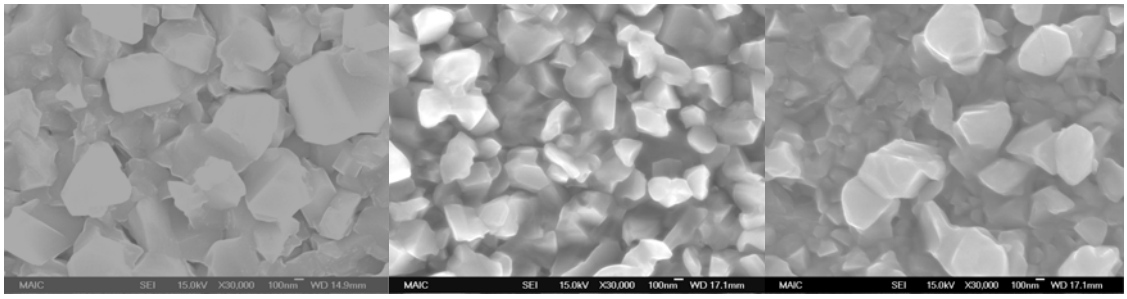

A B C

Figure 4-3. Morphologies of the Cu-rich domain region of CGS films grown by the same recipe at different growth temperatures (X30,000). A) T_{sub} = 386°C. B) T_{sub} = 412°C. C) T_{sub} = 491°C.

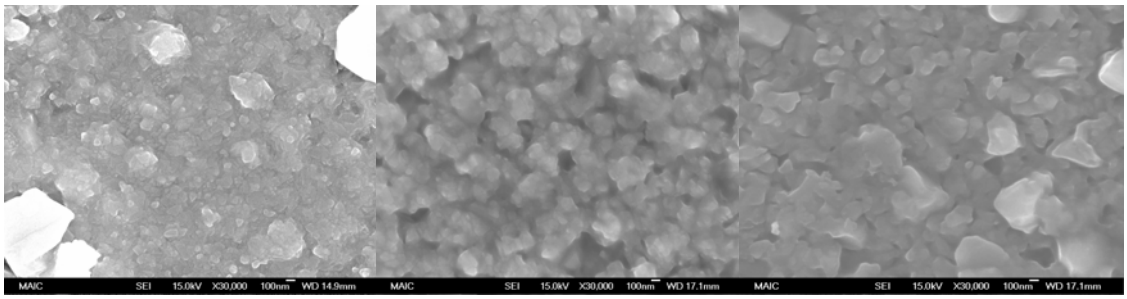

A B C

Figure 4-4. Morphologies of the Ga-rich matrix region of CGS films grown by the same recipe at different growth temperatures (X30,000). A) T_{sub} = 386°C. B) T_{sub} = 412°C. C) T_{sub} = 491°C.

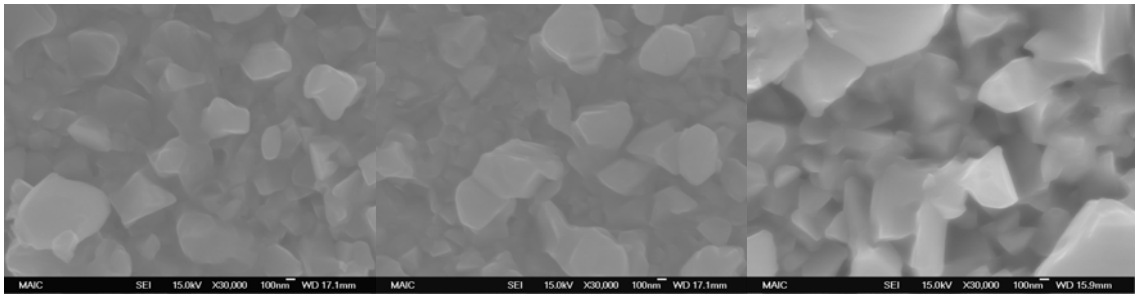

A B C

Figure 4-5. Morphologies of the Cu-rich domain region of CGS films grown with different growth recipes at 491°C (X30,000). A) (.8/1.25). B) (0/.9/1.45/.9). C) (1.15/.95/.75).

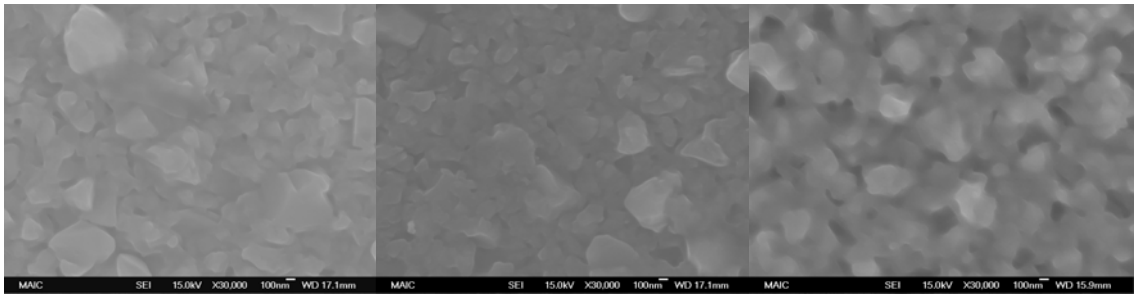

A B C

Figure 4-6. Morphologies of the Ga-rich matrix region of CGS films grown with different growth recipes at 491°C (X30,000). A) (.8/1.25). B) (0/.9/1.45/.9). C) (1.15/.95/.75).

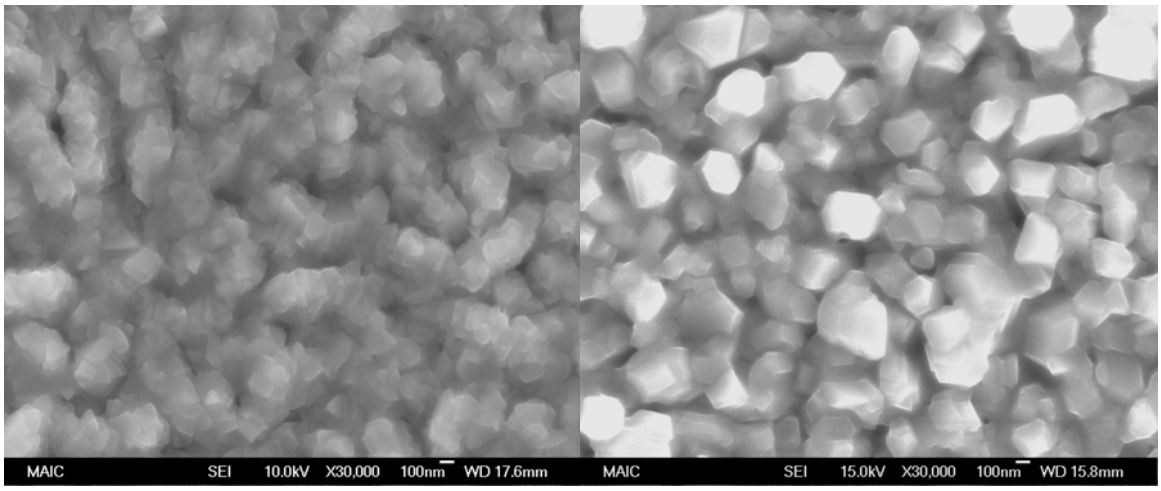

A B

Figure 4-7. Morphologies of CGS films grown by the emulated 3-stage process at 491°C (X30,000). A) Ga-rich. B) Cu-rich.

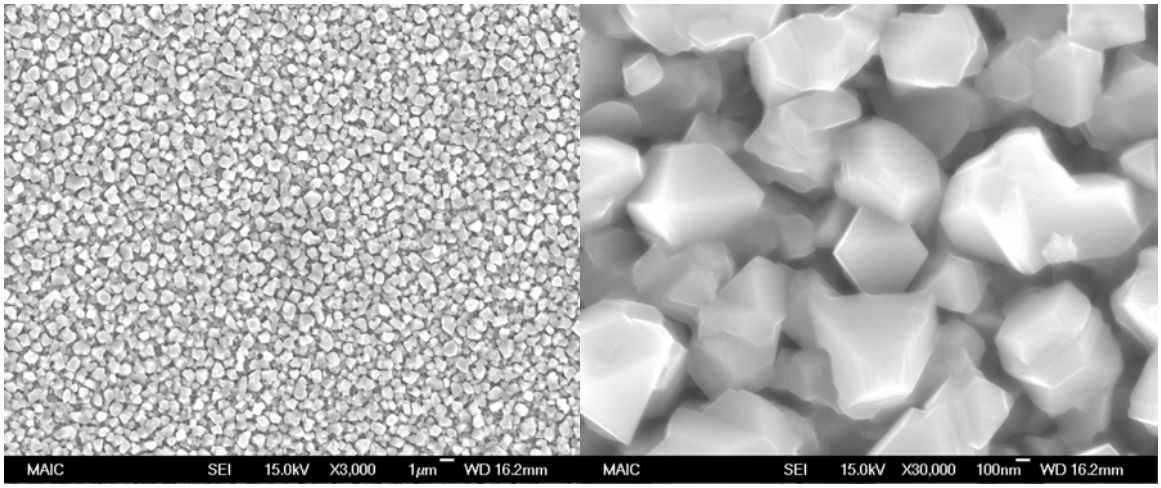

A B

Figure 4-8. Morphology of a Cu-rich film (#542) with large grains and a uniform surface. A) X3000. B) X30,000.

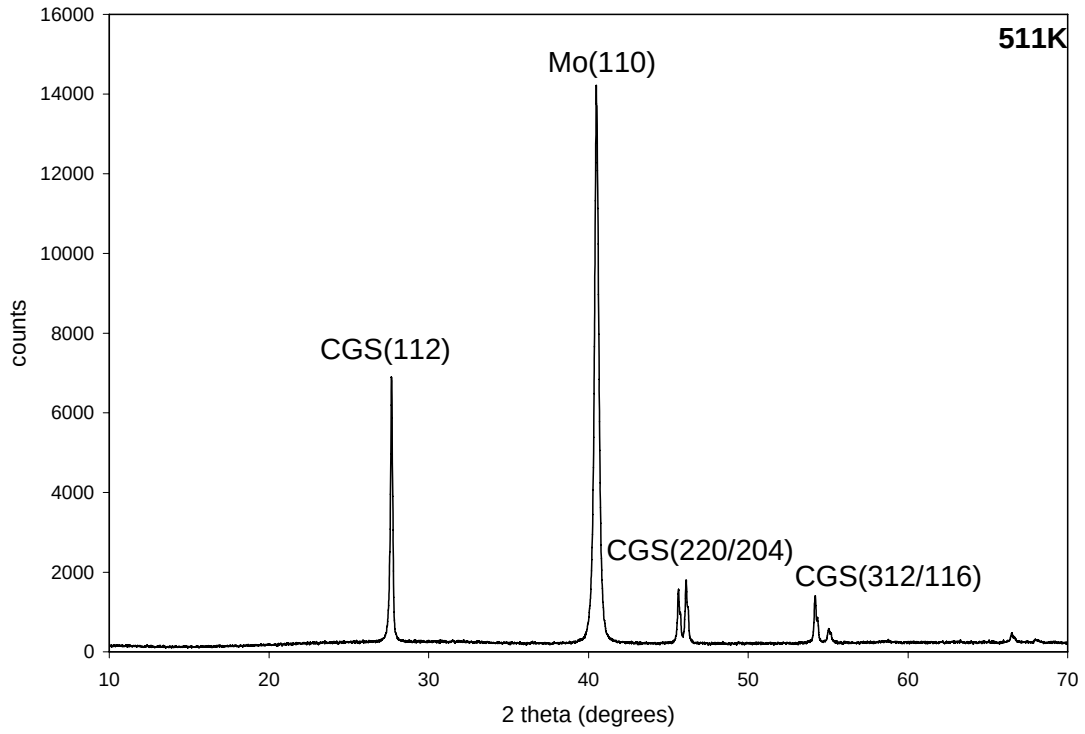

A

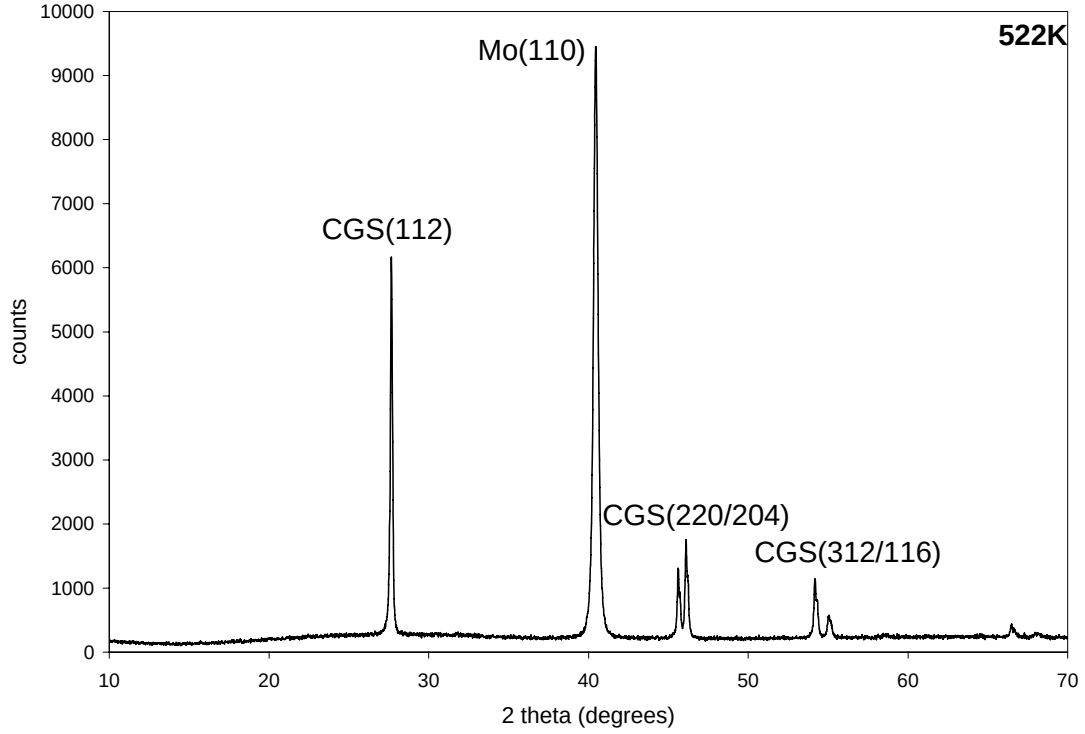

B

Figure 4-9. Diffraction patterns of films grown at different temperatures with the same modified three-stage process. A) T_{sub} = 412°C. B) T_{sub} = 491°C.

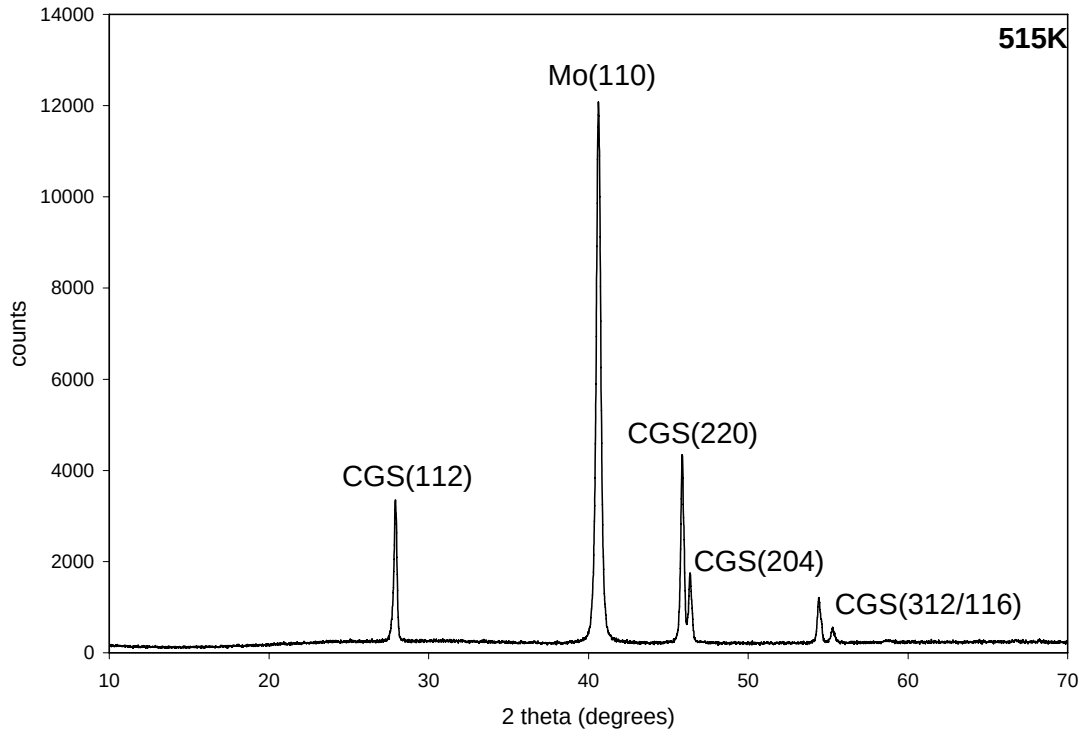

A

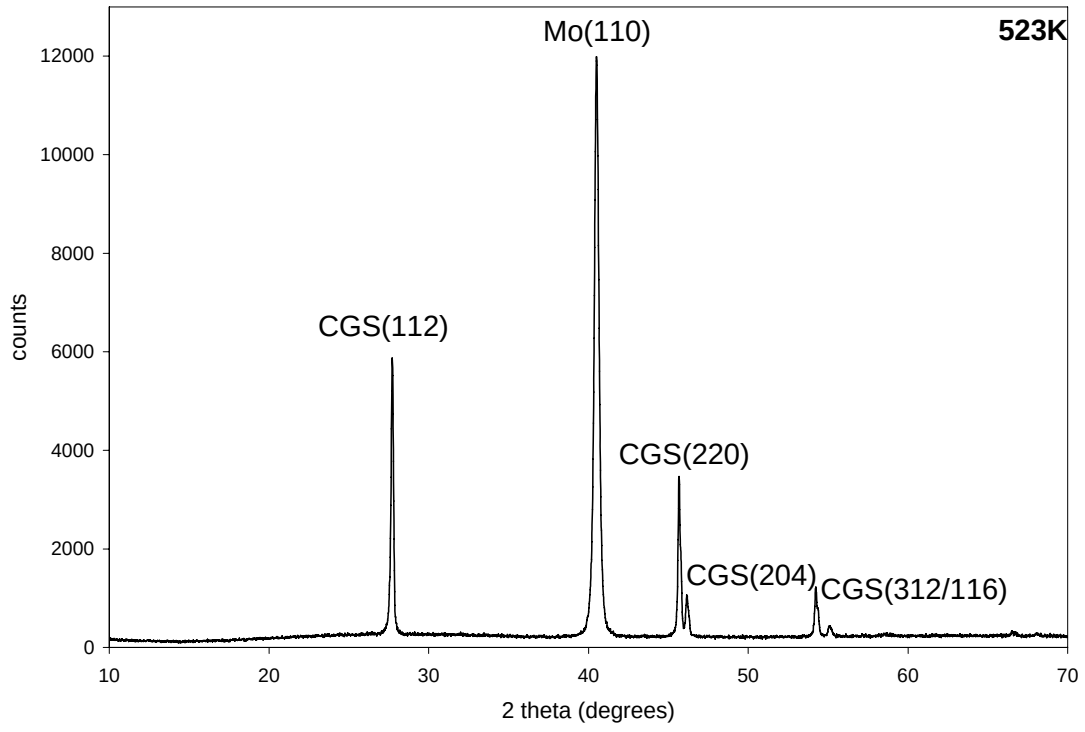

B

Figure 4-10. Diffraction patterns of films grown at different temperatures with the same modified three-stage process featuring an initial GaSe layer. A) T_{sub} = 412°C. B) T_{sub} = 491°C.

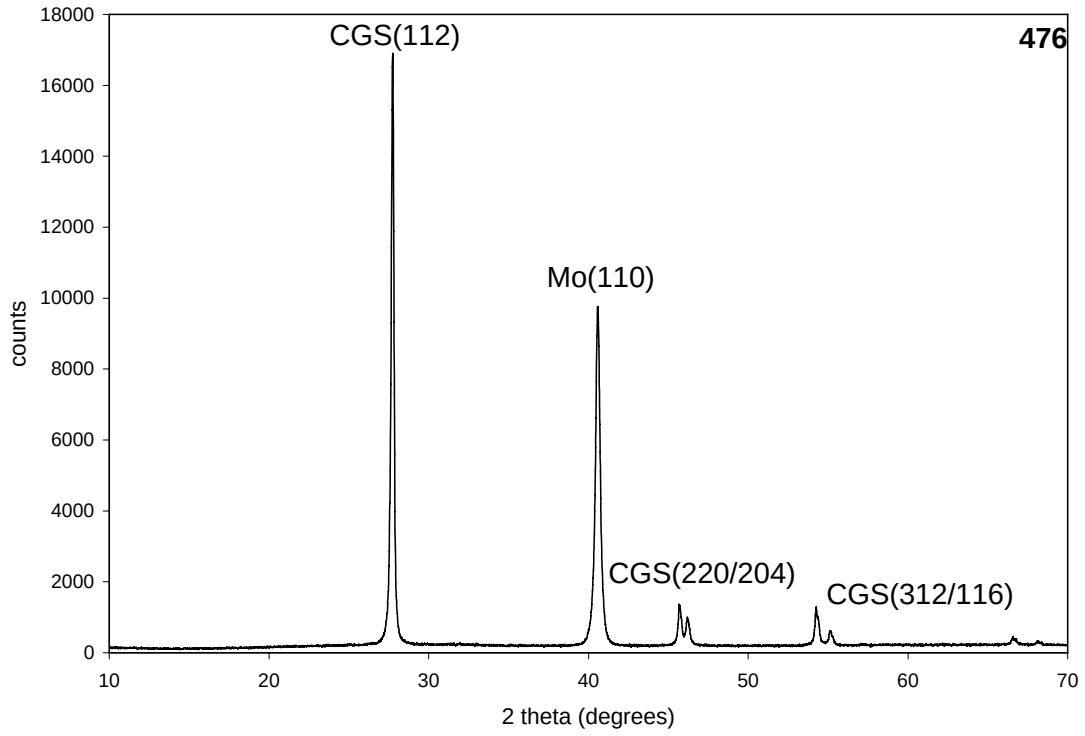

A

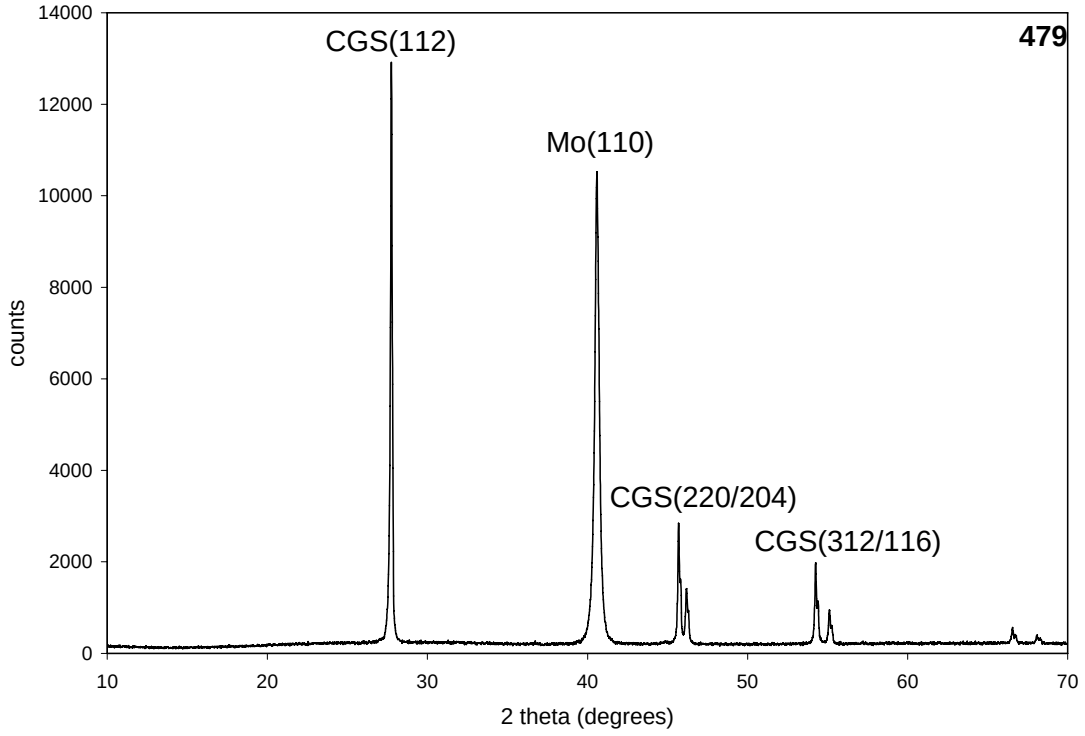

B

Figure 4-11. Diffraction patterns of films grown at different rotational speeds. A) 12 RPM. B) 20 RPM.

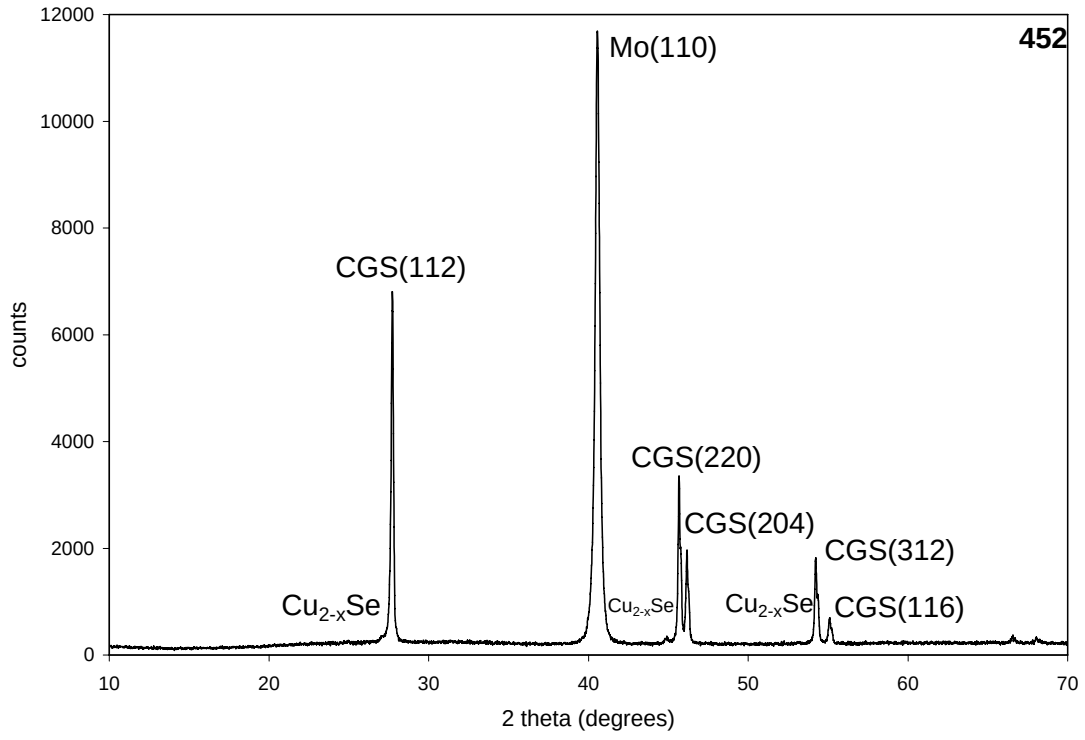

A

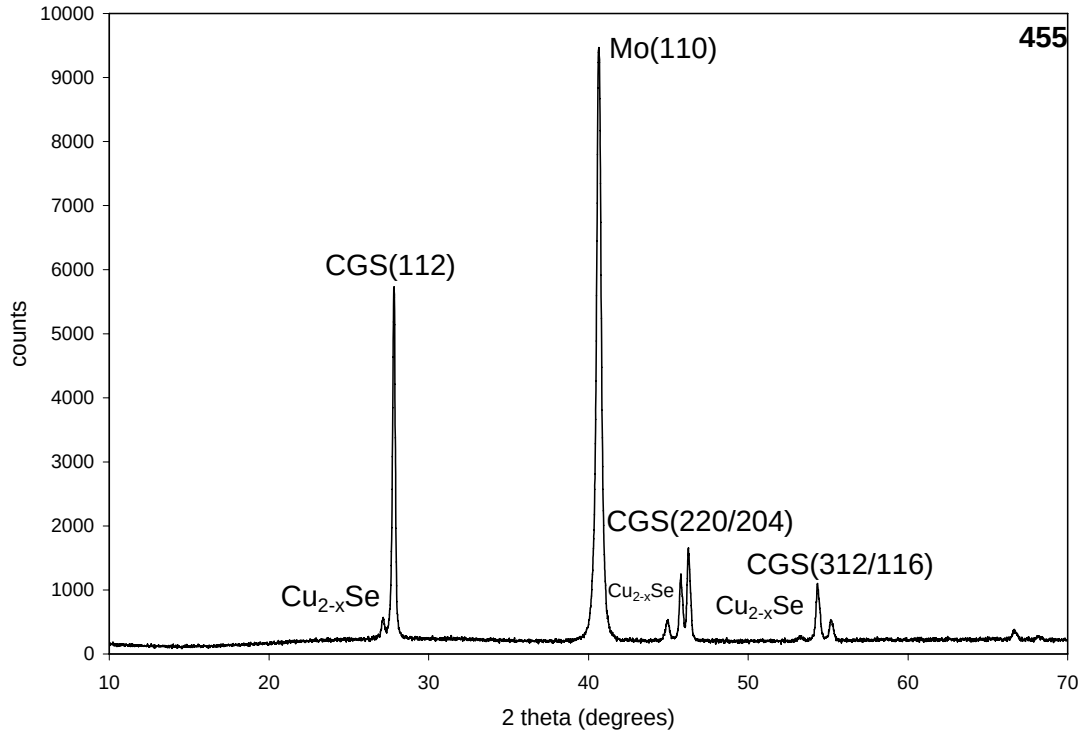

B

Figure 4-12. Diffraction patterns of films grown at different levels of overall Cu-richness. A) Cu/Ga = 1.11. B) Cu/Ga = 1.40.

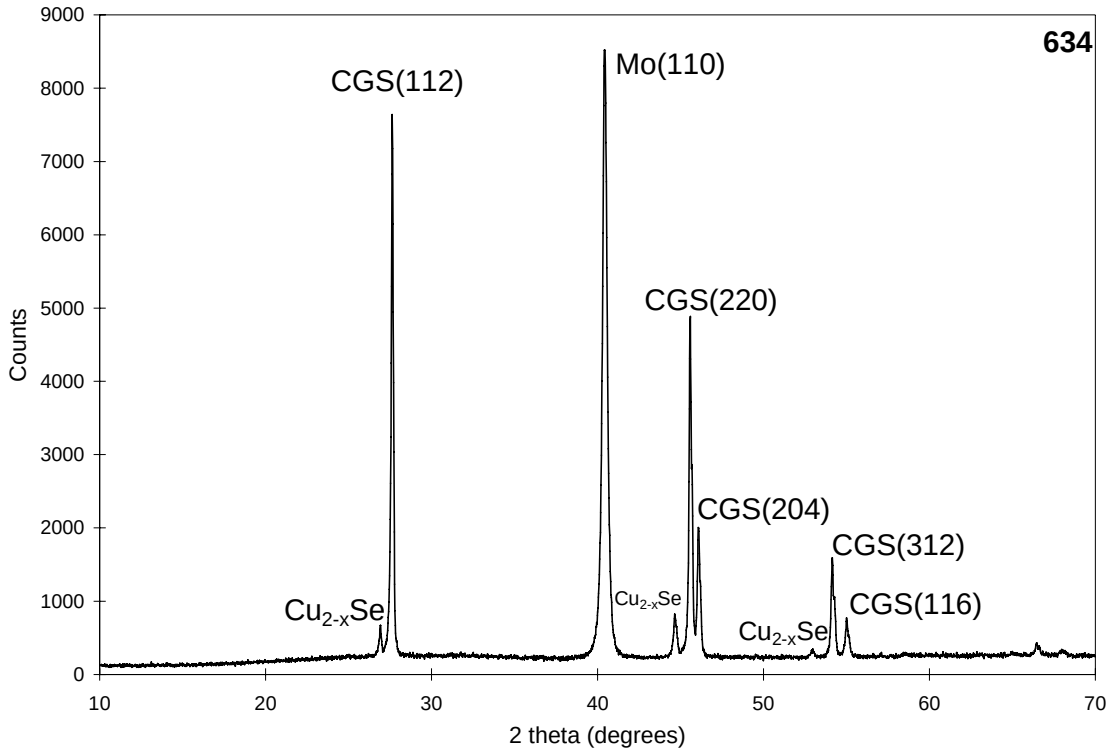

A

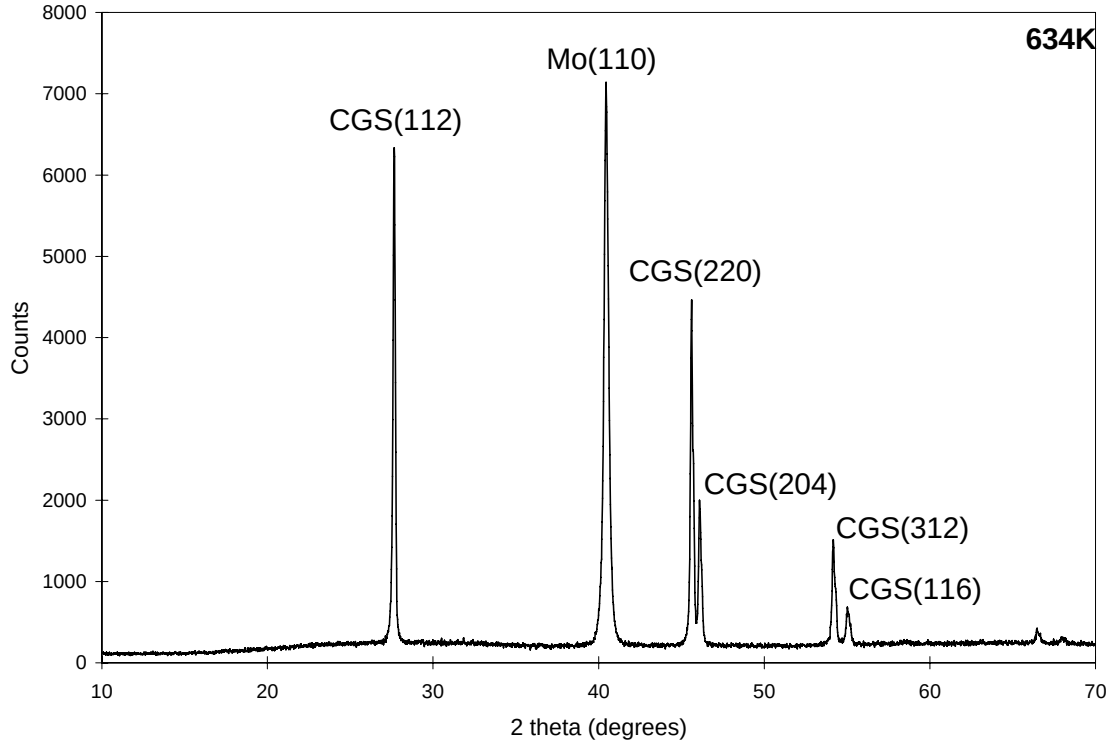

B

Figure 4-13. Effect of KCN-etch on the diffraction pattern of a Cu-rich film. A) Before. B) After.

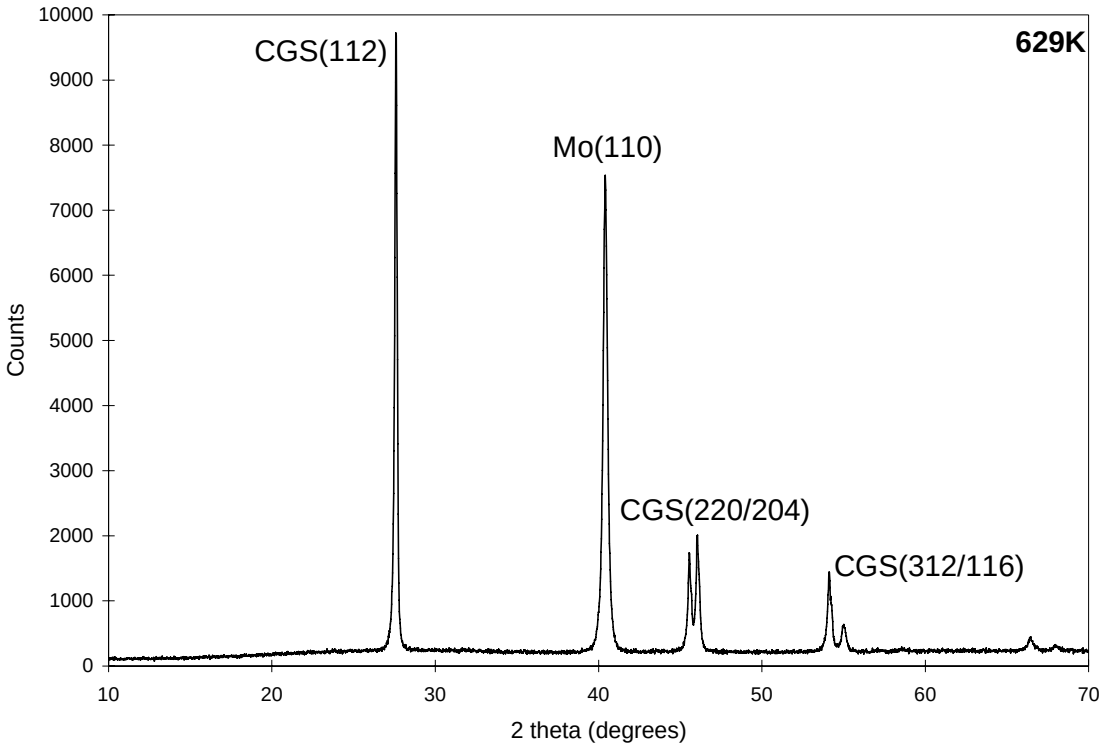

A

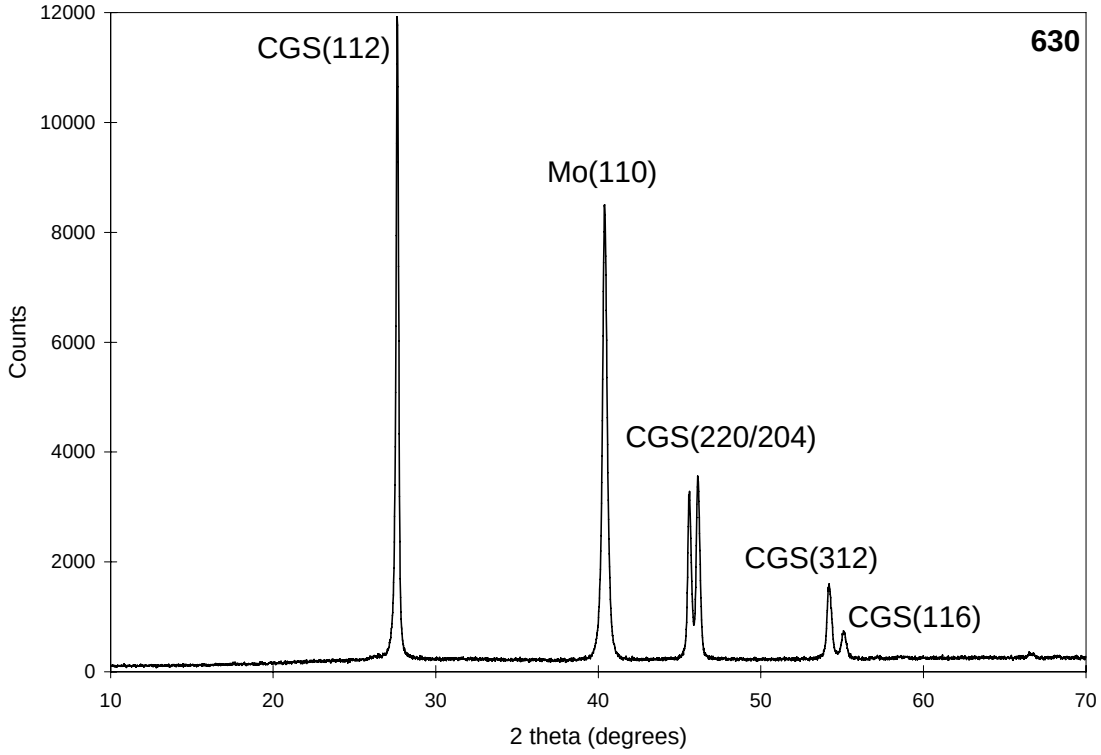

B

Figure 4-14. Diffraction patterns of films grown by the Constant Cu Rate Process. A) KCN-etched Cu-rich. B) Ga-rich.

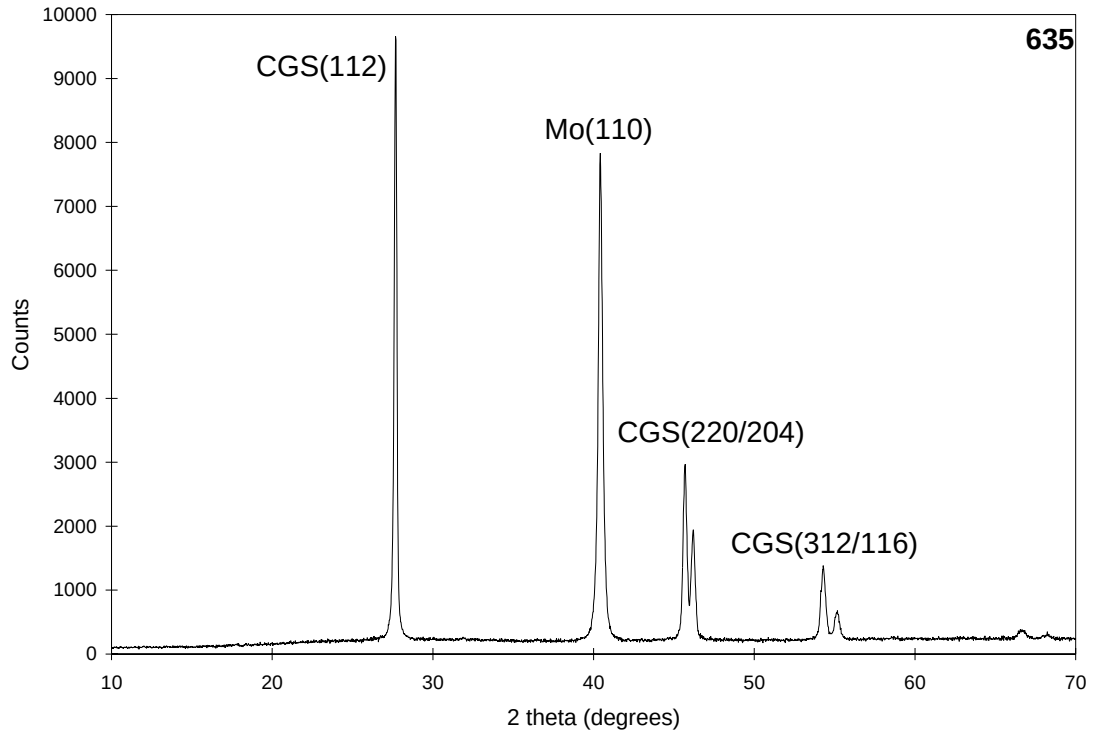

A

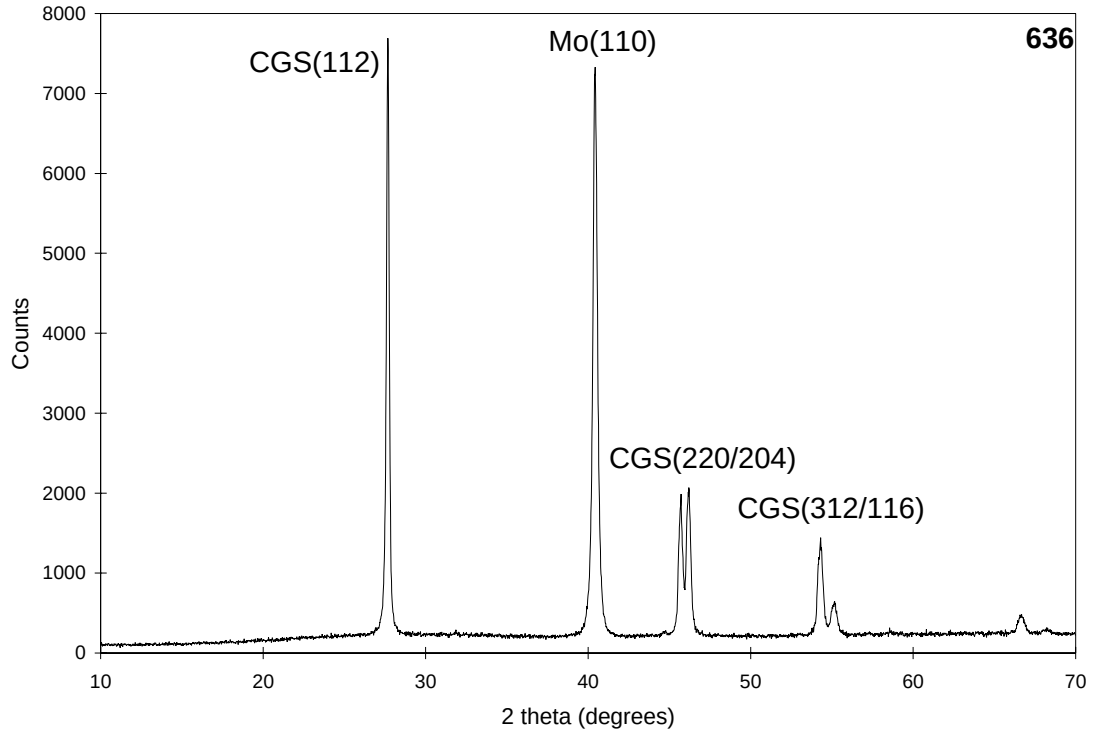

B

Figure 4-15. Diffraction patterns of films grown with varying levels of peak Cu-richness. A) Peak Cu/Ga = 1.3. B) Peak Cu/Ga = 1.6.

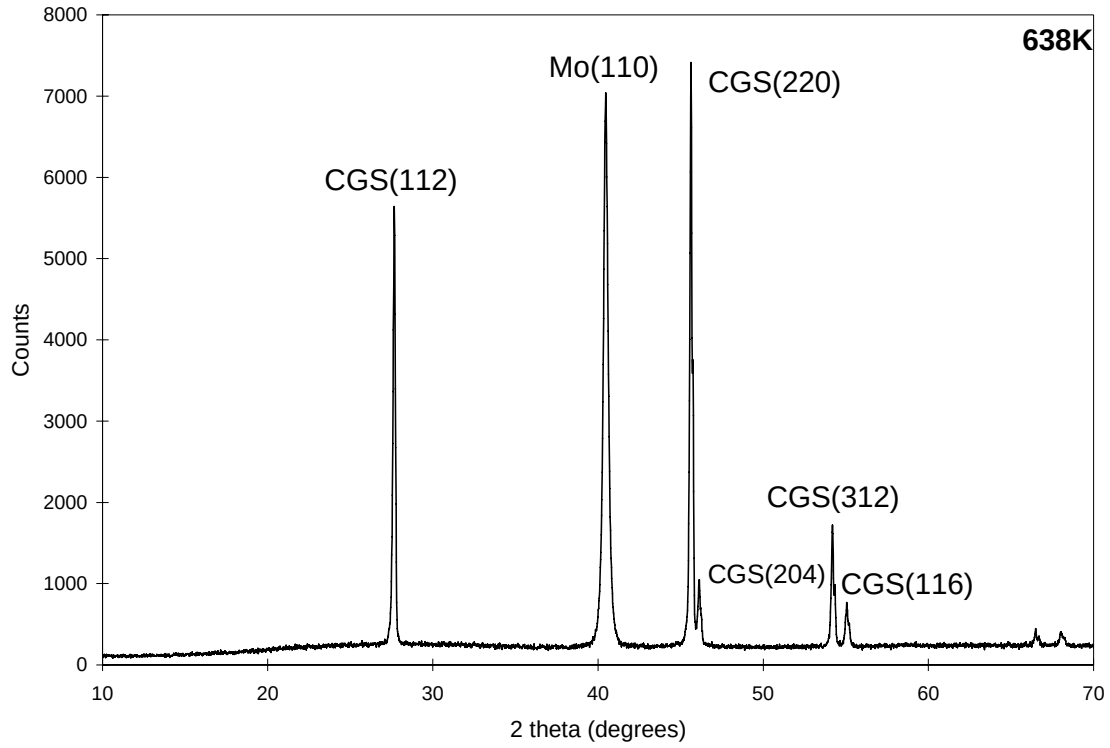

A

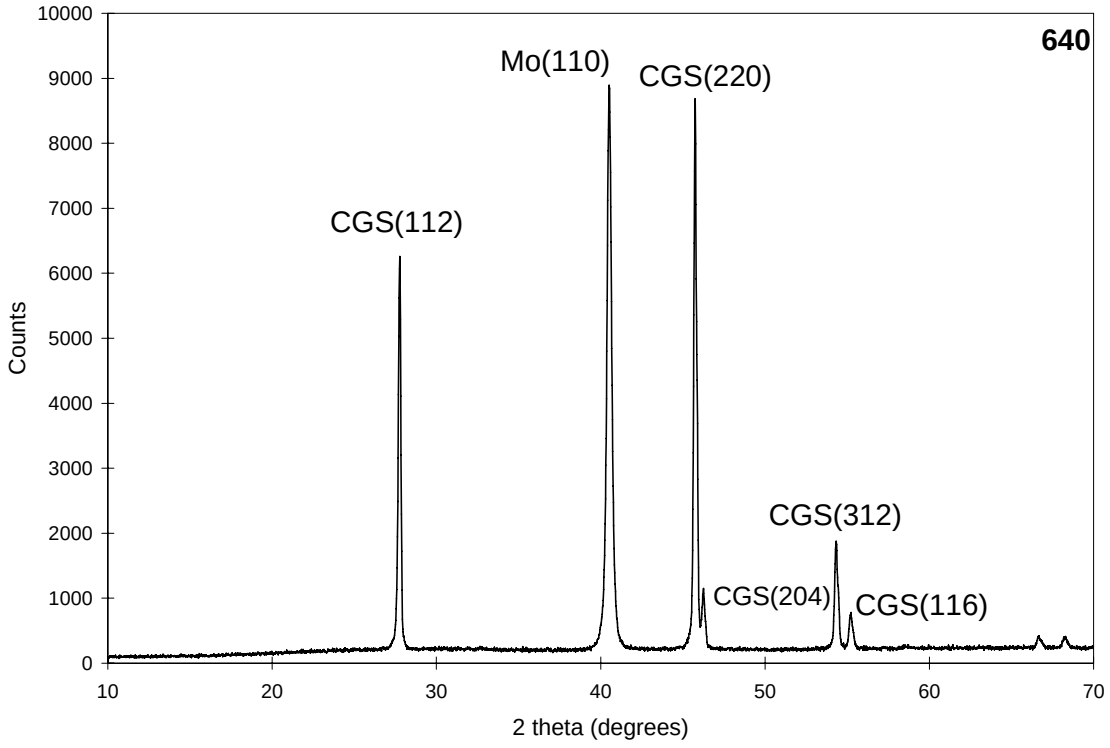

B

Figure 4-16. Diffraction patterns of films grown by the Emulated 3-Stage Process. A) Cu-rich. B) Ga-rich.

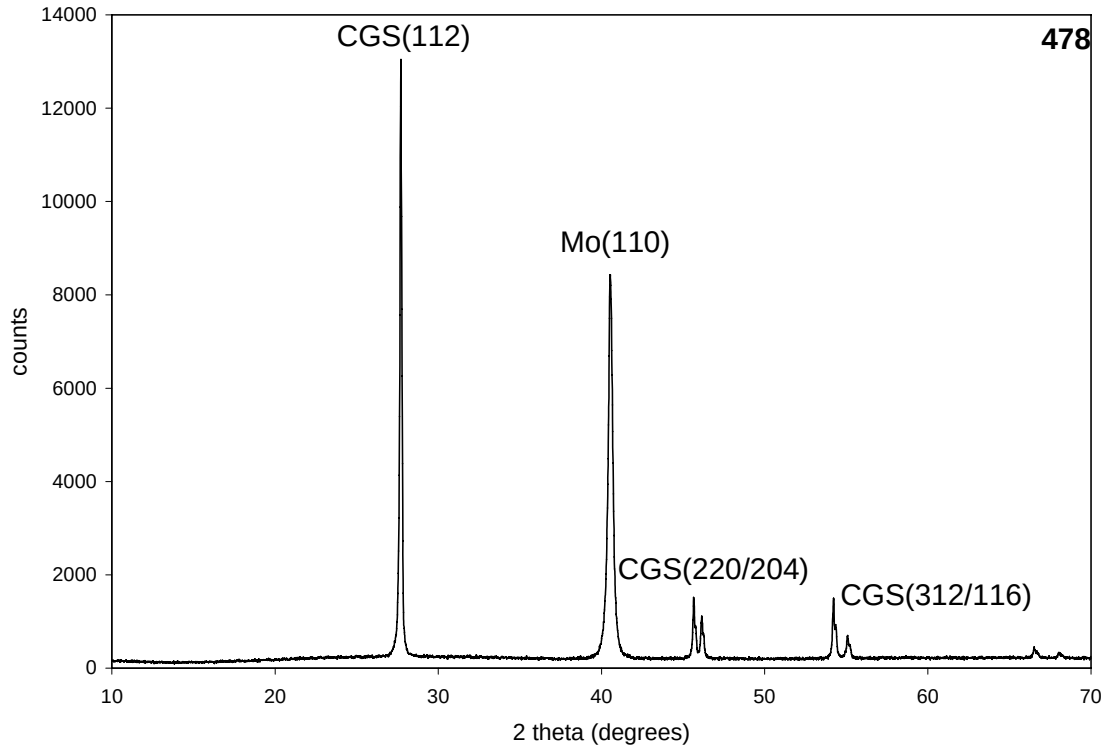

Figure 4-17. Diffraction pattern of a film grown by the Emulated 3-Stage Process that was never Cu-rich.

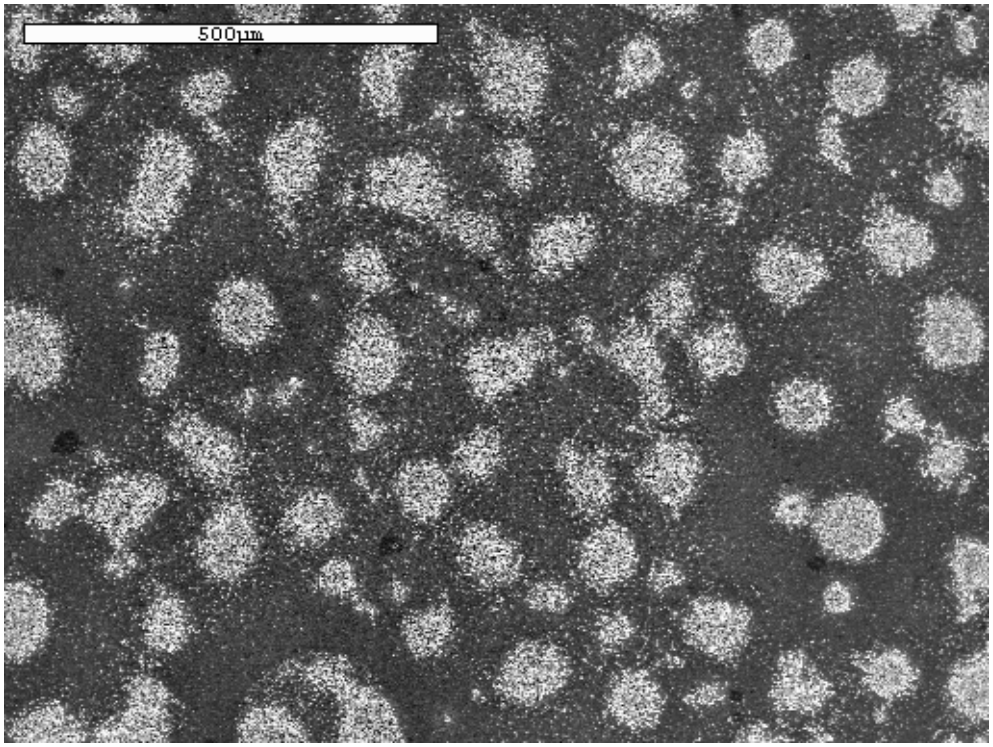

A

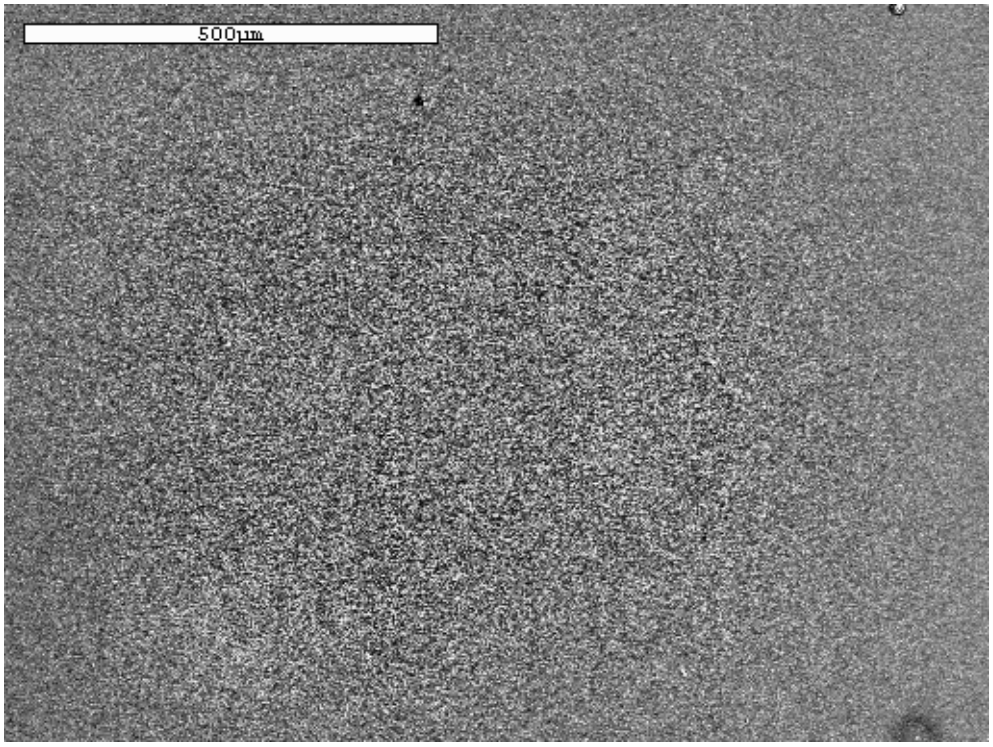

B

Figure 4-18. Surface morphology of films grown by the Constant Cu Rate process (X100). A) Cu-rich. B) Ga-rich.

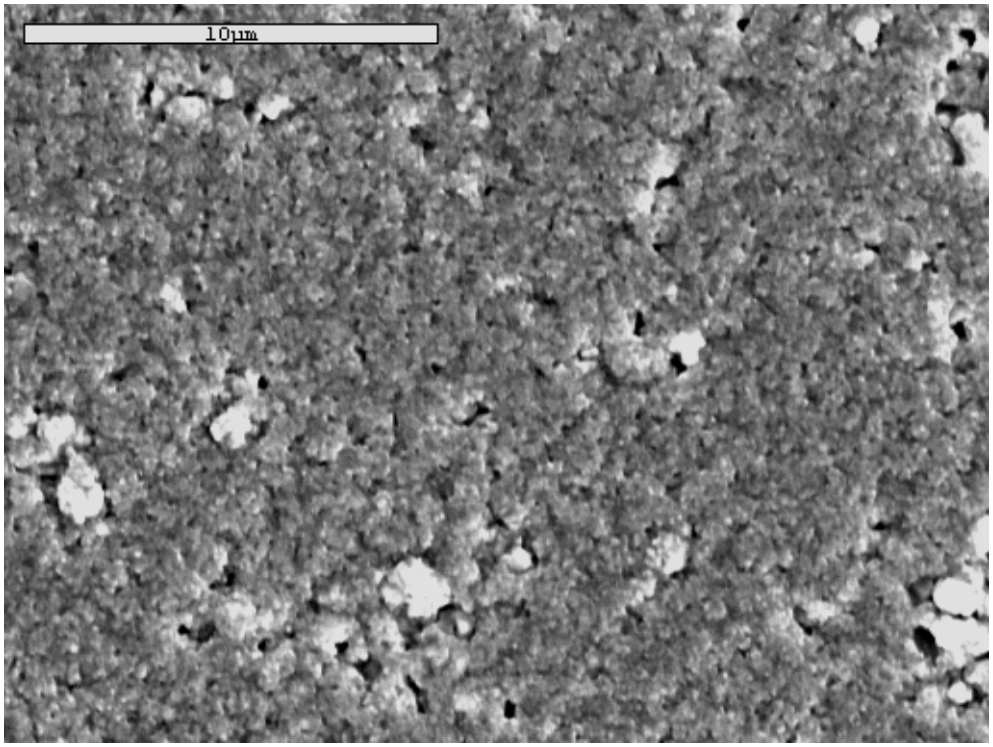

A

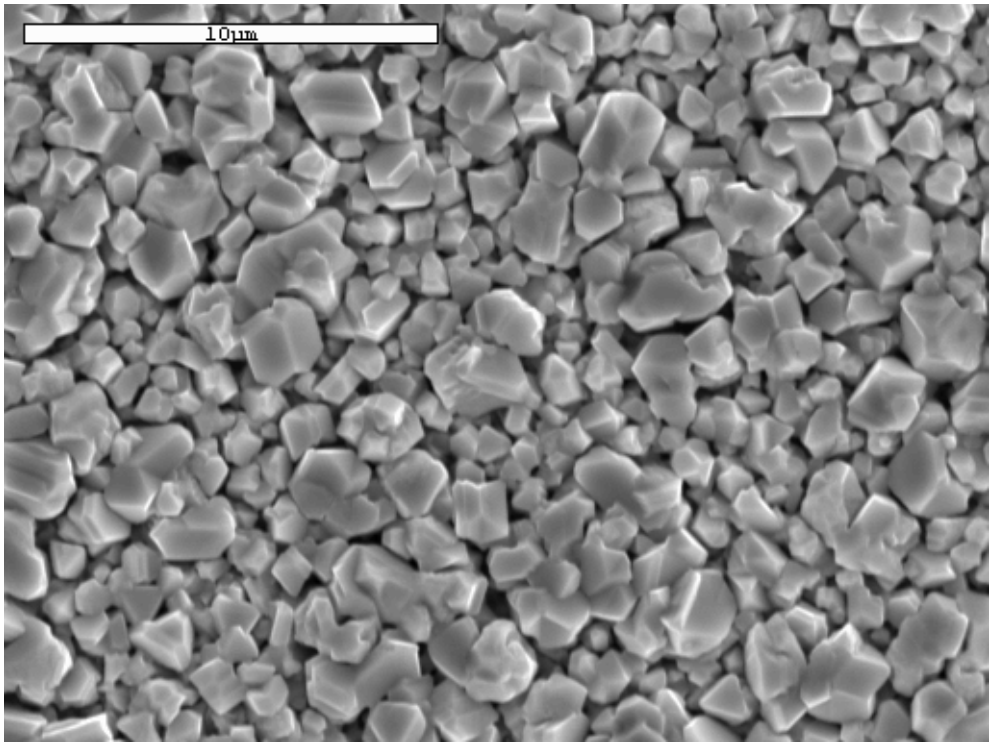

B

Figure 4-19. Surface morphology of a Cu-rich film grown by the Constant Cu Rate Process (X5000). A) Field Region. B) Island Region.

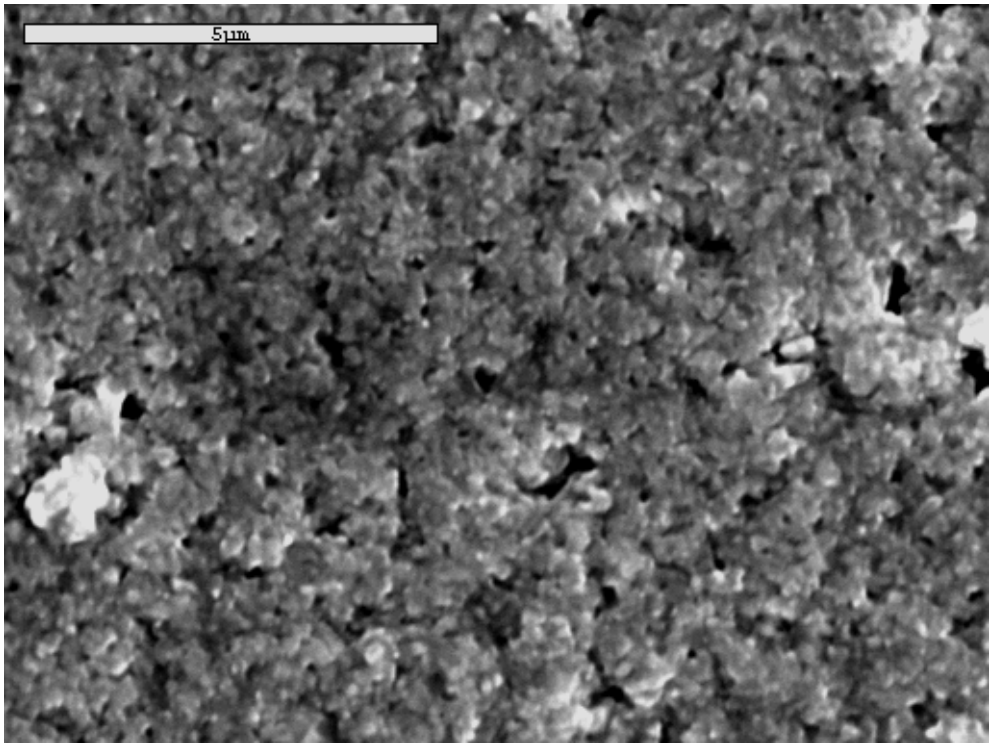

A

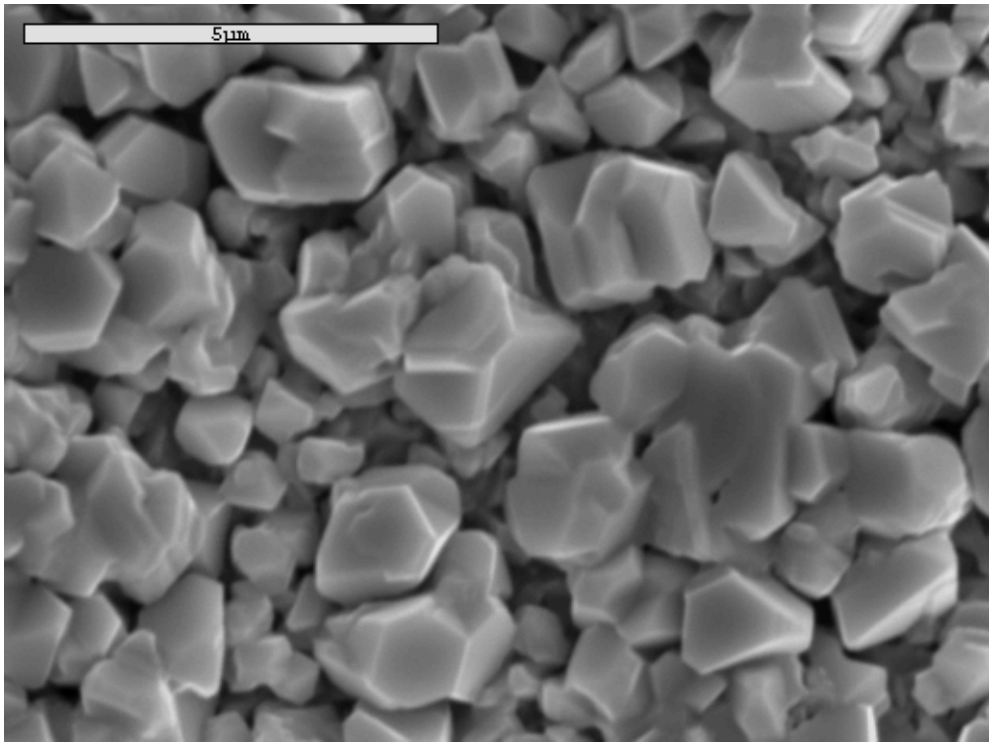

B

Figure 4-20. Surface morphology of a Cu-rich film grown by the Constant Cu Rate Process (X10,000). A) Field Region. B) Island Region.

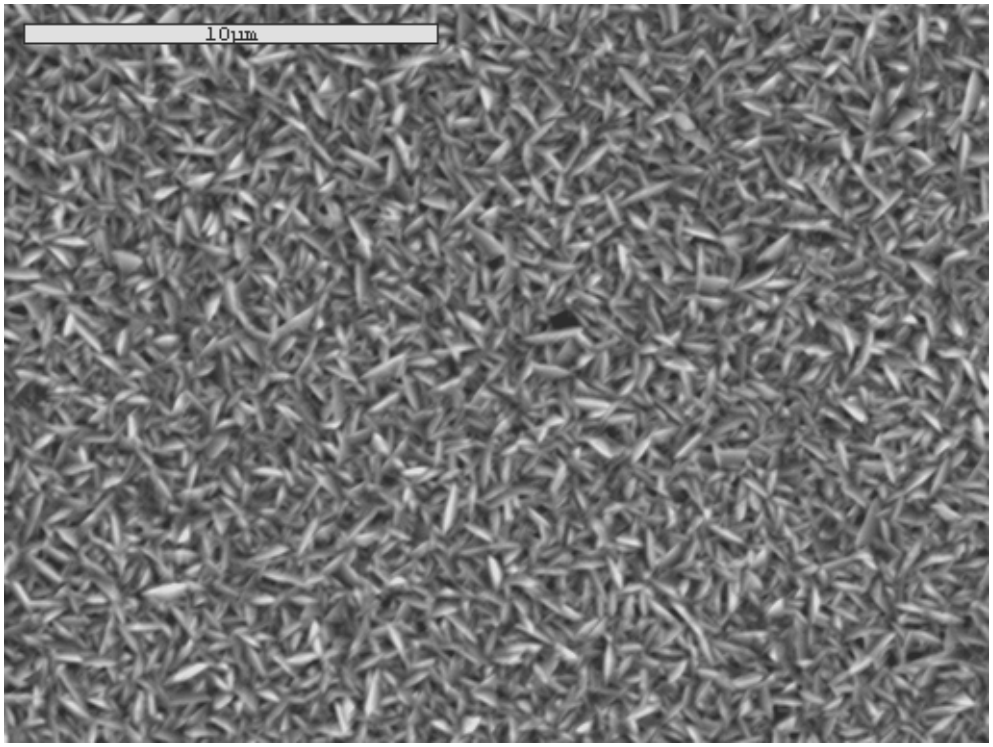

A

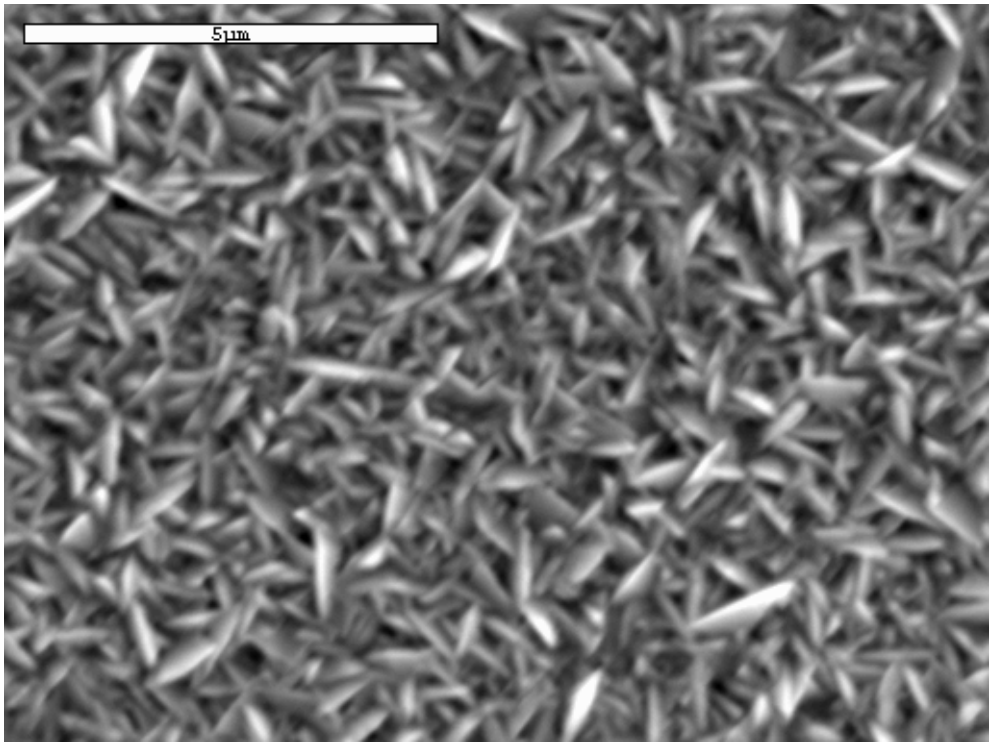

B

Figure 4-21. Surface morphology of a Ga-rich film grown by the Constant Cu Rate Process. A) X5000. B) X10,000.

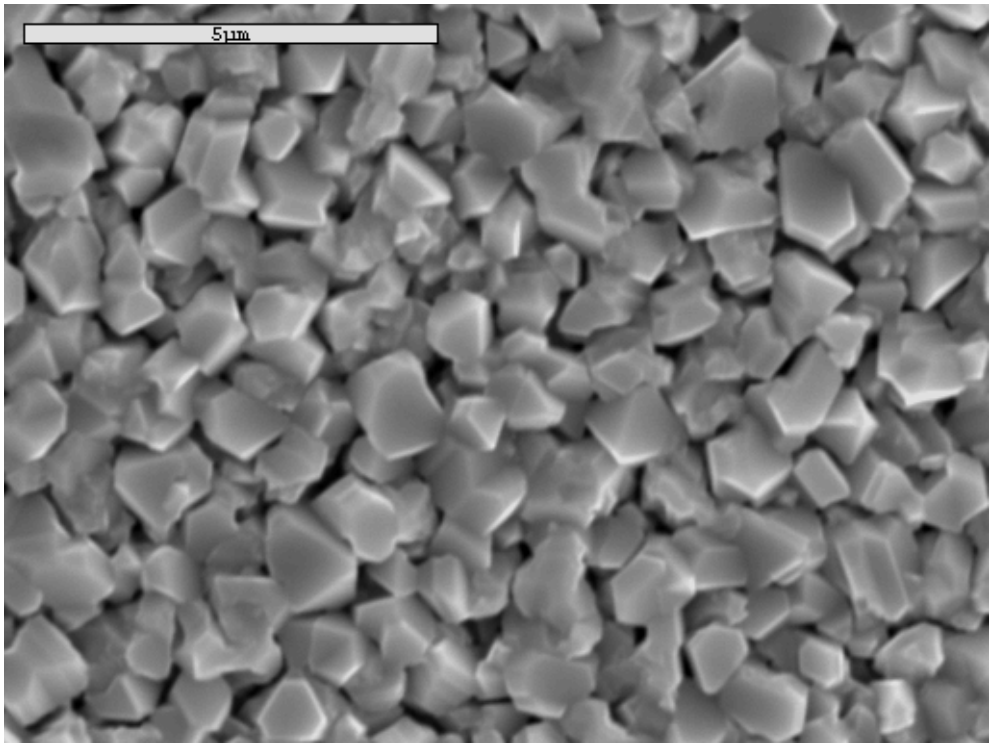

A

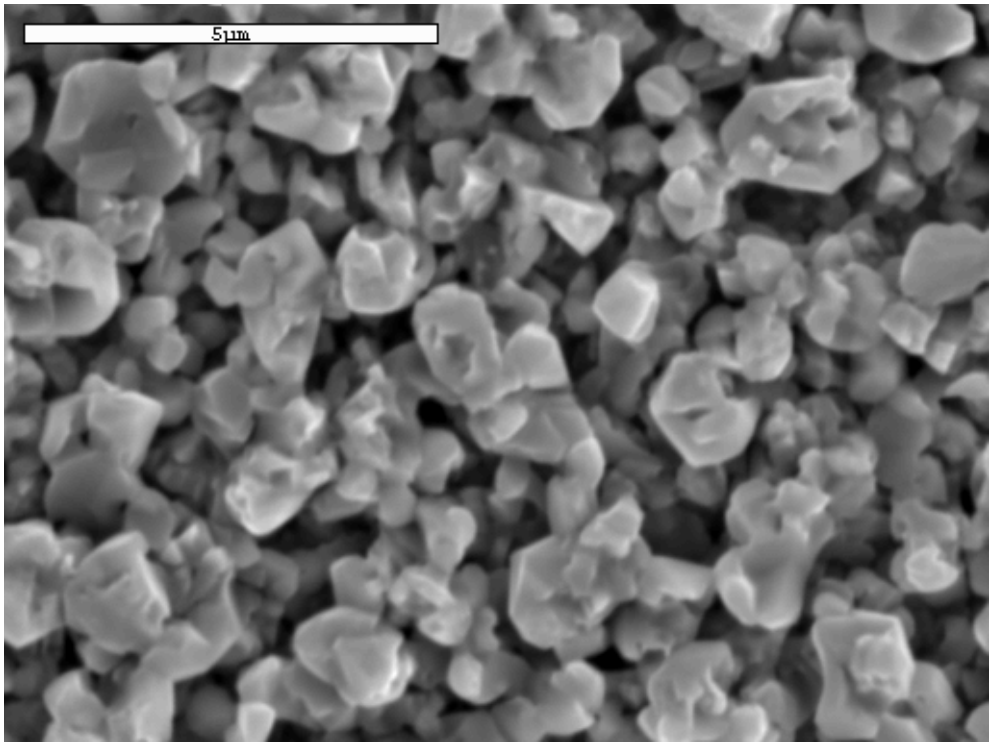

B

Figure 4-22. Effect of KCN-etch on the surface morphology of the island region of a Cu-rich film (X10,000). A) Before. B) After.

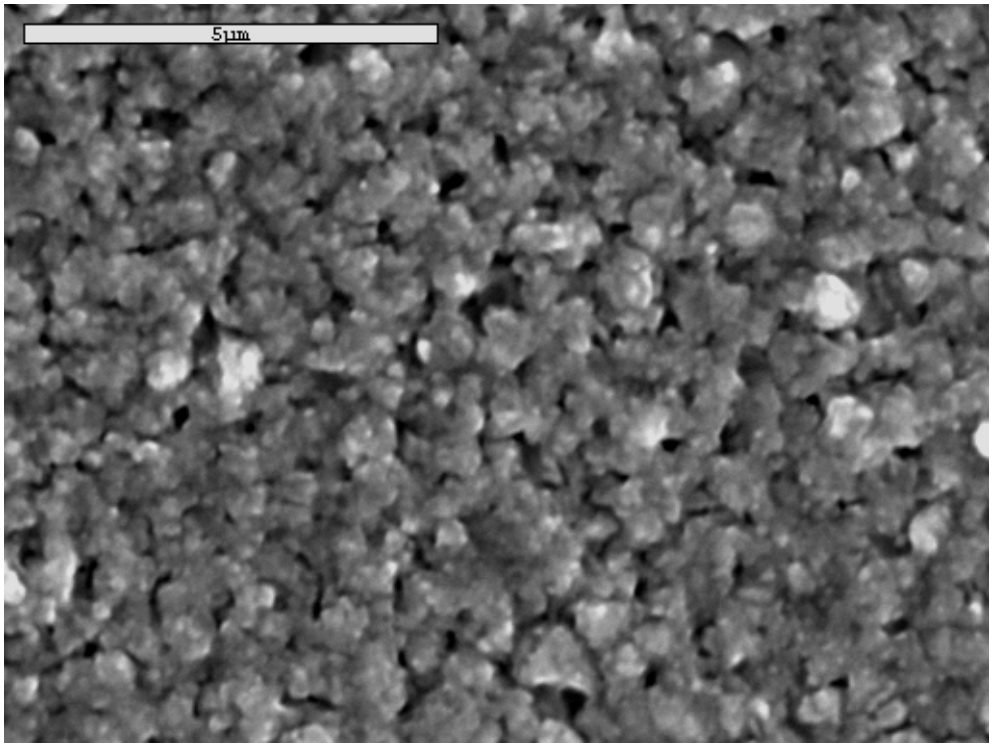

A

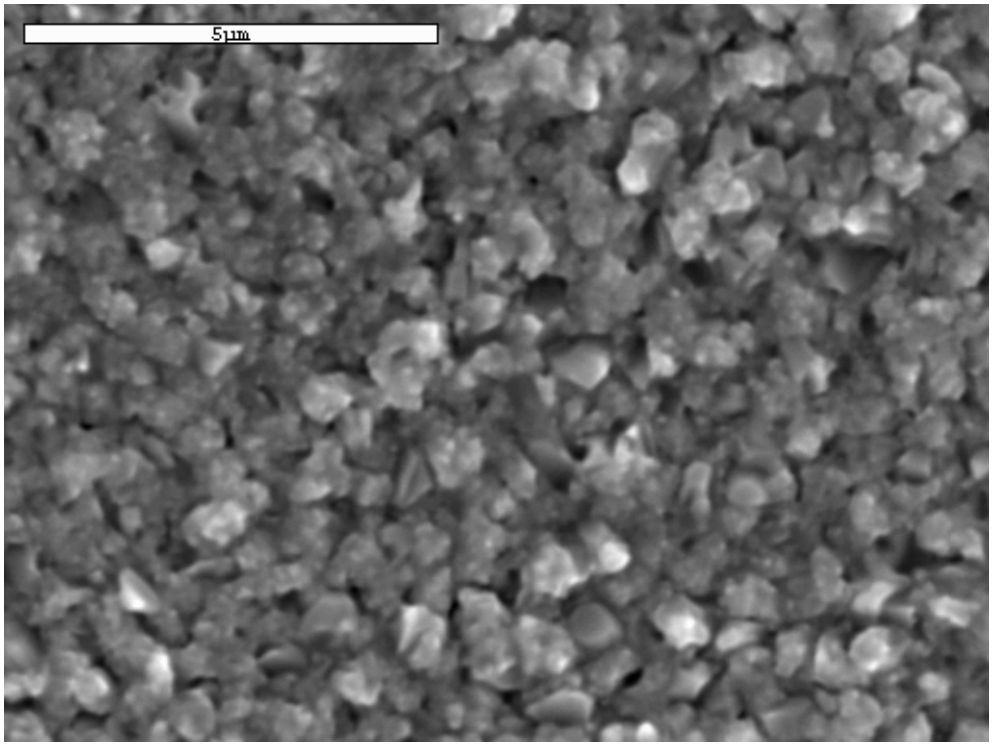

B

Figure 4-23. Effect of KCN-etch on the surface morphology of the field region of a Cu-rich film (X10,000). A) Before. B) After.

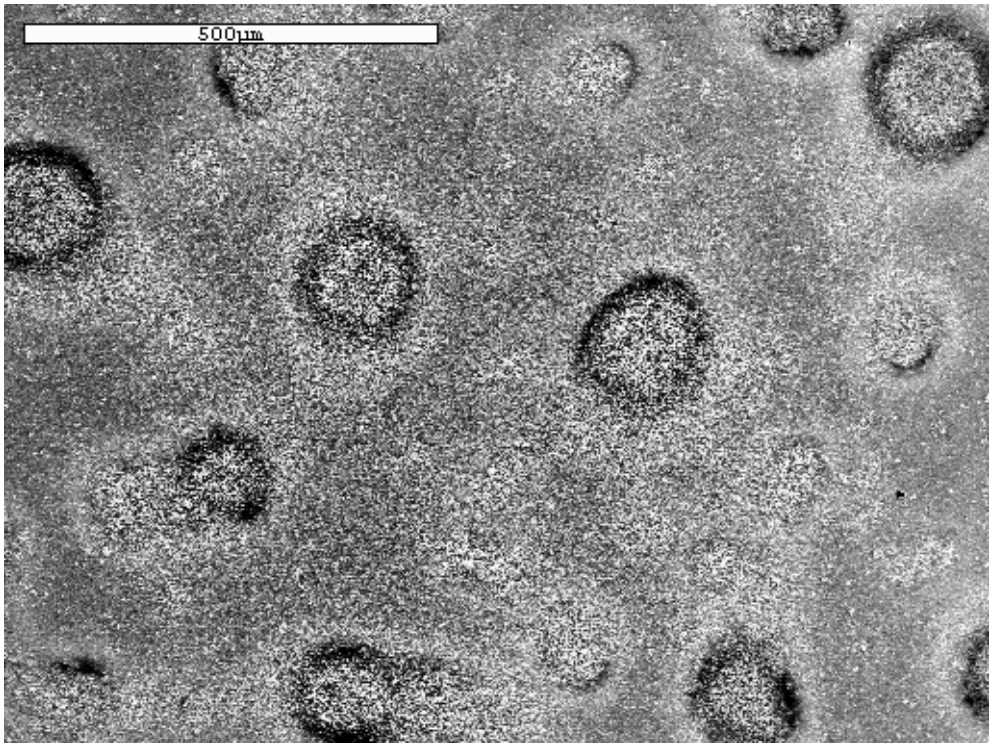

A

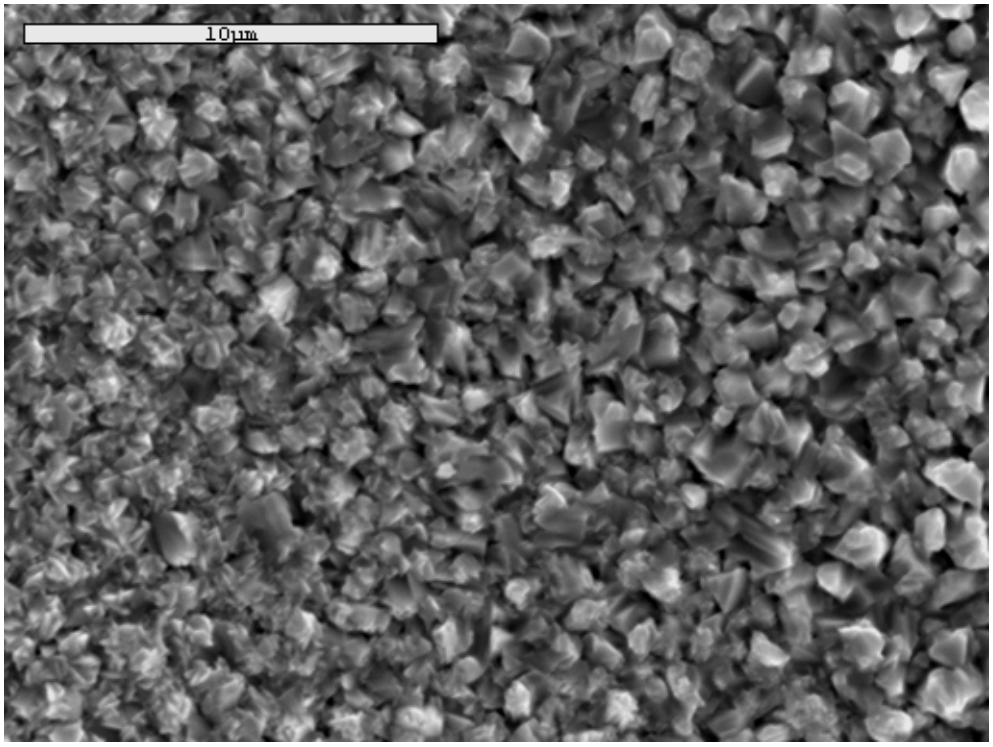

B

Figure 4-24. Surface morphology of a Ga-rich film with rings around the islands A) X100. B) The ring region magnified (X5,000).

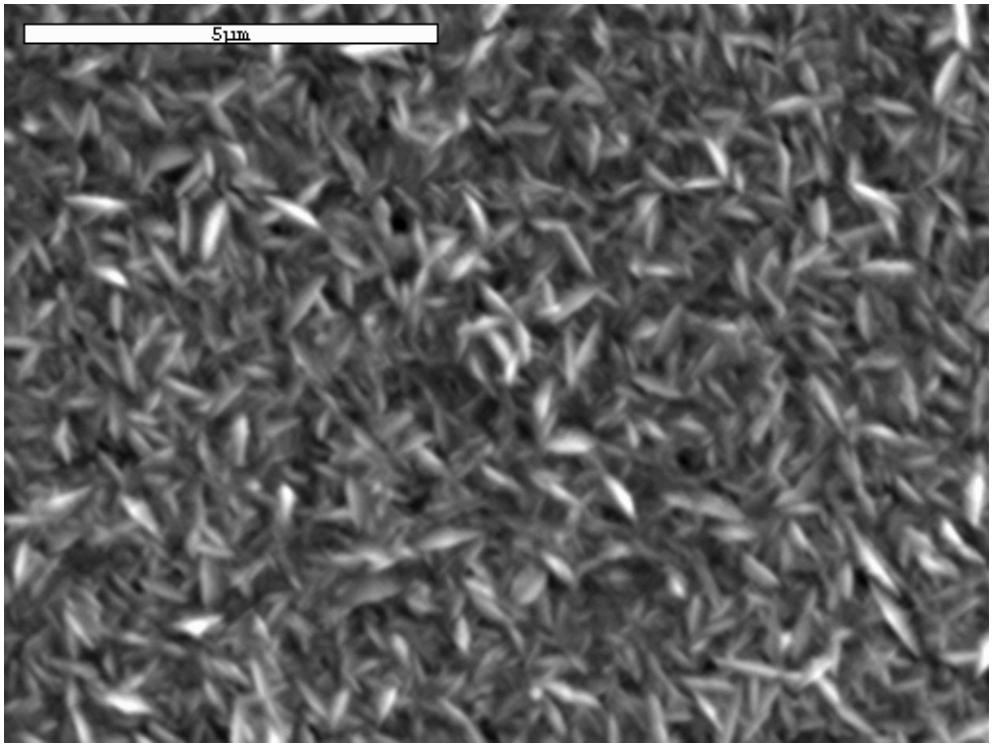

A

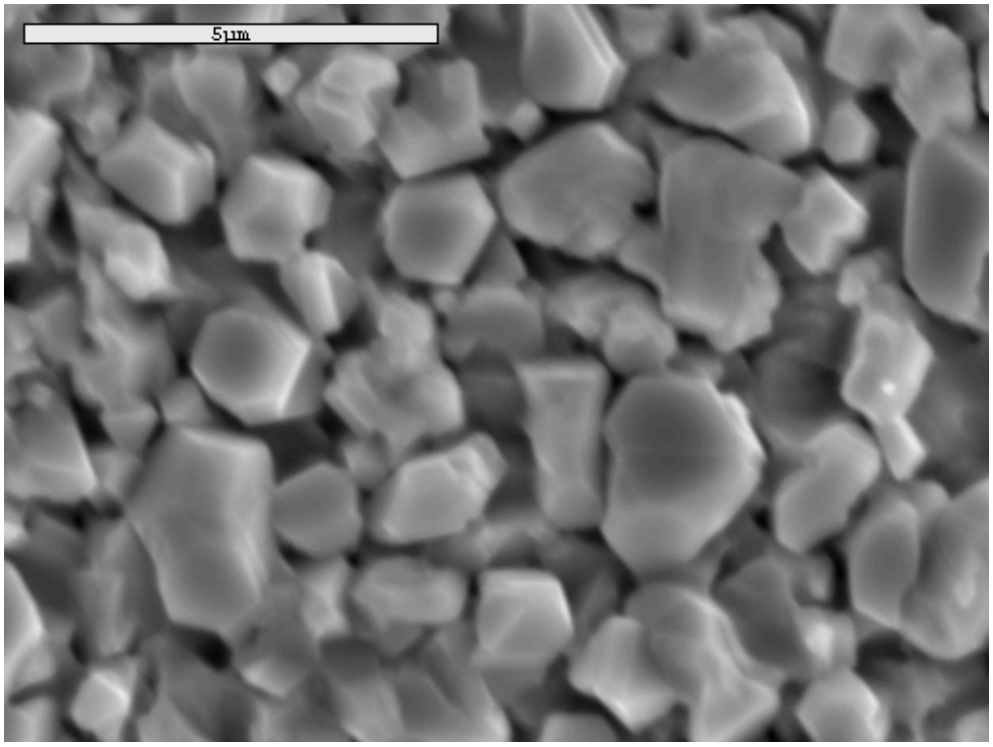

B

Figure 4-25. Distinct grain structure of a Ga-rich film with rings around its islands (X10,000). A) Field region. B) Island region.

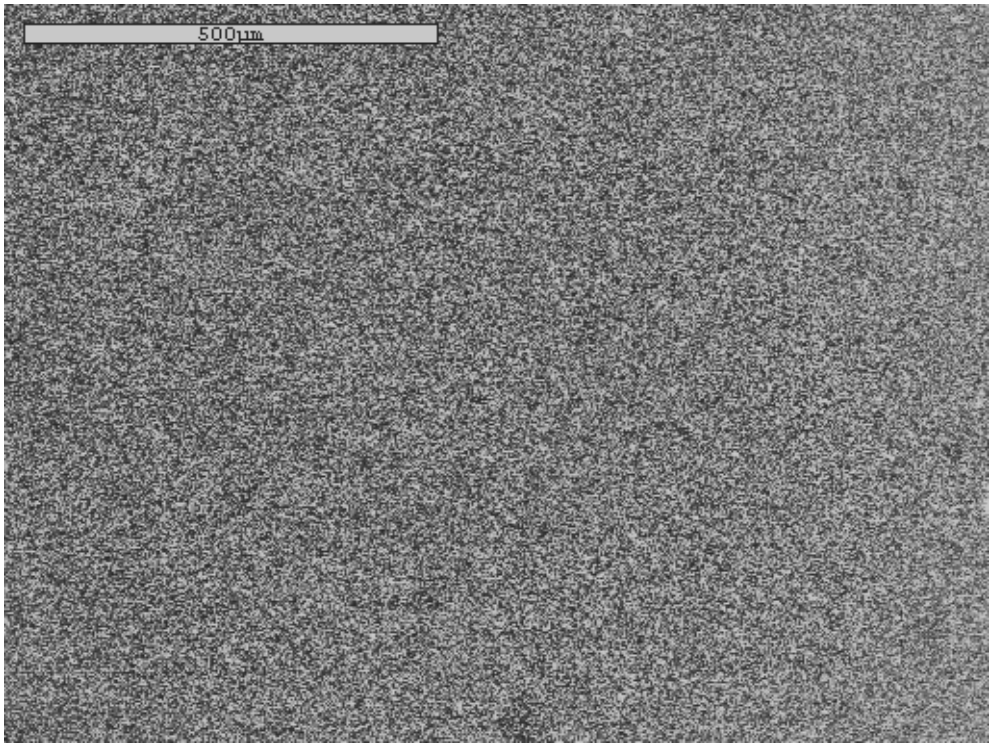

A

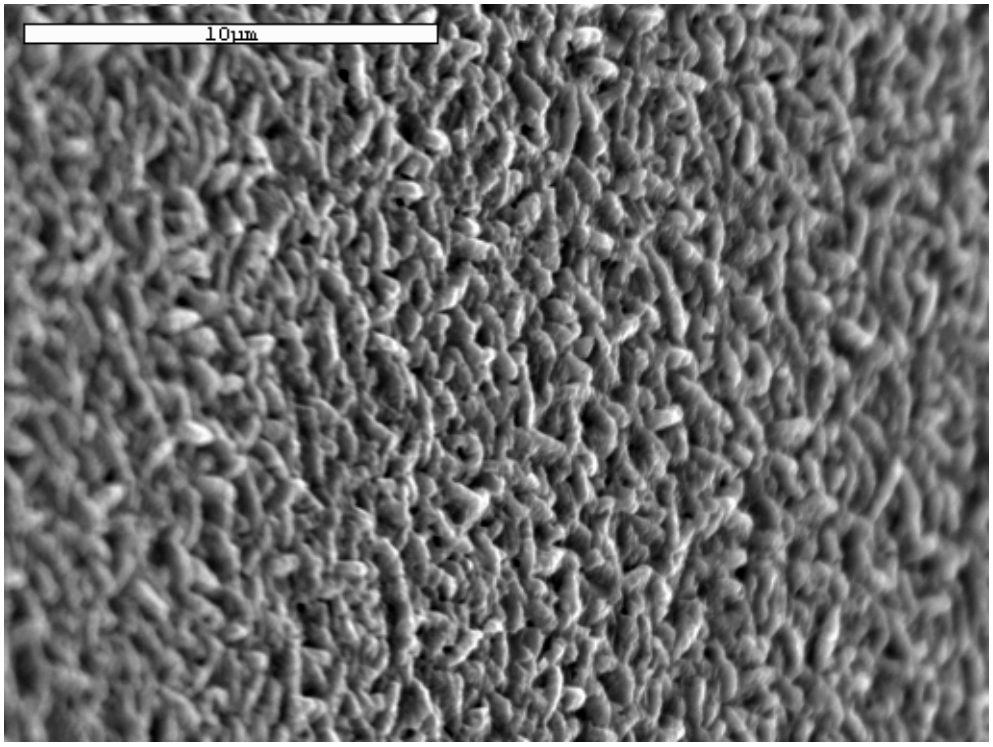

B

Figure 4-26. Surface morphology of a film grown by the Emulated 3-Stage Process. A) X100. B) at a 45° tilt.

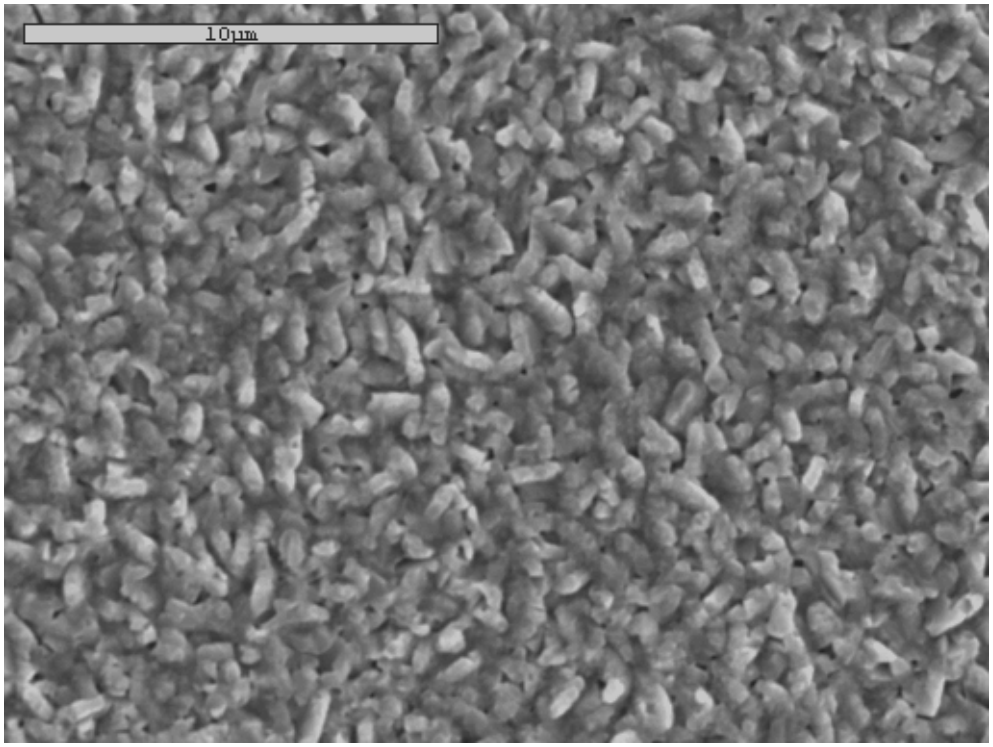

A

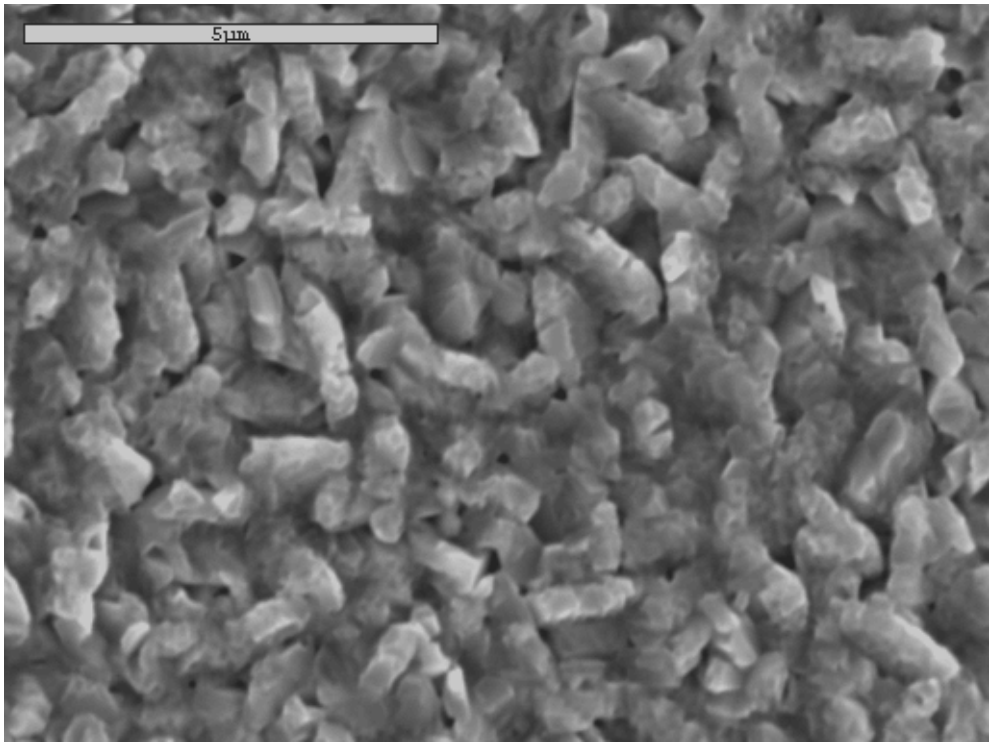

B

Figure 4-27. Surface morphology of a Cu-rich film grown by the Emulated 3-Stage Process. A) X5000. B) X10,000.

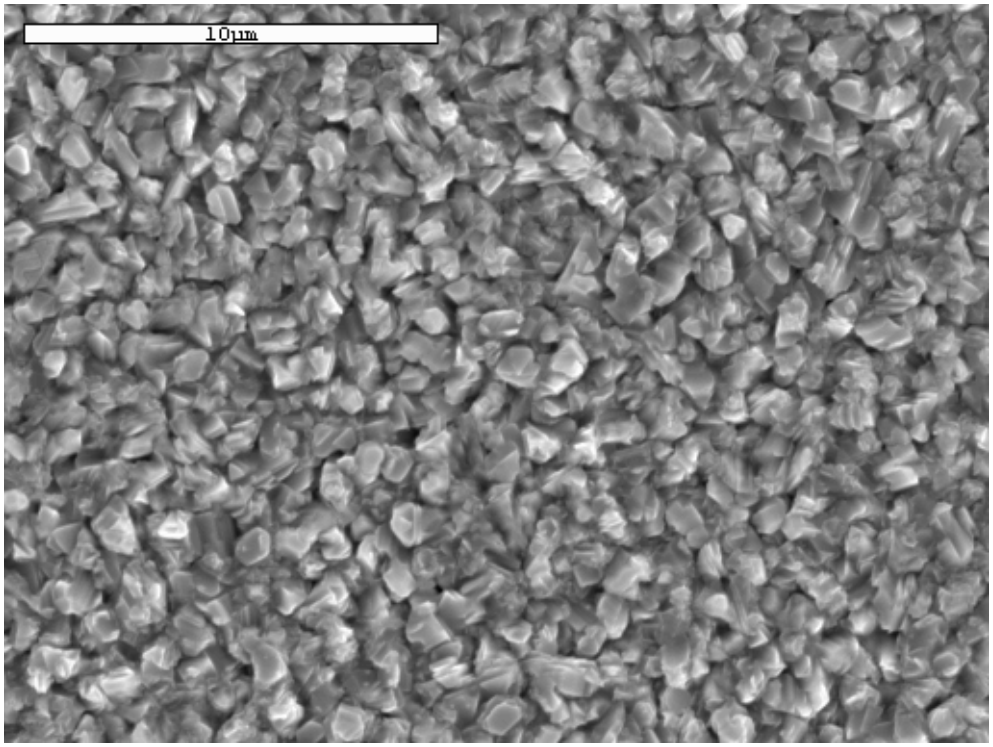

A

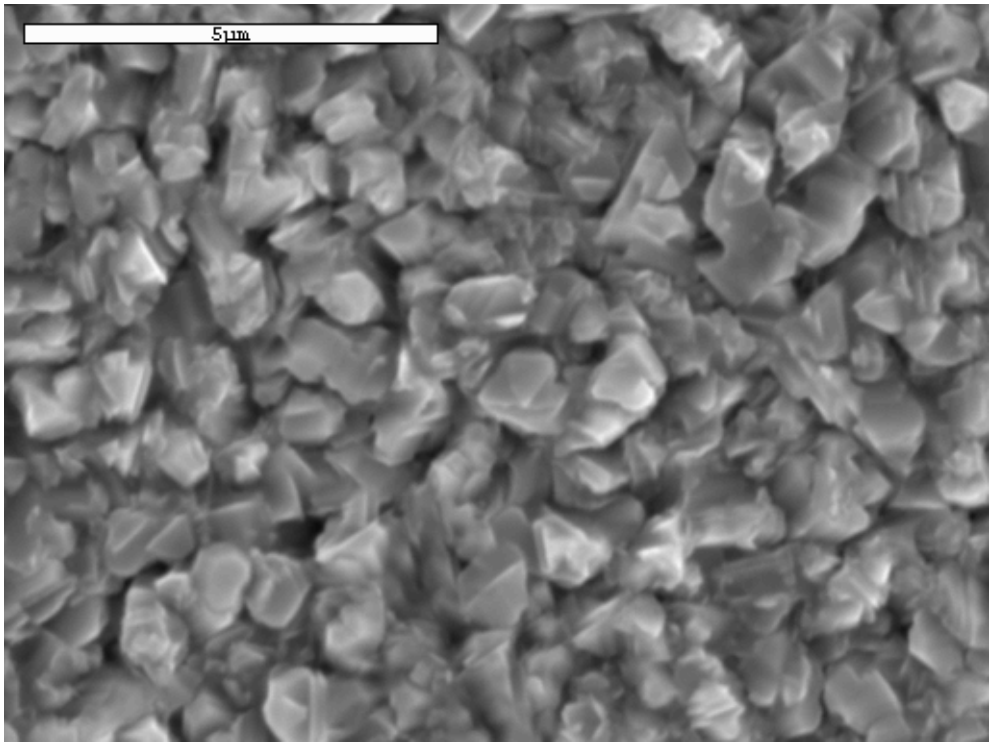

B

Figure 4-28. Surface morphology of a Ga-rich film grown by the Emulated 3-Stage Process. A) X5000. B) X10,000.

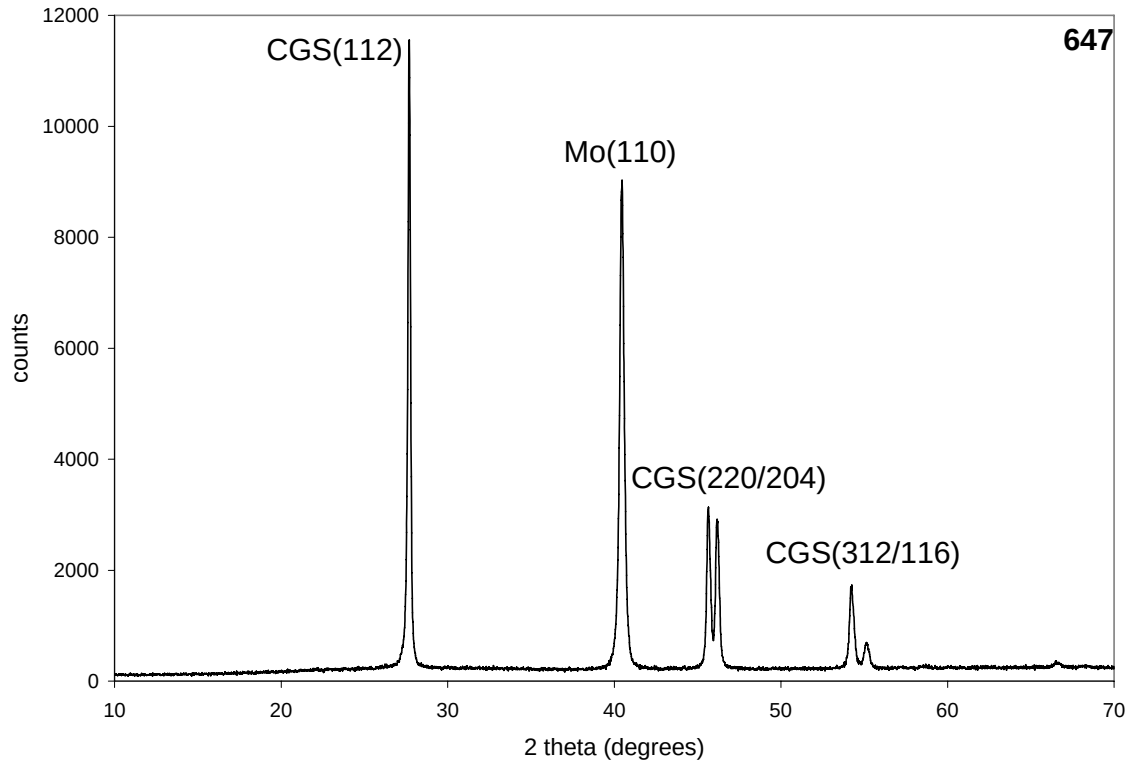

Figure 4-29. Diffraction pattern of a Ga-rich film grown by the Constant Cu Rate process.

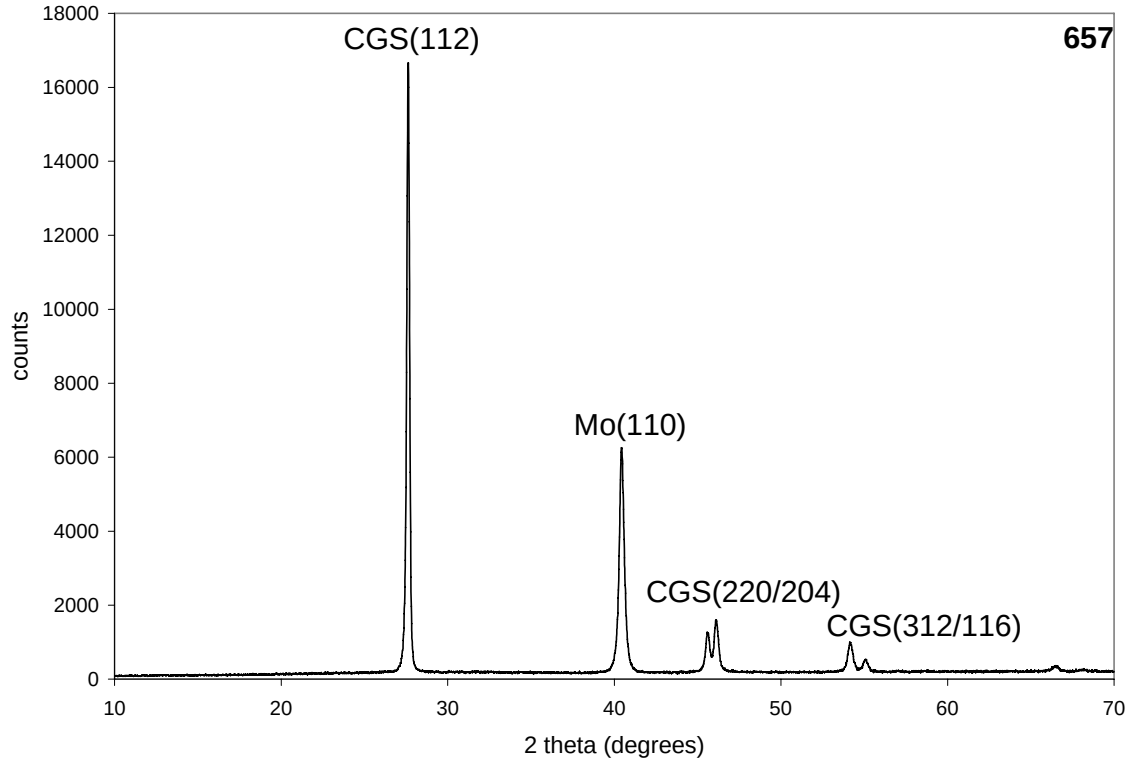

A

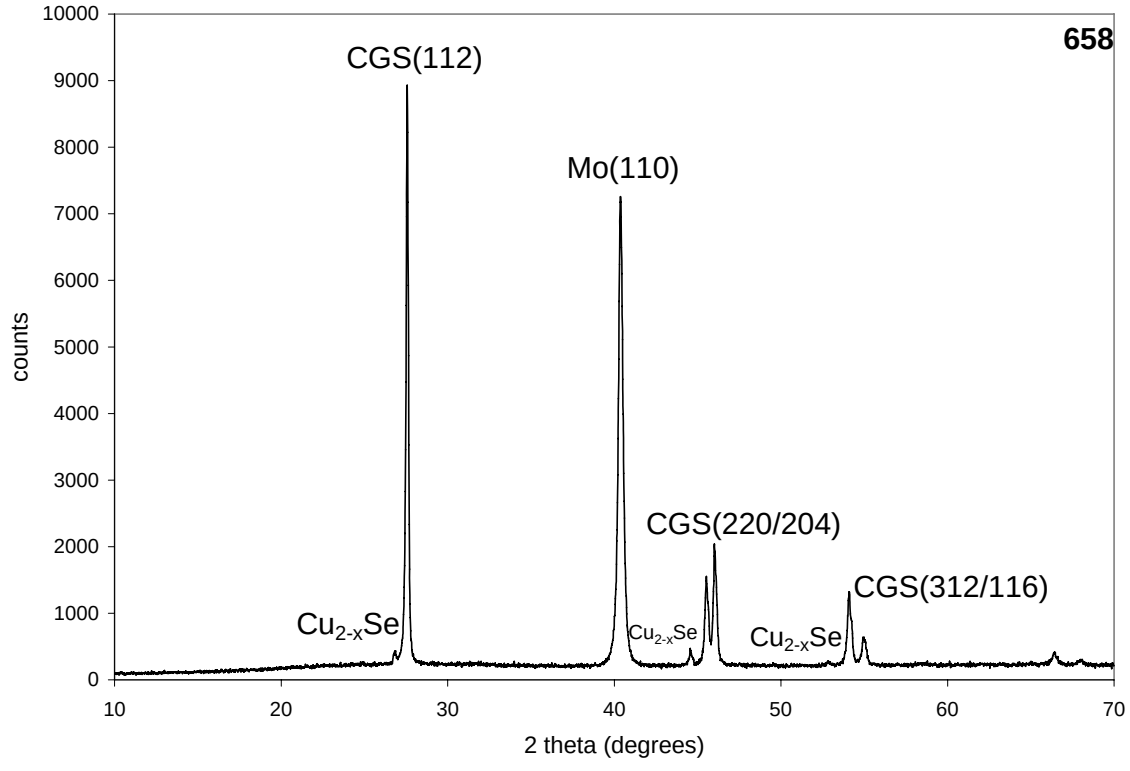

B

Figure 4-30. Diffraction patterns of films grown by the Constant Cu Rate process. A) Stoichiometric. B) Cu-rich.

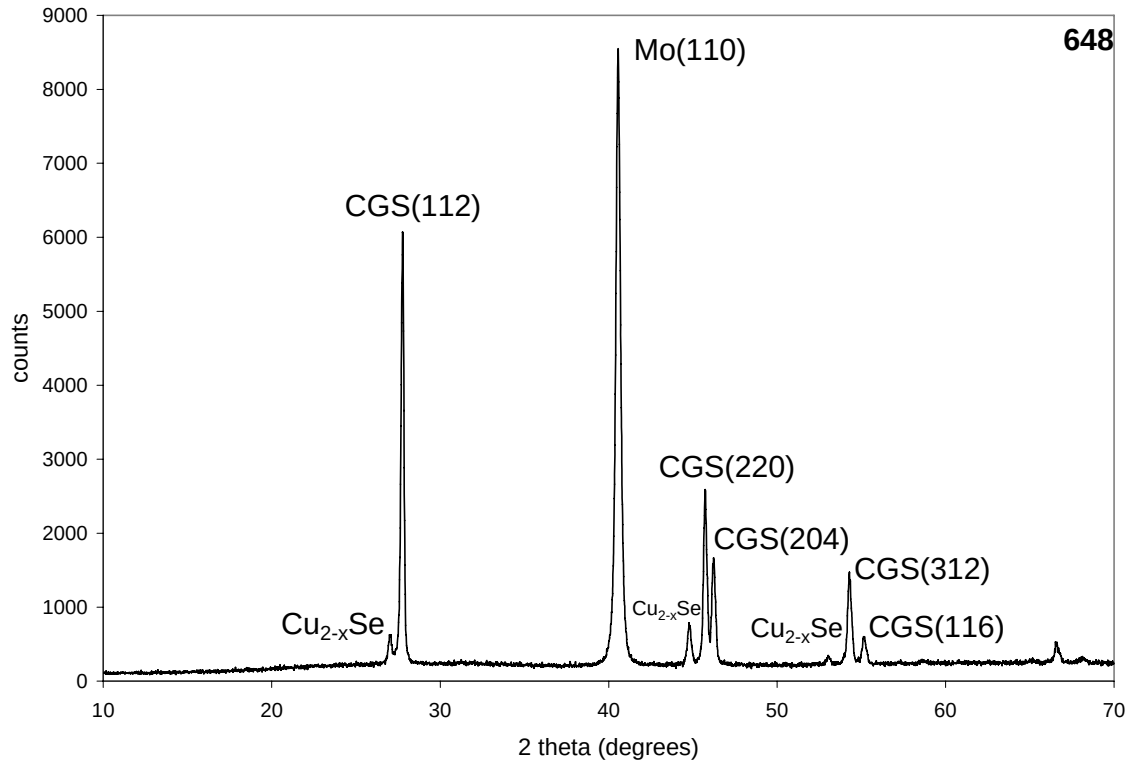

A

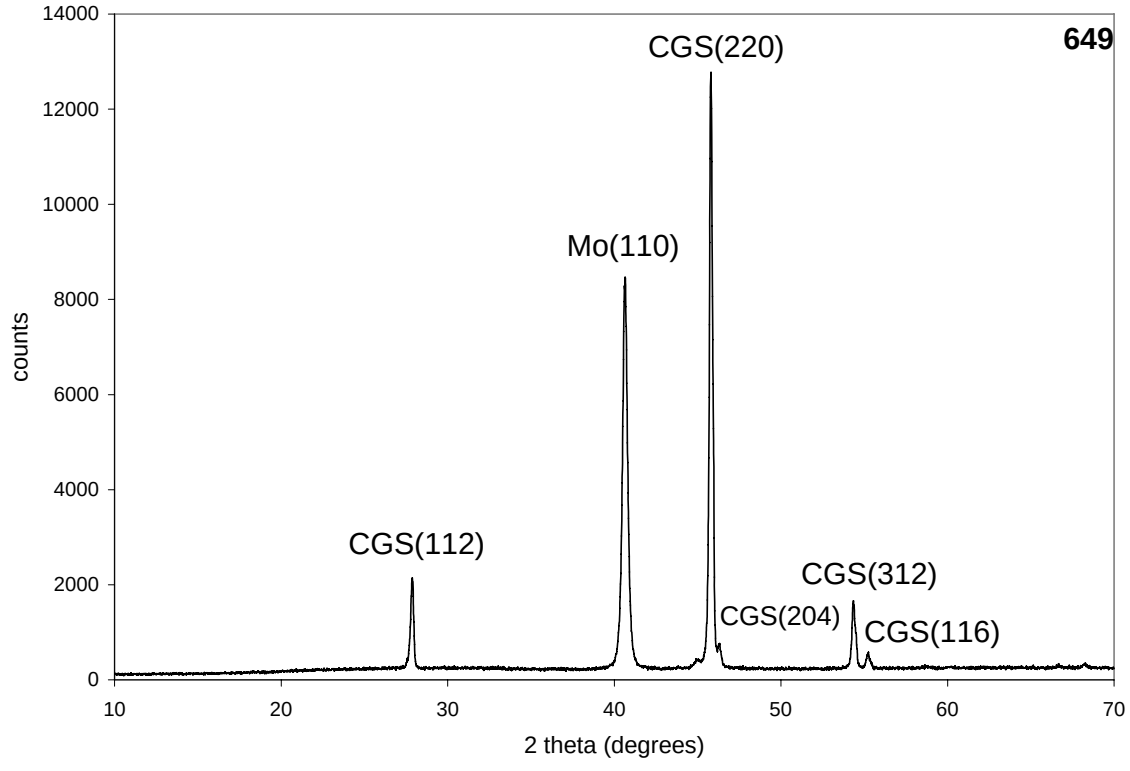

B

Figure 4-31. Diffraction patterns of films grown by 3-stage process. A) Modified 3-Stage Cu-rich film. B) Emulated 3-Stage Ga-rich film.

CHAPTER 5
COPPER GALLIUM DISELENIDE DEVICE FABRICATION

It can be difficult to determine what causes small, but significant, changes in the solar cell parameters when comparing devices. A summary of the properties of the absorbers and devices can pave the way for more careful and controlled experimentation, and the testing of key ideas. Any unique properties or features that have been identified should be noted.

Best Devices in the Literature

A record total area efficiency of 10.2% [142] for $CuGaSe_2$ was achieved at NREL using a thicker absorber and a more Cu-rich condition than the previous best cell [48]. The biggest difference was the addition of a very small amount of In at the end of the growth with In/(In+Ga) < 0.8%. This surface-modified CGS is grown so that the surface region is similar to that of CIGS to minimize defects in the material. The V_{OC} and FF of this new cell were lower compared to the previous record cell, but the J_{SC} increased. This indicates that the recombination mechanisms are different in the two devices. Table 5-1 compares the surface modified CGS I-V results to the previous record cell [142].

Record efficiency of ZnO/CdS/CGS cells went from 6.2 to 9.3% by making the following improvements: slightly Ga-rich absorber composition, the use of Na-containing substrates, and a CdS buffer layer deposition temperature optimized for CGS [111]. Unlike low Ga-content CIGS, the efficiency of single crystals has been higher than polycrystalline CGS solar cells. Saad et al. produced a single crystal CGS solar cell with an efficiency of 9.7% (V_{OC} = 946 mV, J_{SC} = 15.5 mA/cm^2, and FF = 66.5) [143].

The enhancement of the FF seems to be the most important issue in order to achieve high-efficiency CGS cells. CIGS solar cells reach 90% average QE while CGS so far has been limited to about 70% [57]. Current transport through CGS cells is dominated by interface

recombination; the diode ideality factor and the saturation current change drastically under illumination. This may be the main difference to the heterojunctions based on low gallium content CIGS where a relatively small diode factor of 1.5 indicates current transport dominated by recombination in the depletion layer; interface recombination only plays a minor role [63].

Device Fabrication

After the first seven sets of growth runs, samples containing CGS absorber film were sent to James Keane at the National Renewable Energy Laboratory (NREL) to be processed. To eliminate the copper selenide which is known to form in the Cu-rich CGS, all Cu-rich CGS absorber films were etched with a 10% KCN solution for five minutes before being shipped. Also, the 2" x 2" samples were cut in half before being sent. The first six growth series had the misfortune of being shipped while not being protected from the elements. A vacuum sealer was purchased to remedy this situation. Device fabrication completed at NREL included CdS grown by a CBD process followed by the deposition of a high/low resistivity ZnO bilayer film and Ni/Al grid deposition. The first and third growth series had CBD CdS buffer layers deposited on them in-house before being sent to NREL for further processing. Once the devices were sent back to the University of Florida, I-V measurements were taken. For the seventh set of samples, 628-641, the devices were also characterized at NREL and never sent back to the University of Florida. The final CGS growth series was fabricated completely in-house.

World-record surface-modified CGS films are processed with 500-600 Angstroms of CdS using CBD at a bath temperature of ~ 65°C. A ZnO bilayer was then added, containing an undoped ZnO layer (90 nm thick) followed by an Al-doped ZnO layer (about 120 nm thick). A 100 nm thick MgF_2 antireflective coating was deposited using sputtering [142].

The films fabricated completely at the University of Florida had $Zn_xCd_{1-x}S$ buffer layers, instead of the traditional CdS buffers, deposited on them after absorber growth. The CGS films

were cut into 1" x 1" samples and vacuum-sealed after their removal from the vacuum chamber, and they remained so until the buffer was deposited by CBD. The Cu-rich films were etched in a 10% solution of potassium cyanide for five minutes while the Ga-rich films were fabricated as-grown.

The addition of Zn to the most widely used CdS buffer layer material decreases the lattice constant with a lattice match to CGS absorber and produces a more favorable conduction band alignment. Adding Zn enhances both V_{OC} and J_{SC} of the device to yield a higher conversion efficiency for CGS. An aqueous solution of 1.20×10^{-3} M $CdCl_2$ $2(1/2)H_2O$, 1.39×10^{-3} M NH_4Cl, 1.19×10^{-2} M thiourea (H_2NCSNH_2), 6.27×10^{-4} M $ZnCl_2$, and 5.27×10^{-4} M NH_3 was used. The following conditions tend to give the maximum increases in solar-cell conversion efficiencies: CBD bath temperature of 85 °C, duration of bath-deposition t_{dep} = 45-50 minutes, and x_{bath} = 0.2-0.3 (i.e., bath solution containing relative amounts of Zn ranging from 20% to 30%). The chemical bath is kept at the target temperature of 85 °C at all times during film growth. These parameters produce good films on glass and on CGS/CIGS substrates that are visually shiny, uniform, and have no powdery patches. Structural, surface morphology, optical, and electrical analyses show that CdZnS films with a 30% Zn composition should be a successful buffer layer for CGS [144].

The window layer consisted of a 600 nm Al-doped ZnO layer, which was magnetron sputtered. The sheet resistance of the characterization TCO film grown along with the fabricated devices ranged from 38 Ω/square to 45 Ω/square. Cells were completed by evaporation of a Ni (50 nm)/Al (0.3 μm) contact grid and finally defining the cells (0.429 cm^2) by mechanical scribing. No anti-reflective coating is added. For I-V measurement purposes, part of the CGS layer away from the grid was scratched off and an In contact was added to the Mo surface.

Device Characterization

The photo current density - voltage (I-V) characteristics were measured under AM1.5, 100mW/cm^2 illumination at 25°C in our own electrical measurement lab. Dark I-V measurements were taken for a few select samples. The I-V results for the selected devices are summarized in the respective tables for each growth series.

The CGS absorbers for the first growth series, 443-447, had a CdS buffer layer added by CBD in-house at the University of Florida and then were shipped off to NREL for further processing. These films were deposited at a fairly low growth temperature of approximately 386°C. The only device that had an efficiency of at least 1% was #446, which also was the only Cu-rich film in the series. It had a reasonably good short circuit current of 14.4 mA/cm^2, but the cell was severely limited by its extremely low open-circuit voltage of 0.2 V.

Since the first growth series was unsuccessful with a Cu-rich initial stage, we decided to make the initial stage of the next set of runs Ga-rich using our Modified Three-Stage Process. These films were completely processed at NREL and sent back to the University of Florida for electrical characterization. The device parameters are compiled in Table 5-2. An unsuccessful absorber from the previous series, namely #447, and #455-F with a buffer layer added by UF were also sent to NREL to be processed to check the effectiveness of our CBD CdS process. Device #447 showed an efficiency of over 2% with the NREL buffer layer and #455-F had less than half the efficiency of #455, which was completely processed at NREL (1.5 vs 3.3%). No Ga-rich cells were effective; only near stoichiometric and Cu-rich cells showed efficiency greater than 1%. The best cell, #452, had a similar J_{SC} to #446 and a marginally better FF (39% compared to 34%), but its V_{OC} (0.64 V) was much larger resulting in a cell with an efficiency of 3.4%. The slightly Ga-rich cell with a Cu/Ga ratio of 0.97 had the highest J_{SC} of 17.6 mA/cm^2,

but suffered from a lower V_{OC} (0.44 V) and FF (33%) resulting in a lower efficiency of 2.6%. This was also the only absorber that incorporated an initial GaSe layer rather than a Ga-rich layer. The device made from absorber #455 had very similar results to #452 with the only difference being a slightly lower V_{OC}.

All films in the third growth series were either near-stoichiometric or Ga-rich. This growth run series represented the first attempt at using a three-stage growth process in the PMEE reactor. All films received a CBD CdS buffer layer at the University of Florida and then were sent to NREL for processing. All of these devices had efficiencies less than 1%.

Since all successful absorber films grown in the PMEE reactor up to this point were Cu-rich or nearly stoichiometric, we decided to investigate Cu-rich films for device fabrication. This is less than ideal since it requires a cyanide etch to remove the copper selenide secondary phase before buffer layer deposition or the heterojunction will be shorted. The same film processes that had been investigated previously that gave efficiencies greater than 2% were repeated at a slightly higher growth temperature of 412°C. An absorber (#516) that employed the constant copper rate process was also added to see if Ga grading was necessary at a low growth temperature. Table 5-3 shows that all the cells ranged from 2 to 3% efficiency, except for device #513, which started Cu-rich and had a slightly Ga-rich overall composition. It had the lowest J_{SC} and V_{OC} for any of the cells. All the other cells were Cu-rich and had initial GaSe or Ga-rich stages. The most efficient device, #514 with $\eta = 2.9\%$, did not have the highest V_{OC} or J_{SC} in the series, but did have the highest fill factor (64%) of any CGS cell grown by PMEE up to that point. The V_{OC} or J_{SC} of these cells were not better than best of the previous growth series, but across the board these devices all had higher fill factors than had previously been achieved.

Shafarman et al. observed an increase in V_{OC} and FF with an elevated substrate temperature for three different deposition processes. The uniform deposition process gave poorer device performance at 400°C than the Cu-rich growth processes, despite comparable grain sizes in the films. At higher temperatures, there is no advantage to the Cu-rich growth even with increased grain size at 550°C [130]. In general, lower device efficiency with reduced substrate temperature cannot be simply described by changes in grain size, surface morphology, or the availability of sodium. The lower open-circuit voltage and increased recombination current indicate a greater density of intra-grain trap states.

Since high quality copper gallium diselenide films are typically grown at substrate temperatures above 500°C, we felt that we needed to increase the maximum growth temperature employed in the PMEE reactor. We felt that a gap temperature of 900°C, which correlated to a substrate temperature of 491°C, would be a safe maximum operating temperature in our system. This elevated temperature helped us achieve a cell efficiency of greater than 5%. The device parameters of the best CGS cell (#523) grown in our PMEE reactor are shown in Table 5-4 along with the other devices in this growth series. This cell showed an efficiency of 5.3% with J_{sc} = 16.9 mA/cm^2, V_{oc} = 0.476 V and F.F. = 65.5 %. These results are quite good considering the approximated thickness of this sample, possibly only 0.6 μm. Device #521 was very similar to 452 with the highest V_{OC} within this growth series at an elevated temperature, but also suffered from a very low FF. The film that started Cu-rich with a Ga-rich layer added afterwards showed very poor performance because of an extremely low FF. The dark and illuminated I-V curves for device #523 are shown in Figure 5-1.

Rockett et al. showed that the efficiency of devices is improved significantly by the presence of Na during growth. Sodium does not seem to have a specific ongoing effect in

devices; it is only important during film growth to improve the crystal quality. The amount of sodium that is incorporated into a film is dependent on the temperature of the substrate. There can be as much as a 50% increase in device efficiency with Na addition, decreasing at both higher and lower concentrations. Primary improvements are in V_{OC} and often in FF with little or no change in collected current [135].

The quantum efficiency (QE) characteristics of two high-efficiency ZnO/CdS/CGS solar cells measured at UF are shown in Figure 5-2. Both absorbers of #452 and #523 were grown in our PMEE reactor and the CdS buffer layer, ZnO window layer and metallization were prepared by NREL. The comparison of QE characteristics of the two devices shows that the spectral response of #523 in the range of short wavelength (<500 nm) is similar to that of #452, but in the range between 500 and 740 nm, it is much better than that of #452. This means that the improvement of device efficiency (5.3%) in #523 is mainly caused by the improvement of absorber quality. Also, the cut-off wavelength (~ 740 nm) indicates the band gap of the CGS absorber is around 1.7 eV.

The three-stage process may be more ideal in the PMEE reactor at an elevated temperature so we attempted to grow Cu-rich and near-stoichiometric absorber films by the Emulated Three-Stage Process at 491°C. All the films grown by Emulated Three-Stage Process resulted in devices with efficiencies less than 2% as shown in Table 5-5. They suffered from very low short-circuit currents (all less than 10 mA/cm^2), but a V_{OC} of 0.57 V was achieved by device 540. For films #541 and #542, the same process that was used for #523 was repeated, but with the goal of an even higher Cu/Ga ratio to see if an extremely Cu-rich absorber can make a good device after being etched. Device #542, which was grown at 465°C, had a smaller FF than #523

and this resulted in a reduced efficiency while #541 had a larger V_{OC}, but a much smaller FF leading to an efficiency of only 3.1%.

We intended to replicate the process used to grow our most efficient CGS absorber for Sample #634 and Sample #641, but with a thicker absorber layer of 1.5 and 2.0 microns, respectively. The actual thickness was more likely to be about 1.2 and 1.7 μm. We also needed to reduce the substrate temperature to 440 °C to avoid the apparent warping of the rotating platen that seems to be taking place at the higher growth temperature. Table 5-6 shows that the efficiency results for these two cells were unexpectedly low. This may have been the result of limiting the substrate temperature, but they still were not as efficient as the devices that used CGS absorbers grown at 386°C. So it is more likely that the poor film quality demonstrated in the previous chapter is the real reason for the low efficiency. We were able to produce Ga-rich films that led to photovoltaic cells of modest efficiency (see Device #628 and Device #630 in Table 5-6), which generated the highest open-circuit voltages for our CGS cells to date.

Device #634 showed the highest shunt resistance, R_{SHo} = 669 Ω-cm, but it also suffered from a high series resistance of 25 Ω-cm. The best device (#630) had a series resistance of 16 Ω-cm and a shunt resistance of 334 Ω-cm. Device #636, with the lowest R_{So} = 8 Ω-cm, was also destroyed by shunts (R_{SHo} = 12 Ω-cm). The goal is to get a very low series resistance and a very high shunt resistance, for example like R_S = 1.1 Ω-cm and R_{SH} = 3000 Ω-cm in the world record 15% CIS cell [142]. The loss of power due to series resistance is manifested as a drop in FF.

These measurements were done at NREL and they also performed air annealing of two of the devices at 200°C for 2 minutes. The device parameters of #639 improved upon annealing. The V_{OC} improved greatly to 0.60 V, while the FF increased slightly to 56% and the J_{SC} remained unchanged to give an improved efficiency of 2.3%. Device #628 saw its FF decrease

slightly with an increase in V_{OC} to nearly 0.8 V resulting in an efficiency that was nearly the same. A less efficient cell on the same device (#628) saw its V_{OC} increase from 0.77 V to 0.82 V. The J_{SC} for this cell is extremely low at about 5 mA/cm^2. This is likely due to a very high series resistance of 31 Ω-cm. The shunt resistance, R_{SHo} = 477 Ω-cm, was one of the highest of our CGS devices that were tested at NREL.

Kniese et al. observed, using co-evaporation of single elements in an in-line deposition process at a high growth temperature, that Ga-rich CGS grown by a single layer process (7.2%) produced better efficiencies than that grown by a bilayer-like process (6%). The single layer process exhibited a slightly larger V_{OC} and a much larger FF [137]. The reduced J_{SC} and increased FF indicate that there is a difference in the minority carrier collection behavior in the two cells.

The final CGS absorber growth series was completely fabricated into devices in-house at the University of Florida by the procedures described earlier. Table 5-7 shows the results from the I-V characterization of these cells. Only the absorbers with Cu/Ga ratios of greater than one were etched with KCN. None of the as-grown Cu-rich or stoichiometric absorbers produced working solar cells, but we were able to produce our most efficient Ga-rich CGS device. Device #640 featured an absorber grown by the Emulated 3-Stage Process resulting in a 4.9 % efficient cell. We also produced a 4.2 % efficient solar cell from a Ga-rich absorber (#655) grown by the Constant Cu Rate Process. The photo I-V curves for these two devices are shown in Figure 5-3 and Figure 5-4, respectively. The short-circuit current and open-circuit voltage of device #640 are comparable to our best CGS device (#523), but the FF is slightly smaller (57% as compared to 66%). The V_{OC} of each of these cells is still too low for a wide band gap absorber like CGS.

Improvement in this area would likely produce devices with a much higher conversion efficiency.

Conclusions

The best CGS cell produced in the PMEE reactor was fabricated from an absorber grown at the highest allowable substrate temperature, 491°C. Although substrate temperature was not the only factor that limited device performance, it was a key problem. The best cell was rather thin, approximately 0.6 μm, so a thicker absorber under the same conditions should produce a more efficient device. Device annealing should improve the low open-circuit voltage of our devices as can be seen in the gains achieved by the devices that were annealed at NREL. We also demonstrated the ability to completely manufacture CGS devices within our own facilities at the University of Florida. This research effort also produced the most efficient cell fabricated from a Ga-rich CGS absorber. Thin films deposited by both the Emulated Three-Stage Process and the Constant Copper Rate Process were made into devices with conversion efficiencies greater than 4%. Maximum device parameters were achieved on different cells: J_{sc} = 17.6 mA/cm^2 (#457), V_{oc} = 0.82 V (annealed #628), F.F. = 65.5 % (#523), and η = 5.3 (#523).

Table 5-1. Device parameters of record CGS cells produced at NREL.

Device	V_{OC} (V)	J_{SC} (mA/cm^2)	FF (%)	Efficiency (%)
Surface-modified	0.823	18.6	66.8	10.2
Previous record	0.905	14.9	70.8	9.5

Table 5-2. Device parameters for the second CGS absorber growth series.

Device #	V_{OC} (V)	J_{SC} (mA/cm^2)	FF (%)	Efficiency (%)
447	0.536	9.8	40.7	2.1
452	0.640	14.3	38.8	3.4
453	0.355	8.7	32.0	1.0
454	0.310	8.0	33.7	0.8
455-F	0.265	16.7	34.8	1.5
455	0.589	14.5	38.8	3.3
457	0.437	17.6	33.2	2.6

Note: Film #447 was from the first growth series and 455-F had a CdS buffer layer deposited at UF. #456, #458, and #459 showed very low efficiencies.

Table 5-3. Device parameters for the fourth CGS absorber growth series.

Device #	V_{OC} (V)	J_{SC} (mA/cm^2)	FF (%)	Efficiency (%)
510	0.413	11.9	40.8	2.0
511	0.323	15.0	49.3	2.4
512	0.343	11.3	50.1	2.0
513	0.244	7.2	47.6	0.8
514	0.383	12.0	63.7	3.0
515	0.292	13.7	54.0	2.2
516	0.417	9.4	59.1	2.3

Table 5-4. Device parameters for the fifth CGS absorber growth series.

Device #	V_{OC} (V)	J_{SC} (mA/cm^2)	FF (%)	Efficiency (%)
521	0.530	12.6	33.5	2.2
522	0.396	11.4	65.2	2.9
523	0.476	16.9	65.5	5.3
524	0.436	13.7	58.2	3.5
525	0.367	10.9	15.4	0.6

Table 5-5. Device parameters for the sixth CGS absorber growth series.

Device #	V_{OC} (V)	J_{SC} (mA/cm^2)	FF (%)	Efficiency (%)
535	0.444	6.9	45.8	1.4
536	0.421	7.8	44.9	1.5
537	0.478	6.5	45.8	1.4
538	0.454	11.9	35.8	1.9
540	0.571	8.3	37.6	1.8
541	0.557	14.5	38.4	3.1
542	0.481	17.2	54.0	4.5

Table 5-6. Device parameters for the seventh CGS absorber growth series.

Device #	V_{OC} (V)	J_{SC} (mA/cm^2)	FF (%)	Efficiency (%)
628	0.702	6.2	56.0	2.4
629	0.307	3.5	46.9	0.5
630	0.621	10.1	47.8	3.0
634	0.435	4.0	51.8	0.9
635	0.201	7.2	41.9	0.6
636	0.075	7.3	27.9	0.2
637	0.095	4.2	31.2	0.1
638	0.172	8.2	39.7	0.6
639	0.423	6.7	50.0	1.4
641	0.287	7.4	45.5	1.0

Note: I-V characterization was done at NREL.

Table 5-7. Device parameters for the eighth CGS absorber growth series.

Device #	V_{OC} (V)	J_{SC} (mA/cm^2)	FF (%)	Efficiency (%)
640	0.502	16.9	57.4	4.9
647	0.480	13.7	55.7	3.7
649	0.426	16.8	46.3	3.3
655	0.516	14.2	57.8	4.2

Note: Device fabrication was done at UF.

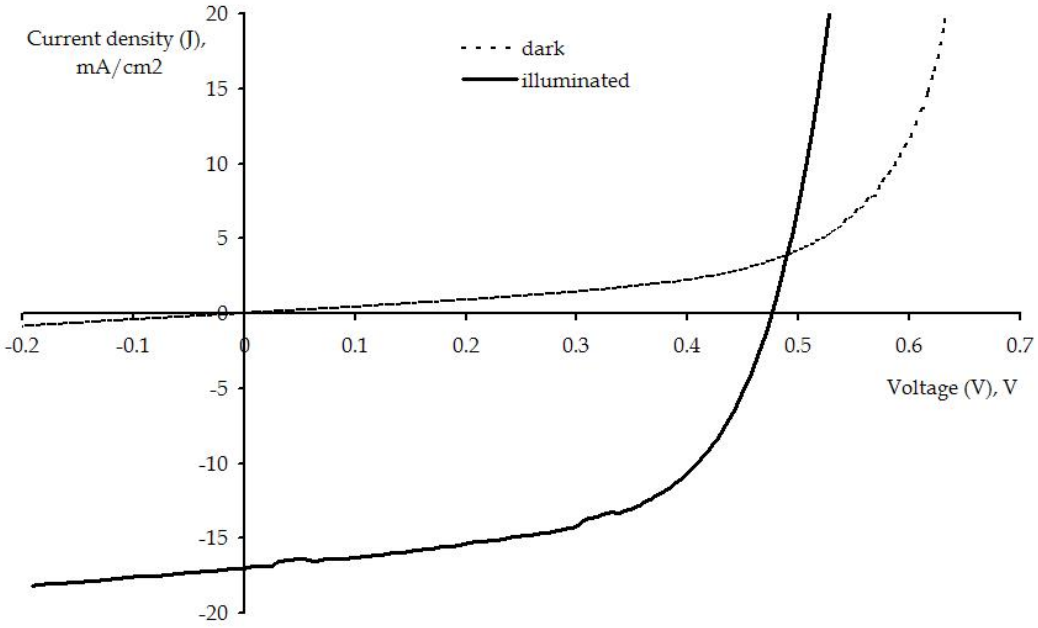

Figure 5-1. Dark and illuminated I-V curves for Device #523.

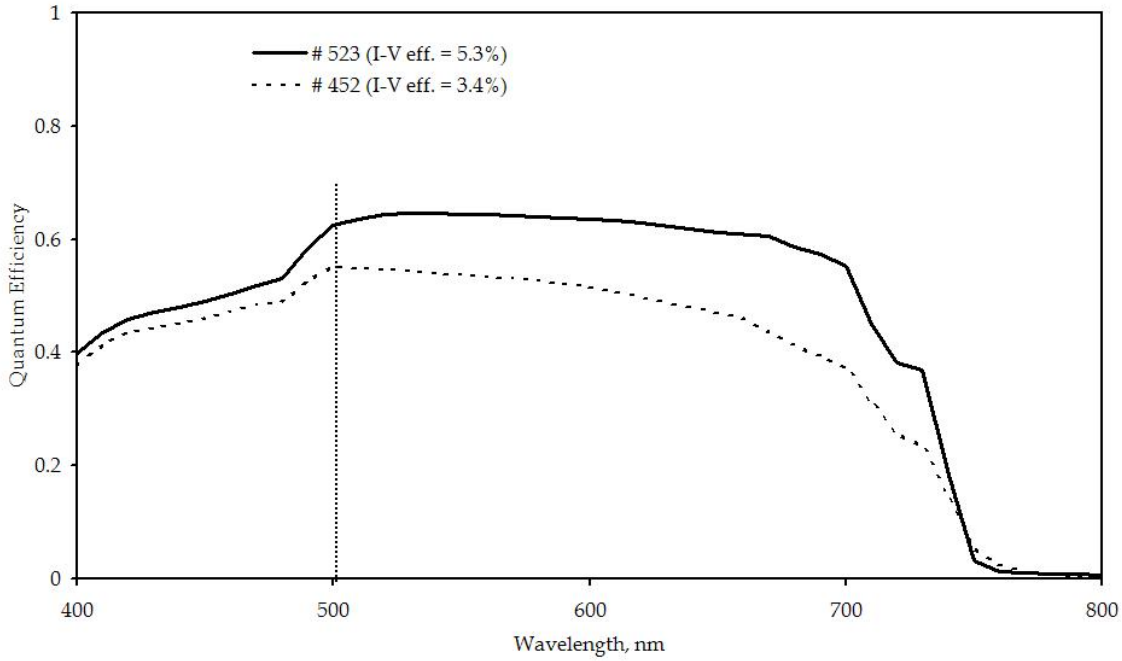

Figure 5-2. Spectral response curves comparing Device #523 and #452.

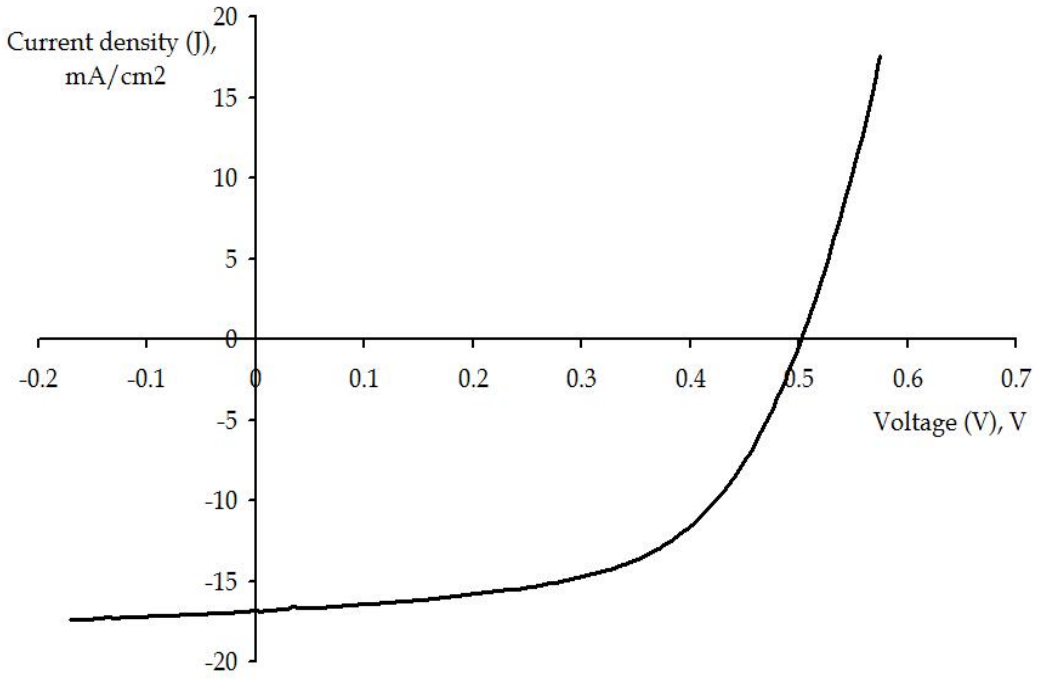

Figure 5-3. Photo I-V curve for Device # 640.

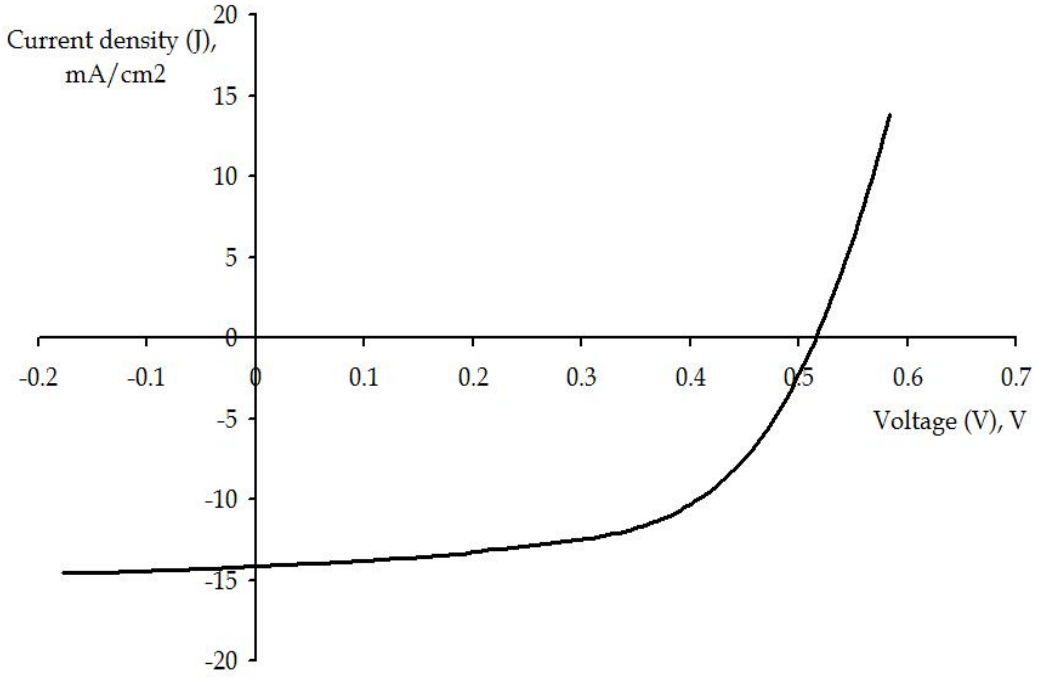

Figure 5-4. Photo I-V curve for Device # 655.

CHAPTER 6
CIGS ABSORBER GROWTH AND DEVICE FABRICATION

So far, achievements in optimizing absorber growth have mainly been directed by intuition; the understanding of CIGS film growth seems to be limited. Voltage differences that could not be accounted for by band gap variations were found to have excellent correlation with trap densities within the CIGS [142]. The performance disparities between devices made using absorber layers fabricated in various facilities may be explained by this assortment of defects. The three-stage process currently leads to the best solar cells produced in the literature. Methods that are used to form epitaxial films, such as MBE or MOCVD, have revealed interesting features for fundamental studies, such as phase segregation and defect formation, but cannot be used to form the base material for high-efficiency solar cells [36].

Best Devices in the Literature

The world record $Cu(In_{1-x}Ga_x)Se_2$ small-area device fabricated at NREL has an efficiency of 19.5% (V_{OC} = 0.694 V, J_{SC} = 35.2 mA/cm^2, FF = 79.7%) [146]. The band gap for this absorber is 1.14 eV (x~0.3). NREL also had the first research team break the 20% efficiency barrier for thin film solar cells: a CIGS cell with η = 21.1% at 14X concentration [106]. The most efficient CIS cell fabricated at UF from an absorber grown in the MEE reactor had previously been 7.1% (V_{OC} = 0.376 V, J_{SC} = 31.0 mA/cm^2, FF = 0.61%) [3].

Growth Matrix

Maximum performance of $Cu(In_{1-x}Ga_x)Se_2$ is attained within an optimum atomic compositional range. This is true for the deviation from stoichiometry (Cu/III ratio) and for the Ga content (x), which directly affects the band gap. Increasing the Ga content mainly increases the band gap by shifting the conduction band position. The composition window is 0.88 < [Cu]/([In]+[Ga]) < 0.95 and [Ga]/([In]+[Ga]) ~ 0.3. Small variations in band gap (or Ga content)

can lead to measurable changes of performance (Contreras, CIGS11). In cell designs with homogenous composition, the optimum Ga/(In+Ga) ratio is a trade-off between V_{OC} and J_{SC} [147].

The use of Ga/(Ga+In) profiles has been found to increase the efficiency of CIGS thin film solar cells [136]. The obtainable composition profiles are strongly dictated by the deposition method. The objective is to vary the band gap in a manner to simultaneously design a lower band gap to enhance the absorption along with a higher band gap to improve the voltage in the same device. By introducing a Ga gradient in the film with higher Ga concentration near the back contact, a back surface field is created. The effect of this back surface field has been observed as an increase mainly in the V_{OC} of the solar cells. Additionally, when thinning down the CIGS film, the back surface field has been found to be efficient in reducing V_{OC} and FF losses caused by the limited thickness of the sample. In order to optimize the Ga profiles, the interdiffusion and intermixing properties of In-rich and Ga-rich CIGS compounds must be taken into account.

An absorber with normal profiling is one where the band gap is increased from front to back [106]. To utilize normal profiling in CIGS, higher Ga content must be added toward the back of the CIGS absorber. This will result in an increase in the conduction band edge and the attainment of an effective force field repelling minority carriers from the back contact. Linear graded absorbers show a correlation between V_{OC}, J_{SC}, and the slope of the grading [148]. The V_{OC} improves with higher Ga contents in the front part of the absorber, while the J_{SC} is affected by the minimum Ga content, but also strongly by the electric fields that determine the current collection.

The double profiling structure incorporates normal profiling plus an inverse profiling in the region adjacent to the surface of the film. A particular case of this double profiling is a notch structure: a low band gap material sandwiched between two wider gap materials. The possibility of attaining higher open-circuit voltages due to the presence of a wider band gap absorber material at the junction structure has potential for optimized photon absorption. The two energy gaps at the front of the double profile structure can be engineered to match certain bands of the terrestrial solar spectrum in order to capture more efficiently from the blue and red spectral regions. The improved quantum efficiency in such a device will translate into enhanced current generation. An additional enhancement of current generation could also come from a field-assisted collection where the increasing conduction band edge found towards the back of the absorber can provide an effective force field for electrons drifting toward the back contact. Devices incorporating a double profiling absorber preserve the high V_{OC} values attained in the normal profiling devices and yield higher J_{SC} for comparable effective band gaps. This can be explained from the enhanced spectral response of the double-profiling structure. Enhancements in V_{OC} and FF could be explained by the reduced dark-current due to the grading in the absorber [106]. In multi-graded absorbers, the absorption and by this, the current, is dominated by the minimum band gap if proper current collection is guaranteed. Furthermore, it has been shown that V_{OC} is correlated to the band gap in the space charge region [148].

In most ungraded solar cells, there is no drift force outside the depletion region to help carriers move toward the junction to be collected. They must rely on diffusion to collect carriers generated outside the depletion region and if the carriers are generated much further than a diffusion length away from the edge of the depletion region, they have only a small probability of being collected. Modeling of an increased band gap in the depletion region showed an

increase in V_{OC} [91]. The uniform incorporation of Ga into the absorber raises the band gap and increases the V_{OC} with this higher V_{OC} being the primary goal of any alloying attempts. Device performance may be further enhanced by nonuniform incorporation. However, graded structures that significantly degrade performance may just as easily result. Therefore, it is important to understand how different compositional profiles arise from different sequential processing steps, and what effects these profiles have on device performance. Material and device parameters other than the band gap vary with composition such as carrier concentration, mobility, diffusion lengths, types of intrinsic defects, and band offsets with CdS.

The price and availability of indium will become a dominant concern for the photovoltaics industry when larger scale production of CIS-based solar cells gets under way. Most high-efficiency CIGS absorbers are currently grown to a thickness of about 2 to 2.5 microns [89]. One way to lessen the need for In would be to reduce the thickness of the absorber layer by at least 50%. Lundberg et al. found that approximately 1% absolute efficiency was lost by reducing the CIGS thickness from 1.8 microns down to 1 micron at the same growth rate [149].

A small growth series was implemented to test the feasibility of $CuIn_{1-x}Ga_xSe_2$ growth in the PMEE reactor. These growth runs were accomplished at a time when the reactor was able to withstand a substrate temperature of 491°C. The details are located in Table 6-1. The Constant Cu Rate Process was used for the deposition of these films because of its simplicity and this leads to ungraded CIGS absorbers. Four different CIGS films were grown with varying thickness with x ~0.3. They ranged from about 0.8 to 1.9 μm. Then x was varied from 0 to 0.4 for films grown slightly thinner than 1 μm (about 0.9 for the CIGS films and about 1.0 for the CIS film). The growth rate varied from about 0.9 to 1.6 Å/s. All of the absorbers were exposed

to the cyanide etch to ensure that no copper selenide secondary phases would be present on the surface.

Absorber Characterization

Orientation

The X-ray diffraction pattern for film #582, as seen in Figure 6-1, showed a slightly stronger (204)/(220) double peak than (112) peak and a much weaker double peak of (116)/(312) orientation. Several additional peaks, which could be clearly ascribed to the CIS structure as well, were very weak and therefore not used for evaluation. The orientation of single step CIGS films did not seem to be dependent upon any of the growth parameters: Cu/(Ga+In) ratio, Ga/(In+Ga) ratio or thickness. The films grown at various thicknesses displayed different diffraction patterns (Figure 6-2), but the orientation did not seem to be related to the thickness. The thinnest film, #575, showed a strong (112) peak, while #578 had a strong (204)/(220) double peak. The film with the greatest thickness, #579, had a very strong (112) peak. The Ga content also seemed to have no specific effect on orientation as can be seen in Figure 6-4. CIGS films with Ga/(Ga+In) ratios from 0 to 0.4 had different diffraction pattern, but no specific trend was followed. This was also true for the Cu/(Ga+In) ratio where a Cu-poor and near-stoichiometric sample are compared in Figure 6-3. As will be revealed below from the literature, orientation strongly depends on substrate type, Se flux ratio, and growth temperature, but preferred orientation in the absorber is not a necessary requirement for attaining high-efficiency.

The high-efficiency CIGS absorbers produced at NREL display a <220/204> type of preferred orientation [150]. They had a ratio of XRD intensity of the <220/204> peak over the <112> peak of ~15.4. Previous absorbers grown at NREL and from other groups have typically been either randomly oriented or, in some cases, (112) oriented [151]. The <220/204> preferred orientation in CIGS is obtained when using relatively high Se overpressures, such as an atomic

flux of Se that is at least four times the flux of the metals. The <112> preferred orientation was obtained using Se overpressures below this value [150].

Precise control of the elemental composition of Se in the vapor flux is not easy to obtain due to the low sticking coefficient of Se. The sticking coefficient of Se onto the substrate increases significantly when adding even small metal fluxes. Umeno et al. have shown that the Se/metal flux ratio affects grain growth and the orientation of the bulk region in CIGS. Precise control of the Se/metal flux ratio is important for improving the crystallinity and thus the device performance [152]. Hanna et al. showed that the Se to metal flux ratio (SMR) has an effect on films deposited at different growth rates. The best devices obtained from fast processes (25 minutes) had an SMR of 4.5, while a higher SMR of 13.5 was required in order to obtain comparable results from slow processes (75 minutes) [153]. All samples were going towards the (220/204) orientation with increasing SMR, which is in agreement with the observations by Contreras. In order to compensate for the lack of Se in the vapor phase, growing CIGS films form additional metal-rich segregations, which lead to shunts in the solar cell. In addition, layers prepared at low SMRs lose indium by way of the formation of the volatile compound, In_2Se.

Growth temperature can also have an effect on the preferred orientation of films grown by the three-stage process. Contreras et al. showed that when Cu is incorporated using a substrate temperature of ~400-500°C, the resulting CIS films consistently present a (220/204) preferred orientation. On the other hand, when Cu deposition occurs at a substrate temperature greater than 500°C, the films begin to show random orientation or somewhat of a (112) texture [154].

At low temperatures, the Na diffusion from the glass to the CIGS layer is suppressed. Lammer et al. observed that a reduction of deposition temperature leads to a total loss of (112) preferential orientation. Na co-evaporation leads to a more pronounced (220/204) orientation, as

normally seen in films for high-efficiency devices [155]. Hanna noted a high Na supply at the beginning by a NaF precursor layer or a strongly reduced Na supply by a Na barrier layer promotes (112) orientation. A fair amount of Na at the beginning of the process as supplied by the standard substrates leads to a (220/204) orientation, for all SMRs [153]. But Contreras believes that sodium, when present at a critical level, can hinder the attainment of the (220/204) preferred orientation. The NREL group says that (220/204) preferred orientation can be attained for Cu-poor materials, but Cu-rich films grown under similar growth conditions tend to be randomly oriented [154].

Morphology

Shafarman et al. showed that at lower temperatures, the uniform flux process appears to give more columnar grains and a smoother surface than CIGS films with a Cu-rich growth period. There is no apparent difference between films grown with Cu-rich flux at either the beginning or middle of deposition [130]. Typical characteristics of the high-efficiency absorbers grown by the three-stage process are a compound grain structure observed in the cross-section view and faceted grains that are visible in plan view [156].

Device Fabrication

The typical device fabrication procedure for highly-efficient CIGS devices at NREL uses CdS deposition where the CIGS thin film is immersed at room temperature and the temperature of the bath is increased to 60°C [156]. 50-60 nm were deposited in 16 minutes. A 90 nm thick undoped ZnO layer and a 120 nm Al_2O_3-doped ZnO layer were deposited. Ni/Al grids were deposited by e-beam evaporation. The total cell area was 0.408 cm^2. A 100 nm MgF_2 film is deposited as an anti-reflective coating.

Our CIGS films were fabricated completely at the University of Florida and had $Zn_xCd_{1-x}S$ buffer layers, instead of the traditional CdS buffers, deposited on them after absorber growth.

The CIGS films were cut into 1" x 1" samples and vacuum-sealed after their removal from the vacuum chamber, and they remained so until the buffer was deposited by CBD. All the CIGS films were etched in a 10% solution of potassium cyanide for five minutes. The procedure for the CBD deposition of $Zn_xCd_{1-x}S$ is exactly the same as the one that we used for CGS as described in Chapter 5.

The window layer consisted of a magnetron sputtered 600 nm Al-doped ZnO layer just like the in-house fabricated CGS devices. The sheet resistance of the characterization TCO film grown along with the fabricated devices is approximately 20 Ω/square. Cells were completed by evaporation of a Ni (50 nm)/Al (0.3 μm) contact grid and finally defining the cells (0.429 cm^2) by mechanical scribing. No anti-reflective coating is added. For I-V measurement purposes, part of the CIGS layer away from the grid was scratched off and an In contact was added to the Mo surface.

Device Characterization

The reference cell method of calculating the illuminated I-V curve described in Chapter 3 was implemented to measure the electrical properties of the CIGS devices. One problem was that the controller that manipulated the operating temperature of the cell was broken. The temperature controller of the cooling system is usually set at ~20°C to keep the reading of the thermocouple and hence the temperature of the test cell at 25 ± 1°C. To rectify the situation, the system was allowed to cool down between measurement runs so that the thermocouple reading was maintained between 25 and 27°C throughout the testing period.

The calibration cell, namely S2049-A1 fabricated in November of 2002, with a total cell area of 0.408 cm^2 was measured on 3/22/04 at NREL with the following parameters for cell #2: V_{OC} = 0.661 V, J_{SC} = 33.73 mA/cm^2, FF =77.47 %, and η = 17.28 %. The goal of the reference method is to match the short-circuit current of the reference cell in our measurement system.

The distance between the lamp and the test cell was decreased when the measured J_{SC} was below 33 mA/cm^2. An acceptable solar simulator intensity was reached giving the following measured calibration cell parameters: V_{OC} = 0.642 V, J_{SC} = 33.62 mA/cm^2, FF =76.09 %, and η = 16.42 %. After the lengthy measurement period of all the cells on eight different CIGS devices with an area of 0.429 cm^2, the calibration cell was measured again to make sure there was no drift in the solar simulator intensity. The following parameters were measured for cell #2: V_{OC} = 0.643 V, J_{SC} = 33.56 mA/cm^2, FF =76.24 %, and η = 16.24 %. These results were satisfactory.

This initial CIGS absorber series produced some interesting results. The most efficient devices ever created in the PMEE reactor were the result of this growth plan. Table 6-2 shows the results of the IV characterization of the illuminated solar cells. Device #582, the $CuInSe_2$ absorber, showed an efficiency of 8.9%. It had a very high open circuit voltage of 0.46 V. Its J_{SC} = 30.5 mA/cm^2 and FF = 64% were also quite good. Figure 6-3 shows the illuminated I-V curve for #582. The highest fill factor (67%) for any device produced from an absorber grown in the PMEE reactor was achieved by #588 resulting in an 8.6 % efficient cell. Both of these films were grown to thicknesses around 1 μm. Figure 6-6 shows how the increased FF of device #588 compared to #575 leads to a higher conversion efficiency despite the fact that #575 has an elevated open circuit voltage. The illuminated I-V curve of device #588 is also compared to the CIGS calibration cell provided by NREL (Figure 6-7), which had a FF greater than 75 % and an efficiency greater than 16 %. Troubling, though, is the relatively poor efficiency of #586 and #587 since they were grown under almost identical conditions as #588.

Solar cell performance generally drops with substrate temperature [157]. Devices fabricated at low substrate temperatures, however, have realized efficiencies that do not fall below the minimum efficiencies obtained at 550°C [158]. Although the observed differences in

defect response between films grown at various temperatures may provide valuable insight into the differences between these materials, they are only one factor affecting device performance.

High-efficiency CIGS absorbers typically require the incorporation of 0.1 at% Na, which enhances the FF and V_{OC}. Rudmann et al. obtained a maximum cell efficiency of 13.8% using the post-deposition of NaF at a substrate temperature of 400°C, while a maximum efficiency of 14.9% was achieved for CIGS cells prepared on SLG at 580°C [159]. Rudmann's group also showed that solar cells with CIGS absorbers deposited on soda-lime glass with an alkali diffusion barrier and external Na incorporation showed a better efficiency (η=14%) than those grown on SLG without the barrier and no outside source of Na (η=12.8%). Cells without any Na showed much lower efficiencies (η=9.5%) [160].

Conclusions

A device with the highest efficiency for any absorber grown in the PMEE reactor was the result of this study. This nearly 9% cell was completely fabricated at the University of Florida revealing our improved processing capabilities. The best cell was produced at a less than ideal growth temperature, with a thickness of approximately one micron, and with no absorber or device annealing. The highest quality absorber also had no gallium content, but a CIGS absorber did result in a device with a slightly lower efficiency (η = 8.6%). This absorber was grown with the Constant Cu Rate Process resulting in no band gap grading, which means there is further room for improvement for CIGS cells.

Table 6-1. CIGS growth series.

Film #	Cu/III ratio	Ga/(In+Ga) ratio	Thickness (μm)
569	0.97	0.30	0.8
575	0.97	0.33	0.85
578	0.97	0.32	1.3
579	1.00	0.30	1.9
582	0.91	0	1.0
586	0.90	0.25	0.9
587	0.99	0.41	0.85
588	0.98	0.21	0.9

Note: All films were KCN-etched before device fabrication.

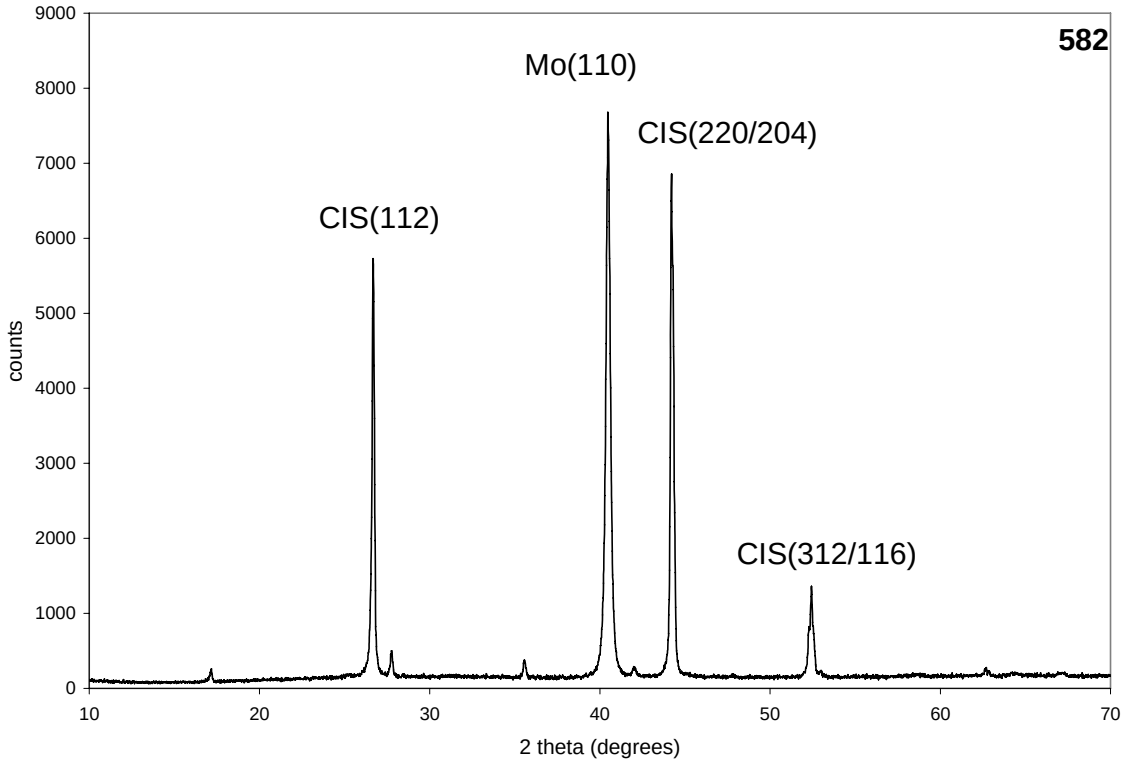

Figure 6-1. Diffraction pattern of CIS film #582.

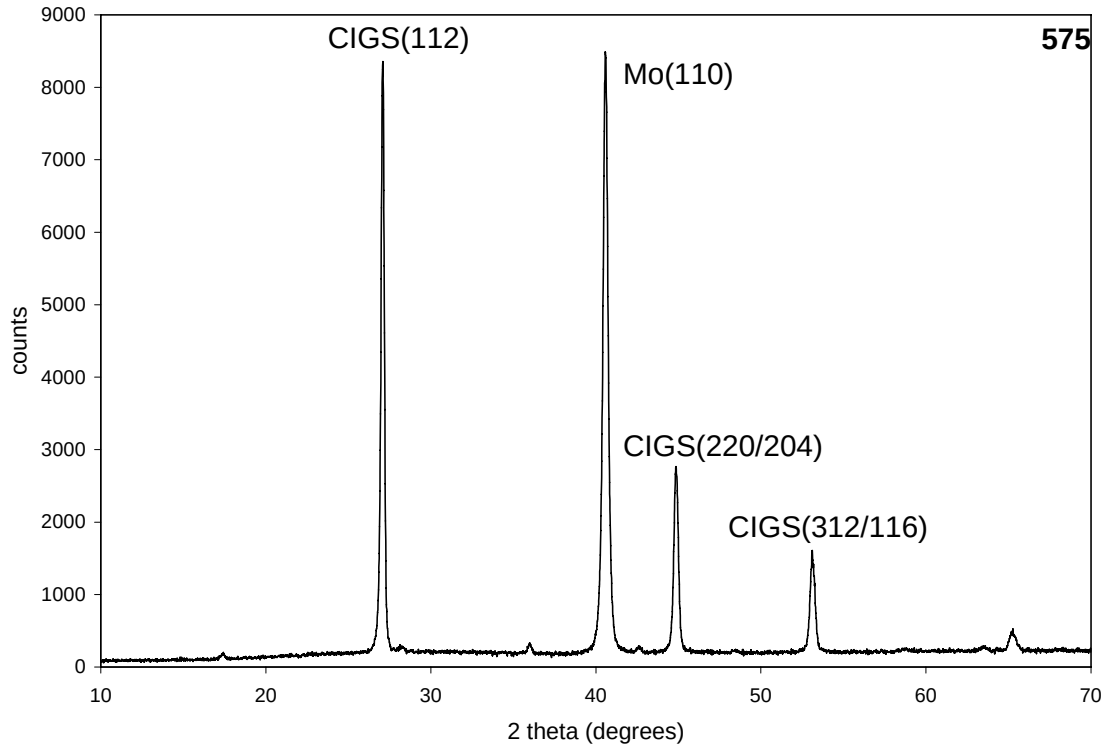

A

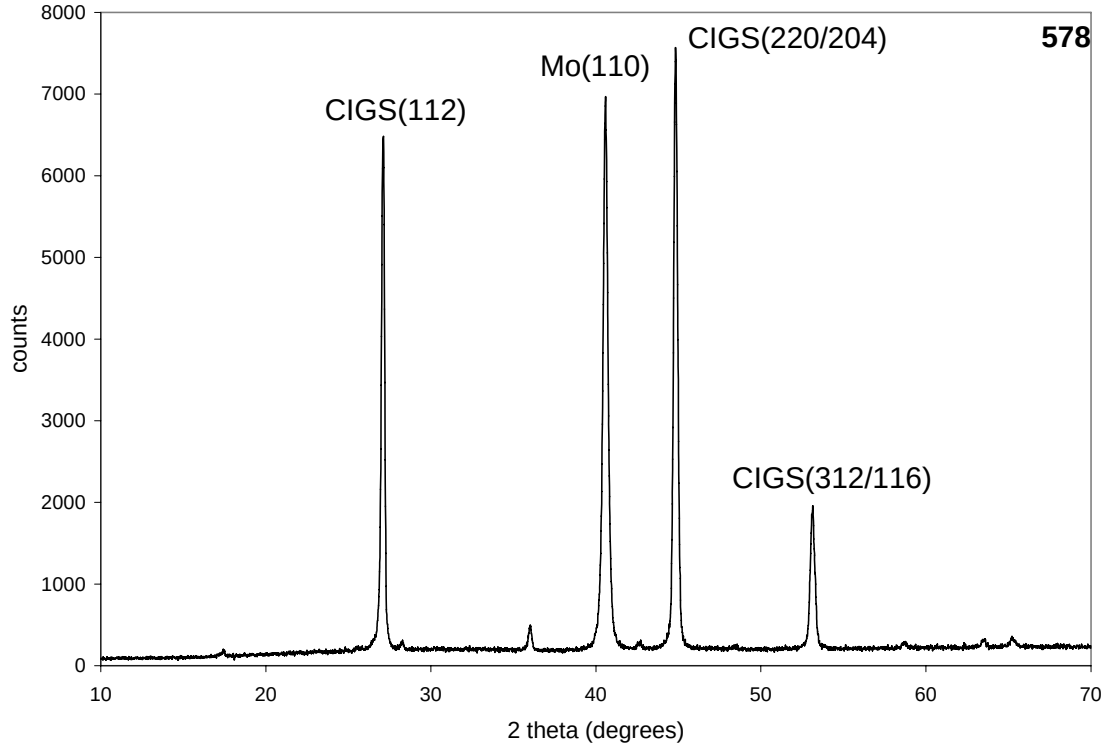

B

Figure 6-2. Diffraction patterns of CIGS films grown to different thicknesses. A) 0.9 μm. B) 1.3 μm.

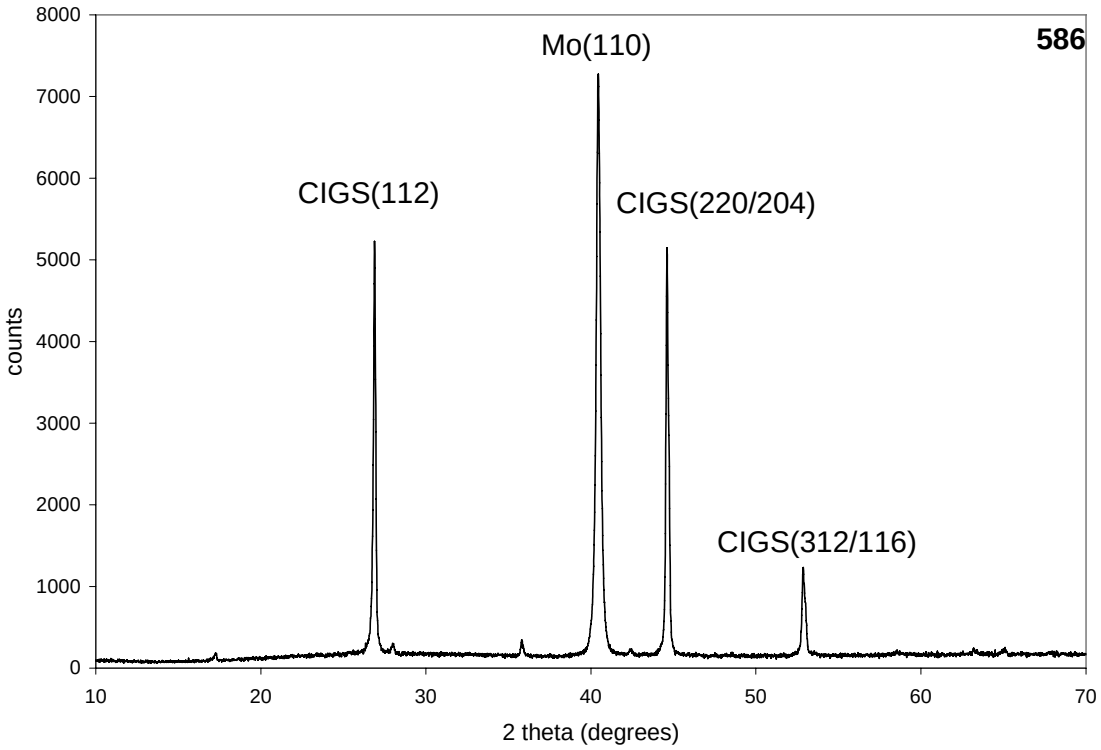

A

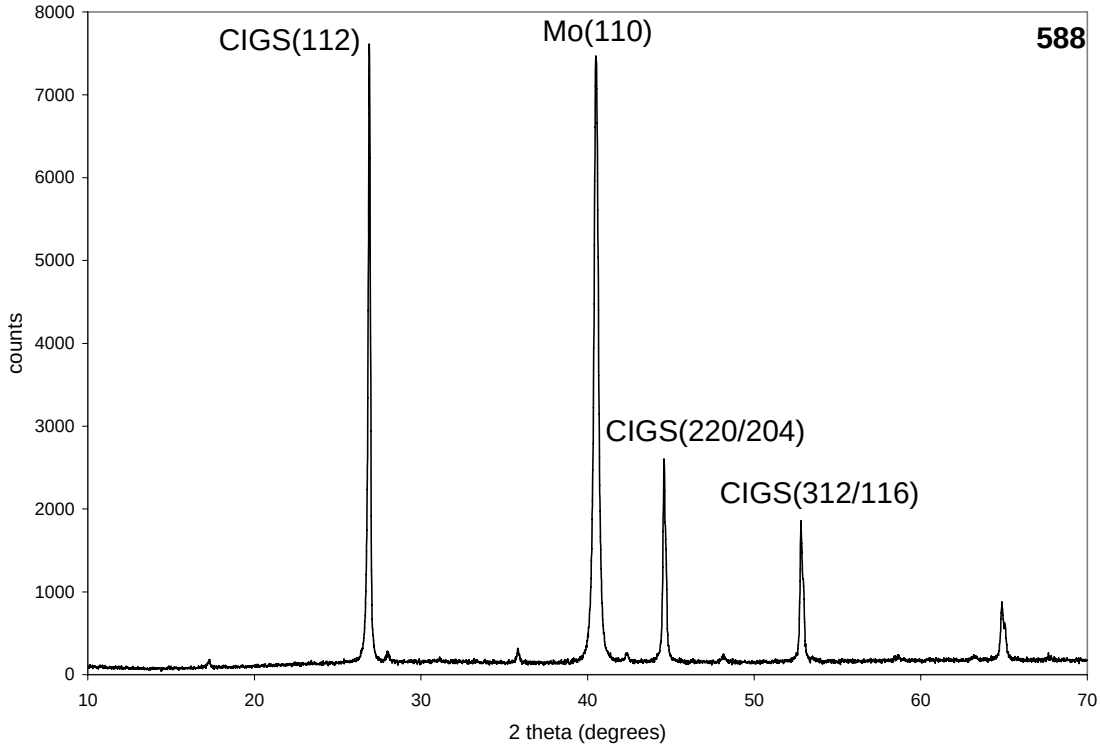

B

Figure 6-3. Diffraction patterns of CIGS films grown with different Cu/III ratios. A) Cu/III = 0.90. B) Cu/III = 0.98.

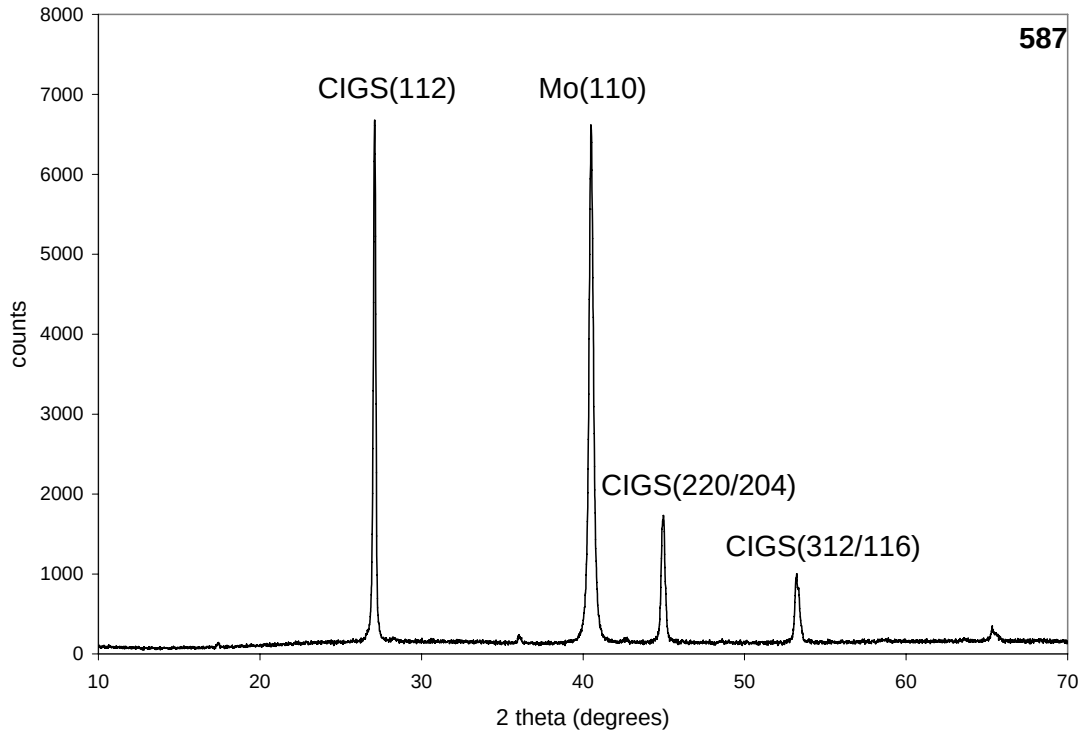

A

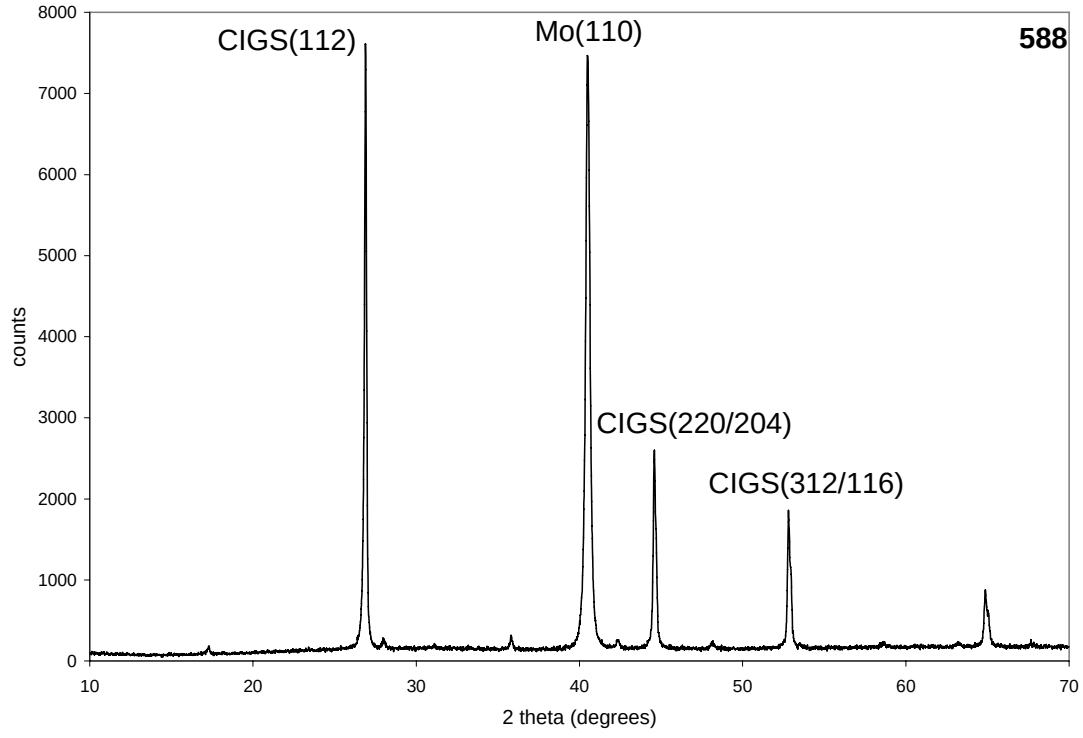

B

Figure 6-4. Diffraction patterns of CIGS films grown with different Ga/III ratios. A) Ga/III = 0.41. B) Ga/III = 0.21.

Table 6-2. Device parameters for the CIGS growth series.

Device #	V_{OC} (V)	J_{SC} (mA/cm^2)	FF (%)	Eff. (%)
569	0.457	24.3	39.4	4.4
575	0.476	26.3	55.5	7.0
578	0.325	26.6	34.2	3.0
582	0.457	30.5	64.0	8.9
586	0.317	21.3	26.8	1.8
587	0.308	18.1	41.7	2.3
588	0.437	29.3	67.0	8.6

Note: Device #579 gave no I-V characteristics.

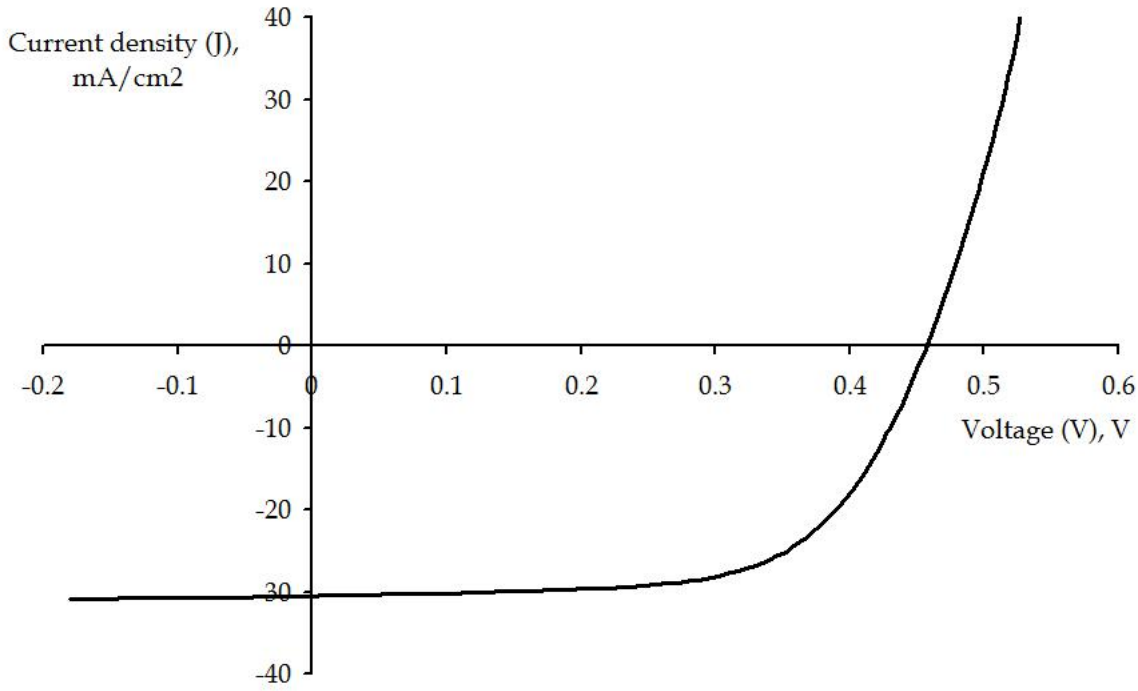

Figure 6-5. Illuminated I-V curve for Device #582.

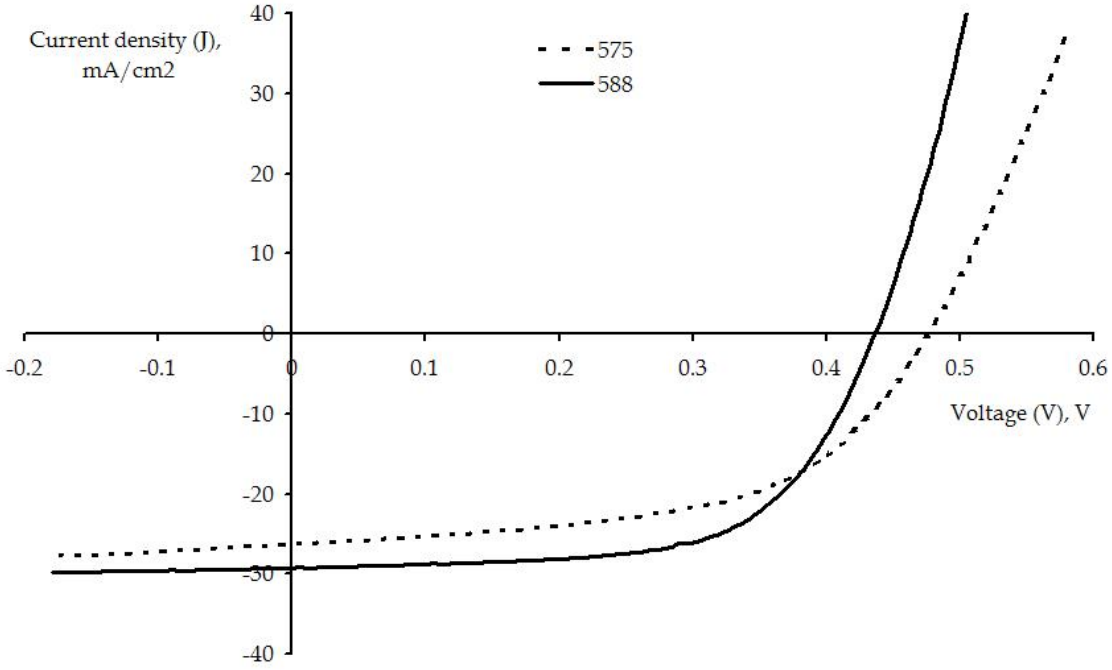

Figure 6-6. Comparison of illuminated I-V curves of Device #575 and #588.

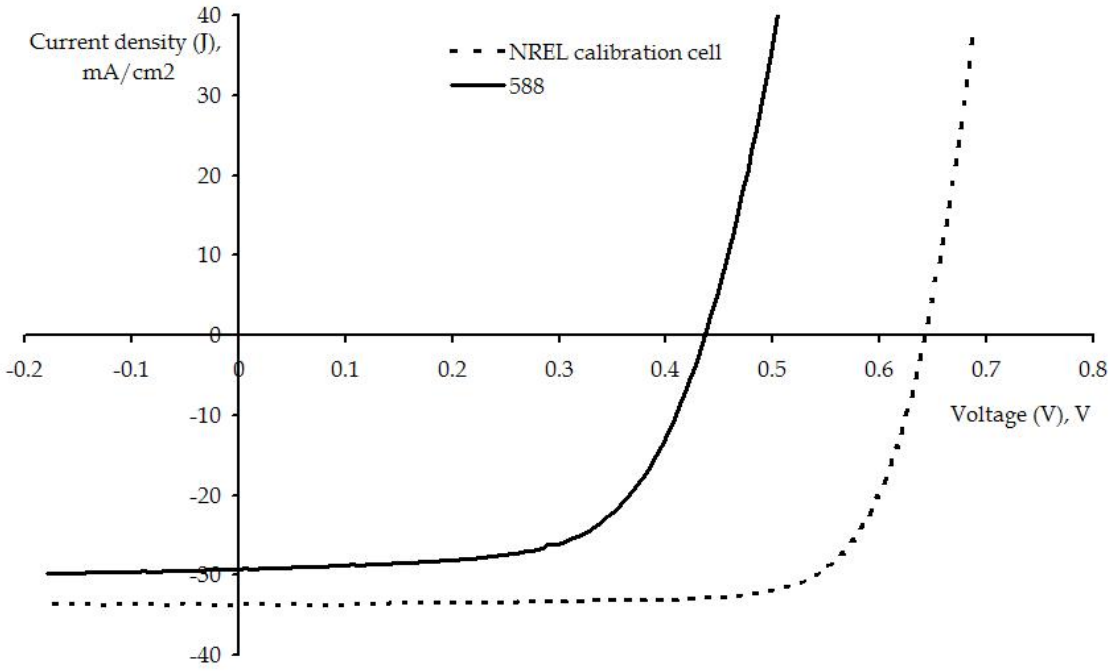

Figure 6-7. Comparison of the illuminated I-V curves of Device #588 and the calibration cell.

CHAPTER 7
DYNAMIC REACTOR MODEL

The prospect of real-time process control for the fabrication of CIS-based modules would accelerate the introduction of a profitable product. Continuous processing of material requires real-time control of the critical growth parameters. Active control in the deposition zone is required to prevent the drift in flux rates that would otherwise occur due to material depletion and dynamic heat redistribution in evaporative sources [161]. Process optimization, e.g. by design of experiments, requires reliable processing conditions, which in turn are only attainable if robust sensors and real-time, in-situ process control strategies are available. A high level of control would lead to a substantial increase in manufacturing yield and further optimization of cell efficiency [162].

The process to be modeled is a rotating disc molecular beam epitaxy reactor. As the high purity raw materials required for MBE growth become more costly, the run-to-run repeatability of the process, as well as the improved uniformity over larger surface areas, becomes increasingly important. The behavior of the thermal effusion sources used in such systems is very non-linear due to the exponential relationship between the rate of evaporation and temperature. Under high vacuum conditions, the case in a MBE reactor, the mean free path of particles is very large and thus molecular flow conditions prevail through most of the reactor. The process dynamics of this reactor should correlate well with an in-line vacuum process.

Flux Modeling

The three sources in the PMEE reactor whose performance is critical to the quality of the films produced are the Cu, In, and Ga effusion sources. These three sources are thermal effusion cells with free evaporating surfaces that have the geometry shown if Figure 7-1. The crucible is

radiatively heated by the filaments through which a regulated current flows. The shutter can be opened or closed in order to precisely control the exposure of the melt to the substrates.

The spatial flux distribution on the substrate as a function of melt height and temperature has already been characterized by Serkan Kincal [163]. The only net source of flux is from the melt surface, in which the mass flow rate is expressed as the product of the flux leaving the surface and the surface area of the melt. The evaporation rate from the surface is governed by Knudsen's effusion equation [163]

$$F_m^i\left(T_m^i\right) = 3.51\times10^{22}\left(\frac{P_V\left(T_m^i\right)}{\sqrt{AW_i T_m^i}}\right) \tag{7-1}$$

where AW_i = Atomic weight of species i

T_m^i = melt temperature of species i

The vapor pressure, P_V, in Equation (7-1) is determined by Antoine's equation

$$P_V\left(T_m^i\right) = \exp\left(A_i + \frac{B_i}{T_m^i}\right) \tag{7-2}$$

where A and B are material specific constants.

Finally, the surface area of the melt can be described by

$$A_m = \pi r_m^2\left(t\right) \tag{7-3}$$

where r_m = the radius of the melt

In all of the calculations by Kincal, the evaporation rate from the melt surface, $F_m(T)$, was set at unity without a loss of generality since the final results can be scaled to any evaporation rate by simply multiplying by the desired value of $F_m(T)$. This normalization makes the results applicable to any material that satisfies Antoine's Law at any temperature of interest.

The flux incident on the substrate is a function of the radial position. The fill level can be varied from a completely full crucible (h_m = 9.0 cm) to an almost empty condition (h_m = 1.0 cm). The deposition rate varies significantly with the melt height and position on the substrate,

making it impossible to use a single value for the flux to estimate the entire flux distribution. These two requirements conflict with the need to have real-time deposition profiles since the calculations involved are numerically intensive.

Fast calculation of fluxes at any melt height can be done on-line by first creating a look-up table with the results shown in Figure 7-2 [163]. Intermediate flux distributions can be estimated very quickly by interpolation from a set of deposition profiles at a series of reference heights. As material exits the crucible during deposition, the melt height is continuously decreasing. Kincal determined that the time rate of change of the melt height (in cm/s) is given by [6]

$$\frac{dh_m^i}{dt} = \frac{-F_m^i\left(T_m^i\right)AW_i}{\pi\rho_m^i N_A}\,\frac{a_3\left(h_m^i\right)^3 + a_2\left(h_m^i\right)^2 + a_1 h_m^i + a_0}{R_B^2 + 2mR_B h_m^i + m^2\left(h_m^i\right)^2} \qquad (7\text{-}4)$$

where ρ_m^i = melt density of species i

N_A = Avogadro's number

h_m^i = melt height of species i

R_B = bottom radius of the crucible

$m = \dfrac{R_E - R_B}{H}$ (R_E = exit radius and H = crucible height)

a_1, a_2, a_3, a_4 are constants related to the geometry of the crucible and are not materials specific.

PMEE Reactor Modeling

The previously described flux model can be incorporated into an overall reactor model that describes the dynamics of thin film deposition. The PMEE reactor can be modeled by a set of differential equations accompanied by a set of algebraic equations. The substrates are not stationary due to the rotating nature of the platen so this dynamic must be incorporated into the model. The change in linear position of the substrate over time is defined by

$$\frac{dx}{dt} = \Omega \cdot 2\pi R_O \qquad (7\text{-}5)$$

where Ω = frequency of rotation

R_O = radius of the center of the platen

The circumference of the platen centerline is given by

$$L = 2\pi R_O \tag{7-6}$$

Finally, the position on the platen, x'(t), is determined by the equation

$$x'(t) = \mathrm{mod}(x, L) \tag{7-7}$$

where mod is the modulus function. For example, $\mathrm{mod}(10,3) = 1$. Position x'(0) = 0 was set as the point directly under the substrate heater as shown in Figure 7-3.

A mass balance on the film for metal species i gives an equation for the differential mass of species i.

$$\frac{dmass_i}{dt} = A_S F_S^i \left(h_m^i(t), x'(t)\right) AW_i \sigma_i \tag{7-8}$$

where
A_S = the area of the deposited film
F_S^i = the atomic flux as a function of melt height ($h_m^i(t)$) and platen position ($x'(t)$)
σ_i = sticking coefficient

F_S was calculated by Kincal [163] and it represents the flux hitting the substrate depending upon the melt height and the position of the substrate in relation to the center of the crucible.

The platen rotates counterclockwise at a constant rate where it travels through all of the deposition zones. In each metal deposition zone, flux strikes the substrate leading to an accumulation of mass and reaction between the assorted elements. The differential masses of each species are then summed to give the total mass balance around the deposited film.

$$\frac{dmass_{tot}}{dt} = \sum \frac{dmass_i}{dt} \tag{7-9}$$

Algebraic equations complement the preceding differentials to give a total description of the system. The film composition of species i (mole fraction) depends on the mass and atomic weight of all the species present in the film.

$$x_i = \frac{\frac{mass_i}{AW_i}}{\frac{mass_i}{AW_i} + \frac{mass_j}{AW_j} + \frac{mass_k}{AW_k}} \tag{7-10}$$

The mole fraction of one of the species can be determined from the others because they all must add up to 1, as follows

$$x_{Se} = 1 - x_{Cu} - x_{In} \tag{7-11}$$

The total mass of a deposited CIGS film is dependent upon the total thickness of that film (τ), the density of the film (ρ), and the deposition area.

$$mass_{tot} = \tau_{CIGS}(t)\,\rho_{CIGS}(t)\,A_S \tag{7-12}$$

Computer code

The model is coded in MATLAB. An M-file (the name given to subroutines in MATLAB) named PMEE_model.m outputs film composition and thickness based on the following input parameters: platen radius, crucible dimensions, substrate area, rotations per minute, deposition time, normalized flux matrix depending on melt height and substrate position, initial melt heights, atomic weight of each species, sticking coefficients, melt temperature of each effusion cell, Antoine coefficients A and B of each species to determine vapor pressure, the density of each species, and the density of the final film. The printout of the m-file is given in Appendix B, which is commented to explain how the program works. SIMULINK is used to solve the differential equations; the total time, the step change in time, and the method of solving ordinary differential equations, such as Euler or Runge-Kutta must be chosen.

Two different models could be developed: one that takes into account the selenium flux or one that assumes the Se flux is distributed in great excess with respect to film stoichiometry. Since the Se flux has not been modeled like the metal effusion sources, and Se is supplied in

excess in the PMEE reactor, the model using excess Se was investigated. This model can be modified in a straightforward fashion to include selenium flux modeling.

A look-up table must be created for the metal flux based on the various melt heights that are possible in the source crucible. The normalized flux on the substrate varies with the radial position of the substrate in relation to the center point of the crucible. Since each metal source has shielding around it, the radial distance away from the middle of the crucible that metal flux can still reach the substrate is limited. As is shown in Figure 7-4 of the cryoshroud, each metal zone sweeps out 40° of the circumference of the reactor. This pertains to approximately 6.2 cm on each side of the crucible center point. So the look-up tables are only relevant up to this distance.

The look-up table for the flux only contains values at certain melt heights so bicubic interpolation is used to calculate the flux at intermediate melt heights. Since the melt height is decreasing throughout the growth run, a new melt height is being continuously calculated. This new melt height is used to calculate the subsequent interpolated flux. The normalized flux for each metal species is then converted into a mass, which accumulates over time on the substrate.

Since the PMEE reactor incorporates a rotating platen, a specific flux distribution hits the substrate during each rotation. The amount of time the substrate remains in the metal deposition zone depends upon the rotational speed of the platen so the mass reaching the substrate per turn is time-dependent. Over a long growth run, the total mass will be the same, but the amount of mass accumulated per rotation differs. A faster rotational speed allows the substrate to see the center of the metal crucible more times during a deposition period, but accumulates less mass per rotation.

This model can be used for any material growth that uses thermal effusion cells with free evaporating surfaces in a rotating disc reactor. Typical PMEE reactor parameters and film properties relevant to Cu-chalcopyrite growth are implemented into the input m-file named input_pmee.m. For the condition of excess Se flux, the composition of Se was set to $x_{Se} = 0.50$.

Conclusions

The PMEE reactor has now been successfully modeled under the condition of excess selenium flux distribution. To represent our system without this stipulation, modeling of the selenium flux from the crucible must be done. One over-simplified solution to this is to model the selenium source as a thermal effusion source with an evaporating free surface. Once film properties are related to the performance parameters of the device, a true predictive model would be accomplished.

The next step is to take known experimental parameters and incorporate them into the model. Knowing initial melt heights, along with melt temperatures and deposition time allows for the modeling of the experimental conditions within the PMEE reactor. Theoretical film composition and thickness can be compared to the actual results to determine the sticking coefficients of each species. These sticking coefficients can be calculated for several different reactor conditions to obtain an error bar of acceptable values.

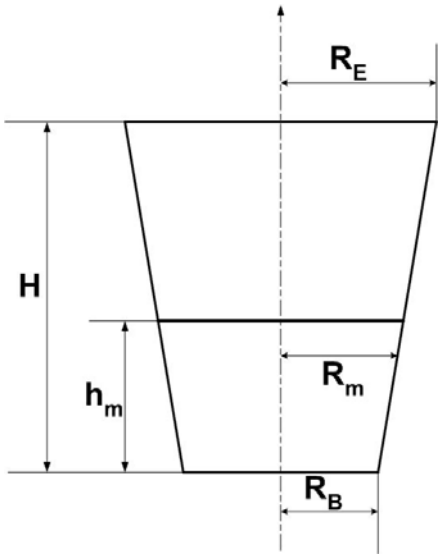

Figure 7-1. Metal source crucible.

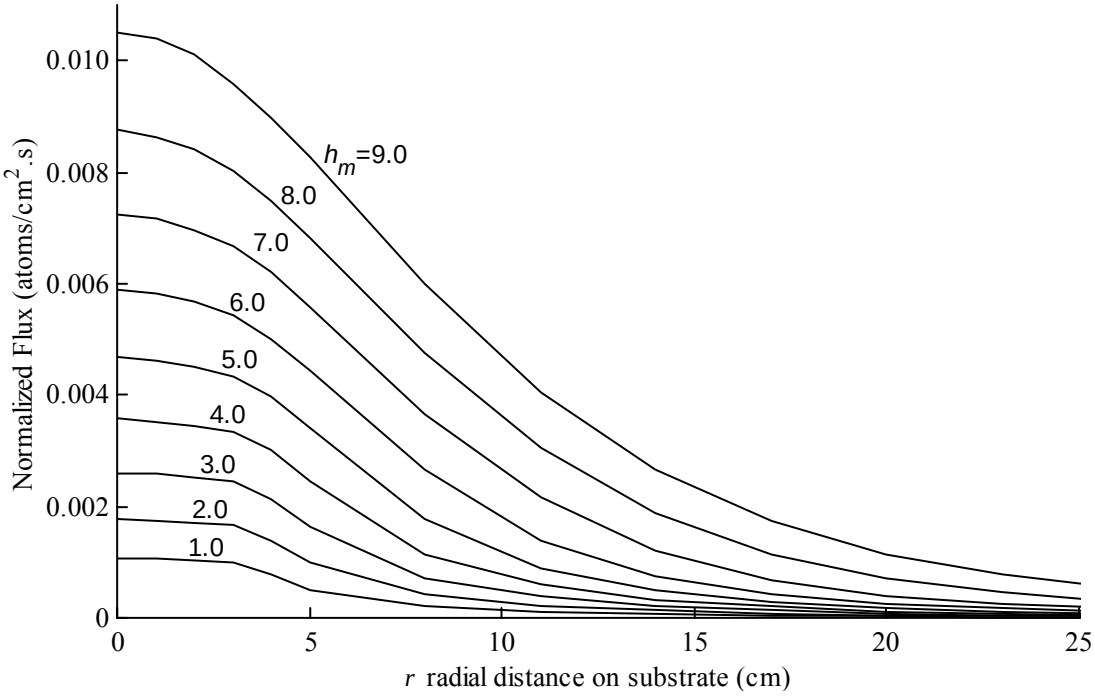

Figure 7-2. Deposition flux $F_S(r)$ (atoms/cm^2-s) on the substrate at nine different melt levels, h_m (cm). The results are normalized to unity evaporation rate from the melt.

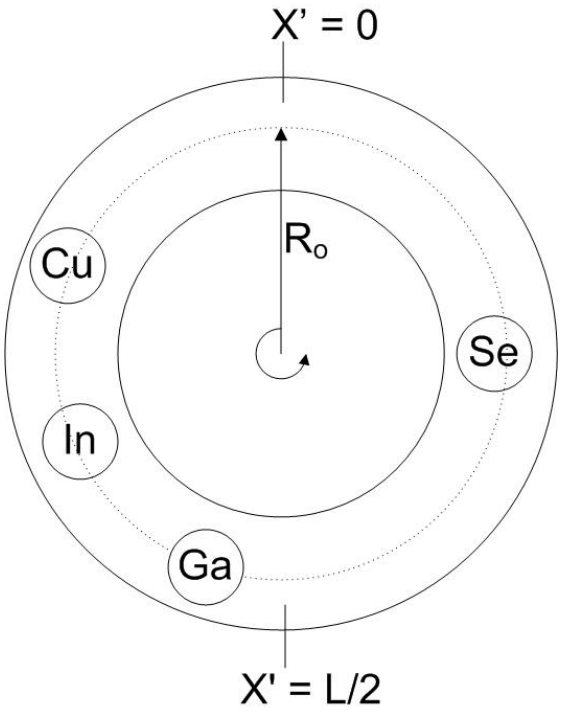

Figure 7-3. Positioning of the sources in the reactor.

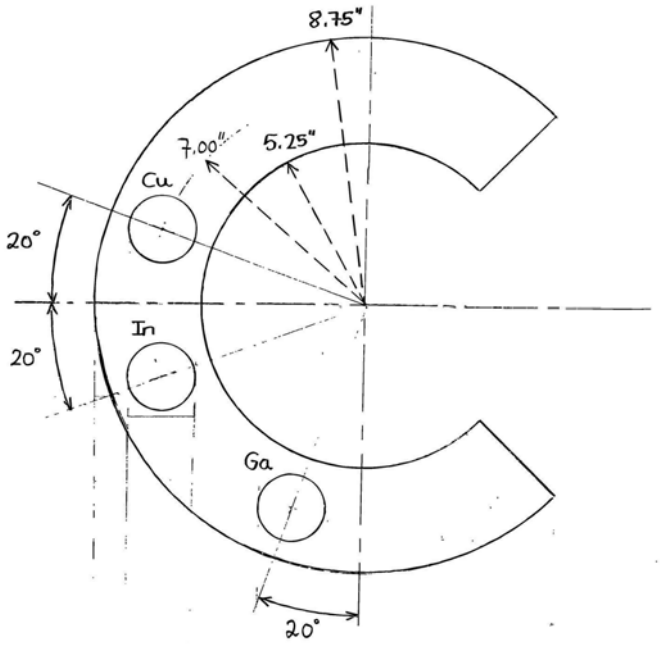

Figure 7-4. Cryoshroud.

CHAPTER 8
CONCLUSIONS AND FUTURE WORK

Conclusions

Growth temperature, growth recipe, and overall Cu/Ga ratio were varied over eight different sets of CGS growth runs. The subsequent effect on film morphology and orientation was noted. The trends observed during film growth became more noticeable when the absorbers were used in the fabrication of solar cell devices. Growth temperature seems to be the most critical variable in achieving high-quality absorber films. The fact that Cu-rich absorbers grown by PMEE have been more successful than Ga-rich ones is likely due to the lower deposition temperature. Ga-rich absorbers produce the highest efficiency CGS cells in the literature, but they are also grown at an elevated temperature of at least 550°C.

The best CGS cell produced in the PMEE reactor was grown at the highest growth temperature available, namely 491°C. The absorber used in this device was rather thin, approximately 0.6 μm, so a thicker absorber under the same conditions should produce a more efficient device. Annealing under the standard conditions at 200°C for 2 minutes should improve the low open-circuit voltage of our best devices. The maximum device parameters achieved by different cells produced from absorbers grown in the PMEE reactor are as follows: J_{sc} = 17.6 mA/cm^2, V_{oc} = 0.82 V, F.F. = 65.5 %, and η = 5.3.

Low Ga-content CIGS growth by PMEE was also studied and resulted in the most efficient solar cell ever produced by our group. This nearly 9% $CuInSe_2$ cell was completely fabricated at the University of Florida revealing our improved processing capabilities. Still, the best cell was produced at a less than ideal growth temperature, with a thickness of only 1 micron, and with no absorber or device annealing. An 8.6% CIGS cell was produced in addition to the CIS cell. Our

CIGS absorbers were grown with the Constant Cu Rate Process, resulting in an ungraded band gap, so further improvements are still possible.

The PMEE reactor has now been successfully modeled under the condition of excess selenium flux distribution. The effusion source flux model developed previously was incorporated into a dynamic reactor model. The integral design issue is the rotating nature of the substrates. Film parameters such as composition and thickness were related to the operation conditions of the reactor and the intrinsic properties of the materials involved in deposition.

Future Work

Since the biggest drawback in using the PMEE reactor to grow polycrystalline films is the limit that we must observe on the maximum substrate growth temperature, a more effective technique may be to grow Cu-Se and Ga-Se bilayer precursors at a low substrate temperature and then anneal the samples at a high temperature for a short period of time to produce $CuGaSe_2$. Successful CGS growth by RTP could lead to the fabrication of tandem cells that use a CGS layer in the design of the top cell.

The growth of Ga-rich CGS absorbers should be investigated more thoroughly. The improvement in device efficiency in the literature was a result of optimal Na incorporation, an optimal buffer layer deposition process, and device annealing in an oxygen atmosphere. The effects of these different processes should be investigated at lower growth temperatures.

Once film properties are related to the performance parameters of the device, a true predictive model would be accomplished. Incorporation of this model into the existing control structure would improve the production efficiency of the PMEE reactor. This would eliminate the need for in-situ measurements of the film properties that are expensive and sometimes difficult to implement.

APPENDIX A
GROWTH RUN DATA

The following tables in this appendix show the PMEE reactor conditions for each growth run described within Chapter 4 and Chapter 6. The film number, along with the growth run objective is presented with the reactor operator and date of experiment in the first part of the table. Target values, such as the metal deposition rates for each sublayer, the gallium primary temperature, and the gap temperature of the substrate heater, are shown in the next section of the table. The values used for the pre-deposition heating of the metal sources can be found in the following segment. Finally, the operation results are displayed; these include temperatures, growth rates, pressures, and the deposition time.

Table A-1. Reactor conditions for Growth Run #443.

Run # 443	Date: 03/22/03
Film: CGS	Operator: Suku Kim, Ryan Acher
Substrate: 2 Mo, 1 Glass	
Objective: To grow thick graded CGS with overall Cu/Ga~0.9	

Target Value

Metal		Se		Substrate Heater	
Cu Rate (A/s)	8.3/6.8/5.3	Cracker (°C)	500	Temp. (°C)	700
In Rate (A/s)	--	Ramp (°C/s)	0.5	Ramp (°C/s)	0.3
Cu tip power (%)	89.9	Crucible (°C)	255	RPM	12
Ga tip power (%)	22			Direction	CCW
Ga primary T (°C)	975				

Total Film Thickness (μm): 1.5

Film Set Value

	Cu	In	Ga
Soak Power (%)	17	--	7
Rise Time (min)	5	--	5
Soak Time (min)	13	--	0

Operation Results

	Cu	In	Ga	Se Crucible	Se Cracker	Heater
Power (%)	16.2	--	11.8-12.0	14.8	9.2	35.5
Tip (°C)	1133-1141	--		--	--	--
Primary (°C)	1089-1096	--	974-976	255.1	500.1	700.1
LSP	8.3/6.8/5.3	--	975	255	500	700
Kc	2	--	2	2	2	2
Ti	2	--	2	2	2	2
Td	0	--	0	0	0	0
Offset	13.2-15.5	--	10	14.9	9.5	35.9
Thick. (kA)	150	--	--	--	--	--

Run time (hr:min:sec): 6:20:55 Headspace P (torr):
Run time (seconds): 22,855 Growth P (torr):

Cu rate

Thickness (kA)	Rate (A/s)
0 - 50	8.29
50 - 100	6.79
100 - 150	5.28

Table A-2. Reactor conditions for Growth Run #444.

Run # 444	Date: 03/23/03
Film: CGS	Operator: Woo Kyoung Kim, Seokhyun Yoon
Substrate: 2 Mo, 1 Glass	
Objective: To grow thick graded CGS with overall Cu/Ga~0.95	

Target Value

Metal		Se		Substrate Heater	
Cu Rate (A/s)	8.6/7.1/5.6	Cracker (°C)	500	Temp. (°C)	700
In Rate (A/s)	--	Ramp (°C/s)	0.5	Ramp (°C/s)	0.3
Cu tip power (%)	89.9	Crucible (°C)	255	RPM	12
Ga tip power (%)	22			Direction	CCW
Ga primary T (°C)	975				

Total Film Thickness (μm): 1.5

Film Set Value

	Cu	In	Ga
Soak Power (%)	17	--	7
Rise Time (min)	5	--	5
Soak Time (min)	13	--	0

Operation Results

	Cu	In	Ga	Se Crucible	Se Cracker	Heater
Power (%)	16.2	--	12.3-12.4	15.9-16.2	9.2-9.3	35.5-36.5
Tip (°C)	1129	--	937	--	--	--
Primary (°C)	1078	--	974-976	255.2	500.3	700
LSP	8.6/7.1/5.6	--	975	255	500	700
Kc	2	--	2	2	2	2
Ti	2	--	2	2	2	2
Td	0	--	0	0	0	0
Offset	16/14.7/13.4	--	10	16.4	10.0	35.4
Thick. (kA)	150	--	--	--	--	--

Run time (hr:min:sec): 6:00:22 Headspace P (torr):
Run time (seconds): 21,622 Growth P (torr):

Cu rate

Thickness (kA)	Rate (A/s)
0 - 50	8.63
50 - 100	--
100 - 150	--

Table A-3. Reactor conditions for Growth Run #445.

Run # 445	Date: 03/24/03
Film: CGS	Operator: Suku Kim, Woo Kyoung Kim
Substrate: 2 Mo, 1 Glass	
Objective: To grow thick graded CGS with overall Cu/Ga~0.95 and a Se temp. change	

Target Value

Metal		Se		Substrate Heater	
Cu Rate (A/s)	8.6/7.1/5.6	Cracker (°C)	500	Temp. (°C)	700
In Rate (A/s)	--	Ramp (°C/s)	0.5	Ramp (°C/s)	0.3
Cu tip power (%)	89.9	Crucible (°C)	230/255	RPM	12
Ga tip power (%)	22			Direction	CCW
Ga primary T (°C)	975				

Total Film Thickness (μm): 1.5

Film Set Value

	Cu	In	Ga
Soak Power (%)	17	--	7
Rise Time (min)	5	--	5
Soak Time (min)	13	--	0

Operation Results

	Cu	In	Ga	Se Crucible	Se Cracker	Heater
Power (%)	15.5/15/--	--	12.1	10.5/15.5	9.1	35
Tip (°C)	1131-1133	--	936	--	--	--
Primary (°C)	1051-1079	--	975	230.4/254.6	500.5	700
LSP	8.6/7.1/5.6	--	975	230/255	500	700
Kc	2	--	2	2	2	2
Ti	2	--	2	2	2	2
Td	0	--	0	0	0	0
Offset	15.5/14.5/12.6	--	10	16.4	9.5	35.9
Thick. (kA)	150	--	--	--	--	--

Run time (hr:min:sec): 6:02:30 Headspace P (torr):
Run time (seconds): 21,750 Growth P (torr):

Cu rate

Thickness (kA)	Rate (A/s)
0 - 50	8.68
50 - 100	7.12
100 - 150	5.57

Table A-4. Reactor conditions for Growth Run #446.

Run # 446	Date: 03/25/03
Film: CGS	Operator: Ryan Kaczynski, Ryan Acher
Substrate: 2 Mo, 1 Glass	
Objective: To grow thick graded CGS with overall Cu/Ga~1.1	

Target Value

Metal		Se		Substrate Heater	
Cu Rate (A/s)	9.8/8.3/6.8	Cracker (°C)	500	Temp. (°C)	700
In Rate (A/s)	--	Ramp (°C/s)	0.5	Ramp (°C/s)	0.3
Cu tip power (%)	89.9	Crucible (°C)	230/255	RPM	12
Ga tip power (%)	22			Direction	CCW
Ga primary T (°C)	975				

Total Film Thickness (μm): 1.5

Film Set Value

	Cu	In	Ga
Soak Power (%)	17	--	7
Rise Time (min)	5	--	5
Soak Time (min)	13	--	0

Operation Results

	Cu	In	Ga	Se Crucible	Se Cracker	Heater
Power (%)	16.5/15.3/--	--	12.0-12.2	9.2/13.1	9.0	34.8-36.2
Tip (°C)	1138-1146	--	936-937	--	--	--
Primary (°C)	1091/1082/1072	--	974-976	230.2/255.2	500.4	699.8-700.5
LSP	9.8/8.3/6.8	--	975	230/255	500	700
Kc	2	--	2	2	2	2
Ti	2	--	2	2	2	2
Td	0	--	0	0	0	0
Offset	16/14.9/--	--	10	9.8/13.6	10.0	35.7
Thick. (kA)	150	--	--	--	--	--

Run time (hr:min:sec): 5:07:50 Headspace P (torr): 3.5×10^{-8}

Run time (seconds): 18,470 Growth P (torr): 6.0×10^{-8}

Cu rate

Thickness (kA)	Rate (A/s)
0 - 50	9.80
50 - 100	8.29
100 - 150	6.81

Table A-5. Reactor conditions for Growth Run #447.

Run # 447	Date: 03/26/03
Film: CGS	Operator: Woo Kyoung Kim, Seokhyun Yoon
Substrate: 1 p-GaAs, 1 Mo, 1 Glass	
Objective: To grow thick graded CGS with overall Cu/Ga~0.95	

Target Value

Metal		Se		Substrate Heater	
Cu Rate (A/s)	8.8/7.3/5.8	Cracker (°C)	500	Temp. (°C)	700
In Rate (A/s)	--	Ramp (°C/s)	0.5	Ramp (°C/s)	0.3
Cu tip power (%)	89.9	Crucible (°C)	260	RPM	12
Ga tip power (%)	22			Direction	CCW
Ga primary T (°C)	975				

Total Film Thickness (μm): 1.5

Film Set Value

	Cu	In	Ga
Soak Power (%)	17	--	7
Rise Time (min)	5	--	5
Soak Time (min)	13	--	0

Operation Results

	Cu	In	Ga	Se Crucible	Se Cracker	Heater
Power (%)	15.9/15.2/14.0	--	11.9-12.0	9.2/13.1	8.7-9.3	37.8-37.9
Tip (°C)	1143/1138/1130	--	935-936	--	--	--
Primary (°C)	1089/1080/1064	--	974-976	259.8/260.3	500.9	699.5-700.6
LSP	8.8/7.3/5.8	--	975	260	500	700
Kc	2	--	2	2	2	2
Ti	2	--	2	2	2	2
Td	0	--	0	0	0	0
Offset	15.7/14.95/13.4	--	10	13.8	10.3	37
Thick. (kA)	150	--	--	--	--	--

Run time (hr:min:sec): 5:53:53 Headspace P (torr):
Run time (seconds): 21,233 Growth P (torr):

Cu rate

Thickness (kA)	Rate (A/s)
0 - 50	8.83
50 - 100	7.31
100 - 150	5.72

Table A-6. Reactor conditions for Growth Run #452.

Run # 452	Date: 04/05/03
Film: CGS	Operator: Ryan Kaczynski
Substrate: 3 Mo, 1 Glass	
Objective: Modified 3-stage CGS with overall Cu/Ga~1.1	

Target Value

Metal		Se		Substrate Heater	
Cu Rate (A/s)	5.54/8.66	Cracker (°C)	500	Temp. (°C)	700
In Rate (A/s)	--	Ramp (°C/s)	0.5	Ramp (°C/s)	0.3
Cu tip power (%)	89.9	Crucible (°C)	260	RPM	12
Ga tip power (%)	22			Direction	CCW
Ga primary T (°C)	975				

Total Film Thickness (μm): 1.1

Film Set Value

	Cu	In	Ga
Soak Power (%)	17	--	7
Rise Time (min)	5	--	5
Soak Time (min)	13	--	0

*Annealing for 30 minutes in Se atmosphere at T = 700°C

Operation Results

	Cu	In	Ga	Se Crucible	Se Cracker	Heater
Power (%)	12.5-13.5	--	12.0-12.1	15.2	9.0	35.0-37.2
Tip (°C)	1127/1144	--	--	--	--	--
Primary (°C)	1054/1089	--	974-976	260.1	500.3	699.4-700.5
LSP	5.54/8.66	--	975	260	500	700
Kc	2	--	2	2	2	2
Ti	2	--	2	2	2	2
Td	0	--	0	0	0	0
Offset	12-13/16	--	10	15.4	9.7	36.1
Thick. (kA)	110	--	--	--	--	--

Run time (hr:min:sec): 4:00:34 Headspace P (torr): 4.0×10^{-8}

Run time (seconds): 14,434 Growth P (torr): 1.7×10^{-8}

Cu rate

Thickness (kA)	Rate (A/s)
0 - 26.72	5.55
26.72 - 110	8.66

Table A-7. Reactor conditions for Growth Run #453.

Run # 453	Date: 04/06/03
Film: CGS	Operator: Woo Kyoung Kim, Seokhyun Yoon
Substrate: 3 Mo, 1 Glass	
Objective: CGS with overall Cu/Ga~0.95	

Target Value

Metal		Se		Substrate Heater	
Cu Rate (A/s)	5.5/9.7/0	Cracker (°C)	500	Temp. (°C)	700
In Rate (A/s)	--	Ramp (°C/s)	0.5	Ramp (°C/s)	0.3
Cu tip power (%)	89.9	Crucible (°C)	260	RPM	12
Ga tip power (%)	22			Direction	CCW
Ga primary T (°C)	975				

Total Film Thickness (μm): 1.0

Film Set Value

	Cu	In	Ga
Soak Power (%)	17	--	7
Rise Time (min)	5	--	5
Soak Time (min)	13	--	0

*Annealing for 30 minutes in Se atmosphere at T = 700°C

Operation Results

	Cu	In	Ga	Se Crucible	Se Cracker	Heater
Power (%)	--/17	--	--	14	9	35-37
Tip (°C)	--/1143	--	--	--	--	--
Primary (°C)	--/1099	--	--	260.2	500.5	700.0
LSP	5.54/9.7	--	975	260	500	700
Kc	2	--	2	2	2	2
Ti	2	--	2	2	2	2
Td	0	--	0	0	0	0
Offset	--/16	--	10	15	10	36.1
Thick. (kA)	110	--	--	--	--	--

Run time (hr:min:sec): 4:13:44 Headspace P (torr):
Run time (seconds): 15,224 Growth P (torr):

Cu rate

Thickness (kA)	Rate (A/s)
0 - 100	8.37

*GaSe was deposited for ~ 54:30 after CGS deposition and before Se annealing

Table A-8. Reactor conditions for Growth Run #454.

Run # 454	Date: 04/07/03
Film: CGS	Operator: Woo Kyoung Kim, Seokhyun Yoon
Substrate: 3 Mo, 1 Glass	
Objective: CGS with overall Cu/Ga~0.95	

Target Value

Metal		Se		Substrate Heater	
Cu Rate (A/s)	6/9.7/9.6/6	Cracker (°C)	500	Temp. (°C)	700
In Rate (A/s)	--	Ramp (°C/s)	0.5	Ramp (°C/s)	0.3
Cu tip power (%)	89.9	Crucible (°C)	260	RPM	12
Ga tip power (%)	22			Direction	CCW
Ga primary T (°C)	975				

Total Film Thickness (μm): 1.0

Film Set Value

	Cu	In	Ga
Soak Power (%)	17	--	7
Rise Time (min)	5	--	5
Soak Time (min)	13	--	0

*Annealing for 30 minutes in Se atmosphere at T = 700°C

Operation Results

	Cu	In	Ga	Se Crucible	Se Cracker	Heater
Power (%)	--/18/17	--	--	14.8-14.9	9.1	35.5-37.5
Tip (°C)	--/1148/1138	--	--	--	--	--
Primary (°C)	--/1104/1091	--	--	260.3	500.4	699.5-700.5
LSP	5.9/9.7/9.6/6.0	--	975	260	500	700
Kc	2	--	2	2	2	2
Ti	2	--	2	2	2	2
Td	0	--	0	0	0	0
Offset	14.2/17.2/16.5	--	10	15.4	10.0	36.1
Thick. (kA)	100	--	--	--	--	--

Run time (hr:min:sec): 4:00:04 Headspace P (torr):
Run time (seconds): 14,404 Growth P (torr):

Cu rate

Thickness (kA)	Rate (A/s)
0 - 10	5.9
10 - 23.71	9.7
23.71 - 45	7.6
45 - 100	6.0

Table A-9. Reactor conditions for Growth Run #455.

Run # 455	Date: 04/08/03
Film: CGS	Operator: Ryan Kaczynski
Substrate: 3 Mo, 1 Glass	
Objective: CGS with overall Cu/Ga~0.95	

Target Value

Metal		Se		Substrate Heater	
Cu Rate (A/s)	6/9.7/9.6/6	Cracker (°C)	500	Temp. (°C)	700
In Rate (A/s)	--	Ramp (°C/s)	0.5	Ramp (°C/s)	0.3
Cu tip power (%)	89.9	Crucible (°C)	260	RPM	12
Ga tip power (%)	22			Direction	CCW
Ga primary T (°C)	975				

Total Film Thickness (μm): 1.0

Film Set Value

	Cu	In	Ga
Soak Power (%)	17	--	7
Rise Time (min)	5	--	5
Soak Time (min)	13	--	0

*Annealing for 30 minutes in Se atmosphere at T = 700°C

Operation Results

	Cu	In	Ga	Se Crucible	Se Cracker	Heater
Power (%)	15.5-18.4	--	12.1-18.4	16	9.3	35.2-37.4
Tip (°C)	1134-1150	--	930	--	--	--
Primary (°C)	1080-1110	--	974-976	260.0	500.2	699.5-700.5
LSP	5.9/9.7/9.6/6.0	--	975	260	500	700
Kc	2	--	2	2	2	2
Ti	2	--	2	2	2	2
Td	0	--	0	0	0	0
Offset	15/19/17/15.7	--	10	16.0	9.7	36.2
Thick. (kA)	100	--	--	--	--	--

Run time (hr:min:sec): 4:11:55 Headspace P (torr): 4.0×10^{-8}

Run time (seconds): 15,115 Growth P (torr): 1.7×10^{-7}

Cu rate

Thickness (kA)	Rate (A/s)
0 - 10	5.89
10 - 23.71	9.67
23.71 - 45	7.56
45 - 100	5.99

Table A-10. Reactor conditions for Growth Run #456.

Run # 456	Date: 04/09/03
Film: CGS	Operator: Seokhyun Yoon
Substrate: 3 Mo, 1 Glass	
Objective: CGS with overall Cu/Ga~0.9	

Target Value

Metal		Se		Substrate Heater	
Cu Rate (A/s)	6/9.7/7.3/5.6	Cracker (°C)	500	Temp. (°C)	700
In Rate (A/s)	--	Ramp (°C/s)	0.5	Ramp (°C/s)	0.3
Cu tip power (%)	89.9	Crucible (°C)	260	RPM	12
Ga tip power (%)	22			Direction	CCW
Ga primary T (°C)	975				

Total Film Thickness (μm): 1.0

Film Set Value

	Cu	In	Ga
Soak Power (%)	17	--	7
Rise Time (min)	5	--	5
Soak Time (min)	13	--	0

*Annealing for 30 minutes in Se atmosphere at T = 700°C

Operation Results

	Cu	In	Ga	Se Crucible	Se Cracker	Heater
Power (%)	14.8-17.5	--	11.9	14.8-15	9.05	35-37
Tip (°C)	1128-1140	--	932.5	--	--	--
Primary (°C)	1075-1144	--	974-976	259.8	500.4	699.5-700.5
LSP	5.9/9.7/7.3/5.6	--	975	260	500	700
Kc	2	--	2	2	2	2
Ti	2	--	2	2	2	2
Td	0	--	0	0	0	0
Offset	14.7-17	--	10	14.8	9.7	36
Thick. (kA)	100	--	--	--	--	--

Run time (hr:min:sec): 4:23:20 Headspace P (torr):
Run time (seconds): 15,800 Growth P (torr):

Cu rate

Thickness (kA)	Rate (A/s)
0 - 10	5.9
10 - 19.4	9.7
19.4 - 45	7.3
45 - 100	5.6

Table A-11. Reactor conditions for Growth Run #457.

Run # 457	Date: 04/10/03
Film: CGS	Operator: Ryan Acher
Substrate: 3 Mo, 1 Glass	
Objective: CGS with overall Cu/Ga~0.96	

Target Value

Metal		Se		Substrate Heater	
Cu Rate (A/s)	0/6/10.3/7.6/5.2	Cracker (°C)	500	Temp. (°C)	700
In Rate (A/s)	--	Ramp (°C/s)	0.5	Ramp (°C/s)	0.3
Cu tip power (%)	89.9	Crucible (°C)	260	RPM	12
Ga tip power (%)	22			Direction	CCW
Ga primary T (°C)	975				

Total Film Thickness (μm): 1.0

Film Set Value

	Cu	In	Ga
Soak Power (%)	17	--	7
Rise Time (min)	5	--	5
Soak Time (min)	13	--	0

*Annealing for 30 minutes in Se atmosphere at T = 700°C

Operation Results

	Cu	In	Ga	Se Crucible	Se Cracker	Heater
Power (%)	--/17.5/--	--	11.8-12.0	14.7	9	36
Tip (°C)	1130-1143	--	932	--	--	--
Primary (°C)	1059-1106	--	974-976	260.1	500.3	699.5-700.5
LSP	5.9/10.3/7.6/5.2	--	975	260	500	700
Kc	2	--	2	2	2	2
Ti	2	--	2	2	2	2
Td	0	--	0	0	0	0
Offset	13.5-17.2	--	10	15	10	36
Thick. (kA)	100.4	--	--	--	--	--

Run time (hr:min:sec): 4:13:25 Headspace P (torr): 4.9×10^{-8}

Run time (seconds): 15,205 Growth P (torr): 1.9×10^{-7}

Cu rate

Thickness (kA)	Rate (A/s)
0 - 10	5.9
10 - 47.3	10.3
47.3 - 73.8	7.6
73.8 - 100.4	5.2

*GaSe was deposited first for 20 minutes

Table A-12. Reactor conditions for Growth Run #458.

Run # 458	Date: 04/11/03
Film: CGS	Operator: Ryan Kaczynski, Woo Kyoung Kim
Substrate: 4 Mo, 1 Glass	
Objective: Modified 3-stage CGS with overall Cu/Ga~0.96	

Target Value

Metal		Se		Substrate Heater	
Cu Rate (A/s)	5.2/8.5/7.8/4.9	Cracker (°C)	500	Temp. (°C)	700
In Rate (A/s)	--	Ramp (°C/s)	0.5	Ramp (°C/s)	0.3
Cu tip power (%)	89.9	Crucible (°C)	260	RPM	12
Ga tip power (%)	22			Direction	CCW
Ga primary T (°C)	975				

Total Film Thickness (μm): 1.0

Film Set Value

	Cu	In	Ga
Soak Power (%)	17	--	7
Rise Time (min)	5	--	5
Soak Time (min)	13	--	0

*Annealing for 30 minutes in Se atmosphere at T = 700°C

Operation Results

	Cu	In	Ga	Se Crucible	Se Cracker	Heater
Power (%)	12.5-13.5	--	12.0-12.1	15.2	9.0	35.0-37.2
Tip (°C)	1127-1144	--	932	--	--	--
Primary (°C)	1054-1089	--	974-976	260.1	500.3	699.4-700.5
LSP	5.2/8.5/7.8/4.9	--	975	260	500	700
Kc	2	--	2	2	2	2
Ti	2	--	2	2	2	2
Td	0	--	0	0	0	0
Offset	12-16.2	--	10	15.4	9.7	36.1
Thick. (kA)	100	--	--	--	--	--

Run time (hr:min:sec): 4:43:39 Headspace P (torr): 4.4×10^{-8}

Run time (seconds): 17,019 Growth P (torr): 1.8×10^{-7}

Cu rate

Thickness (kA)	Rate (A/s)
0 - 10	5.17
10 - 38.8	8.50
38.8 - 50	7.79
50 - 100	4.88

Table A-13. Reactor conditions for Growth Run #459.

Run # 459	Date: 04/12/03
Film: CGS	Operator: Ryan Acher
Substrate: 3 Mo, 1 Glass	
Objective: Modified 3-stage CGS with overall Cu/Ga~0.86	

Target Value

Metal		Se		Substrate Heater	
Cu Rate (A/s)	5.5/7.8/6.8/4.9	Cracker (°C)	500	Temp. (°C)	700
In Rate (A/s)	--	Ramp (°C/s)	0.5	Ramp (°C/s)	0.3
Cu tip power (%)	89.9	Crucible (°C)	260	RPM	12
Ga tip power (%)	22			Direction	CCW
Ga primary T (°C)	975				

Total Film Thickness (μm): 1.0

Film Set Value

	Cu	In	Ga
Soak Power (%)	17	--	7
Rise Time (min)	5	--	5
Soak Time (min)	13	--	0

*Annealing for 30 minutes in Se atmosphere at T = 700°C

Operation Results

	Cu	In	Ga	Se Crucible	Se Cracker	Heater
Power (%)	14.1-16.8	--	11.8-12.1	15.0	9.1	36.5
Tip (°C)	1118-1130	--	930	--	--	--
Primary (°C)	1056-1085	--	974.8-975.2	260.0	500.3	699.5-700.5
LSP	5.5/7.8/6.8/4.9	--	975	260	500	700
Kc	2	--	2	2	2	2
Ti	2	--	2	2	2	2
Td	0	--	0	0	0	0
Offset	13.6-16.3	--	10	15	9.7	36.3
Thick. (kA)	100	--	--	--	--	--

Run time (hr:min:sec): 4:57:30 Headspace P (torr):
Run time (seconds): 17,850 Growth P (torr):

Cu rate

Thickness (kA)	Rate (A/s)
0 - 10.5	5.5
10.5 - 31.2	7.8
31.2 - 46.2	6.8
46.2 - 100	4.9

Table A-14. Reactor conditions for Growth Run #472.

Run # 472	Date: 05/15/03
Film: CGS	Operator: Ryan Kaczynski, Seokhyun Yoon
Substrate: 1 Mo, 1 Glass	
Objective: GaSe/CGS with Cu/Ga~1.25/GaSe	

Target Value

Metal		Se		Substrate Heater	
Cu Rate (A/s)	13.9	Cracker (°C)	500	Temp. (°C)	700
In Rate (A/s)	--	Ramp (°C/s)	0.5	Ramp (°C/s)	0.3
Cu tip power (%)	89.9	Crucible (°C)	250/275	RPM	12
Ga tip power (%)	24			Direction	CCW
Ga primary T (°C)	1007				

Total Film Thickness (μm): 1.1

Film Set Value

	Cu	In	Ga
Soak Power (%)	17	--	7
Rise Time (min)	5	--	5
Soak Time (min)	13	--	0

*Annealing for 30 minutes in Se atmosphere at T = 700°C

Operation Results

	Cu	In	Ga	Se Crucible	Se Cracker	Heater
Power (%)	22.5-22.7	--	13.3-13.5	16/23	9.5	35.8-36
Tip (°C)	1133	--	959	--	--	--
Primary (°C)	1130	--	1006-1008	250.6/276	501	699.6
LSP	13.9	--	1007	250/275	500	700
Kc	2	--	2	2	2	2
Ti	2	--	2	2	2	2
Td	0	--	0	0	0	0
Offset	22.3	--	10	16.3	12.0	35.8
Thick. (kA)	110	--	--	--	--	--

Run time (hr:min:sec): 2:52:01 Headspace P (torr):
Run time (seconds): 10,321 Growth P (torr):

Cu rate

Thickness (kA)	Rate (A/s)
0 - 110	13.99

*GaSe was deposited for 36 minutes before CGS deposition and 5 minutes after

Table A-15. Reactor conditions for Growth Run #474.

Run # 474	Date: 05/19/03
Film: CGS	Operator: Ryan Kaczynski
Substrate: 2 Mo, 1 Glass	
Objective: GaSe/Cu-rich CGS/Ga-rich CGS	

Target Value

Metal		Se		Substrate Heater	
Cu Rate (A/s)	0/14.9/10.3	Cracker (°C)	500	Temp. (°C)	700
In Rate (A/s)	--	Ramp (°C/s)	0.5	Ramp (°C/s)	0.3
Cu tip power (%)	89.9	Crucible (°C)	260/275	RPM	12
Ga tip power (%)	24			Direction	CCW
Ga primary T (°C)	1007				

Total Film Thickness (μm): 1.1

Film Set Value

	Cu	In	Ga
Soak Power (%)	17	--	7
Rise Time (min)	5	--	5
Soak Time (min)	13	--	0

*Annealing for 30 minutes in Se atmosphere at T = 700°C

Operation Results

	Cu	In	Ga	Se Crucible	Se Cracker	Heater
Power (%)	21/19	--	13.2-13.35	16.8/21.5	9.3	35.5-37.0
Tip (°C)	1151/1141	--	958	--	--	--
Primary (°C)	1135/1113	--	1006-1008	260/276	500.3	699.5-700.2
LSP	14.9/10.3	--	1007	260/275	500	700
Kc	2	--	2	2	2	2
Ti	2	--	2	2	2	2
Td	0	--	0	0	0	0
Offset	20.6/18.4	--	10	16.5/19.0	10.0	36.0
Thick. (kA)	110	--	--	--	--	--

Run time (hr:min:sec): 3:19:09 Headspace P (torr): 4.7×10^{-8}

Run time (seconds): 11,949 Growth P (torr): 3.0×10^{-7}

Cu rate

Thickness (kA)	Rate (A/s)
0 - 90	14.9
90 - 110	10.3

*GaSe deposited for 33 minutes before Cu deposition

Table A-16. Reactor conditions for Growth Run #475.

Run # 475	Date: 05/20/03
Film: CGS	Operator: Seokhyun Yoon
Substrate: 2 Mo, 1 Glass	
Objective: GaSe/Cu-rich CGS/Ga-rich CGS, overall Cu/Ga~0.96	

Target Value

Metal		Se		Substrate Heater	
Cu Rate (A/s)	0/14/9.7	Cracker (°C)	500	Temp. (°C)	700
In Rate (A/s)	--	Ramp (°C/s)	0.5	Ramp (°C/s)	0.3
Cu tip power (%)	89.9	Crucible (°C)	260/275	RPM	12
Ga tip power (%)	24			Direction	CCW
Ga primary T (°C)	975				

Total Film Thickness (μm): 1.1

Film Set Value

	Cu	In	Ga
Soak Power (%)	17	--	7
Rise Time (min)	5	--	5
Soak Time (min)	13	--	0

*Annealing for 30 minutes in Se atmosphere at T = 700°C

Operation Results

	Cu	In	Ga	Se Crucible	Se Cracker	Heater
Power (%)	20.6/--	--	13.2	15/16.5	9.3	36-37
Tip (°C)	1155/--	--	958-959	--	--	--
Primary (°C)	1132/--	--	1006-1008	260/276	500.4	699-700
LSP	14/--	--	1007	260/275	500	700
Kc	2	--	2	2	2	2
Ti	2	--	2	2	2	2
Td	0	--	0	0	0	0
Offset	20.3/--	--	10	16.0/19.0	10.0	36.0
Thick. (kA)	110	--	--	--	--	--

Run time (hr:min:sec): 2:56:48 Headspace P (torr): 5.0×10^{-8}

Run time (seconds): 10,608 Growth P (torr): 3.3×10^{-7}

Cu rate

Thickness (kA)	Rate (A/s)
0 - 90	14.0
90 - 110	9.86

*GaSe deposited for 33:50 before Cu deposition

Table A-17. Reactor conditions for Growth Run #476.

Run # 476	Date: 05/21/03
Film: CGS	Operator: Ryan Acher
Substrate: 1 Mo, 1 Glass	
Objective: GaSe/Cu-rich CGS/GaSe, overall Cu/Ga~0.96	

Target Value

Metal		Se		Substrate Heater	
Cu Rate (A/s)	14	Cracker (°C)	500	Temp. (°C)	700
In Rate (A/s)	--	Ramp (°C/s)	0.5	Ramp (°C/s)	0.3
Cu tip power (%)	89.9	Crucible (°C)	260/275	RPM	12
Ga tip power (%)	24			Direction	CCW
Ga primary T (°C)	1007				

Total Film Thickness (μm): 1.1

Film Set Value

	Cu	In	Ga
Soak Power (%)	17	--	7
Rise Time (min)	5	--	5
Soak Time (min)	13	--	0

*Annealing for 30 minutes in Se atmosphere at T = 700°C

Operation Results

	Cu	In	Ga	Se Crucible	Se Cracker	Heater
Power (%)	21.1	--	12.9-13.1	17.6/19	9.1	36.5
Tip (°C)	1153-1159	--	958-960	--	--	--
Primary (°C)	1135-1140	--	1006-1008	260/277	500.4	699.7-700.3
LSP	14	--	1007	260/275	500	700
Kc	2	--	2	2	2	2
Ti	2	--	2	2	2	2
Td	0	--	0	0	0	0
Offset	20.6	--	10	16/19	10.0	36.5
Thick. (kA)	110	--	--	--	--	--

Run time (hr:min:sec): 2:57:30 Headspace P (torr): 3.2-4.1 x 10^{-8}
Run time (seconds): 10,650 Growth P (torr): 3.5-4.1 x 10^{-7}

Cu rate

Thickness (kA)	Rate (A/s)
0 - 110	13.98

*GaSe was deposited for 39:40 before CGS deposition and 6:40 after

Table A-18. Reactor conditions for Growth Run #477.

Run # 477	Date: 05/22/03
Film: CGS	Operator: Woo Kyoung Kim
Substrate: 2 Mo, 1 Glass	
Objective: GaSe/Cu-rich CGS/GaSe, overall Cu/Ga~0.96	

Target Value

Metal		Se		Substrate Heater	
Cu Rate (A/s)	14	Cracker (°C)	500	Temp. (°C)	700
In Rate (A/s)	--	Ramp (°C/s)	0.5	Ramp (°C/s)	0.3
Cu tip power (%)	89.9	Crucible (°C)	260/275	RPM	12
Ga tip power (%)	24			Direction	CCW
Ga primary T (°C)	1007				

Total Film Thickness (μm): 1.1

Film Set Value

	Cu	In	Ga
Soak Power (%)	17	--	7
Rise Time (min)	5	--	5
Soak Time (min)	13	--	0

*Annealing for 30 minutes in Se atmosphere at T = 700°C

Operation Results

	Cu	In	Ga	Se Crucible	Se Cracker	Heater
Power (%)	21.4	--	13.02	15.5/16	9.0	37
Tip (°C)	1161	--	958.3	--	--	--
Primary (°C)	1140	--	1006-1008	260/276	500.5	700.0
LSP	14	--	1007	260/275	500	700
Kc	2	--	2	2	2	2
Ti	2	--	2	2	2	2
Td	0	--	0	0	0	0
Offset	20.8-21	--	10	15.6/18.8	10.0	36.1
Thick. (kA)	110	--	--	--	--	--

Run time (hr:min:sec): 2:57:33 Headspace P (torr): 5×10^{-8}

Run time (seconds): 10,653 Growth P (torr): 5×10^{-7}

Cu rate

Thickness (kA)	Rate (A/s)
0 - 110	14

*GaSe was deposited for 42:54 before CGS deposition and 3:33 after

Table A-19. Reactor conditions for Growth Run #478.

Run # 478	Date: 05/23/03
Film: CGS	Operator: Ryan Kaczynski, Ryan Acher
Substrate: 2 Mo, 1 Glass	
Objective: 3-stage emulation (GaSe/CuSe/GaSe)	

Target Value

Metal		Se		Substrate Heater	
Cu Rate (A/s)	10.8	Cracker (°C)	500	Temp. (°C)	700
In Rate (A/s)	--	Ramp (°C/s)	0.5	Ramp (°C/s)	0.3
Cu tip power (%)	89.9	Crucible (°C)	260/275	RPM	12
Ga tip power (%)	24			Direction	CCW
Ga primary T (°C)	1007				

Total Film Thickness (μm): 1.1

Film Set Value

	Cu	In	Ga
Soak Power (%)	17	--	7
Rise Time (min)	5	--	5
Soak Time (min)	13	--	0

*Annealing for 30 minutes in Se atmosphere at T = 700°C

Operation Results

	Cu	In	Ga	Se Crucible	Se Cracker	Heater
Power (%)	19.9	--	12.9-13.1	15.1/18.3	9.0	36-38
Tip (°C)	1152	--	958-961	--	--	--
Primary (°C)	1125	--	1006-1008	260/277	500.5	699.4-700.4
LSP	10.8	--	1007	260/275	500	700
Kc	2	--	2	2	2	2
Ti	2	--	2	2	2	2
Td	0	--	0	0	0	0
Offset	19.5	--	10	16.0/18.5	10.0	36.8
Thick. (kA)	110	--	--	--	--	--

Run time (hr:min:sec): 5:48:00 Headspace P (torr): 3.8-4.9 x 10^{-8}

Run time (seconds): 20,880 Growth P (torr): 1.3-4.2 x 10^{-7}

Cu rate

Thickness (kA)	Rate (A/s)
0 - 110	10.73

*GaSe was deposited for 2:50:07 before CGS deposition and 7:05 after

Table A-20. Reactor conditions for Growth Run #479.

Run # 479	Date: 05/24/03
Film: CGS	Operator: Woo Kyoung Kim
Substrate: 2 Mo, 1 Glass	
Objective: GaSe/Cu-rich CGS/GaSe, overall Cu/Ga~0.96 at 20 RPM	

Target Value

Metal		Se		Substrate Heater	
Cu Rate (A/s)	14	Cracker (°C)	500	Temp. (°C)	700
In Rate (A/s)	--	Ramp (°C/s)	0.5	Ramp (°C/s)	0.3
Cu tip power (%)	89.9	Crucible (°C)	260/275	RPM	12
Ga tip power (%)	24			Direction	CCW
Ga primary T (°C)	1007				

Total Film Thickness (μm): 1.1

Film Set Value

	Cu	In	Ga
Soak Power (%)	17	--	7
Rise Time (min)	5	--	5
Soak Time (min)	13	--	0

*Annealing for 30 minutes in Se atmosphere at T = 700°C

Operation Results

	Cu	In	Ga	Se Crucible	Se Cracker	Heater
Power (%)	22.7	--	13.4	15.2/20.8	9.0	36.8
Tip (°C)	1142	--	957.4	--	--	--
Primary (°C)	1132	--	1006-1008	260.3/275	500.5	700.0
LSP	14	--	1007	260/275	500	700
Kc	2	--	2	2	2	2
Ti	2	--	2	2	2	2
Td	0	--	0	0	0	0
Offset	22.3	--	10	16.0/17.5	10.0	36.8
Thick. (kA)	110	--	--	--	--	--

Run time (hr:min:sec): 2:57:33 Headspace P (torr): 4×10^{-8}

Run time (seconds): 10,653 Growth P (torr): 4×10^{-7}

Cu rate

Thickness (kA)	Rate (A/s)
0 - 110	14

*GaSe was deposited for 42:54 before CGS deposition and 3:49 after

Table A-21. Reactor conditions for Growth Run #480.

Run # 480	Date: 05/26/03
Film: CGS	Operator: Ryan Kaczynski, Ryan Acher
Substrate: 2 Mo, 1 Glass	
Objective: 3-stage emulation (GaSe/CuSe/GaSe) at 20 RPM	

Target Value

Metal		Se		Substrate Heater	
Cu Rate (A/s)	10.8	Cracker (°C)	500	Temp. (°C)	700
In Rate (A/s)	--	Ramp (°C/s)	0.5	Ramp (°C/s)	0.3
Cu tip power (%)	89.9	Crucible (°C)	260/275	RPM	12
Ga tip power (%)	24			Direction	CCW
Ga primary T (°C)	1007				

Total Film Thickness (μm): 1.1

Film Set Value

	Cu	In	Ga
Soak Power (%)	17	--	7
Rise Time (min)	5	--	5
Soak Time (min)	13	--	0

*Annealing for 30 minutes in Se atmosphere at T = 700°C

Operation Results

	Cu	In	Ga	Se Crucible	Se Cracker	Heater
Power (%)	21.8	--	13.4-13.6	14.6/18.1	9.0	36.8-37.7
Tip (°C)	1133-1140	--	954-958	--	--	--
Primary (°C)	1116-1118	--	1006-1008	260/276	500.5	699.8-700.2
LSP	10.8	--	1007	260/275	500	700
Kc	2	--	2	2	2	2
Ti	2	--	2	2	2	2
Td	0	--	0	0	0	0
Offset	21.05	--	10	15.5/18.5	10.0	37.2
Thick. (kA)	110	--	--	--	--	--

Run time (hr:min:sec): 5:48:00 Headspace P (torr): 3.5-4.8 x 10^{-8}

Run time (seconds): 20,880 Growth P (torr): 1.4-4.5 x 10^{-7}

Cu rate

Thickness (kA)	Rate (A/s)
0 - 110	10.84

*GaSe was deposited for 2:50:00 before CGS deposition and 7:05 after

Table A-22. Reactor conditions for Growth Run #510.

Run # 510	Date: 08/01/03
Film: CGS	Operator: Ryan Kaczynski, Ryan Acher
Substrate: 2 Mo, 1 Glass	
Objective: Repeat Run# 452 with T = 700°C, Cu/Ga~1.1	

Target Value

Metal		Se		Substrate Heater	
Cu Rate (A/s)	5.25/8.2	Cracker (°C)	500	Temp. (°C)	700
In Rate (A/s)	--	Ramp (°C/s)	0.5	Ramp (°C/s)	0.3
Cu tip power (%)	89.9	Crucible (°C)	260	RPM	12
Ga tip power (%)	22			Direction	CCW
Ga primary T (°C)	975				

Total Film Thickness (μm): 1.1

Film Set Value

	Cu	In	Ga
Soak Power (%)	19	--	7
Rise Time (min)	5	--	5
Soak Time (min)	13	--	0

*Annealing for 30 minutes in Se atmosphere at T = 700°C

Operation Results

	Cu	In	Ga	Se Crucible	Se Cracker	Heater
Power (%)	14/16.5	--	16.3-17	15-16	9-11	36-38
Tip (°C)	1118/1125	--	933-936	--	--	--
Primary (°C)	1047/1078	--	974-976	260.1-260.6	499.5-500.5	699.5-700.5
LSP	5.25/8.21	--	975	260	500	700
Kc	2	--	2	2	2	2
Ti	2	--	2	2	2	2
Td	0	--	0	0	0	0
Offset	14.2/15.3	--	10	16.5	10.3	37.0
Thick. (kA)	110	--	--	--	--	--

Run time (hr:min:sec): 4:12:21 Headspace P (torr): 4×10^{-8}

Run time (seconds): 15,141 Growth P (torr): 2×10^{-7}

Cu rate

Thickness (kA)	Rate (A/s)
0 - 26.65	5.25
26.65 - 110	8.28

Table A-23. Reactor conditions for Growth Run #511.

Run # 511	Date: 08/04/03
Film: CGS	Operator: Ryan Kaczynski, Ryan Acher
Substrate: 2 Mo, 1 Glass	
Objective: Repeat Run# 453 with T = 750°C, Cu/Ga~1.1	

Target Value

Metal		Se		Substrate Heater	
Cu Rate (A/s)	6.55/11.45	Cracker (°C)	500	Temp. (°C)	750
In Rate (A/s)	--	Ramp (°C/s)	0.5	Ramp (°C/s)	0.3
Cu tip power (%)	89.9	Crucible (°C)	260	RPM	12
Ga tip power (%)	22			Direction	CCW
Ga primary T (°C)	975				

Total Film Thickness (μm): 1.1

Film Set Value

	Cu	In	Ga
Soak Power (%)	19	--	7
Rise Time (min)	5	--	5
Soak Time (min)	13	--	0

*Annealing for 30 minutes in Se atmosphere at T = 750°C

Operation Results

	Cu	In	Ga	Se Crucible	Se Cracker	Heater
Power (%)	14/19	--	17.1-17.4	15.5-16.5	10-11.5	40-42
Tip (°C)	1120/1140	--	930	--	--	--
Primary (°C)	1058/1100	--	974-976	255-265	499.5-500.5	749-750.3
LSP	6.55/11.45	--	975	260	500	750
Kc	2	--	2	2	2	2
Ti	2	--	2	2	2	2
Td	0	--	0	0	0	0
Offset	14/18.5	--	10	15	10.4	40.0
Thick. (kA)	110	--	--	--	--	--

Run time (hr:min:sec): 3:22:18 Headspace P (torr): 4.5×10^{-8}
Run time (seconds): 12,138 Growth P (torr): 3.0×10^{-7}

Cu rate

Thickness (kA)	Rate (A/s)
0 - 15.7	6.58
15.7 - 110	11.43

*GaSe deposited for 25 minutes after Cu deposition

Table A-24. Reactor conditions for Growth Run #512.

Run # 512	Date: 08/05/03
Film: CGS	Operator: Ryan Kaczynski, Ryan Acher
Substrate: 2 Mo, 1 Glass	
Objective: Reverse process of Run# 511	

Target Value

Metal		Se		Substrate Heater	
Cu Rate (A/s)	8/4.55	Cracker (°C)	500	Temp. (°C)	750
In Rate (A/s)	--	Ramp (°C/s)	0.5	Ramp (°C/s)	0.3
Cu tip power (%)	89.9	Crucible (°C)	260	RPM	12
Ga tip power (%)	22			Direction	CCW
Ga primary T (°C)	975				

Total Film Thickness (μm): 1.1

Film Set Value

	Cu	In	Ga
Soak Power (%)	19	--	7
Rise Time (min)	5	--	5
Soak Time (min)	13	--	0

*Annealing for 30 minutes in Se atmosphere at T = 750°C

Operation Results

	Cu	In	Ga	Se Crucible	Se Cracker	Heater
Power (%)	16.5/13.9	--	16.9-17.6	16.5	9.8	40-42
Tip (°C)	1128/1108	--	925-927	--	--	--
Primary (°C)	1078/1047	--	974-976	259.5-260.5	500.3	749-750.5
LSP	8/4.5	--	975	260	500	750
Kc	2	--	2	2	2	2
Ti	2	--	2	2	2	2
Td	0	--	0	0	0	0
Offset	16/13.5	--	10	16.5	10.4	40.5
Thick. (kA)	110	--	--	--	--	--

Run time (hr:min:sec): 4:53:51 Headspace P (torr): 4.5×10^{-8}
Run time (seconds): 17,631 Growth P (torr): 3.0×10^{-7}

Cu rate

Thickness (kA)	Rate (A/s)
0 - 85.4	7.97
85.4 - 110	4.54

*GaSe deposited for 25 minutes before Cu deposition

Table A-25. Reactor conditions for Growth Run #513.

Run # 513	Date: 08/06/03
Film: CGS	Operator: Ryan Kaczynski, Ryan Acher
Substrate: 2 Mo, 1 Glass	
Objective: Repeat Run# 447 with T = 750°C, Cu/Ga~0.95	

Target Value

Metal		Se		Substrate Heater	
Cu Rate (A/s)	6.7/5.5/4.4	Cracker (°C)	500	Temp. (°C)	750
In Rate (A/s)	--	Ramp (°C/s)	0.5	Ramp (°C/s)	0.3
Cu tip power (%)	89.9	Crucible (°C)	260	RPM	12
Ga tip power (%)	22			Direction	CCW
Ga primary T (°C)	975				

Total Film Thickness (μm): 1.1

Film Set Value

	Cu	In	Ga
Soak Power (%)	19	--	7
Rise Time (min)	5	--	5
Soak Time (min)	13	--	0

*Annealing for 30 minutes in Se atmosphere at T = 750°C

Operation Results

	Cu	In	Ga	Se Crucible	Se Cracker	Heater
Power (%)	14.1-15.6	--	17.5-18.1	16	9.7	40-42.5
Tip (°C)	1110-1123	--	930	--	--	--
Primary (°C)	1048-1068	--	974-976	260-261	500.4	749-750.5
LSP	6.68/5.52/4.3	--	975	260	500	750
Kc	2	--	2	2	2	2
Ti	2	--	2	2	2	2
Td	0	--	0	0	0	0
Offset	13.5-15.0	--	10	17	10.4	40.5
Thick. (kA)	110	--	--	--	--	--

Run time (hr:min:sec): 5:32:04 Headspace P (torr): 6.0×10^{-8}

Run time (seconds): 19,924 Growth P (torr): 3.0×10^{-7}

Cu rate

Thickness (kA)	Rate (A/s)
0 - 44.4	6.7
44.4 - 81	5.5
81 - 110	4.4

Table A-26. Reactor conditions for Growth Run #514.

Run # 514	Date: 08/08/03
Film: CGS	Operator: Woo Kyoung Kim, Seokhyun Yoon
Substrate: 2 Mo, 1 Glass	
Objective: Repeat Run# 452 with T = 750°C, Cu/Ga~1.1	

Target Value

Metal		Se		Substrate Heater	
Cu Rate (A/s)	4.65/7.25	Cracker (°C)	500	Temp. (°C)	750
In Rate (A/s)	--	Ramp (°C/s)	0.5	Ramp (°C/s)	0.3
Cu tip power (%)	89.9	Crucible (°C)	260	RPM	12
Ga tip power (%)	22			Direction	CCW
Ga primary T (°C)	975				

Total Film Thickness (μm): 1.1

Film Set Value

	Cu	In	Ga
Soak Power (%)	19	--	7
Rise Time (min)	5	--	5
Soak Time (min)	13	--	0

*Annealing for 30 minutes in Se atmosphere at T = 750°C

Operation Results

	Cu	In	Ga	Se Crucible	Se Cracker	Heater
Power (%)	13.7/--	--	--	--	--	--
Tip (°C)	1111/--	--	--	--	--	--
Primary (°C)	1044/--	--	--	--	--	--
LSP	4.65/7.25	--	975	260	500	700
Kc	2	--	2	2	2	2
Ti	2	--	2	2	2	2
Td	0	--	0	0	0	0
Offset	13.0/--	--	10	--	--	--
Thick. (kA)	110	--	--	--	--	--

Run time (hr:min:sec): 4:45:45 Headspace P (torr):
Run time (seconds): 17,145 Growth P (torr):

Cu rate

Thickness (kA)	Rate (A/s)
0 - 26.7	4.71
26.7 - 110	7.25

Table A-27. Reactor conditions for Growth Run #515.

Run # 515	Date: 08/11/03
Film: CGS	Operator: Seokhyun Yoon
Substrate: 2 Mo, 1 Glass	
Objective: Graded Cu-rich CGS	

Target Value

Metal		Se		Substrate Heater	
Cu Rate (A/s)	0/5.3/8.4/5.2	Cracker (°C)	500	Temp. (°C)	750
In Rate (A/s)	--	Ramp (°C/s)	0.5	Ramp (°C/s)	0.3
Cu tip power (%)	89.9	Crucible (°C)	260	RPM	12
Ga tip power (%)	22			Direction	CCW
Ga primary T (°C)	975				

Total Film Thickness (μm): 1.1

Film Set Value

	Cu	In	Ga
Soak Power (%)	19	--	7
Rise Time (min)	5	--	5
Soak Time (min)	13	--	0

*Annealing for 30 minutes in Se atmosphere at T = 750°C

Operation Results

	Cu	In	Ga	Se Crucible	Se Cracker	Heater
Power (%)	14.7/--/--	--	18.05	15-17	8.8-9.2	39-41
Tip (°C)	1118/--/--	--	926	--	--	--
Primary (°C)	1055/1092/--	--	974-976	260-261	500-501	749-750
LSP	5.3/8.3/5.3	--	975	260	500	750
Kc	2	--	2	2	2	2
Ti	2	--	2	2	2	2
Td	0	--	0	0	0	0
Offset	14.1/17.5/--	--	10	18	11	42
Thick. (kA)	110	--	--	--	--	--

Run time (hr:min:sec): 4:37:29 Headspace P (torr):
Run time (seconds): 16,649 Growth P (torr):

Cu rate

Thickness (kA)	Rate (A/s)
0 - 18.8	5.30
18.8 - 98.9	8.42
98.9 - 110	5.59

*GaSe deposited for 26:40 before Cu deposition

Table A-28. Reactor conditions for Growth Run #516.

Run # 516	Date: 08/12/03
Film: CGS	Operator: Woo Kyoung Kim
Substrate: 2 Mo, 1 Glass	
Objective: Cu-rich CGS with constant Cu rate throughout growth run	

Target Value

Metal		Se		Substrate Heater	
Cu Rate (A/s)	6	Cracker (°C)	500	Temp. (°C)	750
In Rate (A/s)	--	Ramp (°C/s)	0.5	Ramp (°C/s)	0.3
Cu tip power (%)	89.9	Crucible (°C)	260	RPM	12
Ga tip power (%)	22			Direction	CCW
Ga primary T (°C)	975				

Total Film Thickness (μm): 1.1

Film Set Value

	Cu	In	Ga
Soak Power (%)	19	--	7
Rise Time (min)	5	--	5
Soak Time (min)	13	--	0

*Annealing for 30 minutes in Se atmosphere at T = 750°C

Operation Results

	Cu	In	Ga	Se Crucible	Se Cracker	Heater
Power (%)	15	--	17.8-18	15-16	10	40-42
Tip (°C)	1120	--	925	--	--	--
Primary (°C)	1065	--	974.5-975.5	260-261	500.0	750.0
LSP	6	--	975	260	500	750
Kc	2	--	2	2	2	2
Ti	2	--	2	2	2	2
Td	0	--	0	0	0	0
Offset	14.3	--	10	17.3	10.0	41
Thick. (kA)	110	--	--	--	--	--

Run time (hr:min:sec): 5:05:33 Headspace P (torr): 5-9 x 10^{-8}

Run time (seconds): 18,333 Growth P (torr): 5 x 10^{-7}

Cu rate

Thickness (kA)	Rate (A/s)
0 - 110	6.0

Table A-29. Reactor conditions for Growth Run #521.

Run # 521	Date: 09/29/03
Film: CGS	Operator: Ryan Kaczynski
Substrate: 1 Mo, 1 Glass	
Objective: Repeat Run# 452 with T = 900°C (0.8/1.25)	

Target Value

Metal		Se		Substrate Heater	
Cu Rate (A/s)	5.4/8.4	Cracker (°C)	500	Temp. (°C)	900
In Rate (A/s)	--	Ramp (°C/s)	0.5	Ramp (°C/s)	0.3
Cu tip power (%)	89.9	Crucible (°C)	265	RPM	12
Ga tip power (%)	22			Direction	CCW
Ga primary T (°C)	978				

Total Film Thickness (μm): 1.1

Film Set Value

	Cu	In	Ga
Soak Power (%)	19	--	7
Rise Time (min)	5	--	5
Soak Time (min)	13	--	0

*Annealing for 30 minutes in Se atmosphere at T = 900°C

Operation Results

	Cu	In	Ga	Se Crucible	Se Cracker	Heater
Power (%)	14.5/17.7	--	17.7-17.8	19-20	11.9	53-57.8
Tip (°C)	1120/1138	--	928-931	--	--	--
Primary (°C)	1056/1090	--	977-979	265.0	500.3	898-900.5
LSP	5.4/8.4	--	978	265	500	900
Kc	2	--	2	2	2	2
Ti	2	--	2	2	2	2
Td	0	--	0	0	0	0
Offset	13.5/16.8	--	10	20.0	12.5	54.0
Thick. (kA)	110	--	--	--	--	--

Run time (hr:min:sec): 4:07:20 Headspace P (torr): 1.8×10^{-7}

Run time (seconds): 14,840 Growth P (torr): 2.5×10^{-6}

Cu rate

Thickness (kA)	Rate (A/s)
0 - 26.72	5.43
26.72 - 110	8.40

Table A-30. Reactor conditions for Growth Run #522.

Run # 522	Date: 09/30/03
Film: CGS	Operator: Seokhyun Yoon
Substrate: 1 Mo, 1 Glass	
Objective: Repeat Run# 453 with T = 900°C (0.8/1.4/0)	

Target Value

Metal		Se		Substrate Heater	
Cu Rate (A/s)	5.4/8.4/0	Cracker (°C)	500	Temp. (°C)	900
In Rate (A/s)	--	Ramp (°C/s)	0.5	Ramp (°C/s)	0.3
Cu tip power (%)	89.9	Crucible (°C)	265	RPM	12
Ga tip power (%)	22			Direction	CCW
Ga primary T (°C)	978				

Total Film Thickness (μm): 1.1

Film Set Value

	Cu	In	Ga
Soak Power (%)	19	--	7
Rise Time (min)	5	--	5
Soak Time (min)	13	--	0

*Annealing for 30 minutes in Se atmosphere at T = 900°C

Operation Results

	Cu	In	Ga	Se Crucible	Se Cracker	Heater
Power (%)	15/18.6	--	17.1	19.9	12.1-12.3	55-57
Tip (°C)	1118/1130	--	928	--	--	--
Primary (°C)	1050/1097	--	977-979	264.5-265.5	500.3	897-900
LSP	5.4/8.4	--	978	265	500	900
Kc	2	--	2	2	2	2
Ti	2	--	2	2	2	2
Td	0	--	0	0	0	0
Offset	13/16	--	10	19.5	12.5	54.0
Thick. (kA)	110	--	--	--	--	--

Run time (hr:min:sec): 4:06:01 Headspace P (torr): 2.1×10^{-7}

Run time (seconds): 14,761 Growth P (torr): 1.6×10^{-6}

Cu rate

Thickness (kA)	Rate (A/s)
0 - 13	5.4
13 - 110	8.4

*GaSe deposited for 35 minutes after Cu deposition

Table A-31. Reactor conditions for Growth Run #523.

Run # 523	Date: 10/01/03
Film: CGS	Operator: Woo Kyoung Kim
Substrate: 1 Mo, 1 Glass	
Objective: Repeat Run# 515 with T = 900°C (0/0.9/1.45/0.9)	

Target Value

Metal		Se		Substrate Heater	
Cu Rate (A/s)	5.85/9.43/5.85	Cracker (°C)	500	Temp. (°C)	900
In Rate (A/s)	--	Ramp (°C/s)	0.5	Ramp (°C/s)	0.3
Cu tip power (%)	89.9	Crucible (°C)	265	RPM	12
Ga tip power (%)	22			Direction	CCW
Ga primary T (°C)	975				

Total Film Thickness (μm): 1.1

Film Set Value

	Cu	In	Ga
Soak Power (%)	19	--	7
Rise Time (min)	5	--	5
Soak Time (min)	13	--	0

*Annealing for 30 minutes in Se atmosphere at T = 900°C

Operation Results

	Cu	In	Ga	Se Crucible	Se Cracker	Heater
Power (%)	--/18.8/--	--	17.5-17.6	20-20.5	12.2	55-57
Tip (°C)	--/1136/--	--	928	--	--	--
Primary (°C)	--/1100/--	--	974-976	264.5-265.5	500.2	897-900
LSP	5.85/9.43/5.85	--	975	265	500	900
Kc	2	--	2	2	2	2
Ti	2	--	2	2	2	2
Td	0	--	0	0	0	0
Offset	15/17.75	--	10	19.5	12.5	55.0
Thick. (kA)	110	--	--	--	--	--

Run time (hr:min:sec): 4:11:10 Headspace P (torr): 1.8×10^{-7}

Run time (seconds): 15,070 Growth P (torr): 1.8×10^{-6}

Cu rate

Thickness (kA)	Rate (A/s)
0 - 17.5	5.85
17.5 - 99.5	9.43
99.5 - 110	5.85

*GaSe deposited for 25 minutes before Cu deposition

Table A-32. Reactor conditions for Growth Run #524.

Run # 524	Date: 10/02/03
Film: CGS	Operator: Seokhyun Yoon
Substrate: 1 Mo, 1 Glass	
Objective: Repeat Run# 453 with T = 900°C (0/1.4/0.8)	

Target Value

Metal		Se		Substrate Heater	
Cu Rate (A/s)	0/9.1/5.2	Cracker (°C)	500	Temp. (°C)	900
In Rate (A/s)	--	Ramp (°C/s)	0.5	Ramp (°C/s)	0.3
Cu tip power (%)	89.9	Crucible (°C)	258	RPM	12
Ga tip power (%)	22			Direction	CCW
Ga primary T (°C)	975				

Total Film Thickness (μm): 1.1

Film Set Value

	Cu	In	Ga
Soak Power (%)	19	--	7
Rise Time (min)	5	--	5
Soak Time (min)	13	--	0

*Annealing for 30 minutes in Se atmosphere at T = 900°C

Operation Results

	Cu	In	Ga	Se Crucible	Se Cracker	Heater
Power (%)	19.3/15.3	--	17.9	19.9-20.3	12.2-12.5	55-58
Tip (°C)	1139/1125	--	924	--	--	--
Primary (°C)	1101/1064	--	977-979	256-258	500.1	897-900
LSP	9.1/5.2	--	978	258	500	900
Kc	2	--	2	2	2	2
Ti	2	--	2	2	2	2
Td	0	--	0	0	0	0
Offset	18.4/14.8	--	10	19.5	12.5	55.0
Thick. (kA)	110	--	--	--	--	--

Run time (hr:min:sec): 4:13:03 Headspace P (torr): 1.0×10^{-7}
Run time (seconds): 15,183 Growth P (torr): 1.0×10^{-6}

Cu rate

Thickness (kA)	Rate (A/s)
0 - 88.7	9.1
88.7 - 110	5.2

*GaSe deposited for 25 minutes before Cu deposition

Table A-33. Reactor conditions for Growth Run #525.

Run # 525	Date: 10/03/03
Film: CGS	Operator: Ryan Kaczynski
Substrate: 2 Mo, 1 Glass	
Objective: Repeat Run# 513 with T = 900°C (1.15/0.95/0.75)	

Target Value

Metal		Se		Substrate Heater	
Cu Rate (A/s)	7.5/6.2/4.9	Cracker (°C)	500	Temp. (°C)	900
In Rate (A/s)	--	Ramp (°C/s)	0.5	Ramp (°C/s)	0.3
Cu tip power (%)	89.9	Crucible (°C)	265	RPM	12
Ga tip power (%)	22			Direction	CCW
Ga primary T (°C)	978				

Total Film Thickness (μm): 1.1

Film Set Value

	Cu	In	Ga
Soak Power (%)	19	--	7
Rise Time (min)	5	--	5
Soak Time (min)	13	--	0

*Annealing for 30 minutes in Se atmosphere at T = 900°C

Operation Results

	Cu	In	Ga	Se Crucible	Se Cracker	Heater
Power (%)	15-17.3	--	17.7-18.1	19.5	12.1	55-60
Tip (°C)	1116-1133	--	924	--	--	--
Primary (°C)	1060-1083	--	977-979	265.2	500.1	898-900
LSP	7.5/6.2/4.9	--	978	265	500	900
Kc	2	--	2	2	2	2
Ti	2	--	2	2	2	2
Td	0	--	0	0	0	0
Offset	14.2-16.3	--	10	20.0	12.5	56.0
Thick. (kA)	110	--	--	--	--	--

Run time (hr:min:sec): 4:57:40 Headspace P (torr): 1.0-1.8 x 10^{-7}
Run time (seconds): 17,860 Growth P (torr): 1.0-1.4 x 10^{-6}

Cu rate

Thickness (kA)	Rate (A/s)
0 - 44.4	7.46
44.4 - 81.1	6.17
81.1 - 110	4.85

Table A-34. Reactor conditions for Growth Run #535.

Run # 535	Date: 12/05/03
Film: CGS	Operator: Ryan Kaczynski
Substrate: 2 Mo, 1 Glass	
Objective: 3-stage emulation (GaSe/CuSe/GaSe) at T = 822/900°C	

Target Value

Metal		Se		Substrate Heater	
Cu Rate (A/s)	9.83	Cracker (°C)	500	Temp. (°C)	822/900
In Rate (A/s)	--	Ramp (°C/s)	0.5	Ramp (°C/s)	0.3
Cu tip power (%)	89.9	Crucible (°C)	265	RPM	12
Ga tip power (%)	24			Direction	CCW
Ga primary T (°C)	1005				

Total Film Thickness (μm): 1.0

Film Set Value

	Cu	In	Ga
Soak Power (%)	19	--	7
Rise Time (min)	5	--	5
Soak Time (min)	13	--	0

Operation Results

	Cu	In	Ga	Se Crucible	Se Cracker	Heater
Power (%)	19-19.4	--	18.5-19.3	22/18	12.1	52/58-62
Tip (°C)	1144	--	943-947	--	--	--
Primary (°C)	1107-1115	--	1004-1006	265.0	500.0	822.5/900.5
LSP	10	--	1005	265	500	822/900
Kc	2	--	2	2	2	2
Ti	2	--	2	2	2	2
Td	0	--	0	0	0	0
Offset	18-19.5	--	10	22/18.7	12.0	51/59
Thick. (kA)	100	--	--	--	--	--

Run time (hr:min:sec): 5:47:52 Headspace P (torr): 7.5×10^{-8} - 1.0×10^{-7}

Run time (seconds): 20,872 Growth P (torr): 3.0×10^{-7} - 1.0×10^{-6}

Cu rate

Thickness (kA)	Rate (A/s)
0 - 100	9.84

*GaSe was deposited for 2:49:30 before CuSe deposition and 8:55 after

Table A-35. Reactor conditions for Growth Run #536.

Run # 536	Date: 12/12/03
Film: CGS	Operator: Ryan Kaczynski
Substrate: 2 Mo, 1 Glass	
Objective: 3-stage emulation (GaSe/CuSe/GaSe) at T = 822/900°C	

Target Value

Metal		Se		Substrate Heater	
Cu Rate (A/s)	10	Cracker (°C)	500	Temp. (°C)	822/900
In Rate (A/s)	--	Ramp (°C/s)	0.5	Ramp (°C/s)	0.3
Cu tip power (%)	89.9	Crucible (°C)	265	RPM	12
Ga tip power (%)	24			Direction	CCW
Ga primary T (°C)	1005				

Total Film Thickness (μm): 1.0

Film Set Value

	Cu	In	Ga
Soak Power (%)	19	--	7
Rise Time (min)	5	--	5
Soak Time (min)	13	--	0

Operation Results

	Cu	In	Ga	Se Crucible	Se Cracker	Heater
Power (%)	17.3-18.5	--	18.7-18.9	21/18	12.3	50-53/58-62
Tip (°C)	1153-1156	--	940-945	--	--	--
Primary (°C)	1108-1113	--	1004-1006	265.9	499.9	823/901
LSP	10.0	--	1005	265	500	822/900
Kc	2	--	2	2	2	2
Ti	2	--	2	2	2	2
Td	0	--	0	0	0	0
Offset	16.5-17.7	--	10	21.5/18.5	12.0	51/60
Thick. (kA)	100	--	--	--	--	--

Run time (hr:min:sec): 6:01:33 Headspace P (torr): 7.5×10^{-8} - 1.5×10^{-7}

Run time (seconds): 21,693 Growth P (torr): 2.8×10^{-7} - 9.5×10^{-7}

Cu rate

Thickness (kA)	Rate (A/s)
0 - 100	10.00

*GaSe was deposited for 3:05:12 before CuSe deposition and 9:44 after

Table A-36. Reactor conditions for Growth Run #537.

Run # 537	Date: 12/13/03
Film: CGS	Operator: Ryan Kaczynski, Ryan Acher
Substrate: 2 Mo, 1 Glass	
Objective: Thin 3-stage emulation (GaSe/CuSe/GaSe) at T = 822/900°C	

Target Value

Metal		Se		Substrate Heater	
Cu Rate (A/s)	10	Cracker (°C)	500	Temp. (°C)	822/900
In Rate (A/s)	--	Ramp (°C/s)	0.5	Ramp (°C/s)	0.3
Cu tip power (%)	89.9	Crucible (°C)	265	RPM	12
Ga tip power (%)	24			Direction	CCW
Ga primary T (°C)	1005				

Total Film Thickness (μm): 0.5

Film Set Value

	Cu	In	Ga
Soak Power (%)	19	--	7
Rise Time (min)	5	--	5
Soak Time (min)	13	--	0

Operation Results

	Cu	In	Ga	Se Crucible	Se Cracker	Heater
Power (%)	19.5	--	18.8-19.3	21	12	52/58-62
Tip (°C)	1136-1150	--	941	--	--	--
Primary (°C)	1101-1109	--	1004-1006	265.3	500.0	822.5/901
LSP	10.0	--	1005	265	500	822/900
Kc	2	--	2	2	2	2
Ti	2	--	2	2	2	2
Td	0	--	0	0	0	0
Offset	17.3-19.5	--	10	21.5/18.5	12.0	51.5/62
Thick. (kA)	50.0	--	--	--	--	--

Run time (hr:min:sec): 3:01:15 Headspace P (torr): 4.4-8.3 x 10^{-8}

Run time (seconds): 10,875 Growth P (torr): 1.9-7.8 x 10^{-7}

Cu rate

Thickness (kA)	Rate (A/s)
0 - 100	9.95

*GaSe was deposited for 1:32:36 before CuSe deposition and 4:52 after

Table A-37. Reactor conditions for Growth Run #538.

Run # 538	Date: 12/15/03
Film: CGS	Operator: Ryan Kaczynski
Substrate: 2 Mo, 1 Glass	
Objective: Cu-rich, constant-rate CGS with GaSe start	

Target Value

Metal		Se		Substrate Heater	
Cu Rate (A/s)	13	Cracker (°C)	500	Temp. (°C)	900
In Rate (A/s)	--	Ramp (°C/s)	0.5	Ramp (°C/s)	0.3
Cu tip power (%)	89.9	Crucible (°C)	265	RPM	12
Ga tip power (%)	24			Direction	CCW
Ga primary T (°C)	1005				

Total Film Thickness (μm): 1.0

Film Set Value

	Cu	In	Ga
Soak Power (%)	19	--	7
Rise Time (min)	5	--	5
Soak Time (min)	13	--	0

Operation Results

	Cu	In	Ga	Se Crucible	Se Cracker	Heater
Power (%)	22.1-22.5	--	18.6-18.9	18.5	12.1	58-62
Tip (°C)	1142-1148	--	941-943	--	--	--
Primary (°C)	1124-1130	--	1004-1006	265.5	500.0	899-901
LSP	13.0	--	1005	265	500	822/900
Kc	2	--	2	2	2	2
Ti	2	--	2	2	2	2
Td	0	--	0	0	0	0
Offset	21.3-22.0	--	10	18.5	12.0	60.0
Thick. (kA)	100.0	--	--	--	--	--

Run time (hr:min:sec): 2:17:26 Headspace P (torr): 6.5×10^{-8} - 1.0×10^{-7}

Run time (seconds): 8,246 Growth P (torr): 3.6×10^{-7} - 6.0×10^{-7}

Cu rate

Thickness (kA)	Rate (A/s)
0 - 100	12.98

*GaSe deposited for 9 minutes before Cu deposition

Table A-38. Reactor conditions for Growth Run #540.

Run # 540	Date: 12/17/03
Film: CGS	Operator: Ryan Kaczynski
Substrate: 2 Mo, 1 Glass	
Objective: 3-stage emulation (GaSe/CuSe/GaSe) at T = 822/900°C	

Target Value

Metal		Se		Substrate Heater	
Cu Rate (A/s)	12.6	Cracker (°C)	500	Temp. (°C)	822/900
In Rate (A/s)	--	Ramp (°C/s)	0.5	Ramp (°C/s)	0.3
Cu tip power (%)	89.9	Crucible (°C)	265	RPM	12
Ga tip power (%)	24			Direction	CCW
Ga primary T (°C)	1005				

Total Film Thickness (μm): 1.0

Film Set Value

	Cu	In	Ga
Soak Power (%)	19	--	7
Rise Time (min)	5	--	5
Soak Time (min)	13	--	0

Operation Results

	Cu	In	Ga	Se Crucible	Se Cracker	Heater
Power (%)	20.5-21.5	--	19.0-19.3	21.3/19.2	12.1	50/58-62
Tip (°C)	1140-1144	--	935-943	--	--	--
Primary (°C)	1116-1122	--	1004-1006	265-266	499.9	823/901
LSP	12.6	--	1005	265	500	822/900
Kc	2	--	2	2	2	2
Ti	2	--	2	2	2	2
Td	0	--	0	0	0	0
Offset	20.0-21.5	--	10	21.5/18.5	12.0	51/63
Thick. (kA)	100	--	--	--	--	--

Run time (hr:min:sec): 4:34:45 Headspace P (torr): 3.2×10^{-8} - 1.4×10^{-7}

Run time (seconds): 16,485 Growth P (torr): 1.8×10^{-7} - 9.3×10^{-7}

Cu rate

Thickness (kA)	Rate (A/s)
0 - 100	12.60

*GaSe deposited for 2:12:17 before CuSe deposition and 10:10 after

Table A-39. Reactor conditions for Growth Run #541.

Run # 541	Date: 12/18/03
Film: CGS	Operator: Woo Kyoung Kim
Substrate: 2 Mo, 1 Glass	
Objective: Repeat Run# 523 with T = 822/900°C (0/1/1.6/1)	

Target Value

Metal		Se		Substrate Heater	
Cu Rate (A/s)	5.8/9.4/5.8	Cracker (°C)	500	Temp. (°C)	822/900
In Rate (A/s)	--	Ramp (°C/s)	0.5	Ramp (°C/s)	0.3
Cu tip power (%)	89.9	Crucible (°C)	265	RPM	12
Ga tip power (%)	22			Direction	CCW
Ga primary T (°C)	975				

Total Film Thickness (μm): 1.1

Film Set Value

	Cu	In	Ga
Soak Power (%)	19	--	7
Rise Time (min)	5	--	5
Soak Time (min)	13	--	0

*Annealing for 30 minutes in Se atmosphere at T = 900°C

Operation Results

	Cu	In	Ga	Se Crucible	Se Cracker	Heater
Power (%)	17.4/19.9/--	--	17.8	18.1	12.2	59-62
Tip (°C)	1114/1132/--	--	912	--	--	--
Primary (°C)	1066/1101/--	--	974-976	264.5-265.5	500.2	897
LSP	5.8/9.4/5.8	--	975	265	500	900
Kc	2	--	2	2	2	2
Ti	2	--	2	2	2	2
Td	0	--	0	0	0	0
Offset	17/19.2/16.5	--	10	18	12.5	55.0
Thick. (kA)	110.5	--	--	--	--	--

Run time (hr:min:sec): 4:11:10 Headspace P (torr): 1.0×10^{-7}

Run time (seconds): 15,070 Growth P (torr): $5\text{-}7 \times 10^{-7}$

Cu rate

Thickness (kA)	Rate (A/s)
0 - 10.5	5.8
10.5 - 94.75	9.4
94.75 - 110.5	5.8

*GaSe deposited for 25 minutes before Cu deposition

Table A-40. Reactor conditions for Growth Run #542.

Run # 542	Date: 12/19/03
Film: CGS	Operator: Woo Kyoung Kim
Substrate: 2 Mo, 1 Glass	
Objective: Repeat Run# 523 with T = 850°C (0/1.2/1.6/1.0)	

Target Value

Metal		Se		Substrate Heater	
Cu Rate (A/s)	7/9.4/5.8	Cracker (°C)	500	Temp. (°C)	850
In Rate (A/s)	--	Ramp (°C/s)	0.5	Ramp (°C/s)	0.3
Cu tip power (%)	89.9	Crucible (°C)	265	RPM	12
Ga tip power (%)	22			Direction	CCW
Ga primary T (°C)	978				

Total Film Thickness (μm): 1.15

Film Set Value

	Cu	In	Ga
Soak Power (%)	19	--	7
Rise Time (min)	5	--	5
Soak Time (min)	13	--	0

*Annealing for 30 minutes in Se atmosphere at T = 850°C

Operation Results

	Cu	In	Ga	Se Crucible	Se Cracker	Heater
Power (%)	17-19.4	--	18.1	18.4	12.1	55-56
Tip (°C)	1125-1137	--	--	--	--	--
Primary (°C)	1077-1170	--	977-979	265.5-265.7	500.2	849.5-850.4
LSP	7.0/9.4/5.8	--	978	265	500	850
Kc	2	--	2	2	2	2
Ti	2	--	2	2	2	2
Td	0	--	0	0	0	0
Offset	16.4-18.9	--	10	19.5	12.5	55.0
Thick. (kA)	115.6	--	--	--	--	--

Run time (hr:min:sec): 4:06:22 Headspace P (torr): 9.0×10^{-8}

Run time (seconds): 14,782 Growth P (torr): 3.6×10^{-7}

Cu rate

Thickness (kA)	Rate (A/s)
0 - 12.2	7.0
12.2 - 93	9.36
93 - 115.6	5.85

*GaSe deposited for 25 minutes before Cu deposition

Table A-41. Reactor conditions for Growth Run #569.

Run # 569	Date: 03/19/04
Film: CIGS	Operator: Ryan Kaczynski
Substrate: 2 Mo	
Objective: Constant rate CIGS	

Target Value

Metal		Se		Substrate Heater	
Cu Rate (A/s)	12.5	Cracker (°C)	500	Temp. (°C)	900
In Rate (A/s)	7.5	Ramp (°C/s)	0.5	Ramp (°C/s)	0.3
Cu tip power (%)	84.9	Crucible (°C)	265	RPM	12
Ga tip power (%)	22			Direction	CCW
Ga primary T (°C)	978				

Total Film Thickness (μm): 1.0

Film Set Value

	Cu	In	Ga
Soak Power (%)	19	39	7
Rise Time (min)	5	5	5
Soak Time (min)	13	13	0

Operation Results

	Cu	In	Ga	Se Crucible	Se Cracker	Heater
Power (%)	25.3	36	19.0	20.5-22	10.7-10.8	62-64
Tip (°C)	1127	--	907	--	--	--
Primary (°C)	1139	922	977-979	264.7-265	500.7	899-900.5
LSP	12.5	7.5	978	265	500	900
Kc	2	2	2	2	2	2
Ti	2	2	2	2	2	2
Td	0	0	0	0	0	0
Offset	22.2	35.4	10	21	12.0	62.0
Thick. (kA)	100	59.92	--	--	--	--

Run time (hr:min:sec): 2:13:22 Headspace P (torr): 6.3-8.7 x 10^{-8}

Run time (seconds): 8002 Growth P (torr): 1.7-2.5 x 10^{-7}

Rate

Cu		In	
Thickness (kA)	Rate (A/s)	Thickness (kA)	Rate (A/s)
0 - 100	12.50	0 - 59.9	7.49

Table A-42. Reactor conditions for Growth Run #575.

Run # 575	Date: 04/26/04
Film: CIGS	Operator: Ryan Kaczynski
Substrate: 4 Mo, 1 Glass	
Objective: Constant rate CIGS, x~0.3	

Target Value

Metal		Se		Substrate Heater	
Cu Rate (A/s)	12.5	Cracker (°C)	500	Temp. (°C)	900
In Rate (A/s)	8	Ramp (°C/s)	0.5	Ramp (°C/s)	0.3
Cu tip power (%)	84.9	Crucible (°C)	265	RPM	12
Ga tip power (%)	22			Direction	CCW
Ga primary T (°C)	978				

Total Film Thickness (μm): 1.0

Film Set Value

	Cu	In	Ga
Soak Power (%)	19	39	7
Rise Time (min)	5	5	5
Soak Time (min)	13	13	0

Operation Results

	Cu	In	Ga	Se Crucible	Se Cracker	Heater
Power (%)	22-24	36	19-19.3	22-22.5	10.7-10.8	58.5-63.5
Tip (°C)	1132-1136	--	927-934	--	--	--
Primary (°C)	1133-1139	942-966	977-979	264.7-265.3	501.3	898-901
LSP	12.5	8.0	978	265	500	900
Kc	2	2	2	2	2	2
Ti	2	2	2	2	2	2
Td	0	0	0	0	0	0
Offset	21.8-22.0	35.5-37.0	10	23	12.0	61.0
Thick. (kA)	100	64.1	--	--	--	--

Run time (hr:min:sec): 2:13:33 Headspace P (torr): 1.2×10^{-7}

Run time (seconds): 8013 Growth P (torr): $7.8\text{-}9.0 \times 10^{-7}$

Rate

Cu		In	
Thickness (kA)	Rate (A/s)	Thickness (kA)	Rate (A/s)
0 - 100	12.48	0 - 64.1	8.00

Table A-43. Reactor conditions for Growth Run #578.

Run # 578	Date: 05/03/04
Film: CIGS	Operator: Ryan Kaczynski
Substrate: 3 Mo, 1 Glass	
Objective: Thick, constant rate CIGS, x~0.3	

Target Value

Metal		Se		Substrate Heater	
Cu Rate (A/s)	12.5	Cracker (°C)	500	Temp. (°C)	900
In Rate (A/s)	8	Ramp (°C/s)	0.5	Ramp (°C/s)	0.3
Cu tip power (%)	84.9	Crucible (°C)	265	RPM	12
Ga tip power (%)	22			Direction	CCW
Ga primary T (°C)	978				

Total Film Thickness (μm): 1.5

Film Set Value

	Cu	In	Ga
Soak Power (%)	19	39	7
Rise Time (min)	5	5	5
Soak Time (min)	13	13	0

Operation Results

	Cu	In	Ga	Se Crucible	Se Cracker	Heater
Power (%)	22-23.5	36-37.5	19.5-20.1	22-22.5	9-9.5	59-63.5
Tip (°C)	1129-1140	--	916-927	--	--	--
Primary (°C)	1133-1140	941-971	977-979	264.8-265.4	501.7	899-901
LSP	12.5	8.0	978	265	500	900
Kc	2	2	2	2	2	2
Ti	2	2	2	2	2	2
Td	0	0	0	0	0	0
Offset	22-22.8	35.8-36.5	10	23	12.0	61.0
Thick. (kA)	150	96.13	--	--	--	--

Run time (hr:min:sec): 3:20:24 Headspace P (torr): 1.2×10^{-7}

Run time (seconds): 12,024 Growth P (torr): $8.5\text{-}9.5 \times 10^{-7}$

Rate

Cu		In	
Thickness (kA)	Rate (A/s)	Thickness (kA)	Rate (A/s)
0 - 100	12.48	0 - 64.1	8.00

Table A-44. Reactor conditions for Growth Run #579.

Run # 579	Date: 05/04/04
Film: CIGS	Operator: Ryan Kaczynski
Substrate: 3 Mo, 1 Glass	
Objective: Thick, constant rate CIGS, x~0.3	

Target Value

Metal		Se		Substrate Heater	
Cu Rate (A/s)	12.5	Cracker (°C)	500	Temp. (°C)	900
In Rate (A/s)	8	Ramp (°C/s)	0.5	Ramp (°C/s)	0.3
Cu tip power (%)	84.9	Crucible (°C)	265	RPM	12
Ga tip power (%)	22			Direction	CCW
Ga primary T (°C)	978				

Total Film Thickness (μm): 2.0

Film Set Value

	Cu	In	Ga
Soak Power (%)	19	39	7
Rise Time (min)	5	5	5
Soak Time (min)	13	13	0

Operation Results

	Cu	In	Ga	Se Crucible	Se Cracker	Heater
Power (%)	23-25	37-37.5	20.4-20.7	22.6-23.6	9-9.7	59.5-64
Tip (°C)	1129-1145	--	914-920	--	--	--
Primary (°C)	1133-1150	945-975	977-979	264.7-265.3	501.3	899-901
LSP	12.5	8.0	978	265	500	900
Kc	2	2	2	2	2	2
Ti	2	2	2	2	2	2
Td	0	0	0	0	0	0
Offset	22.5-23.5	36.0-36.7	10	23	12.0	61.0
Thick. (kA)	200	128	--	--	--	--

Run time (hr:min:sec): 4:26:26
Run time (seconds): 15,986
Headspace P (torr): 8.0×10^{-8} - 1.2×10^{-7}
Growth P (torr): 7.0×10^{-7} - 1.0×10^{-6}

Rate

Cu		In	
Thickness (kA)	Rate (A/s)	Thickness (kA)	Rate (A/s)
0 - 100	12.51	0 - 64.1	8.00

Table A-45. Reactor conditions for Growth Run #582.

Run # 582	Date: 05/11/04
Film: CIS	Operator: Ryan Kaczynski
Substrate: 3 Mo, 1 Glass	
Objective: Constant rate CIS, x=0	

Target Value

Metal		Se		Substrate Heater	
Cu Rate (A/s)	12.5	Cracker (°C)	500	Temp. (°C)	900
In Rate (A/s)	12.25	Ramp (°C/s)	0.5	Ramp (°C/s)	0.3
Cu tip power (%)	84.9	Crucible (°C)	265	RPM	12
Ga tip power (%)	--			Direction	CCW
Ga primary T (°C)	--				

Total Film Thickness (μm): 1.0

Film Set Value

	Cu	In	Ga
Soak Power (%)	19	39	--
Rise Time (min)	5	5	--
Soak Time (min)	13	13	--

Operation Results

	Cu	In	Ga	Se Crucible	Se Cracker	Heater
Power (%)	21.5-25	38.3-39.5	--	23.8-24	9.5-10.4	59-63.5
Tip (°C)	1137-1150	--	--	--	--	--
Primary (°C)	1140-1148	965-992	--	264.5	500.8	898-901
LSP	12.5	12.25	--	265	500	900
Kc	2	2	--	2	2	2
Ti	2	2	--	2	2	2
Td	0	0	--	0	0	0
Offset	22.3-23.0	37.8-38.2	--	23	12.0	61.0
Thick. (kA)	100	128	--	--	--	--

Run time (hr:min:sec): 2:13:10 Headspace P (torr): 6-9 x 10^{-8}

Run time (seconds): 7990 Growth P (torr): 4-7 x 10^{-7}

Rate

Cu		In	
Thickness (kA)	Rate (A/s)	Thickness (kA)	Rate (A/s)
0 - 100	12.52	0 - 97.6	12.22

Table A-46. Reactor conditions for Growth Run #586.

Run # 586	Date: 05/17/04
Film: CIGS	Operator: Ryan Kaczynski
Substrate: 3 Mo, 1 Glass	
Objective: Constant rate CIGS, x<0.3	

Target Value

Metal		Se		Substrate Heater	
Cu Rate (A/s)	15.0	Cracker (°C)	500	Temp. (°C)	900
In Rate (A/s)	11.5	Ramp (°C/s)	0.5	Ramp (°C/s)	0.3
Cu tip power (%)	84.9	Crucible (°C)	265	RPM	12
Ga tip power (%)	22			Direction	CCW
Ga primary T (°C)	978				

Total Film Thickness (μm): 1.0

Film Set Value

	Cu	In	Ga
Soak Power (%)	23	39	7
Rise Time (min)	5	5	5
Soak Time (min)	13	13	0

Operation Results

	Cu	In	Ga	Se Crucible	Se Cracker	Heater
Power (%)	23.5-24.5	37-38	20.6-20.9	23.3-23.8	12.1	59-64
Tip (°C)	1143-1148	--	916-919	--	--	--
Primary (°C)	1149-1158	965-987	977-979	264.6-264.9	500.0	898-901
LSP	15.0	11.5	978	265	500	900
Kc	2	2	2	2	2	2
Ti	2	2	2	2	2	2
Td	0	0	0	0	0	0
Offset	22.8-24.5	36.6-38.0	10	23	12.0	61.0
Thick. (kA)	100	76.52	--	--	--	--

Run time (hr:min:sec): 1:51:06 Headspace P (torr): 5-9 x 10^{-8}

Run time (seconds): 6666 Growth P (torr): 3-4 x 10^{-7}

Rate

Cu		In	
Thickness (kA)	Rate (A/s)	Thickness (kA)	Rate (A/s)
0 - 100	15.0	0 - 76.5	11.48

Table A-47. Reactor conditions for Growth Run #587.

Run # 587	Date: 05/18/04
Film: CIGS	Operator: Ryan Kaczynski
Substrate: 3 Mo, 1 Glass	
Objective: Constant rate CIGS, x>0.3	

Target Value

Metal		Se		Substrate Heater	
Cu Rate (A/s)	10.0	Cracker (°C)	500	Temp. (°C)	900
In Rate (A/s)	4.85	Ramp (°C/s)	0.5	Ramp (°C/s)	0.3
Cu tip power (%)	84.9	Crucible (°C)	265	RPM	12
Ga tip power (%)	22			Direction	CCW
Ga primary T (°C)	978				

Total Film Thickness (μm): 1.0

Film Set Value

	Cu	In	Ga
Soak Power (%)	20	35	7
Rise Time (min)	5	5	5
Soak Time (min)	13	13	0

Operation Results

	Cu	In	Ga	Se Crucible	Se Cracker	Heater
Power (%)	20.5-22.1	34-34.8	20.4-20.6	22.5-22.7	11.8	60.7-65
Tip (°C)	1125-1134	--	917-920	--	--	--
Primary (°C)	1120-1130	920-933	977-979	265.2-265.5	500.1	898-900.5
LSP	10.0	4.85	978	265	500	900
Kc	2	2	2	2	2	2
Ti	2	2	2	2	2	2
Td	0	0	0	0	0	0
Offset	21-21.4	33.7-34.5	10	23-23.5	12.0	61.5
Thick. (kA)	100	48.3	--	--	--	--

Run time (hr:min:sec): 2:46:27 Headspace P (torr): 4-8 x 10^{-8}

Run time (seconds): 9987 Growth P (torr): 2.5-5 x 10^{-7}

Rate

Cu		In	
Thickness (kA)	Rate (A/s)	Thickness (kA)	Rate (A/s)
0 - 100	10.01	0 - 48.3	4.84

Table A-48. Reactor conditions for Growth Run #588.

Run # 588	Date: 05/19/04
Film: CIGS	Operator: Ryan Kaczynski
Substrate: 4 Mo, 1 Glass	
Objective: Constant rate CIGS, x<0.3	

Target Value

Metal		Se		Substrate Heater	
Cu Rate (A/s)	18	Cracker (°C)	500	Temp. (°C)	900
In Rate (A/s)	14.8	Ramp (°C/s)	0.5	Ramp (°C/s)	0.3
Cu tip power (%)	84.9	Crucible (°C)	265	RPM	12
Ga tip power (%)	22			Direction	CCW
Ga primary T (°C)	978				

Total Film Thickness (μm): 1.0

Film Set Value

	Cu	In	Ga
Soak Power (%)	23.5	39	7
Rise Time (min)	5	5	5
Soak Time (min)	13	13	0

Operation Results

	Cu	In	Ga	Se Crucible	Se Cracker	Heater
Power (%)	25-26	39.3-40	20.7-20.9	23.6-20.9	11.9-12.1	60-65
Tip (°C)	1147-1150	--	916-918	--	--	--
Primary (°C)	1166-1171	980-1005	977-979	264.7	500.0	898-901
LSP	18.0	14.8	978	265	500	900
Kc	2	2	2	2	2	2
Ti	2	2	2	2	2	2
Td	0	0	0	0	0	0
Offset	21.8-22	38.5-41.0	10	23.0	12.0	61.5
Thick. (kA)	100	82.14	--	--	--	--

Run time (hr:min:sec): 1:32:40 Headspace P (torr): 4-7 x 10^{-8}

Run time (seconds): 5560 Growth P (torr): 2-3 x 10^{-7}

Rate

Cu		In	
Thickness (kA)	Rate (A/s)	Thickness (kA)	Rate (A/s)
0 - 100	17.99	0 - 82.1	14.77

Table A-49. Reactor conditions for Growth Run #628.

Run # 628	Date: 07/18/05
Film: CGS	Operator: Ryan Kaczynski
Substrate: 3 Mo	
Objective: Ga-rich, constant rate CGS	

Target Value

Metal		Se		Substrate Heater	
Cu Rate (A/s)	10.7	Cracker (°C)	500	Temp. (°C)	800
In Rate (A/s)	--	Ramp (°C/s)	0.5	Ramp (°C/s)	0.3
Cu tip power (%)	76.9	Crucible (°C)	265	RPM	12
Ga tip power (%)	24			Direction	CCW
Ga primary T (°C)	970				

Total Film Thickness (μm): 1.5

Film Set Value

	Cu	In	Ga
Soak Power (%)	14	--	7
Rise Time (min)	5	--	5
Soak Time (min)	13	--	0

Operation Results

	Cu	In	Ga	Se Crucible	Se Cracker	Heater
Power (%)	12.3-13.1	--	9.4-9.6	21-21.4	11.9-12.1	56.0-61.0
Tip (°C)	1105-1118	--	958-963	--	--	--
Primary (°C)	--	--	969-971	265.3-265.6	500.0	798-800.5
LSP	10.5	--	970	265	500	800
Kc	2	--	2	2	2	2
Ti	2	--	2	2	2	2
Td	0	--	0	0	0	0
Offset	13.6-16.3	--	10	22.0	12.0	57-58
Thick. (kA)	150	--	--	--	--	--

Run time (hr:min:sec): 3:53:56 Headspace P (torr): 9.0×10^{-8} - 1.0×10^{-7}

Run time (seconds): 14,036 Growth P (torr): 4×10^{-7}

Cu rate

Thickness (kA)	Rate (A/s)
5	11.57
10	11.12
100	10.74
150	10.69

Table A-50. Reactor conditions for Growth Run #629.

Run # 629	Date: 07/20/05
Film: CGS	Operator: Ryan Kaczynski
Substrate: 3 Mo	
Objective: Cu-rich, constant rate CGS	

Target Value

Metal		Se		Substrate Heater	
Cu Rate (A/s)	13.5	Cracker (°C)	500	Temp. (°C)	800
In Rate (A/s)	--	Ramp (°C/s)	0.5	Ramp (°C/s)	0.3
Cu tip power (%)	76.9	Crucible (°C)	265	RPM	12
Ga tip power (%)	24			Direction	CCW
Ga primary T (°C)	970				

Total Film Thickness (μm): 1.5

Film Set Value

	Cu	In	Ga
Soak Power (%)	15	--	7
Rise Time (min)	5	--	5
Soak Time (min)	13	--	0

Operation Results

	Cu	In	Ga	Se Crucible	Se Cracker	Heater
Power (%)	14.8-15.9	--	9.5-9.6	19.8-21.4	11.9-12.0	56.5-60.5
Tip (°C)	1114-1126	--	958-963	--	--	--
Primary (°C)	--	--	969-971	265.7-266.1	500.0	798-800.5
LSP	13.5	--	970	265	500	800
Kc	2	--	2	2	2	2
Ti	2	--	2	2	2	2
Td	0	--	0	0	0	0
Offset	13.0	--	10	22.0	12.0	57.5
Thick. (kA)	150	--	--	--	--	--

Run time (hr:min:sec): 3:05:01 Headspace P (torr): 5-8 x 10^{-8}

Run time (seconds): 11,101 Growth P (torr): 2.7-3.7 x 10^{-7}

Cu rate

Thickness (kA)	Rate (A/s)
5	14.40
10	14.00
100	13.54
150	13.51

Table A-51. Reactor conditions for Growth Run #630.

Run # 630	Date: 07/22/05
Film: CGS	Operator: Ryan Kaczynski
Substrate: 3 Mo	
Objective: Ga-rich, constant rate CGS	

Target Value

Metal		Se		Substrate Heater	
Cu Rate (A/s)	10.5	Cracker (°C)	500	Temp. (°C)	800
In Rate (A/s)	--	Ramp (°C/s)	0.5	Ramp (°C/s)	0.3
Cu tip power (%)	76.9	Crucible (°C)	265	RPM	12
Ga tip power (%)	24			Direction	CCW
Ga primary T (°C)	970				

Total Film Thickness (μm): 1.5

Film Set Value

	Cu	In	Ga
Soak Power (%)	13	--	7
Rise Time (min)	5	--	5
Soak Time (min)	13	--	0

Operation Results

	Cu	In	Ga	Se Crucible	Se Cracker	Heater
Power (%)	13.1-14.2	--	9.5-9.7	21.0-21.5	11.9-12.0	57.0-60.6
Tip (°C)	1105-1117	--	957-963	--	--	--
Primary (°C)	--	--	969-971	265.3-265.6	500.0	798-800.5
LSP	10.5	--	970	265	500	800
Kc	2	--	2	2	2	2
Ti	2	--	2	2	2	2
Td	0	--	0	0	0	0
Offset	11.4-12.8	--	10	22.0	12.0	57.5
Thick. (kA)	150	--	--	--	--	--

Run time (hr:min:sec): 3:58:08 Headspace P (torr): 5.2-7.7 x 10^{-8}

Run time (seconds): 14,288 Growth P (torr): 2.4-3.6 x 10^{-7}

Cu rate

Thickness (kA)	Rate (A/s)
5	10.42
10	10.59
100	10.52
150	10.50

Table A-52. Reactor conditions for Growth Run #634.

Run # 634	Date: 08/03/05
Film: CGS	Operator: Ryan Kaczynski
Substrate: 3 Mo	
Objective: Cu-rich growth based on Run# 523 at T = 800°C	

Target Value

Metal		Se		Substrate Heater	
Cu Rate (A/s)	14/19/14	Cracker (°C)	500	Temp. (°C)	800
In Rate (A/s)	--	Ramp (°C/s)	0.5	Ramp (°C/s)	0.3
Cu tip power (%)	76.9	Crucible (°C)	265	RPM	12
Ga tip power (%)	24			Direction	CCW
Ga primary T (°C)	970				

Total Film Thickness (μm): 1.5

Film Set Value

	Cu	In	Ga
Soak Power (%)	15	--	7
Rise Time (min)	5	--	5
Soak Time (min)	13	--	0

Operation Results

	Cu	In	Ga	Se Crucible	Se Cracker	Heater
Power (%)	15/18/16	--	9.3-9.5	20.7-21.0	11.8-12.1	58.0-61.5
Tip (°C)	1124/1147/1134	--	955-961	--	--	--
Primary (°C)	--	--	969-971	265.5-265.7	500.0	798.2-800
LSP	14/19/14	--	970	265	500	800
Kc	2	--	2	2	2	2
Ti	2	--	2	2	2	2
Td	0	--	0	0	0	0
Offset	12.5/15/13	--	10	22.0	12.0	58.0
Thick. (kA)	150	--	--	--	--	--

Run time (hr:min:sec): 2:37:45 Headspace P (torr): 7.5×10^{-8} - 1.0×10^{-7}

Run time (seconds): 9,465 Growth P (torr): $3.5\text{-}4.0 \times 10^{-7}$

Cu rate

Thickness (kA)	Rate (A/s)
0 - 23	14.13
23 - 136.5	18.99
136.5 - 150	14.06

*GaSe deposited for 15 minutes before Cu deposition

Table A-53. Reactor conditions for Growth Run #635.

Run # 635	Date: 08/04/05
Film: CGS	Operator: Ryan Kaczynski
Substrate: 3 Mo	
Objective: Ga-rich CGS by modified 3-stage process	

Target Value

Metal		Se		Substrate Heater	
Cu Rate (A/s)	15.3/8.2	Cracker (°C)	500	Temp. (°C)	800
In Rate (A/s)	--	Ramp (°C/s)	0.5	Ramp (°C/s)	0.3
Cu tip power (%)	76.9	Crucible (°C)	265	RPM	12
Ga tip power (%)	24			Direction	CCW
Ga primary T (°C)	970				

Total Film Thickness (μm): 1.5

Film Set Value

	Cu	In	Ga
Soak Power (%)	15	--	7
Rise Time (min)	5	--	5
Soak Time (min)	13	--	0

Operation Results

	Cu	In	Ga	Se Crucible	Se Cracker	Heater
Power (%)	16/12	--	9.2-9.4	21.0-22.0	11.8-12.0	59.0-62.0
Tip (°C)	1134/1114	--	952-962	--	--	--
Primary (°C)	--	--	969-971	265.0-265.5	500.1	798.0-800
LSP	15.3/8.2	--	970	265	500	800
Kc	2	--	2	2	2	2
Ti	2	--	2	2	2	2
Td	0	--	0	0	0	0
Offset	12.5/10	--	10	22.0	12.0	58-59
Thick. (kA)	150	--	--	--	--	--

Run time (hr:min:sec): 3:55:24 Headspace P (torr): 5.0×10^{-8} - 1.0×10^{-7}

Run time (seconds): 14,124 Growth P (torr): $2.5\text{-}4.5 \times 10^{-7}$

Cu rate

Thickness (kA)	Rate (A/s)
0 - 91.5	15.27
91.5 - 150	8.20

*GaSe deposited for 16:40 minutes before Cu deposition

Table A-54. Reactor conditions for Growth Run #636.

Run # 636	Date: 08/05/05
Film: CGS	Operator: Ryan Kaczynski
Substrate: 3 Mo	
Objective: Ga-rich CGS by modified 3-stage process	

Target Value

Metal		Se		Substrate Heater	
Cu Rate (A/s)	19.0/8.22	Cracker (°C)	500	Temp. (°C)	800
In Rate (A/s)	--	Ramp (°C/s)	0.5	Ramp (°C/s)	0.3
Cu tip power (%)	76.9	Crucible (°C)	265	RPM	12
Ga tip power (%)	24			Direction	CCW
Ga primary T (°C)	970				

Total Film Thickness (μm): 1.5

Film Set Value

	Cu	In	Ga
Soak Power (%)	17	--	7
Rise Time (min)	5	--	5
Soak Time (min)	13	--	0

Operation Results

	Cu	In	Ga	Se Crucible	Se Cracker	Heater
Power (%)	17/12	--	9.3-9.5	21.2-21.8	11.9-12.0	59.0-63.0
Tip (°C)	1150/1118	--	952-960	--	--	--
Primary (°C)	--	--	969-971	265.1-265.5	500.1	798.0-800
LSP	19.0/8.2	--	970	265	500	800
Kc	2	--	2	2	2	2
Ti	2	--	2	2	2	2
Td	0	--	0	0	0	0
Offset	15/11	--	10	22.0	12.0	60.0
Thick. (kA)	150	--	--	--	--	--

Run time (hr:min:sec): 3:53:27 Headspace P (torr): 4.5×10^{-8} - 1.0×10^{-7}

Run time (seconds): 14,007 Growth P (torr): $2.5\text{-}4.0 \times 10^{-7}$

Cu rate

Thickness (kA)	Rate (A/s)
0 - 76	18.99
76 - 150	8.22

*GaSe deposited for 16:40 minutes before Cu deposition

Table A-55. Reactor conditions for Growth Run #637.

Run # 637	Date: 08/10/05
Film: CGS	Operator: Ryan Kaczynski
Substrate: 3 Mo	
Objective: Stoichiometric CGS by modified 3-stage process	

Target Value

Metal		Se		Substrate Heater	
Cu Rate (A/s)	15.27/10.16	Cracker (°C)	500	Temp. (°C)	800
In Rate (A/s)	--	Ramp (°C/s)	0.5	Ramp (°C/s)	0.3
Cu tip power (%)	76.9	Crucible (°C)	265	RPM	12
Ga tip power (%)	24			Direction	CCW
Ga primary T (°C)	970				

Total Film Thickness (μm): 1.5

Film Set Value

	Cu	In	Ga
Soak Power (%)	15	--	7
Rise Time (min)	5	--	5
Soak Time (min)	13	--	0

Operation Results

	Cu	In	Ga	Se Crucible	Se Cracker	Heater
Power (%)	16.7/13.5	--	9.3-9.5	21.5-22.3	12.0-12.2	60.0-63.0
Tip (°C)	1141/1127	--	952-958	--	--	--
Primary (°C)	--	--	969-971	264.8-265.2	500.0	798.0-800
LSP	15.3/10.2	--	970	265	500	800
Kc	2	--	2	2	2	2
Ti	2	--	2	2	2	2
Td	0	--	0	0	0	0
Offset	14.5/12	--	10	22.0	12.0	60.0
Thick. (kA)	150	--	--	--	--	--

Run time (hr:min:sec): 3:36:36 Headspace P (torr): 5.5 x 10^{-8} - 1.0 x 10^{-7}

Run time (seconds): 12,996 Growth P (torr): 2.5-5.0 x 10^{-7}

Cu rate

Thickness (kA)	Rate (A/s)
0 - 84	15.27
84 - 150	10.16

*GaSe deposited for 16:40 minutes before Cu deposition

Table A-56. Reactor conditions for Growth Run #638.

Run # 638	Date: 08/11/05
Film: CGS	Operator: Ryan Kaczynski
Substrate: 3 Mo	
Objective: Cu-rich using 2-stage process	

Target Value

Metal		Se		Substrate Heater	
Cu Rate (A/s)	14.6	Cracker (°C)	500	Temp. (°C)	800
In Rate (A/s)	--	Ramp (°C/s)	0.5	Ramp (°C/s)	0.3
Cu tip power (%)	76.9	Crucible (°C)	265	RPM	12
Ga tip power (%)	24			Direction	CCW
Ga primary T (°C)	970				

Total Film Thickness (μm): 1.5

Film Set Value

	Cu	In	Ga
Soak Power (%)	15	--	7
Rise Time (min)	5	--	5
Soak Time (min)	13	--	0

Operation Results

	Cu	In	Ga	Se Crucible	Se Cracker	Heater
Power (%)	16.8-17.5	--	9.5-9.6	21.5/24.5	12.1-12.7	59-62
Tip (°C)	1136-1139	--	945-957	--	--	--
Primary (°C)	--	--	969-971	264.0-265.5	499.6	798-800
LSP	14	--	970	265	500	800
Kc	2	--	2	2	2	2
Ti	2	--	2	2	2	2
Td	0	--	0	0	0	0
Offset	14.7-14.9	--	10	22.0-23.5	12.0	60.0
Thick. (kA)	150	--	--	--	--	--

Run time (hr:min:sec): 5:56:57 Headspace P (torr): 5.0×10^{-8} - 1.0×10^{-7}

Run time (seconds): 21,417 Growth P (torr): $2.5\text{-}5.0 \times 10^{-7}$

Cu rate

Thickness (kA)	Rate (A/s)
0 - 150	14.02

*GaSe deposited for 2:58:35 before CuSe deposition

Table A-57. Reactor conditions for Growth Run #639.

Run # 639	Date: 08/12/05
Film: CGS	Operator: Ryan Kaczynski
Substrate: 3 Mo	
Objective: Stoichiometric CGS by modified 3-stage process	

Target Value

Metal		Se		Substrate Heater	
Cu Rate (A/s)	19/9.8	Cracker (°C)	500	Temp. (°C)	800
In Rate (A/s)	--	Ramp (°C/s)	0.5	Ramp (°C/s)	0.3
Cu tip power (%)	76.9	Crucible (°C)	265	RPM	12
Ga tip power (%)	24			Direction	CCW
Ga primary T (°C)	970				

Total Film Thickness (μm): 1.5

Film Set Value

	Cu	In	Ga
Soak Power (%)	17	--	7
Rise Time (min)	5	--	5
Soak Time (min)	13	--	0

Operation Results

	Cu	In	Ga	Se Crucible	Se Cracker	Heater
Power (%)	18.0/14.0	--	9.6-9.7	21.7-22.2	11.8-12.0	59.0-62.0
Tip (°C)	1150/1125	--	952-957	--	--	--
Primary (°C)	--	--	969-971	264.9-265.1	500.0	798.0-800
LSP	19.0/9.8	--	970	265	500	800
Kc	2	--	2	2	2	2
Ti	2	--	2	2	2	2
Td	0	--	0	0	0	0
Offset	16/13	--	10	22.0	12.0	60.0
Thick. (kA)	150	--	--	--	--	--

Run time (hr:min:sec): 3:29:10 Headspace P (torr): 4.5×10^{-8} - 1.0×10^{-7}

Run time (seconds): 12,550 Growth P (torr): $2.2\text{-}5.0 \times 10^{-7}$

Cu rate

Thickness (kA)	Rate (A/s)
0 - 91.5	15.27
91.5 - 150	8.20

*GaSe deposited for 16:40 minutes before Cu deposition

Table A-58. Reactor conditions for Growth Run #640.

Run # 640	Date: 08/15/05
Film: CGS	Operator: Ryan Kaczynski
Substrate: 3 Mo	
Objective: Ga-rich using 3-stage process	

Target Value

Metal		Se		Substrate Heater	
Cu Rate (A/s)	19.0	Cracker (°C)	500	Temp. (°C)	800
In Rate (A/s)	--	Ramp (°C/s)	0.5	Ramp (°C/s)	0.3
Cu tip power (%)	76.9	Crucible (°C)	265	RPM	12
Ga tip power (%)	24			Direction	CCW
Ga primary T (°C)	970				

Total Film Thickness (μm): 1.5

Film Set Value

	Cu	In	Ga
Soak Power (%)	17	--	7
Rise Time (min)	5	--	5
Soak Time (min)	13	--	0

Operation Results

	Cu	In	Ga	Se Crucible	Se Cracker	Heater
Power (%)	17.6-18.5	--	9.6-9.7	21.7/24.0	12.0-12.7	60-65
Tip (°C)	1142-1145	--	946-958	--	--	--
Primary (°C)	--	--	969-971	264.0-265.1	499.6	798-800
LSP	19	--	970	265	500	800
Kc	2	--	2	2	2	2
Ti	2	--	2	2	2	2
Td	0	--	0	0	0	0
Offset	15.5	--	10	22.0	12.0	60-61
Thick. (kA)	150	--	--	--	--	--

Run time (hr:min:sec): 6:20:00 Headspace P (torr): 5.0×10^{-8} - 1.0×10^{-7}

Run time (seconds): 22,800 Growth P (torr): $2.0\text{-}6.0 \times 10^{-7}$

Cu rate

Thickness (kA)	Rate (A/s)
0 - 150	19.17

*GaSe deposited for 3:24:35 before CuSe deposition and 45 minutes after

Table A-59. Reactor conditions for Growth Run #641.

Run # 641	Date: 08/17/05
Film: CGS	Operator: Ryan Kaczynski
Substrate: 3 Mo	
Objective: Thick Cu-rich growth based on Run# 523 at T = 800°C	

Target Value

Metal		Se		Substrate Heater	
Cu Rate (A/s)	14/19/14	Cracker (°C)	500	Temp. (°C)	800
In Rate (A/s)	--	Ramp (°C/s)	0.5	Ramp (°C/s)	0.3
Cu tip power (%)	76.9	Crucible (°C)	265	RPM	12
Ga tip power (%)	24			Direction	CCW
Ga primary T (°C)	970				

Total Film Thickness (μm): 2.0

Film Set Value

	Cu	In	Ga
Soak Power (%)	15	--	7
Rise Time (min)	5	--	5
Soak Time (min)	13	--	0

Operation Results

	Cu	In	Ga	Se Crucible	Se Cracker	Heater
Power (%)	25/29/22	--	9.4-9.6	21.3-21.8	11.9-12.1	61.7-64.7
Tip (°C)	1162/1190/1155	--	942-958	--	--	--
Primary (°C)	--	--	969-971	265.1-265.3	500.0	798.0-799.6
LSP	14/19/14	--	970	265	500	800
Kc	2	--	2	2	2	2
Ti	2	--	2	2	2	2
Td	0	--	0	0	0	0
Offset	25/26/19	--	10	22.0	12.0	61.0
Thick. (kA)	200	--	--	--	--	--

Run time (hr:min:sec): 3:31:01 Headspace P (torr): 5.0×10^{-8} - 1.0×10^{-7}

Run time (seconds): 12,661 Growth P (torr): 2.0-5.0 x 10^{-7}

Cu rate

Thickness (kA)	Rate (A/s)
0 - 31	13.95
31 - 182	18.99
182 - 200	14.00

*GaSe deposited for 20 minutes before Cu deposition

Table A-60. Reactor conditions for Growth Run #647.

Run # 647	Date: 12/07/05
Film: CGS	Operator: Ryan Kaczynski
Substrate: 3 Mo	
Objective: Ga-rich, constant rate CGS	

Target Value

Metal		Se		Substrate Heater	
Cu Rate (A/s)	8.5	Cracker (°C)	500	Temp. (°C)	800
In Rate (A/s)	--	Ramp (°C/s)	0.5	Ramp (°C/s)	0.3
Cu tip power (%)	76.9	Crucible (°C)	265	RPM	12
Ga tip power (%)	24			Direction	CCW
Ga primary T (°C)	970				

Total Film Thickness (μm): 1.5

Film Set Value

	Cu	In	Ga
Soak Power (%)	10	--	7
Rise Time (min)	5	--	5
Soak Time (min)	13	--	0

Operation Results

	Cu	In	Ga	Se Crucible	Se Cracker	Heater
Power (%)	13.0-14.5	--	9.4-9.7	22.0-22.3	12.1-12.2	61.8-64.1
Tip (°C)	1105-1119	--	945-952	--	--	--
Primary (°C)	--	--	969-971	264.7-265.0	500.0	798-799.8
LSP	8.5	--	970	265	500	800
Kc	2	--	2	2	2	2
Ti	2	--	2	2	2	2
Td	0	--	0	0	0	0
Offset	11.0-13.0	--	10	22.0	12.0	61.0
Thick. (kA)	150	--	--	--	--	--

Run time (hr:min:sec): 4:54:18 Headspace P (torr): 5.5-6.5 x 10^{-8}

Run time (seconds): 17,658 Growth P (torr): 3.2-5.0 x 10^{-7}

Cu rate

Thickness (kA)	Rate (A/s)
5	7.53
10	8.13
80	8.57
150	8.50

Table A-61. Reactor conditions for Growth Run #648.

Run # 648	Date: 12/08/05
Film: CGS	Operator: Ryan Kaczynski
Substrate: 3 Mo	
Objective: Cu-rich growth based on Run #523 at T = 800°C	

Target Value

Metal		Se		Substrate Heater	
Cu Rate (A/s)	11/14.5/11	Cracker (°C)	500	Temp. (°C)	800
In Rate (A/s)	--	Ramp (°C/s)	0.5	Ramp (°C/s)	0.3
Cu tip power (%)	76.9	Crucible (°C)	265	RPM	12
Ga tip power (%)	24			Direction	CCW
Ga primary T (°C)	970				

Total Film Thickness (μm): 1.5

Film Set Value

	Cu	In	Ga
Soak Power (%)	13	--	7
Rise Time (min)	5	--	5
Soak Time (min)	13	--	0

Operation Results

	Cu	In	Ga	Se Crucible	Se Cracker	Heater
Power (%)	15.5/17.5/16	--	9.4-9.7	21.4-21.8	11.9-12.1	62.0-63.8
Tip (°C)	1121/1139/1129	--	943-953	--	--	--
Primary (°C)	--	--	969-971	265.5-265.7	500.0	798-799.5
LSP	11/14.5/11	--	970	265	500	800
Kc	2	--	2	2	2	2
Ti	2	--	2	2	2	2
Td	0	--	0	0	0	0
Offset	12.5/15.2/14	--	10	22.0	12.0	61.0
Thick. (kA)	150	--	--	--	--	--

Run time (hr:min:sec): 3:24:43 Headspace P (torr): 4.0-6.7 x 10^{-8}

Run time (seconds): 12,283 Growth P (torr): 2.2-3.6 x 10^{-7}

Cu rate

Thickness (kA)	Rate (A/s)
0 - 21.3	11.04
21.3 - 128.7	14.50
128.7 - 150	10.94

*GaSe deposited for 16:40 before Cu deposition

Table A-62. Reactor conditions for Growth Run #649.

Run # 649	Date: 12/10/05
Film: CGS	Operator: Ryan Kaczynski
Substrate: 3 Mo	
Objective: Ga-rich using 3-stage process	

Target Value

Metal		Se		Substrate Heater	
Cu Rate (A/s)	15.0	Cracker (°C)	500	Temp. (°C)	800
In Rate (A/s)	--	Ramp (°C/s)	0.5	Ramp (°C/s)	0.3
Cu tip power (%)	76.9	Crucible (°C)	265	RPM	12
Ga tip power (%)	24			Direction	CCW
Ga primary T (°C)	970				

Total Film Thickness (μm): 1.5

Film Set Value

	Cu	In	Ga
Soak Power (%)	17	--	7
Rise Time (min)	5	--	5
Soak Time (min)	13	--	0

Operation Results

	Cu	In	Ga	Se Crucible	Se Cracker	Heater
Power (%)	17-18	--	9.6-9.9	21.0-24.0	12.1-12.7	63.0-65.0
Tip (°C)	1146-1150	--	942-952	--	--	--
Primary (°C)	1109-1112	--	969-971	265.5-265.7	499.7	798-799
LSP	15.0	--	970	265	500	800
Kc	2	--	2	2	2	2
Ti	2	--	2	2	2	2
Td	0	--	0	0	0	0
Offset	14-16	--	10	22.0	12.0	61.0
Thick. (kA)	150	--	--	--	--	--

Run time (hr:min:sec): 7:53:48 Headspace P (torr): 5.0×10^{-8} - 1.0×10^{-7}

Run time (seconds): 28,428 Growth P (torr): $2.5\text{-}6.0 \times 10^{-7}$

Cu rate

Thickness (kA)	Rate (A/s)
5	14.0
100	15.05
150	15.06

*GaSe deposited for 4:37:47 before CuSe deposition and 30 minutes after

Table A-63. Reactor conditions for Growth Run #652.

Run # 652	Date: 02/07/06
Film: CGS	Operator: Ryan Kaczynski
Substrate: 3 Mo	
Objective: Constant rate CGS	

Target Value

Metal		Se		Substrate Heater	
Cu Rate (A/s)	10.9	Cracker (°C)	500	Temp. (°C)	800
In Rate (A/s)	--	Ramp (°C/s)	0.5	Ramp (°C/s)	0.3
Cu tip power (%)	76.9	Crucible (°C)	265	RPM	12
Ga tip power (%)	24			Direction	CCW
Ga primary T (°C)	970				

Total Film Thickness (μm): 1.5

Film Set Value

	Cu	In	Ga
Soak Power (%)	10	--	7
Rise Time (min)	5	--	5
Soak Time (min)	13	--	0

Operation Results

	Cu	In	Ga	Se Crucible	Se Cracker	Heater
Power (%)	10.3-13.4	--	9.1-9.4	23.0-24.0	12.2	62-65
Tip (°C)	1110-1122	--	966-969	--	--	--
Primary (°C)	1054	--	970-971	263.9-264.3	499.9	798.5-800.0
LSP	10.9	--	970	265	500	800
Kc	2	--	2	2	2	2
Ti	2	--	2	2	2	2
Td	0	--	0	0	0	0
Offset	8.2-11.0	--	10	22.0	12.0	62.0
Thick. (kA)	150	--	--	--	--	--

Run time (hr:min:sec): 3:48:58
Run time (seconds): 13,738
Headspace P (torr): 6-8 x 10^{-8}
Growth P (torr): 4.5-6 x 10^{-7}

Cu rate

Thickness (kA)	Rate (A/s)
5	13.3
20	11.5
80	11.1
150	10.92

Table A-64. Reactor conditions for Growth Run #653.

Run # 653	Date: 02/09/06
Film: CGS	Operator: Ryan Kaczynski
Substrate: 3 Mo	
Objective: Ga-rich, constant rate CGS	

Target Value

Metal		Se		Substrate Heater	
Cu Rate (A/s)	10.9	Cracker (°C)	500	Temp. (°C)	800
In Rate (A/s)	--	Ramp (°C/s)	0.5	Ramp (°C/s)	0.3
Cu tip power (%)	76.9	Crucible (°C)	265	RPM	12
Ga tip power (%)	24			Direction	CCW
Ga primary T (°C)	970				

Total Film Thickness (μm): 1.5

Film Set Value

	Cu	In	Ga
Soak Power (%)	8	--	7
Rise Time (min)	5	--	5
Soak Time (min)	13	--	0

Operation Results

	Cu	In	Ga	Se Crucible	Se Cracker	Heater
Power (%)	10.5-11.5	--	9.1-9.4	23.0-24.0	12.1-12.2	62-65
Tip (°C)	1114-1125	--	966-969	--	--	--
Primary (°C)	1057	--	969-971	264.0-264.5	499.9	798.0-799.7
LSP	10.9	--	970	265	500	800
Kc	2	--	2	2	2	2
Ti	2	--	2	2	2	2
Td	0	--	0	0	0	0
Offset	8.5-10.0	--	10	22.0	12.0	62.0
Thick. (kA)	150	--	--	--	--	--

Run time (hr:min:sec): 3:48:58 Headspace P (torr): 5.5-8 x 10^{-8}

Run time (seconds): 13,738 Growth P (torr): 4-6 x 10^{-7}

Cu rate

Thickness (kA)	Rate (A/s)
5	11.0
20	10.9
100	10.94
150	10.92

Table A-65. Reactor conditions for Growth Run #654.

Run # 654	Date: 02/14/06
Film: CGS	Operator: Ryan Kaczynski
Substrate: 3 Mo	
Objective: Cu-rich, constant rate CGS	

Target Value

Metal		Se		Substrate Heater	
Cu Rate (A/s)	12.7	Cracker (°C)	500	Temp. (°C)	800
In Rate (A/s)	--	Ramp (°C/s)	0.5	Ramp (°C/s)	0.3
Cu tip power (%)	76.9	Crucible (°C)	265	RPM	12
Ga tip power (%)	24			Direction	CCW
Ga primary T (°C)	970				

Total Film Thickness (μm): 1.5

Film Set Value

	Cu	In	Ga
Soak Power (%)	10	--	7
Rise Time (min)	5	--	5
Soak Time (min)	13	--	0

Operation Results

	Cu	In	Ga	Se Crucible	Se Cracker	Heater
Power (%)	12.0-13.0	--	9.2-9.3	21.3-21.8	12.2-12.3	62-65
Tip (°C)	1121-1132	--	965-968	--	--	--
Primary (°C)	1071-1073	--	969-971	265.1-265.4	499.9	798.0-799.7
LSP	12.7	--	970	265	500	800
Kc	2	--	2	2	2	2
Ti	2	--	2	2	2	2
Td	0	--	0	0	0	0
Offset	9.5-10.8	--	10	22.0	12.0	62.0
Thick. (kA)	150	--	--	--	--	--

Run time (hr:min:sec): 3:17:42 Headspace P (torr): 4.8-7.0 x 10^{-8}

Run time (seconds): 11,682 Growth P (torr): 2.7-3.7 x 10^{-7}

Cu rate

Thickness (kA)	Rate (A/s)
5	12.75
30	12.71
100	12.67
150	12.65

Table A-66. Reactor conditions for Growth Run #655.

Run # 655	Date: 02/23/06
Film: CGS	Operator: Ryan Kaczynski
Substrate: 3 Mo	
Objective: Ga-rich, constant rate CGS	

Target Value

Metal		Se		Substrate Heater	
Cu Rate (A/s)	10.3	Cracker (°C)	500	Temp. (°C)	800
In Rate (A/s)	--	Ramp (°C/s)	0.5	Ramp (°C/s)	0.3
Cu tip power (%)	76.9	Crucible (°C)	265	RPM	12
Ga tip power (%)	24			Direction	CCW
Ga primary T (°C)	970				

Total Film Thickness (μm): 1.5

Film Set Value

	Cu	In	Ga
Soak Power (%)	9	--	7
Rise Time (min)	5	--	5
Soak Time (min)	13	--	0

Operation Results

	Cu	In	Ga	Se Crucible	Se Cracker	Heater
Power (%)	9.0-10.3	--	9.2-9.5	24.0	12.2	64-65
Tip (°C)	1115-1127	--	962-966	--	--	--
Primary (°C)	1053-1055	--	969-971	264.0	499.7	798.0-799.3
LSP	10.3	--	970	265	500	800
Kc	2	--	2	2	2	2
Ti	2	--	2	2	2	2
Td	0	--	0	0	0	0
Offset	7.0-8.5	--	10	22.0	12.0	62.0
Thick. (kA)	150	--	--	--	--	--

Run time (hr:min:sec): 4:03:17 Headspace P (torr): 5.5-6.5 x 10^{-8}

Run time (seconds): 14,597 Growth P (torr): 3.0-4.5 x 10^{-7}

Cu rate

Thickness (kA)	Rate (A/s)
5	11.47
50	10.36
100	10.28
150	10.28

Table A-67. Reactor conditions for Growth Run #656.

Run # 656	Date: 03/14/06
Film: CGS	Operator: Ryan Kaczynski
Substrate: 3 Mo	
Objective: Cu-rich, constant rate CGS	

Target Value

Metal		Se		Substrate Heater	
Cu Rate (A/s)	12.1	Cracker (°C)	500	Temp. (°C)	800
In Rate (A/s)	--	Ramp (°C/s)	0.5	Ramp (°C/s)	0.3
Cu tip power (%)	76.9	Crucible (°C)	265	RPM	12
Ga tip power (%)	24			Direction	CCW
Ga primary T (°C)	970				

Total Film Thickness (μm): 1.5

Film Set Value

	Cu	In	Ga
Soak Power (%)	10	--	7
Rise Time (min)	5	--	5
Soak Time (min)	13	--	0

Operation Results

	Cu	In	Ga	Se Crucible	Se Cracker	Heater
Power (%)	10.3-11.8	--	9.1-9.4	22.0-23.0	12.1	64-66
Tip (°C)	1126-1168	--	966-969	--	--	--
Primary (°C)	1067-1073	--	969-971	264.8-265.3	499.9	798.5-800.0
LSP	12.1	--	970	265	500	800
Kc	2	--	2	2	2	2
Ti	2	--	2	2	2	2
Td	0	--	0	0	0	0
Offset	8.0-9.7	--	10	23.0	12.0	63.0
Thick. (kA)	150	--	--	--	--	--

Run time (hr:min:sec): 3:26:23 Headspace P (torr): 9×10^{-8} - 1×10^{-7}

Run time (seconds): 12,383 Growth P (torr): $4.3\text{-}5 \times 10^{-7}$

Cu rate

Thickness (kA)	Rate (A/s)
5	13.3
20	12.5
100	12.11
150	12.11

Table A-68. Reactor conditions for Growth Run #657.

Run # 657	Date: 03/16/06
Film: CGS	Operator: Ryan Kaczynski
Substrate: 3 Mo	
Objective: Ga-rich, constant rate CGS	

Target Value

Metal		Se		Substrate Heater	
Cu Rate (A/s)	10.0	Cracker (°C)	500	Temp. (°C)	800
In Rate (A/s)	--	Ramp (°C/s)	0.5	Ramp (°C/s)	0.3
Cu tip power (%)	76.9	Crucible (°C)	265	RPM	12
Ga tip power (%)	24			Direction	CCW
Ga primary T (°C)	970				

Total Film Thickness (μm): 1.5

Film Set Value

	Cu	In	Ga
Soak Power (%)	8	--	7
Rise Time (min)	5	--	5
Soak Time (min)	13	--	0

Operation Results

	Cu	In	Ga	Se Crucible	Se Cracker	Heater
Power (%)	9.6-10.9	--	9.3-9.6	22-23	12.3	64-66
Tip (°C)	1117-1128	--	963-963	--	--	--
Primary (°C)	1057-1059	--	969-971	264.8-265.0	499.9	798.0-799.2
LSP	10.0	--	970	265	500	800
Kc	2	--	2	2	2	2
Ti	2	--	2	2	2	2
Td	0	--	0	0	0	0
Offset	8.0-8.8	--	10	22.0	12.0	62.0
Thick. (kA)	150	--	--	--	--	--

Run time (hr:min:sec): 4:10:06 Headspace P (torr): 4.7-6.3 x 10^{-8}

Run time (seconds): 15,006 Growth P (torr): 2.4-3.7 x 10^{-7}

Cu rate

Thickness (kA)	Rate (A/s)
5	10.27
20	10.18
100	10.01
150	10.00

Table A-69. Reactor conditions for Growth Run #658.

Run # 658	Date: 03/24/06
Film: CGS	Operator: Ryan Kaczynski
Substrate: 3 Mo	
Objective: Constant rate CGS	

Target Value

Metal		Se		Substrate Heater	
Cu Rate (A/s)	11.0	Cracker (°C)	500	Temp. (°C)	800
In Rate (A/s)	--	Ramp (°C/s)	0.5	Ramp (°C/s)	0.3
Cu tip power (%)	76.9	Crucible (°C)	265	RPM	12
Ga tip power (%)	24			Direction	CCW
Ga primary T (°C)	970				

Total Film Thickness (μm): 1.5

Film Set Value

	Cu	In	Ga
Soak Power (%)	8	--	7
Rise Time (min)	5	--	5
Soak Time (min)	13	--	0

Operation Results

	Cu	In	Ga	Se Crucible	Se Cracker	Heater
Power (%)	11.0-13.0	--	9.3-9.6	21.5-22.2	12.2-12.3	64-66
Tip (°C)	1121-1133	--	960-964	--	--	--
Primary (°C)	1070-1072	--	969-971	264.9-265.2	499.9	797.8-799.0
LSP	11.0	--	970	265	500	800
Kc	2	--	2	2	2	2
Ti	2	--	2	2	2	2
Td	0	--	0	0	0	0
Offset	9.0-11.0	--	10	22.0	12.0	62.0
Thick. (kA)	150	--	--	--	--	--

Run time (hr:min:sec): 3:48:02 Headspace P (torr): 5-7 x 10^{-8}

Run time (seconds): 13,682 Growth P (torr): 3-4 x 10^{-7}

Cu rate

Thickness (kA)	Rate (A/s)
5	10.73
20	10.91
100	10.93
150	10.96

Table A-70. Reactor conditions for Growth Run #659.

Run # 659	Date: 04/14/06
Film: CGS	Operator: Ryan Kaczynski
Substrate: 3 Mo	
Objective: Constant rate CGS	

Target Value

Metal		Se		Substrate Heater	
Cu Rate (A/s)	10.5	Cracker (°C)	500	Temp. (°C)	800
In Rate (A/s)	--	Ramp (°C/s)	0.5	Ramp (°C/s)	0.3
Cu tip power (%)	76.9	Crucible (°C)	265	RPM	12
Ga tip power (%)	24			Direction	CCW
Ga primary T (°C)	970				

Total Film Thickness (μm): 1.5

Film Set Value

	Cu	In	Ga
Soak Power (%)	8	--	7
Rise Time (min)	5	--	5
Soak Time (min)	13	--	0

Operation Results

	Cu	In	Ga	Se Crucible	Se Cracker	Heater
Power (%)	11.0-14.0	--	9.3-9.6	22.6-22.8	12.2-12.3	64-65
Tip (°C)	1115-1130	--	960-964	--	--	--
Primary (°C)	1067-1070	--	969-971	264.6-264.7	499.9	798.0-798.7
LSP	10.5	--	970	265	500	800
Kc	2	--	2	2	2	2
Ti	2	--	2	2	2	2
Td	0	--	0	0	0	0
Offset	9.0-11.5	--	10	22.0	12.0	62.0
Thick. (kA)	150	--	--	--	--	--

Run time (hr:min:sec): 3:59:19 Headspace P (torr): 5.4-6.7 x 10^{-8}

Run time (seconds): 14,359 Growth P (torr): 3.9-4.5 x 10^{-7}

Cu rate

Thickness (kA)	Rate (A/s)
5	10.08
20	10.36
100	10.41
150	10.45

Table A-71. Reactor conditions for Growth Run #660.

Run # 660	Date: 05/09/06
Film: CGS	Operator: Ryan Kaczynski
Substrate: 3 Mo	
Objective: Constant rate CGS	

Target Value

Metal		Se		Substrate Heater	
Cu Rate (A/s)	9.5	Cracker (°C)	500	Temp. (°C)	800
In Rate (A/s)	--	Ramp (°C/s)	0.5	Ramp (°C/s)	0.3
Cu tip power (%)	76.9	Crucible (°C)	265	RPM	12
Ga tip power (%)	24			Direction	CCW
Ga primary T (°C)	970				

Total Film Thickness (μm): 1.5

Film Set Value

	Cu	In	Ga
Soak Power (%)	8	--	7
Rise Time (min)	5	--	5
Soak Time (min)	13	--	0

Operation Results

	Cu	In	Ga	Se Crucible	Se Cracker	Heater
Power (%)	11.8-13.4	--	9.2-9.4	23.0	12.2-12.3	65-66
Tip (°C)	1113-1123	--	958-962	--	--	--
Primary (°C)	1067	--	969-971	264.5	499.9	796.0-799.0
LSP	9.5	--	970	265	500	800
Kc	2	--	2	2	2	2
Ti	2	--	2	2	2	2
Td	0	--	0	0	0	0
Offset	10-11.8	--	10	22.0	12.0	63.0
Thick. (kA)	150	--	--	--	--	--

Run time (hr:min:sec): 4:24:00 Headspace P (torr): 5.5-8.0 x 10^{-8}

Run time (seconds): 15,840 Growth P (torr): 4.5-6.0 x 10^{-7}

Cu rate

Thickness (kA)	Rate (A/s)
5	9.63
20	9.46
100	9.46
150	9.47

Table A-72. Reactor conditions for Growth Run #661.

Run # 661	Date: 05/11/06
Film: CGS	Operator: Ryan Kaczynski
Substrate: 3 Mo	
Objective: Constant rate CGS	

Target Value

Metal		Se		Substrate Heater	
Cu Rate (A/s)	9.0	Cracker (°C)	500	Temp. (°C)	800
In Rate (A/s)	--	Ramp (°C/s)	0.5	Ramp (°C/s)	0.3
Cu tip power (%)	76.9	Crucible (°C)	265	RPM	12
Ga tip power (%)	24			Direction	CCW
Ga primary T (°C)	970				

Total Film Thickness (μm): 1.5

Film Set Value

	Cu	In	Ga
Soak Power (%)	8	--	7
Rise Time (min)	5	--	5
Soak Time (min)	13	--	0

Operation Results

	Cu	In	Ga	Se Crucible	Se Cracker	Heater
Power (%)	12.4-13.1	--	9.2-9.5	22.5-22.7	12.1-12.2	65-66
Tip (°C)	1115-1122	--	956-963	--	--	--
Primary (°C)	1062-1063	--	969-971	264.6-264.7	499.9	795.0-798.5
LSP	9.0	--	970	265	500	800
Kc	2	--	2	2	2	2
Ti	2	--	2	2	2	2
Td	0	--	0	0	0	0
Offset	10-11.2	--	10	22.0	12.0	62.0
Thick. (kA)	150	--	--	--	--	--

Run time (hr:min:sec): 4:37:40 Headspace P (torr): 4.5-6.0 x 10^{-8}

Run time (seconds): 16,660 Growth P (torr): 4.0-5.5 x 10^{-7}

Cu rate

Thickness (kA)	Rate (A/s)
5	8.49
10	8.97
100	9.03
150	9.00

Table A-73. Reactor conditions for Growth Run #662.

Run # 662	Date: 05/12/06
Film: CGS	Operator: Ryan Kaczynski
Substrate: 3 Mo	
Objective: Constant rate CGS	

Target Value

Metal		Se		Substrate Heater	
Cu Rate (A/s)	10.2	Cracker (°C)	500	Temp. (°C)	800
In Rate (A/s)	--	Ramp (°C/s)	0.5	Ramp (°C/s)	0.3
Cu tip power (%)	76.9	Crucible (°C)	265	RPM	12
Ga tip power (%)	24			Direction	CCW
Ga primary T (°C)	970				

Total Film Thickness (μm): 1.5

Film Set Value

	Cu	In	Ga
Soak Power (%)	9	--	7
Rise Time (min)	5	--	5
Soak Time (min)	13	--	0

Operation Results

	Cu	In	Ga	Se Crucible	Se Cracker	Heater
Power (%)	13.9-14.6	--	9.3-9.5	20.9-21.5	12.1	65-66
Tip (°C)	1120-1130	--	955-961	--	--	--
Primary (°C)	1075	--	969-971	264.5	499.9	798.5-799.2
LSP	10.2	--	970	265	500	800
Kc	2	--	2	2	2	2
Ti	2	--	2	2	2	2
Td	0	--	0	0	0	0
Offset	12-13	--	10	22.0	12.0	63.0
Thick. (kA)	150	--	--	--	--	--

Run time (hr:min:sec): 4:04:07 Headspace P (torr): 3.8-5.5 x 10^{-8}

Run time (seconds): 14,647 Growth P (torr): 2.5-3.6 x 10^{-7}

Cu rate

Thickness (kA)	Rate (A/s)
5	9.54
20	10.19
100	10.26
150	10.24

Table A-74. Reactor conditions for Growth Run #666.

Run # 666	Date: 07/21/06-07/22/06
Film: CGS	Operator: Ryan Kaczynski
Substrate: 4 Mo	
Objective: Bilayer CGS (CuSe/GaSe)	

Target Value

Metal		Se		Substrate Heater	
Cu Rate (A/s)	14.0	Cracker (°C)	500	Temp. (°C)	440/250
In Rate (A/s)	--	Ramp (°C/s)	0.5	Ramp (°C/s)	0.3
Cu tip power (%)	76.9	Crucible (°C)	265	RPM	12
Ga tip power (%)	24			Direction	CCW
Ga primary T (°C)	980				

Total Film Thickness (μm): 1.5

Film Set Value

	Cu	In	Ga
Soak Power (%)	15	--	7
Rise Time (min)	5	--	5
Soak Time (min)	13	--	0

Operation Results

	Cu	In	Ga	Se Crucible	Se Cracker	Heater
Power (%)	16.2-16.7	--	11.3-11.7	23	12.9	24/10
Tip (°C)	1127-1135	--	956-958	--	--	--
Primary (°C)	1091-1096	--	979-982	264.5	499.5	440.5/252
LSP	14.0	--	980	265	500	440/250
Kc	2	--	2	2	2	2
Ti	2	--	2	2	2	2
Td	0	--	0	0	0	0
Offset	15.0	--	10	22.0	12.0	25.0/15.0
Thick. (kA)	150	--	--	--	--	--

Run time (hr:min:sec): 5:58:22 Headspace P (torr): 2.6-3.9 x 10^{-8}

Run time (seconds): 21,502 Growth P (torr): 2.4 x 10^{-8} - 1.2 x 10^{-7}

Cu rate

Thickness (kA)	Rate (A/s)
5	14.5
20	14.4
100	14.05
150	14.02

APPENDIX B
REACTOR MODEL

This appendix includes the MATLAB code for two M-files needed to run the SIMULINK program pmee_sim: an input file named pmee_input that creates a vector of all the growth and reactor related parameters and an S-file named pmee_model that generates compositions and film thickness based on the growth conditions.

Input_PMEE.m

```
% Input file
% Defines the parameters and other
% configuration elements needed to
% run PMEE_sim

% by R. Kaczynski  3/23/07

% Assigns a value to "film" to determine which metal sources are "on"
film     =  input('Film deposition (0=CIGS, 1=CIS, 2=CGS)?')              ;

hm_Cu0   =  input('Initial Copper melt height (cm)?')                     ;
Tm_Cu    =  input('Melt temperature of Copper (C)?')                      ;

% If the film is CGS, there will be no In flux
if film  == 2
   hm_In0   =  0                                                          ;
   Tm_In    =  0                                                          ;
else
   hm_In0   =  input('Initial Indium melt height (cm)?')                  ;
   Tm_In    =  input('Melt temperature of Indium (C)?')                   ;
end

% If the film is CIS, there will be no Ga flux
if film  == 1
   hm_Ga0   =  0                                                          ;
   Tm_Ga    =  0                                                          ;
else
   hm_Ga0   =  input('Initial Gallium melt height (cm)?')                 ;
   Tm_Ga    =  input('Melt temperature of Gallium (C)?')                  ;
end

RPM      =  input('Rotations per minute?')                                ;

% PMEE reactor dimensions in centimeters (cm)
% Platen centerline radius
Ro       =  17.78                                                         ;
% Crucible bottom radius
Rb       =  0.26                                                          ;
% Crucible exit radius
Re       =  1.44                                                          ;
```

```
% Crucible height
H        =  9                                                              ;
% Platen circumference
L        =  2*pi*Ro                                                        ;

% Dimensionless unit
m        =  (Re-Rb)/H                                                      ;

% Geometric constants relating to the crucible's dimensions
gc0      =  -0.14417                                                       ;
gc1      =  0.47195                                                        ;
gc2      =  -0.10846                                                       ;
gc3      =  0.015233                                                       ;

% Dimension of a square substrate (cm)
w        =  5                                                              ;
% Substrate area (cm^2)
As       =  w^2                                                            ;

% Avogadro's constant
NA       =  602200000000000000000000                                       ;

% Atomic weights (g/mol)
AW_Cu    =  63.546                                                         ;
AW_In    =  114.82                                                         ;
AW_Ga    =  69.72                                                          ;
AW_Se    =  78.96                                                          ;

% Constants A and B for Antoine's equation
A_Cu     =  9.284                                                          ;
B_Cu     =  -17073                                                         ;
A_In     =  8.073                                                          ;
B_In     =  -12136                                                         ;
A_Ga     =  8.558                                                          ;
B_Ga     =  -14658                                                         ;

% Densities (g/cm^3)
rho_Cu   =  8.9                                                            ;
rho_In   =  7.31                                                           ;
rho_Ga   =  5.91                                                           ;
rho_film =  5.6                                                            ;

% Sticking Coefficients (value of 0 to 1)
sigma_Cu =  1                                                              ;
sigma_In =  1                                                              ;
sigma_Ga =  1                                                              ;

% Evaporation rate of Cu
Fm_Cu    =  3510000000000000000000*exp(A_Cu+(B_Cu/(Tm_Cu+273))) ...
            /sqrt(AW_Cu*(Tm_Cu+273))                                       ;
```

```
% Evaporation rate of In
% If the film is CGS, the In shutter is closed
if film  == 2
   Fm_In =  0                                                              ;
else
   Fm_In =  3510000000000000000000*exp(A_In+(B_In/(Tm_In+273))) ...
            /sqrt(AW_In*(Tm_In+273))                                       ;
end

% Evaporation rate of Ga
% If the film is CIS, the Ga shutter is closed
if film  == 1
   Fm_Ga =  0                                                              ;
else
   Fm_Ga =  3510000000000000000000*exp(A_Ga+(B_Ga/(Tm_Ga+273))) ...
            /sqrt(AW_Ga*(Tm_Ga+273))                                       ;
end

% Degrees swept out by each metal zone in the reactor
deg      =  40                                                             ;
% Distance from the crucible center point to the zone edge
edge     =  L*(deg/360)*0.5                                                ;


%  Load normalized flux matrix NF

   load NF

%  Build parameters vector

p        =  [  hm_Cu0,     hm_In0,     hm_Ga0,     RPM,        L,        ...
               Fm_Cu,      Fm_In,      Fm_Ga,      AW_Cu,      AW_In,    ...
               AW_Ga,      AW_Se,      rho_Cu,     rho_In,     rho_Ga,   ...
               rho_film,   NA,         gc0,        gc1,        gc2,      ...
               gc3,        Rb,         m,          edge,       As,       ...
               sigma_Cu,   sigma_In,   sigma_Ga                          ]  ;
```

PMEE_model.m

```
% PMEE model
% function that outputs Cu/(Ga+In) ratio,
% Ga/(Ga+In) ratio, and thickness as well
% as the new melt heights after a growth
% run simulation in PMEE_sim

% by R. Kaczynski  3/23/07

function [sys, x0]   =  pmee_model(t,x,u,flag,p,NF)

% Assign physical parameter values from p

hm_Cu0   =  p(1)  ;  Fm_Cu =  p(6)  ;  AW_Cu =  p(9)  ;  rho_Cu   =  p(13) ;
hm_In0   =  p(2)  ;  Fm_In =  p(7)  ;  AW_In =  p(10) ;  rho_In   =  p(14) ;
hm_Ga0   =  p(3)  ;  Fm_Ga =  p(8)  ;  AW_Ga =  p(11) ;  rho_Ga   =  p(15) ;
                                       AW_Se =  p(12) ;  rho_film =  p(16) ;
```

```
RPM      =  p(4)  ;  gc0   =  p(18) ;  NA    =  p(17) ;  sigma_Cu =  p(26) ;
L        =  p(5)  ;  gc1   =  p(19) ;  edge  =  p(24) ;  sigma_In =  p(27) ;
Rb       =  p(22) ;  gc2   =  p(20) ;  As    =  p(25) ;  sigma_Ga =  p(28) ;
m        =  p(23) ;  gc3   =  p(21) ;

% Vectors that define the rows and columns of NF

Height   =  9:-0.5:0                                                        ;
Dist     =  0:0.5:30.5                                                      ;


if flag  == 0

   size_states       =  7                                                   ;
   size_disc_states  =  0                                                   ;
   size_outputs      =  6                                                   ;
   size_inputs       =  1                                                   ;
   size_disc_roots   =  0                                                   ;
   size_feedthrough  =  0                                                   ;

   sys      =  [  size_states,   size_disc_states, size_outputs,  ...
                  size_inputs,   size_disc_roots,  size_feedthrough  ]      ;

   % Initial condition vector
     % The initial mass of In is set to a very small number
     % greater than 0 to avoid "division by zero" errors
   x0 =  [  0; hm_Cu0;  hm_In0;  hm_Ga0;  0; 0.00000000000000000001; 0; ]  ;

elseif   abs(flag)   == 1

   % Differential position
   exdot    =  (RPM/60)*L                                                   ;

   % Position of the substrate on the platen
   exprime  =  mod(x(1),L)                                                  ;


   % Differential melt height of Cu
   hm_Cudot =  -((Fm_Cu*AW_Cu)/(pi*rho_Cu*NA))*((gc3*(x(2))^3+gc2*(x(2))^2...
               +gc1*x(2)+gc0)/(Rb^2+2*m*Rb*x(2)+(m^2)*(x(2))^2))             ;

   % If the substrate is in the first half of
   % the Cu deposition zone
   if exprime  >  L/4-2*edge  &  exprime  <  L/4-edge

      % Position of the substrate within the deposition zone
      pos   =  edge-(exprime-(L/4-2*edge))                                  ;

      % Interpolated normalized Cu flux reaching the substrate
      Fs_Cu =  interp2(Dist,Height,NF,pos,x(2),'cubic')                     ;
```

```
% If the substrate is in the second half of
% the Cu deposition zone
elseif   exprime  >  L/4-edge &  exprime  <  L/4

   pos   =  exprime-(L/4-edge)                                    ;
   Fs_Cu =  interp2(Dist,Height,NF,pos,x(2),'cubic')              ;

% If the substrate is outside the Cu deposition zone,
% there is no Cu flux reaching the substrate
else
   Fs_Cu =  0                                                     ;
end


% Differential melt height of In
hm_Indot =  -((Fm_In*AW_In)/(pi*rho_In*NA))*((gc3*(x(3))^3+gc2*(x(3))^2...
            +gc1*x(3)+gc0)/(Rb^2+2*m*Rb*x(3)+(m^2)*(x(3))^2))       ;

% If the substrate is in the first half of
% the In deposition zone
if exprime  >  L/4   &  exprime  <  L/4+edge

   pos   =  edge-(exprime-(L/4))                                  ;

   % Interpolated normalized In flux reaching the substrate
   Fs_In =  interp2(Dist,Height,NF,pos,x(3),'cubic')              ;

% If the substrate is in the second half of
% the In deposition zone
elseif   exprime  >  L/4+edge &  exprime  <  L/4+2*edge

   pos   =  exprime-(L/4+edge)                                    ;
   Fs_In =  interp2(Dist,Height,NF,pos,x(3),'cubic')              ;

% If the substrate is outside the In deposition zone,
% there is no In flux reaching the substrate
else
   Fs_In =  0                                                     ;
end


% Differential melt height of Ga
hm_Gadot =  -((Fm_Ga*AW_Ga)/(pi*rho_Ga*NA))*((gc3*(x(4))^3+gc2*(x(4))^2...
            +gc1*x(4)+gc0)/(Rb^2+2*m*Rb*x(4)+(m^2)*(x(4))^2))       ;

% If the substrate is in the first half of
% the Ga deposition zone
if exprime  >  L/2-2*edge  &  exprime  <  L/2-edge

   pos   =  edge-(exprime-(L/2-2*edge))                           ;

   % Interpolated normalized Ga flux reaching the substrate
   Fs_Ga =  interp2(Dist,Height,NF,pos,x(4),'cubic')              ;
```

```
    % If the substrate is in the second half of
    % the Ga deposition zone
    elseif   exprime  >  L/2-edge &  exprime  <  L/2

       pos   =  exprime-(L/2-edge)                                    ;
       Fs_Ga = interp2(Dist,Height,NF,pos,x(4),'cubic')               ;

    % If the substrate is outside the Ga deposition zone,
    % there is no Ga flux reaching the substrate
    else
       Fs_Ga =  0                                                     ;
    end


    % Differential mass of each metal species on the substrate
    mass_Cudot  =  As*Fm_Cu*Fs_Cu*(AW_Cu/NA)*sigma_Cu                  ;
    mass_Indot  =  As*Fm_In*Fs_In*(AW_In/NA)*sigma_In                  ;
    mass_Gadot  =  As*Fm_Ga*Fs_Ga*(AW_Ga/NA)*sigma_Ga                  ;


    sys      =  [  exdot       ;  hm_Cudot    ;  hm_Indot    ;  hm_Gadot ;...
                   mass_Cudot  ;  mass_Indot  ;  mass_Gadot              ]  ;

elseif   flag ==  3

    % Position
    ex       =  x(1)                                                   ;

    % Melt heights
    hm_Cu    =  x(2)                                                   ;
    hm_In    =  x(3)                                                   ;
    hm_Ga    =  x(4)                                                   ;

    % Deposited mass
    mass_Cu  =  x(5)                                                   ;
    mass_In  =  x(6)                                                   ;
    mass_Ga  =  x(7)                                                   ;

    % Se flux is supplied in excess so the mass of Se
    % is set so that comp_Se = 0.5
    mass_Se  =  ((x(5)/AW_Cu)+(x(6)/AW_In)+(x(7)/AW_Ga))*AW_Se         ;

    % Composition
    comp_Cu  =  (mass_Cu/AW_Cu)/...

    ((mass_Cu/AW_Cu)+(mass_In/AW_In)+(mass_Ga/AW_Ga)+(mass_Se/AW_Se))  ;

    comp_In  =  (mass_In/AW_In)/...

    ((mass_Cu/AW_Cu)+(mass_In/AW_In)+(mass_Ga/AW_Ga)+(mass_Se/AW_Se))  ;

    comp_Ga  =  (mass_Ga/AW_Ga)/...

    ((mass_Cu/AW_Cu)+(mass_In/AW_In)+(mass_Ga/AW_Ga)+(mass_Se/AW_Se))  ;
```

```
   comp_Se  =  (mass_Se/AW_Se)/...

   ((mass_Cu/AW_Cu)+(mass_In/AW_In)+(mass_Ga/AW_Ga)+(mass_Se/AW_Se))       ;

   % Cu/(Ga+In) ratio
   Cu_III   =  comp_Cu/(comp_In+comp_Ga)                                  ;

   % Ga/(Ga+In) ratio
   Ga_III   =  comp_Ga/(comp_In+comp_Ga)                                  ;

   % Film thickness (microns)
   thick    =  ((mass_Cu+mass_In+mass_Ga+mass_Se)/(rho_film*As))*10000    ;

   sys      =  [  hm_Cu;   hm_In;   hm_Ga;   ...
                  Cu_III;  Ga_III;  thick    ]                           ;

else

   sys      =  []                                                        ;

end
```

LIST OF REFERENCES

[1] B.J. Stanbery, C-H. Chang, S. Kim, S. Kincal, G. Lippold, S.P. Ahrenkiel, L. Li, T.J. Anderson, M.M. Al-Jassim, in: A. Mascarenhas, D. Folstaedt, B. Joyce, T. Suzuki (Eds.), Mat. Res. Soc. Symp. I Proc. 583, 2000, 195-200.

[2] F.R. White, A.H. Clark, M.C. Graf, S.P. Grindle, L.L. Kazmerski, J. Vac. Sci. Technol. 16 (1979) 287-289.

[3] B.J. Stanbery, Heteroepitaxy and Nucleation Control for the Growth of Metal Chalcogenides Using Activated Reactant Sources, Ph.D. Thesis, Department of Chemical Engineering, University of Florida, 2001.

[4] S. Kim, Growth Kinetics and Processings of Copper Indium Diselenide-Based Thin Films, Ph.D. Thesis, Department of Chemical Engineering, University of Florida, 2003.

[5] P. Chow, Molecular Beam Epitaxy, in: J.L. Vossen, W. Kern, ed., Thin Film Processes II (Academic Press, San Diego, 1991) 133-175.

[6] S.Kincal, Modeling and Control of Multiple Thermal Effusion Sources and Substrate Temperature in Molecular Beam Epitaxy Reactors, Ph.D. Thesis, Department of Chemical Engineering, University of Florida, 2002.

[7] N.S. Lewis, Basic Research Needs for Solar Energy Utilization, Report on the Basic Energy Sciences Workshop on Solar Energy Utilization, U.S. Department of Energy Office of Basic Energy Sciences, 2005.

[8] K. Zweibel, Harnessing Solar Power: The Photovoltaics Challenge (Plenum Press, New York, 1990).

[9] S.S. Li, Semiconductor Physical Electronics (Plenum Press, New York, 1993).

[10] D.L. King, W.E. Boyson, J.A. Kratochvil, Proc. 29th IEEE PVSC, New Orleans, LA, 2002, 1356-1361.

[11] T.J. Gillespie, C.H. Marshall, M. Contreras, J. Keane, Solar Energy Mater. Solar Cells 59 (1999) 27-34.

[12] M. Powalla, D. Hariskos, E. Lotter, M. Oertel, J. Springer, D. Stellbogen, B. Dimmler, R. Schaffler, Thin Solid Films 431-432 (2003) 523-533.

[13] S.K. Deb, Proc. 4th World Renewable Energy Congress, Denver, CO, 1996, 375-379.

[14] S. Guha, Proc. 31st IEEE PVSC, Lake Buena Vista, FL, 2005, 12-16.

[15] L.L. Kazmerski, Proc. 29th IEEE PVSC, New Orleans, LA, 2002, 21-27.

[16] D.M. Chapin, C.S. Fuller, G.L. Pearson, J. Appl. Phys. 25 (1954) 676-677.

[17] J.L. Shay, S. Wagner, H.M. Kasper, Appl. Phys. Lett. 27 (1975) 89-90.

[18] L.L. Kazmerski, F.R. White, G.K. Margon, Appl. Phys. Lett. 29 (1976) 268-270.

[19] W.S. Chen, J.M. Stewart, W.E. Devaney, R.A. Mickelsen, B.J. Stanbery, Proc. 16th IEEE PVSC, San Diego, CA, 1982, 781-785

[20] A.S. Grove, Physics and Technology of Semiconductor Devices (John Wiley and Sons, Inc., New York, 1967).

[21] P. Wurfel, Physics of Solar Cells: From Principles to New Concepts (Wiley-VCH, Weinheim, 2005).

[22] H.J. Moller, Semiconductors for Solar Cells (Artech House, Boston, 1993).

[23] W.R. Runyan, Semiconductor Measurements and Instrumentation (McGraw-Hill, New York, 1975).

[24] J. Muller, J. Nowoczin, H. Schmitt, Thin Solid Films 496 (2006) 364-370.

[25] A. Goetzberger, C. Hebling, H-W. Schock, Materials Science and Engineering R 40 (2003) 1-46.

[26] R.D. Wieting, Proc. 29th IEEE PVSC, New Orleans, LA, 2002, 478-483.
[27] B. Dimmler, M. Powalla, R. Schaeffler, Proc. 31st IEEE PVSC, Lake Buena Vista, FL, 2005, 189-194.
[28] J.A. Abushama, S. Johnston, R. Noufi, Journal of Physics and Chemistry of Solids 66 (2005) 1855-1857.
[29] J.L. Shay, B. Tell, H.M. Kasper, L.M. Schiavone, Physical Review B 7 (1973) 4485-4490.
[30] H-W. Schock, R. Noufi, Prog. Photovolt. Res. Appl. 8 (2000) 151-160.
[31] V.G. Lambrecht, Mater. Res. Bull. 8 (1973) 1383.
[32] J.E. Jaffe, A. Zunger, Phys. Rev. B 28 (1983) 5822-5847.
[33] L. Mandel, R.D. Tomlinson, M.J. Hampshire, J. Appl. Cryst. 10 (1977) 130-131.
[34] J. Parkes, R.D. Tomlinson, M.J. Hampshire, J. Appl. Cryst. 6 (1973) 414-416.
[35] A. Gerhard, W. Harneit, S. Brehme, A. Bauknecht, U. Fiedeler, M.Ch. Lux-Steiner, S. Siebentritt, Thin Solid Films 387 (2001) 67-70.
[36] Y. Hamakawa, Thin Film Solar Cells: Next Generation Photovoltaics and Its Applications (Springer, New York, 2004).
[37] B.J. Stanbery, Proc. 31st IEEE PVSC, Lake Buena Vista, FL, 2005, 355-358.
[38] R. Wieting, R. Gay, H. Ngyuen, J. Palm, C. Rischmiller, A. Seapan, D. Tarrant, D. Willet, Proc. 31st IEEE PVSC, Lake Buena Vista, FL, 2005, 177-182.
[39] U. Rau, Jpn. J. Appl. Phys. 39 (2000) Suppl. 39-1, 389-394.
[40] D. Liao, A. Rockett, Proc. 29th IEEE PVSC, New Orleans, LA, 2002, 515-518.
[41] S. Siebentritt, Thin Solid Films, 403-404 (2002) 1-8.
[42] C.-S. Jiang, R. Noufi, K. Ramanathan, J.A. Abushama, H.R. Moutinho, M.M. Al-Jassim, Appl. Phys. Lett. 85 (2004) 2625-2627.
[43] J.L. Shay, B. Tell, H.M. Kasper, L.M. Schiavone, Phys. Rev. B 5 (1972) 5003-5005.
[44] W. Horig, H. Neumann, B. Schumann, G. Kuhn, Phys. Status Solidi 85 (1978) K57.
[45] G.L. Gu, B.H. Tseng, H.L. Hwang, Journal of Physics and Chemistry of Solids 64 (2003) 1901-1906.
[46] K. Yoshino, N. Mitani, T. Ikari, P. Fons, S. Niki, A. Yamada, Solar Energy Mater. Solar Cells 67 (2001) 173-178.
[47] V. Nadenau, G. Lippold, U. Rau, H.W. Schock, Journal of Crystal Growth 233 (2001) 13-21.
[48] D.L. Young, J. Keane, A. Duda, J.A. Abushama, C.L. Perkins, M. Romero, R. Noufi, Prog. Photovolt. Res. Appl. 11 (2003) 535-541.
[49] M. Saad, A. Kassis, Solar Energy Mater. Solar Cells 77 (2003) 415-422.
[50] C.H. Henry, J. Appl. Phys. 51 (1980) 4494-4500.
[51] V. Nadenau, U. Rau, A. Jasenek, H.W. Schock, J. Appl. Phys. 87 (2000) 584-593.
[52] A. Jasenek, U. Rau, V. Nadenau, H.W. Schock, J. Appl. Phys. 87 (2000) 594-602.
[53] A. Bauknecht, S. Siebentritt, A. Gerhard, W. Harneit, S. Brehme, J.Albert, S.Rushworth, M.Ch. Lux-Steiner, Thin Solid Films 361-362 (2000) 426-431.
[54] B.A. Monsour, M.A. El-Hagary, Thin Solid Films 256 (1995) 165-170.
[55] A. Meeder, L. Weinhardt, R. Stresing, D. Fuertes Marron, R. Wurz, S.M. Babu, T. Schedel-Niedrig, M.Ch. Lux-Steiner, C. Heske, E. Umbach, Journal of Physics and Chemistry of Solids 64 (2003) 1553-1557.
[56] M.A. Contreras, H. Wiesner, J. Tuttle, K. Ramanathan, R. Noufi, Solar Energy Mater. Solar Cells 49 (1997) 239-247.

[57] S. Siebentritt, Thin Solid Films 403-404 (2002) 1-8.
[58] U. Rau, M. Schmidt, A. Jasenek, G. Hanna, H.W. Schock, Solar Energy Mater. Solar Cells 67 (2001) 137-143.
[59] U. Rau, A. Jasenek, H.W. Schock, P. Engelhardt, Th. Meyer, Thin Solid Films 361-362 (2000) 298-302.
[60] C.H. Huang, S.S. Li, T.J. Anderson, Proc. 29th IEEE PVSC, New Orleans, LA, 2002, 748-751.
[61] J.H. Schon, Ch. Kloc, E. Bucher, Thin Solid Films 361-362 (2000) 411-414.
[62] C. Persson, Y.J. Zhao, S. Lany, A. Zunger, Phys. Rev. B 72 (2005) 035211 1-14.
[63] A. Kassis, M. Saad, Solar Energy Mater. Solar Cells 80 (2003) 491-499.
[64] G.A. Medvedkin, T. Nishi, Y. Katsumata, H. Miyake, K. Sato, Solar Energy Mater. Solar Cells 75 (2003) 135-143.
[65] J.H. Schon, E. Bucher, Thin Solid Films 387 (2001) 23-25.
[66] J.H. Schon, E. Arushanov, N. Fabre, E. Bucher, Solar Energy Mater. Solar Cells 61 (2000) 417-426.
[67] B. Tell, J.L. Shay, H.M. Kasper, Phys. Rev. B 4 (1971) 2463-2471.
[68] M. Nanu, L. Reijnen, B. Meester, J. Schoonman, A. Goosens, Chem. Vap. Deposition 10 (2004) 45-49.
[69] J.M. Masse, J.C. Manthurathil, D.R. Locher, Bull. Am. Phys. Soc. 20 (1975) 696.
[70] D. Braunger, Th. Durr, D. Hariskos, Ch. Noble, Th. Walter, N. Wieser, H.W. Schock, Proc. 25th IEEE PVSC, Washington, D.C., 1996, 1001-1004
[71] M.S. Branch, P.R. Berndt, J.R. Botha, A.W.R. Leitch, J. Weber, Thin Solid Films 431-432 (2003) 94-98.
[72] S. Zweigart, S.M. Sun, G. Bilger, H.W. Schock, Solar Energy Mater. Solar Cells 41/42 (1996) 219-229.
[73] M.L. Chenene, V. Alberts, B.C. Cuamba, Proc. 3rd WCPEC, Osaka, Japan, 2003, 406-409.
[74] M. Rusu, S. Wiesner, D. Fuertes Marron, A. Meeder, S. Doka, W. Bohne, S. Linder, Th. Schedel-Niedrig, Ch. Giesen, M. Heuken, M.Ch. Lux-Steiner, Thin Solid Films 451-452 (2004) 556-561.
[75] L.L. Kerr, S. Kim, S. Kincal, M. Ider, S. Yoon, T.J. Anderson, Proc. 29th IEEE PVSC, New Orleans, LA, 2002, 676-679.
[76] M.E. Calixto, P.J. Sebastian, R.N. Bhattacharya, R. Noufi, Solar Energy Mater. Solar Cells 59 (1999) 75-84.
[77] D.L. Schulz, C.J. Curtis, A. Cram, J.L. Alleman, A. Mason, R.J. Matson, J.D. Perkins, D.S. Ginley, Proc. 26th IEEE PVSC, Anaheim, CA, 1997, 483-486.
[78] V.J. Kapur, A. Bansal, P. Le, O.I. Asensio, Proc. 29th IEEE PVSC, New Orleans, LA, 2002, 688-691.
[79] W. Schockley, H. Queisser, J. Appl. Phys. 32 (1961) 510-519.
[80] R.A. Sherif, R.R. King, N.H. Karam, D.R. Lillington, Proc. 31st IEEE PVSC, Lake Buena Vista, FL, 2005, 17-22.
[81] T.J. Coutts, K.A. Emery, J.S. Ward, Prog. Photovolt. Res. Appl. 10 (2002) 1-9.
[82] M. Symko-Davies, Proc. 31st IEEE PVSC, Lake Buena Vista, FL, 2005, 41-413.
[83] P. Mahawela, S. Jeedigunta, C.S. Ferekides, D.L. Morel, Proc. 29th IEEE PVSC, New Orleans, LA, 2002, 724-727.

[84] T. Nakada, Y. Hirabayashi, T. Tokado, D. Ohmori, Proc. 3rd WCPEC, Osaka, Japan, 2003, 2880-2884.
[85] F.J. Haug, H. Zogg, A.N. Tiwari, Proc. 29th IEEE PVSC, New Orleans, LA, 2002, 728-731.
[86] W. N. Shafarman, P.D. Paulson, Proc. 31st IEEE PVSC, Lake Buena Vista, FL, 2005, 231-234.
[87] D. L.Young, J.H. Abushama, R. Noufi, X. Li, J. Keane, T.A. Gessert, J.S. Ward, M. Contreras, M. Symko-Davies, T.J. Coutts, Proc. 29th IEEE PVSC, New Orleans, LA, 2002, 608-611.
[88] T. Schlenker, M.L. Valero, H.W. Schock, J.H. Werner, Journal of Crystal Growth 264 (2004) 178-183.
[89] K. Ramanathan, J. Keane, R. Noufi, Proc. 31st IEEE PVSC, Lake Buena Vista, FL, 2005, 195-198.
[90] B.J. Stanbery, C.H. Chang, T.J. Anderson, Proc. 11th International Conference on Ternary and Multinary Compounds, Salford, UK, 1997, 915-922.
[91] A.M. Gabor, J.R. Tuttle, M.H. Bode, A. Franz, A.L. Tennant, M.A. Contreras. R. Noufi, D.G. Jensen, A.M. Hermann, Solar Energy Mater. Solar Cells 41/42 (1996) 247-260.
[92] R. Hunger, K. Sakurai, A. Yamada, P. Fons, K. Iwata, K. Matsubara, S. Niki, Thin Solid Films 431-432 (2003) 16-21.
[93] J.W. Olesik, Inductively Coupled Plasma – Optical Emission Spectroscopy, in: C.R. Brundle, C.A. Evans, Jr., S. Wilson, ed., Encyclopedia of Materials Characterization (Butterworth-Heinemann, Stoneham, MA, 1992) 198-213.
[94] J.B. Bindell, Scanning Electron Microscopy, in: C.R. Brundle, C.A. Evans, Jr., S. Wilson, ed., Encyclopedia of Materials Characterization (Butterworth-Heinemann, Stoneham, MA, 1992) 70-84.
[95] M.F. Toney, X-Ray Diffraction, in: C.R. Brundle, C.A. Evans, Jr., S. Wilson, ed., Encyclopedia of Materials Characterization (Butterworth-Heinemann, Stoneham, MA, 1992) 198-213.
[96] H.S. Ullal, Proc. 28th IEEE PVSC, Anchorage, AK, 2000, 418-423.
[97] H.A. Al-Thani, F.S. Hasoon, M. Young, Sally Asher, J.L. Alleman, M.M. Al-Jassim, D.L. Williamson, Proc. 29th IEEE PVSC, New Orleans, LA, 2002, 720-723.
[98] K. Orgassa, H.W. Schock, J.H. Werner, Thin Solid Films 431-432 (2003) 387-391.
[99] G.M. Hanket, U.P. Singh, E. Eser, W.N. Shafarman, R.W. Birkmire, Proc. 29th IEEE PVSC, New Orleans, LA, 2002, 567-570.
[100] Y. Hashimoto, T. Satoh, S. Shimakawa, T. Negami, Proc. 3rd WCPEC, Osaka, Japan, 2003, 574-577.
[101] D. Bremaud, D. Rudmann, G. Bilger, H. Zogg, A. N. Tiwari, Proc. 31st IEEE PVSC, Lake Buena Vista, FL, 2005,
[102] A. Yamada, P. Fons, K. Matsubara, K. Iwata, K. Sakurai, S. Niki, Thin Solid Films 431-432 (2003) 277-284.
[103] O. Schenker, M. Klenk, E. Bucher, Thin Solid Films 361-362 (2000) 454-457.
[104] V. Nadenau, D. Hariskos, H.W. Schock, 14th Eur. PVSEC, Barcelona, Spain, 1997, 1250.
[105] K.T. Ramakrishna, P.J. Reddy, J. Appl. Phys. 25 (1992) 1345-1348.
[106] M.A. Contreras, J. Tuttle, A. Gabor, A. Tennant, K. Ramanathan, S. Asher, A. Franz, J. Keane, L.Wang, R. Noufi, Solar Energy Mater. Solar Cells 41/42 (1996) 231-246.

[107] L. Olsen, P. Eschbach, S. Kundu, Proc. 29th IEEE PVSC, New Orleans, LA, 2002, 652-655.
[108] J.S. Ward, K. Ramanathan, F.S. Hasoon, T.J. Coutts, J. Keane, M.A. Contreras, T. Moriarty, R. Noufi, Prog. Photovolt. Res. Appl. 10 (2002) 41-46.
[109] K. Ramanathan, F.S. Hasoon, S. Smith, A. Mascrahenas, H. Al-Thani, J. Alleman, H.S. Ullal, J. Keane, Proc. 29th IEEE PVSC, New Orleans, LA, 2002, 523-526.
[110] T. Nakada, A. Kunioka, Appl. Phys. Lett. 74 (1999) 2444-2446.
[111] A. Jasenek, U. Rau, V. Nadenau, D. Thiess, H.W. Schock, Thin Solid Films 361-362 (2000) 415-419.
[112] K. Ramanathan, F.S. Hasoon, S. Smith, D.L. Young, M.A. Contreras, P.K. Johnson, A.O. Pudov, J.R. Sites, Journal of Physics and Chemistry of Solids 64 (2003) 1495-1498.
[113] M. Bar, Ch.H. Fischer, H.J. Muffler, B. Leupolt, Th.P. Niesen, F. Karg, M.Ch. Lux-Steiner, Proc. 29th IEEE PVSC, New Orleans, LA, 2002, 636-639.
[114] B. Sang, W.N Shafarman, R.W. Birkmire, Proc. 29th IEEE PVSC, New Orleans, LA, 2002, 632-635.
[115] D. Hariskos, S. Spiering, M. Powalla, Thin Solid Films 480-481 (2005) 99-104.
[116] M.Ch. Lux-Steiner, A. Ennaoui, Ch.H. Fischer, A. Jager Waldau, J. Klaer, R. Klenk, R. Konenkamp, Th. Matthes, R. Scheer, S. Siebentritt, A. Weidinger, Thin Solid Films 361-362 (2000) 533-539.
[117] A. Bauknecht, U. Blieske, T. Kampschulte, J. Albert, H. Sehnert, M.Ch. Lux-Steiner, A. Klein, W. Jaegermann, Appl. Phys. Lett. 74 (1999) 1099-1101.
[118] M. Rusu, P. Gashin, A. Simaskevich, Solar Energy 72 (2002) 235-241.
[119] A. Klein, W. Jaegerman, J. Fritsche, R. Hunger, D. Kraft, F. Sauberlich, T. Schulmeyer, B. Spath, Proc. 31st IEEE PVSC, Lake Buena Vista, FL, 2005, 205-210.
[120] K. Ramanathan, R. Bhattacharya, J. Granata, J. Webb, D. Niles, M. Contreras, H. Wiesner, F. Hasoon, R. Noufi, Proc. 26th IEEE PVSC, Anaheim, CA, 1997, 319-322.
[121] H.S. Ullal, K. Zweibel, B. von Roedern, Proc. 29th IEEE PVSC, New Orleans, LA, 2002, 472-477.
[122] S.H. Wei, X. Nie, S.B. Zhang, Proc. 29th IEEE PVSC, New Orleans, LA, 2002, 496-499.
[123] C.H. Huang, Alternative Buffer Layers, Device Modeling and Characterization of Copper-Indium-Diselenide-Based Thin-Film Solar Cells, Ph.D. Thesis, Department of Electrical and Computer Engineering, University of Florida, 2002.
[124] A. Meeder, D. Fuertes Marron, V. Chu, J.P. Conde, A. Jager-Waldau, A. Rumberg, M.Ch. Lux-Steiner, Thin Solid Films 403-404 (2002) 495-499.
[125] M. Klenk, O. Schenker, E. Bucher, Thin Solid Films 361-362 (2000) 229-233.
[126] R. Caballero, C. Guillen, Thin Solid Films 403-404 (2002) 107-111.
[127] V. Nadenau, D. Hariskos, H.W. Schock, M. Krejci, F.J. Haug, A.N. Tiwari, H. Zogg, G. Kostorz, J. Appl. Phys. 85 (1999) 534-542.
[128] B.M. Keyes, P. Dippo, W. Metzger, J. Abushama, R. Noufi, Proc. 29th IEEE PVSC, New Orleans, LA, 2002, 511-514.
[129] R. Scheer, M. Wilhelm, H.J. Lewerenz, H.W. Schock, L. Stolt, Solar Energy Mater. Solar Cells 49 (1997) 299-309.
[130] W.N. Shafarman, J. Zhu, Thin Solid Films 361-362, (2000) 473-477.
[131] I.L. Repins, D.C. Fisher, M.E. Beck, J.S. Britt, Proc. 31st IEEE PVSC, Lake Buena Vista, FL, 2005, 311-314.

[132] M. Purwins, A. Weber, P. Berwian, G. Muller, F. Hergert, S. Jost, R. Hock, Journal of Crystal Growth 287 (2006) 408-413.
[133] J. Abushama, S. Johnston, R. Ahrenkiel, R. Crandall, D. Young, R. Noufi, in: R. Noufi et al. (Eds.), Mat. Res. Soc. Symp. Proc. 763, 2003, 255-260.
[134] F.J. Haug, M. Krejci, H. Zogg, A.N. Tiwari, M. Kirsch, S. Siebentritt, Thin Solid Films 361-362 (2000) 239-242.
[135] A. Rockett, Thin Solid Films 480-481 (2005) 2-7.
[136] M. Bodegard, O. Lundberg, J. Lu, L. Stolt, Thin Solid Films 431-432 (2003) 46-52.
[137] R. Kniese, M. Lammer, U. Rau, M. Powalla, Thin Solid Films 451-452 (2004) 430-433.
[138] G. Orsal, F. Mailly, N. Romain, M.C. Artaud, S. Rushworth, S. Duchemin, Thin Solid Films 361-362 (2000) 135-139.
[139] T. Wada, S. Nishiwaki, N. Kohara, T. Negami, S. Niki, R. Suzuki, T. Ohdaira, S. Ishibashi, A. Yamada, Jpn. J. Appl. Phys. 39 (2000) suppl. 39-1, 8-13.
[140] A. Yamada, Y. Makita, S. Niki, A. Obara, P. Fons, H. Shibata, Microelectronics Journal 27 (1996) 53-58.
[141] Kerr, Growth, Characterization and Thermodynamic Modeling of Absorber and Transparent Conducting Oxides for Copper Indium Diselenide Based Thin Film Solar Cells, Ph.D. Thesis, Department of Chemical Engineering, University of Florida, 2004.
[142] J. Abushama, R. Noufi, S. Johnston, S. Ward, X. Wu, Proc. 31st IEEE PVSC, Lake Buena Vista, FL, 2005, 299-302.
[143] M. Saad, H. Riazi, E. Bucher, M.Ch. Lux-Steiner, Appl. Phys. A 62 (1996) 181-185.
[144] J.Song, S.S. Li, S. Yoon, W.K. Kim, J. Kim, J. Chen, V. Craciun, T.J. Anderson, O.D. Crisalle, F. Ren, Proc. 31st IEEE PVSC, Lake Buena Vista, FL, 2005, 449-452.
[145] D.G. Jensen, Proc. 31st IEEE PVSC, Lake Buena Vista, FL, 2005, 351-354.
[146] M.A. Contreras, K. Ramanathan, J. Abushama, F. Hasoon, D.L. Young, B. Egaas, R. Noufi, Prog. Photovolt. Res. Appl. 13 (2005) 209-216.
[147] G. Voorwinden, R. Kniese, M. Powalla, Thin Solid Films 431-432 (2003) 538-542.
[148] T. Dullweber, G. Hanna, W. Shams-Kolahi, A. Schwartzlander, M.A. Contreras, R. Noufi, H.W. Schock, Thin Solid Films 361-362 (2000) 478-481.
[149] O.Lundberg, M. Bodegard, L. Stolt, Thin Solid Films 431-432 (2003) 26-30.
[150] M.A. Contreras, M.J. Romero, R. Noufi, Thin Solid Films 511-512 (2006) 51-54.
[151] M.A. Contreras, B. Egaas, K. Ramanathan, J. Hiltner, A. Swartlander, F. Hasoon, R. Noufi, Prog. Photovolt. Res. Appl. 7 (1999) 311-316.
[152] Y. Umeno, T. Nakada, Proc. 3rd WCPEC, Osaka, Japan, 2003, 380-383.
[153] G. Hanna, J. Mattheis, V. Laptev, Y. Yamamoto, U. Rau, H.W. Schock, Thin Solid Films 431-432 (2003) 31-36.
[154] M.A. Contreras, B. Egaas, D. King, A. Swartzlander, T. Dullweber, Thin Solid Films 361-362 (2000) 167-171.
[155] M. Lammer, A. Eicke, M. Powalla, Proc. 29th IEEE PVSC, New Orleans, LA, 2002, 696-699.
[156] K. Ramanathan, M.A. Contreras, C.L. Perkins, S. Asher, F.S. Hasoon, J. Keane, D. Young, M. Romero, W. Metzger, R. Noufi, J. Ward, A. Duda, Prog. Photovolt. Res. Appl. 11(2003) 225-230.
[157] B. Marsen, S. Marsillac, S. Dorn, R. Rocheleau, Proc. 31st IEEE PVSC, Lake Buena Vista, FL, 2005, 386-389.

[158] J.T. Heath, J.D. Cohen, W.N. Shafarman, Proc. 29th IEEE PVSC, New Orleans, LA, 2002, 596-599.
[159] D. Rudmann, D. Bremaud, A.F. da Cunha, G. Bilger, A. Strohm, M. Kaelin, H. Zogg, A.N. Tiwari, Thin Solid Films 480-481 (2005) 55-60.
[160] D. Rudman, G. Bilger, M. Kaelin, F.J. Haug, H. Zogg, A.N. Tiwari, Thin Solid Films 431-432 (2003) 37-40.
[161] S. Wiedeman, M.E. Beck, R. Butcher, I. Repins, N. Gomez, B. Joshi, R.G. Wendt, J.S. Britt, Proc. 29th IEEE PVSC, New Orleans, LA, 2002, 575-578.
[162] M.E. Beck, S. Wiedeman, R. Huntington, J. VanAlsburg, E. Kanto, R. Butcher, J.S. Britt, Proc. 31st IEEE PVSC, Lake Buena Vista, FL, 2005, 211-214.
[163] S. Kincal, O.D. Crisalle, Proc. American Control Conference, Chicago, IL, 2000, 4001-4005.

BIOGRAPHICAL SKETCH

Ryan Michael Kaczynski was born in Amherst, NY on January 11, 1979. He grew up in the small Western New York town of Newfane and was named valedictorian of his graduating senior class in June 1997. He then attended Cornell University in Ithaca, NY where he received his Bachelor of Science degree in chemical engineering in May 2001. In August 2001, he joined the graduate program in the Chemical Engineering department at the University of Florida (UF) to pursue the degree of Doctor of Philosophy. While at UF, he became a member of the multi-disciplinary Copper Indium Diselenide (CIS) solar cell group headed by Dr. Oscar D. Crisalle (his advisor), Dr. Timothy J. Anderson, and Dr. Sheng S. Li.